Master thesis

The application of double-curved precast concrete elements for the project Green Planet

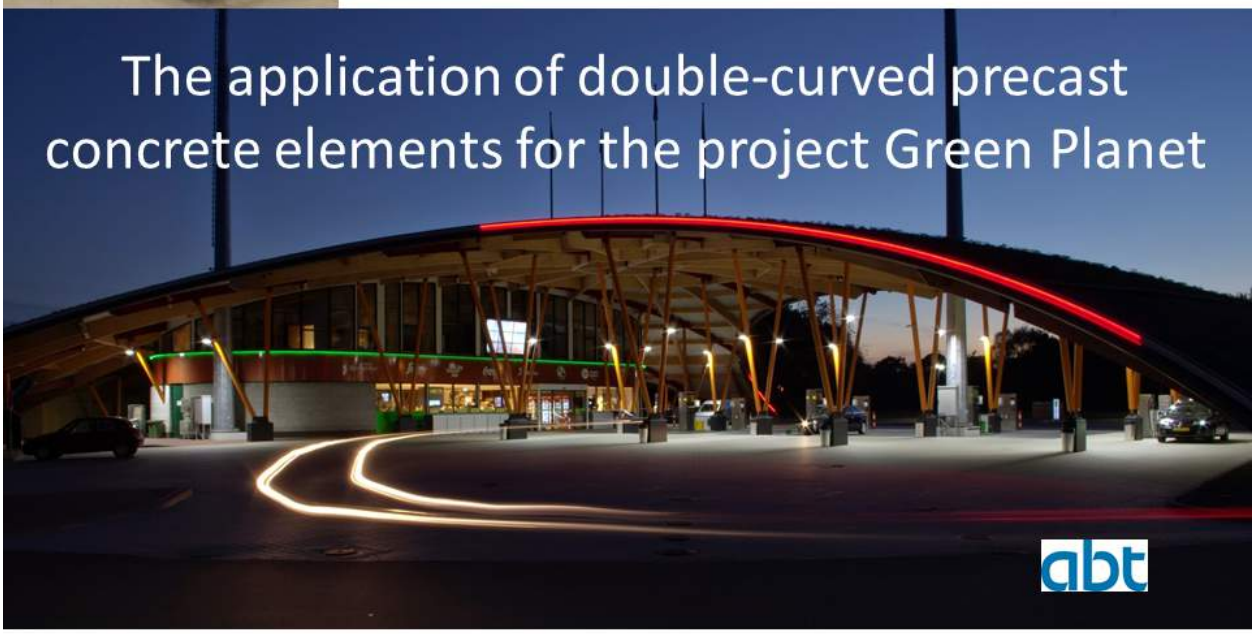

TU Delft

Sietse Witterholt

August 2016

Delft University of Technology
Faculty of Civil Engineering and Geosciences
Building Engineering – Structural Design

Graduate committee
Prof. Ir. R. Nijsse
Dr. Ir. H.R.Schipper
Dr. Ir. P.C.J. Hoogenboom
Dr. Ir. S. Grünewald
Ir. J.A.M. van Vliet

Preface

This final report is a result of my Master thesis for the Master Building Engineering of the faculty of Civil Engineering and Geosciences at the Delft University of Technology. The research was performed at the Structural and Building Engineering section and in cooperation with ABT in Velp. It focuses on the application of double-curved precast concrete elements for which project Green Planet was selected.

Elaborating on extensive investigations on how to produce unique double-curved precast elements with a flexible formwork, I had the great opportunity to explore the integration of the elements into an actual design. This offered both an investigation and designing challenge. This thesis presents the transformation of a timber/steel structure into a customized concrete structure which is double-curved. With a structural analysis and optimization using finite element analysis a suitable design is created in this thesis. Furthermore, an investigation in connecting curved concrete elements in finite element analysis is presented. In the end the viability of the design, concerning execution and costs, is addressed.

For completing this Master thesis I would like to thank my graduation committee Prof. Ir. R. Nijsse, Dr. Ir. H.R.Schipper, Dr. Ir. P.C.J. Hoogenboom, Dr. Ir. S. Grunewald and Ir. J.A.M. van Vliet for their guidance and sharing their knowledge, experience and ideas on the subject. Also, I would like to thank Ir. D.C. van Keulen for sharing his knowledge about detailing.

Sietse Witterholt
August 2016

Summary

Double-curved structures, or shell structures, can transfer forces very efficiently. The thickness to span ratio is very small which can lead to a very economical design. Especially when a relatively cheap building material like concrete is used. Concrete dome structures, for example, combine the strengths of both material and building shape. The building process of these structures, however, is generally very labor intensive.
Concrete shell structures can be build on site making use of a huge temporary supportive structure to cast the concrete on, but they can be (partially) prefabricated as well, like the Palazzetto dello Sport in Rome. Prefabricating structures is a popular building method because it allows manufacturing in a controlled environment and it often provides a quick and simple erection on site. A disadvantage of prefabricating is usually the complexity of the required connections. It is interesting to combine both building methods, i.e. prefabricate the supportive structure and make it contribute to the structural integrity of the structure. In this way the advantages of both methods are combined: reduce the complexity of the connections because of the in-situ concrete layer and integrate the supportive structure in the design for a more cost efficient erection. This thesis studies the feasibility of such a building method, making use of a concrete shell structure consisting of double-curved precast concrete elements.
The project Green Planet, a (gas) station built along the A32 highway in the north of the Netherlands, is a double-curved structure built just recently (designed by ABT). The main structure consists of laminated wood beams and steel roof panels. The height is 9 meters and the diameter 75 meters, making it a large span sphere shaped shell structure, except that it is supported by columns (see Figure 1). However, this construction could have been executed in concrete as well, self-supporting and without columns. This provides a perfect application for this research and besides the feasibility of the building method it will be possible to study the economically competitiveness compared to other building methods as well.

Figure 1: A top view of the project Green Planet

The shape of the Green Planet shell structure is challenging and requires the production of many uniquely shaped double-curved elements. Normally, the prefabrication of all these different elements would be very expensive. One year ago, however, H.R. Schipper finished a PhD research demonstrating that the prefabrication of double-curved concrete elements is possible with an adjustable formwork. This 'flexible mould method' offers a cost efficient way of manufacturing the elements with a re-usable mould. This Master thesis contributes to this research by studying a practical application of the double-curved elements produced with the adjustable formwork.
The structural behavior of the Green Planet shell is analyzed by using a finite element analysis (FEA) program, Scia Engineer. To verify the unusual shape of the shell structure the results are compared to results of comparable but more traditional shell structures. It was compared with a cylinder structure, a regular dome structure and a weakened (by an oculus in the top) dome structure with comparable dimensions and boundary conditions. The conclusion was that the Green Planet shell is best defined as a very stiff cylinder structure. An analysis with realistic loads in conformation with the codes indicated that various wind loads are normative for the internal forces on the structure. The structure is mainly subjected to compressive forces and only in certain areas, along the edge of the shell or near the supports, tension forces arise. Additionally, the analysis confirms that large thrust forces will act on the foundation.
Therefore, special attention went out to the foundation and a model in which the supports were connected by long steel tension cables was analyzed. It was found that due to small settlements caused by the elongation of the cables the resistance against buckling will never suffice. For this reason it is recommended to make use of post-tension cables or another special foundation that will prevent these small settlements.
The analysis resulted in a Green Planet shell with a thickness of 250 mm, a material strength C45/55 and the supports are hinged to prevent settlements. In order to investigate the

influence of the connections between the precast elements on the behavior of the structure, the model is segmented. Unfortunately, this segmentation was slightly impeded by the limitations of the FEA program. But, together with the other boundary conditions it was possible to create a realistic segmentation plan.
In order to be able to model the connections in the FEA program it was necessary to determine the spring stiffness they represent. The spring stiffness of the connection is divided in an axial, rotational and shear stiffness part. For each stiffness a formula was composed and tested with theoretical and FEA models. When combined again these formulas represent a three-dimensional connection stiffness and this was tested with other FEA models as well. It was concluded that the combined formula is appropriate to simulate a connection stiffness in Scia Engineer. Additionally, the research indicated that a large connection stiffness reduction has a relatively small influence on the buckling behavior of a concrete dome structure.
The combined formulas for the connection stiffness were applied to the Green Planet model as well. In this case the connection stiffness would simulate a continuous concrete shell structure. When the stiffness of all connections is halved it would simulate a construction that's weakened considerably because of the connections. Connections that cause the stiffness of a continuous concrete section to halve are deemed straightforward to design. The comparison results showed that there is a small maximum difference of 0,5% between the Green Planet models if the stiffness of the connections is halved. Therefore, a simple connection will suffice for the final Green Planet design.
For the execution of the Green Planet design a few proposals are presented addressing the connection design, the execution method and the foundation. The overall conclusion is that it's technically feasible to design an alternative for project Green Planet, making use of a concrete shell structure consisting of double-curved precast concrete elements. The economically competitiveness of this alternative, however, is not achieved and it is questionable if this possible at all since the original design is very economic. But, it must be noted that the original Green Planet design is supported by columns while the presented alternative structure offers a column free space, structurally and in the end economically this makes a big difference.
This study offers a lot of ideas and challenges for future research. One example of a most interesting challenge would be to design the proposed connection in a specialized FEA program and compare the results with practical experiments.

Contents

I Introduction to the research **8**

1 Introduction **9**
1.1 Introduction to the problem and research objectives 9
1.2 Approach 10

2 Literature review **12**
2.1 Reference projects 12
2.2 Mechanics 21
2.3 Adjustable formwork 34

II Green Planet: design and optimization **44**

3 Dome analysis **45**
3.1 Introduction 45
3.2 Shell parameters 45
3.3 Linear elastic analysis: theory vs FEA 47
3.4 Linear buckling analysis: theory vs FEA 56
3.5 Discussion 58

4 Shell structures comparison **61**
4.1 Introduction 61
4.2 Weakened dome analysis 62
4.3 Arch analysis 65
4.4 Cylinder structure analysis 69
4.5 Asymmetrical loaded dome 74
4.6 Green Planet analysis 78
4.7 Comparison 83
4.8 Discussion 89

5 Design Green Planet analysis **90**
5.1 Introduction 90
5.2 Loading 90
5.3 Analysis Green Planet 95
5.4 Mesh study 106
5.5 Thickness study 108

5.6 Material strength study . . . 110
5.7 Optimizing thickness and material strength . . . 110
5.8 Foundation . . . 113
5.9 Geometrical non-linear analysis . . . 117

III Green Planet: segmentation and detailing 118

6 Segmentation 119
6.1 Introduction . . . 119
6.2 Segmentation options . . . 120
6.3 Finite element modeling . . . 123
6.4 Effect of segmentation . . . 125

7 Detailing 127
7.1 Introduction . . . 127
7.2 Axial connection . . . 127
7.3 Rotational connection . . . 133
7.4 Shear connection . . . 138
7.5 Application connection design . . . 144
7.6 Connecting Green Planet . . . 165

IV Green Planet: execution and costs 172

8 Execution and costs 173
8.1 Introduction . . . 173
8.2 Feasibility . . . 173
8.3 Connections . . . 176
8.4 Execution method . . . 177
8.5 Production of the elements . . . 180
8.6 Foundation . . . 180
8.7 Costs . . . 181

V Final remarks 182

9 Conclusions and recommendations 183
9.1 Introduction . . . 183
9.2 Conclusions . . . 183
9.3 Recommendations . . . 187

Bibliography 190

A Top displacement hemispherical dome with potential energy 196

Part I

Introduction to the research

Chapter 1

Introduction

1.1 Introduction to the problem and research objectives

1.1.1 Introduction to the problem

Everywhere architects are engaged to adapt their buildings to a certain environment or make it stand out. In the latter case the aim is to design a unique building that lingers in peoples minds. An icon using form to emphasize it's functional use for example. Regularly, shell structures are chosen for this purpose. These structures break the linearity of daily practicality. Thus, the building appeals to the imagination and constitutes a landmark herein.
A supposedly future landmark is the (gas) service station built along the A32 highway in the north of the Netherlands. The unique feature being offering sustainable fuels, is publicly exhibited by means of the shape of the structure. The shape simulates a portion of the earth's surface. The surface of the globe on which we live and which is endangered of being compromised by the use of non-renewable fuels. In short, it's called project Green Planet. This shape is a shell structure, which consists of laminated wood beams and steel roof panels. The height is 9 meters and the diameter 75 meters, making it a large span shell structure, except that it is supported by columns. However, this construction could have been executed in concrete as well, self-supporting and without supports.
In this case different technical reasons militate against the execution of a concrete shell structure. A shell structure with the most ideal shape with respect to transferring loads does not have spherical curvatures. Bending stresses will arise, which require more reinforcement and an increased thickness. In addition, the execution of such a shell structure is very labor intensive. This is mainly due to the necessary formwork. Furthermore, the structure requires a large foundation to resist large horizontal forces. Moreover, high economic interests come with this design. The foundation of this shell structure is a good example of an economic interest. In addition to the intensive labor required for the construction of a concrete foundation and the associated costs, comes another practical disadvantage with this concrete structure. If chosen they should have given priority to an archaeological investigation, which would have slowed down the project.
When the shape of the design is considered it can be concluded that in particular the required complexity of the formwork and the related costs thereof prevent the structure

from being designed in concrete. An alternative would be the application of load-bearing double-curved concrete elements. These precast elements can be produced with a flexible/adjustable and reusable mould. As a result, the elements can be easily custom-made. Some supportive structure remains necessary however but can, depending on the implementation, be reduced to a stability construction.
In this research the Green Planet design is used to investigate the application of prefabricated double-curved concrete elements. In addition, costs will be quantified to determine if the future design can be competitive with the current design.

1.1.2 Research objectives

The aim of this master thesis is to investigate the application of double-curved elements produced with an adjustable formwork. The application is predetermined and is the project Green Planet. A lot of aspects need to be considered to come to a balanced design. In the end the main question will be if the final design is economically competitive with the original design. Therefore, the main research question of this thesis is:

> Is it possible to design an economically competitive and technically feasible alternative for project Green Planet, making use of a concrete shell structure consisting of double-curved precast concrete elements?

To answer this research question the following sub-goals have been defined:

- Validate a suitable finite element analysis program. The Green Planet design will be modeled in a finite element analysis (FEA) program for an accurate analysis of the shell structure, so it's necessary to validate the program.
- Design a suitable model for the Green Planet structure, analyze and optimize it. The original design has a spherical shape that needs to be maintained in the design. It has to be transformed into a design suitable for the building material concrete and therefore the model needs to be analyzed and optimized. This is important with respect to the technical feasibility of the design.
- Find a good segment distribution. The design needs to be segmented in a proper way to install the precast elements.
- Design a suitable connection. There's no standard solution available for connecting the concrete elements. The best option needs to be explored and the effect on the shell behavior must be investigated.
- Find the best execution method. Shell structures are often economically unfavorable due to specific requirements during the building phase. It is necessary to find the most practical way of building the shell structure.
- Provide a cost indication. This will determine whether the design is economically competitive.

1.2 Approach

The thesis consists of five parts which will cover the sub-goals that were introduced:

Part I Introduction to the research Chapter 1 'Introduction' gives a short introduction to the problem and the research objectives. Chapter 2 'Literature review' starts with a number of reference projects and addresses the main aspects that accompany the design of a shell structure. Furthermore, the mechanics of shell structures are studied in depth to support the (further on) extensive investigation on the technical feasibility, which is one of the sub-goals. The relatively unknown concept of the adjustable formwork is presented here as well, from development to production, to provide a good idea what the specific features are of a shell structure and how the elements are best produced and applied in the end.

Part II Green Planet: design and optimization Chapter 3 'Dome analysis' is the chapter where Scia Engineer is used for getting familiar with a FEA program. The theory of shell mechanics is used to compare results from with the FEA program. In Chapter 4 'Shell structures comparison' it is investigated whether the Green Planet model that was created gives a realistic output with respect to theoretically verifiable models. Thereafter, in Chapter 5 'Design Green Planet analysis', realistic loads are applied to the model and it's results are analyzed. Some features of the shell design are optimized.

Part III Green Planet: segmentation and detailing Chapter 6 'Segmentation' will present the whole process of the segmentation of the Green Planet shell design. Chapter 7 'Detailing' will elaborate upon the design of connections which can be used in a FEA program like Scia Engineer. First the different aspects of a connection are tested separately. After that, more tests follow until in the end the connection is tested on the Green Planet model.

Part IVGreen Planet: execution and costs Chapter 8 'Execution and costs' will shortly discuss aspects with regard to the execution of the structure. A cost indication of the new Green Planet design will be presented as well as a cost comparison with the original design.

Part V Final remarks Chapter 9 'Conclusions and recommendations' will summarize the most important findings and conclusions, whilst the recommendations will give directions for future research.

Chapter 2

Literature review

2.1 Reference projects

2.1.1 Introduction

Shell structures don't need an introduction because they're everywhere. But, in order to build one it's necessary to apply the knowledge gathered through history. For this, an overview will be given introducing different prefabricated shells built to date. For those reference projects various important factors are studied and discussed in order to set a foundation for the different aspects required to design a shell structure.

2.1.2 Examples of prefabricated shell structures

History has left a great heritage of concrete shell structures. These shell structures can be divided into categories depending on their realization method. Such as, structures build in-situ and structures that made use of prefabricated elements. This last category is the most interesting regarding the theme of the thesis. The category of prefabricated concrete shell structures can be broken down again into two divisions: one where the precast elements form the main load bearing structure and one which makes use of precast elements assembled on a supporting structure.
Here, a short chronological overview of prefabricated concrete shell structures will be presented. Additionally, reference is made to each structure's important design factors: the type of concrete used, the structural division of the panels, the type of formwork, the connections, realization method and foundation. Distinction is made between shell structures and freeform structures, in which the latter one structurally relies on added strength and stiffness rather than an independent curvature transferring load through membrane forces.

2.1.3 Shell structures

Palazzetto dello Sport, [11] [32] [20]

Place	Rome, Italy
Year	1957
Architect/Engineer	Piere Luigi Nervi, together with architect Annibale Vitellozzi
Dimensions	Span is 60 m, height is 7 m an thickness is 25 mm
Concrete	Reinforced concrete (ferrocement)
Structural division	The shape is based on a sphere, from which diamond shapes where derived
Formwork	Slightly curved masonry with 'ribs', on which the mesh was folded and concrete applied
Realization	Precast elements were hoisted on the scaffolding by two cranes, subsequently reinforcement was placed and concrete poured
Connection	In-situ concrete connection: reinforcement is placed in between and over the precast elements, working together with the reinforcement already sticking out of the elements, then the concrete is poured
Foundation	The self supporting roof is supported by transitional conical elements which lay on 36 Y-shaped pillars connected at the bottom by a prestressed concrete ring (80 m diameter)

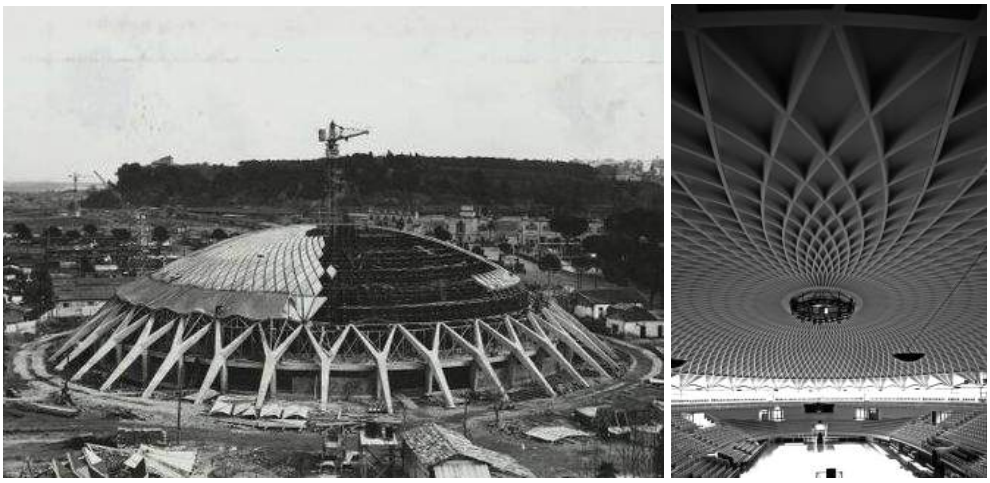

Figure 2.1: (a) Construction of the shell, www.impresedilinews.it (b) Palazzetto dello Sport

Philips pavilion: Le Poème Électronique, [1] [33] [19]

Place	Brussels, Belgium
Year	1958
Architect/Engineer	Le Corbusier/H.C. Duyster
Dimensions	The height was $\pm$17 m, the thickness of the panels is 50 mm
Concrete	Reinforced concrete
Structural division	Several hyperbolic paraboloid and conoid surfaces were divided into ($\pm$56) different elements. Every element is unique and measures around 700x700 mm and is 50 mm thick
Formwork	Sand hills stabilized by cement on which a, by wooden planks divided, surface was poured
Realization	A temporary complex wooden scaffolding is erected to supported the precast elements, which are placed closely together and later hold together with post tensioned cables
Connection	The surfaces are poured together by means of a reinforced concrete beam, with reinforcement sticking out for the later applied steel cables. Those cables are tensioned, both on inner and outer side of the surface, in order to obtain a monolithic surface.
Foundation	The self supporting concrete elements rest on the tilted concrete beams and a concrete foundation floor, supported by wooden foundation piles

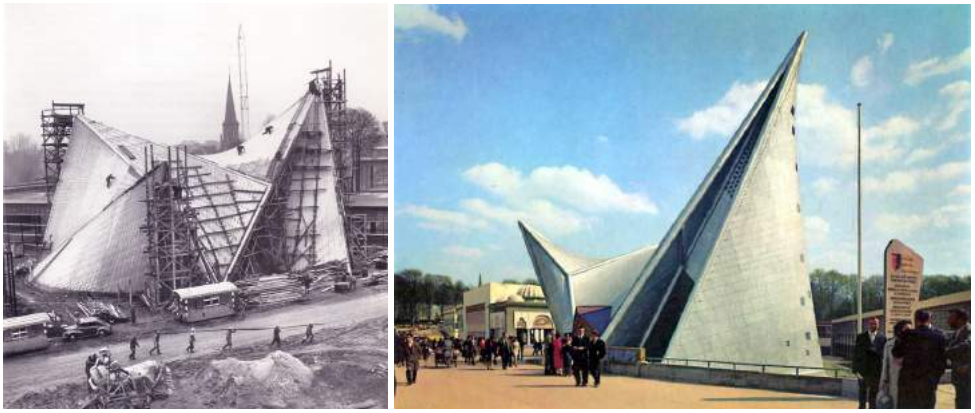

Figure 2.2: (a) Construction of the walls (b) Philips pavilion: Le Poème Électronique

Sydney Opera House, [59] [44]

Place	Sydney, Australia
Year	1973
Architect/Engineer	Jorn Urzon/Ove Arup & Partners
Dimensions	Highest shell point is around 45m above the foundation column
Concrete	Concrete, dense for that time
Structural division	The shape is based on a sphere, its radius is approximately 74m
Formwork	Steel-framed plywood, length of elements could be varied
Realization	Adjustable and movable steel erection arch for placing the ribs, tower cranes for the concrete segments
Connection	Adhesives (epoxy resin) in first place (for the ribs), then bolted with hydraulic jacks and anchored with post tension cables to the pedestal anchorage columns
Foundation	The shells are self supporting and rest on special columns. Four large columns, pedestals, which bear a section are tied together transversely and longitudinally by a post tensioned connecting beam, separate from the base structure

Figure 2.3: (a) Construction of the shells (b) Sydney Opera House

American Air Museum, [45] [13]

Place	Duxford, U.S.A.
Year	1997
Architect/Engineer	Foster & Parteners/Ove Arup & Partners
Dimensions	Span is 90 m, length is 100 m and roof is 2x100 mm thick with 900 mm gap
Concrete	Reinforced concrete
Structural division	The curved elements dimensions are obtained by rotating a circle along the torus shape
Formwork	Six different moulds, creating six different elements, dimensions approx 12x4x0,1 m. Including inverted t-shaped elements for the lower and flat elements for the top layer
Realization	Temporary steel scaffolding
Connection	In-situ 'wet' reinforced concrete connection
Foundation	Plinth construction, in the form of a triangle, acting as tension ring resisting both vertical and horizontal forces from the self supporting roof structure

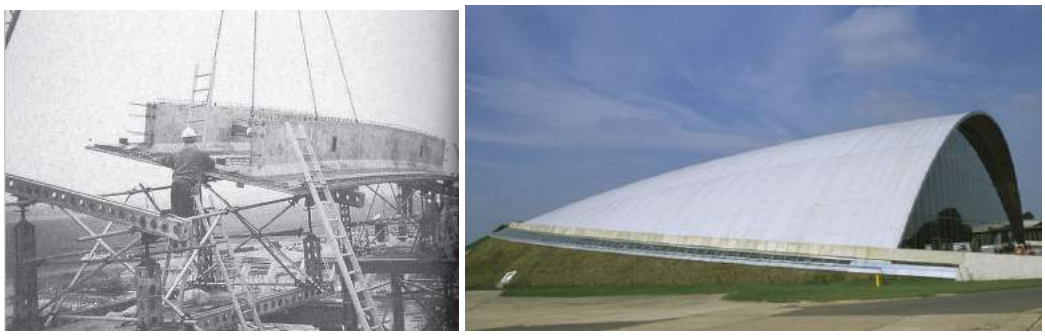

Figure 2.4: (a) Construction shell (b) American Air Museum

The Shawnessy LRT station canopies [55]

Place	Calgary, Canada
Year	2003
Architect/Engineer	CPV Group Architects & Engineers Ltd.
Dimensions	The length is 5 m, width is 6 m and the thickness is 20 mm
Concrete	UHPC (Ductal) with poly-vinyl alcohol fibres, compressive strength: 150 N/mm^2 and flexural strength: 18 N/mm^2
Structural division	The conical shape was divided in two halves
Formwork	Two closed steel plate moulds, for all canopies, one for the left and one for the right side. Besides, for the column a vertical steel plate mould was used. The other parts were moulded in a traditional way
Realization	A steel framework supported the assembled canopy. After transport it was lifted on temporary supports. While standing above the column, the struts where lifted in place, with a temporary lifting device. Then, the struts where connected to the column and the canopy
Connection	A bolted connection, injected with grout, is used for the shell elements. A welded connection is used for the strut an column connection. A pin connection is used for connecting the strut and the canopy, and, three canopies to each other
Foundation	The shell is simply supported by a precast column and three precast struts

Figure 2.5: (a) Construction of the shell (b) The Shawnessy LRT station

2.1.4 Freeform structures

Millau toll station, [13]

Place	Millau, France
Year	2004
Architect/Engineer	Michel Herbert/Eiffage TP
Dimensions	The length is 98 m, the width is 23 m and the thickness ranging from 100 to 850 mm (hollow core elements)
Concrete	Carecem with 20 mm long fibres (1,5-3% volume)
Structural division	The structure is just cut in the transverse direction, creating elements of 28 m long
Formwork	Special steel formwork (PERI), where the next element is cast on top of the already and just cast, and in the building the adjacent, element. Because of this, the elements fit flawless
Realization	The elements are transported and hoisted on temporary steel scaffolding
Connection	Bolted connection between the elements, in the end all post tensioned together with 12 tension strands
Foundation	The roof structure is placed on steel columns

Figure 2.6: (a) Construction of the roof (b) Millau toll station, [3]

Heydar Aliyev cultural center, [2] [6] [5]

Place	Baku, Azerbaijan
Year	2012
Architect/Engineer	Zaha Hadid/AKT, Tuncal Engineers
Dimensions	The height of the roof is 74 m and the thickness of the panels 8-13 mm (but supported by a steel space frame)
Concrete	Fine grain high performance concrete with glass fibre mats
Structural division	The panels are divided with a special penalization program
Formwork	Using customized single-use moulds made from 3d milled Styrofoam blocks and CNC-cut 2d milled ribs, the ribbed panels only 8-13 mm thick where made
Realization	By crane the elements are placed and fixed on the steel frame
Connection	The elements are simply fixed to the steel frame with screws
Foundation	The elements are supported by a huge 3d curved self supporting steel space frame

Figure 2.7: (a) Panalisation of the roof (b) Heydar Aliyev cultural center, www.dezeen.com

2.1.5 Conclusions

Seven different precast double curved structures were discussed. They represent more or less the possibilities and the experience gained in these kind of structures so far. Logically, over time, due to the introduction of computers and 3d technology and other developments, the shape and the materials used for the designs became more advanced. What else can be concluded from these designs is elaborated on in this section.

Mechanics As already mentioned, the shell structures transfer the loads mainly by membrane forces rather than bending, because of their curvature. Clearly this was the case with the discussed shells, as the shells where self supporting thin and slender shells while this wouldn't be possible if they had to carry large bending moments. Although, some structures needed ribs in order to increase their flexural rigidity. However, the theory is confirmed by the two freeform structures as well, which couldn't rely on much shell behavior, in which either an increase of inertia or a supporting structure for the concrete was necessary.

Concrete The first structures made use of normal reinforced concrete panels. Meanwhile, in the last decade, a large jump seems to be made into the high- or ultra high performance concrete in combination with fibres. Perhaps, making the concrete shell structures interesting again. Because, this rather new material offers great structural advantages, making much slender construction possible. Furthermore, troubles with getting reinforcement in the panels belong to history, now that there are flexible fibres taking care of macro and micro cracking. On the other hand, it has to be taken in consideration that the material is still experimental in the sense that there's no regulation yet and the preparation and material costs are high. For example, the Arnhem central station, which was researched for this overview too; it was uncertain for a long time whether they should use prefabricated concrete elements for its complex double-curved roof or not. In the end, it was chosen to use a more straightforward method with steel, because of the costs resulting from a longer construction time and a bigger risk profile, Van Dijk et al. [50]. Nevertheless, the high performance concrete is a promising material to apply to shell structures in the future.

Structural division Structural division of the surface is carefully thought of in most discussed designs. Where Nervi designed an analytical shape to easily divide his diamond shaped elements it was a 3d paneling program which aided the designers of the Heydar Aliyev Center with the division of the cladding panels covering the double-curved structure.
Important features here are the rationalization of the shape, the limitation of unique elements and the re-use of formwork, which is directly linked to the realization phase and the costs. There are some exceptions like the Philips pavilion and the Millau toll station, where no panel shape is the same. This can partly be attributed to the fact that these were expensive prestige projects, labor was cheap in the early days or there was simply no other method that was much better. Anyhow, it can be concluded that it is preferred to pay good attention to the structural division in order to limit the use of different moulds, affecting the costs.

Formwork It is already stated that designers try to limit the use of different moulds in order to limit the costs. Besides, every project made use of a different mould type for creating panels, no general mould could be derived from the discussed designs. These two observations pave the way for a new technique, like the flexible mould. In addition, this could also be an alternative for projects now cast in-situ or complex designs, like the Arnhem station, where costs become a major issue.

Realization The paneled structures are generally supported by temporary steel scaffolding during construction. The needed crane capacity depends on the weight and dimensions of the elements, determining also the speed of the realization. The transportation costs are the reason for three of the projects to make the elements on site. This is, due to the weather, like in Australia with the Sydney Opera house, not always beneficial for producing the elements and the working conditions. Furthermore, a lot depends on the designed connections for the elements.

Connection The most common connections in the precast structures were the wet connection, bolted connection and post tensioned cable connection. The wet connection is used for the earliest structures, but not for the high performance concrete designs. The bolted connection was used for both types, especially for the high performance concrete constructions. Furthermore, the cable connection is often used as a post tensioned connection, where compression forces are introduced in the elements, causing the elements to structurally work together.

Foundation The foundation is often skipped in the provided structural information. The discussed designs rest mainly on a few structurally important points, like columns. However, these columns are not only connected with the foundation in the ground but transversely or/and longitudinally as well. Some structures are therefore connected with a continuous ring or edge beam.

2.2 Mechanics

2.2.1 Introduction

This chapter presents the mechanics of shell structures. At first it is discussed how shell surfaces can be generated and which methods are available. After that the mechanics are explained by means of analytical theories and numerical methods. Furthermore, the failure of shells is studied including the main failure load which is buckling. Then, some attention is payed to the difference between prefabricated shells and monolithic shells, because the theories and failure loads don't specifically mention something about prefabricated shells. Finally, some words are spent on the optimization methods for shell designing.

2.2.2 Curve and surface geometry

The possibilities are endless when it comes to a (shell structures) shape. The order of the complexity of the edges can be subdivided into four categories, from which the surface is determined (Figure 2.8). Ultimately, as shown, there are infinite shapes which can be created.

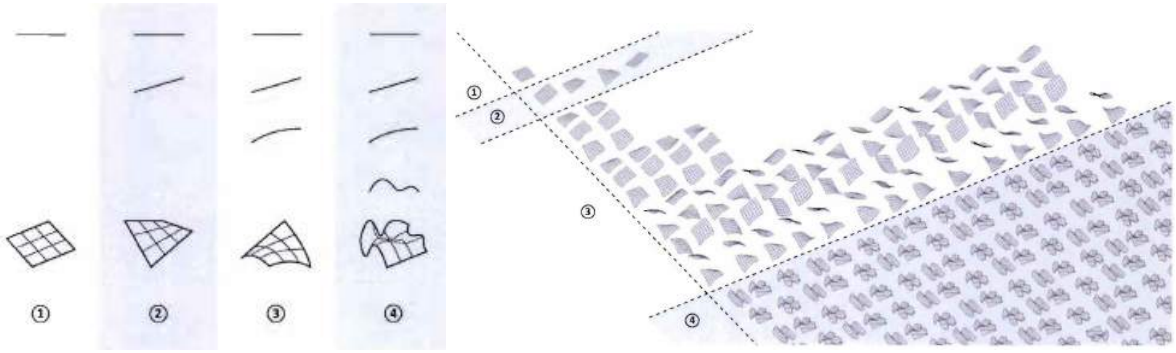

Figure 2.8: Order of edge curves with corresponding surface possibilities, Verhaegh [54]

With these possibilities come many developed techniques to create shells. To maintain an overview the shapes need to be rationalized and categorized in a certain way. This can be done on the basis of the way the surface is generated, based on a geometrical or non-geometrical definition.

Geometrical defined surfaces Geometrical defined surfaces are surfaces based on mathematical formulas. So, the complexity of the building shape increases linear with the complexity of the describing functions. However, a building surface can already appear geometrically very complex, while simple functions are applied. Because of this property these surfaces where used in many forms during the first half of the twentieth century, Billington [7]. These surfaces where also called 'analytical forms'. These forms where used to create buildings by putting several shapes together or leaving some segments out. Typical geometrical defined surfaces are the surface of revolution, the ruled surface and translational surface. Later, a free-form surface could be added to this list, like the NURBS surface.

Surface of revolution A surface of revolution is created by rotating a certain curve (the meridian or generatrix) around an axis, which is called the axis of revolution (or directrix), see Figure 2.9. This results in synclastic surfaces like conical shells, circular domes, torus shapes, paraboloids, ellipsoids of revolution and hyperboloids of revolution.

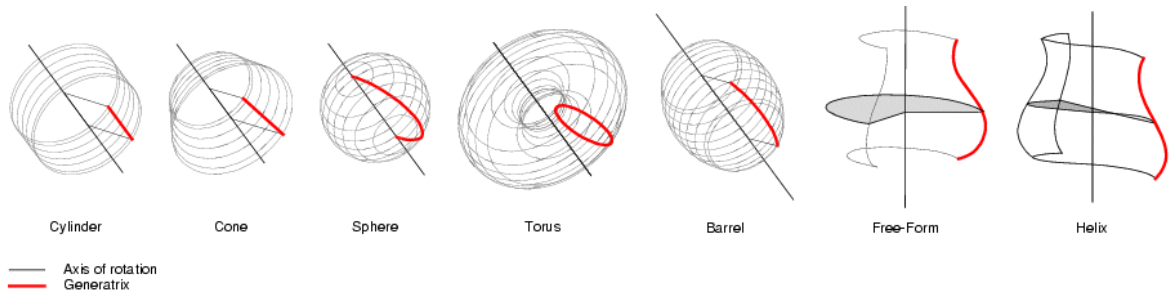

Figure 2.9: Surfaces of revolution, catiadoc.free.fr

Ruled surface A ruled surface is created by connecting two curves or surfaces (directrixes) by straight lines (generatrix). The straight lines remain parallel to a prescribed direction or plane, see Figure 2.10a. The surface that is obtained is anticlastic.

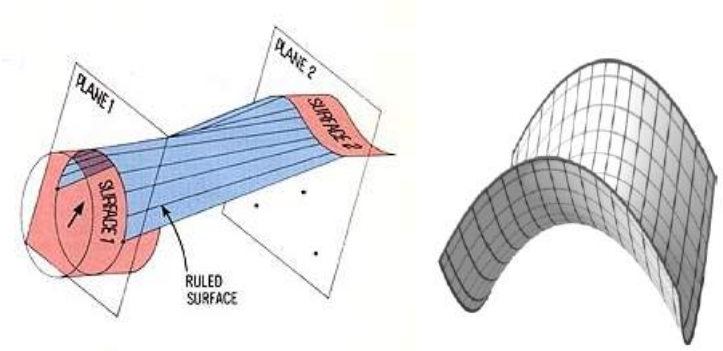

Figure 2.10: (a) Ruled surface, www.plmworld.org (b) Translational surface, www.geometrie.tugraz.at

Translational surface A translational surface is created by sliding a curve (generatrix) along another curve (directrix). The orientation of the surface generating curve remains constant, see the example in Figure 2.10b. In this way synclastic, anticlastic or monoclastic surfaces are formed, depending on the shape of the generating and directing curves.

Free-form surface A free-form surface is a surface that doesn't have rigid radial dimensions, like the geometrical shapes that were described earlier, and is not described by fixed functions, Peerdeman [35]. There are different methods to realize a free-form surface, such as the Bézier surface, Gordon surface or Coons surface method, but most (CAD) systems nowadays use non-uniform rational B-Spline (NURBS) mathematics to create a free-form surface, Piegl [36]. With this method it's possible to create almost all shapes that

one can imagine and, therefore, it can be used from illustrating to manufacturing industry. Architects use NURBS to design free-form structures like BLOB structures.
A NURBS surface is a generalization of B-Splines, Hoogenboom [17]. The surface is determined by a degree, weighted control points and a knot vector. The degree determines usually whether NURBS curves are lines or polylines (1 degree), circles (2), cubic free-form curves (3) or quintic free-form curves (5), Vambersky and Wagemans [49]. The control points determine the shape of the NURBS curve, by moving the control points the shape can be changed. Normally the weight given to the control points is the same, but if not the shape is influenced by the weights, making the curve rational. The knot vector is a sequence of parameter values that determines where and how the control points affect the NURBS curve. The knot vector divides the parametric space in the intervals mentioned before, usually referred to as knot spans. The individual knot values are not meaningful by themselves; only the ratios of the difference between the knot values matter.
Eventually, the NURBS surface is created by means of the evaluation rule, a mathematical formula that takes a number and assigns a point. The number the evaluation rule starts with is called a parameter. The evaluation rule is like a black box; converting a parameter into a point location. The degree, control points and knots determine how the black box works, Vambersky and Wagemans [49].

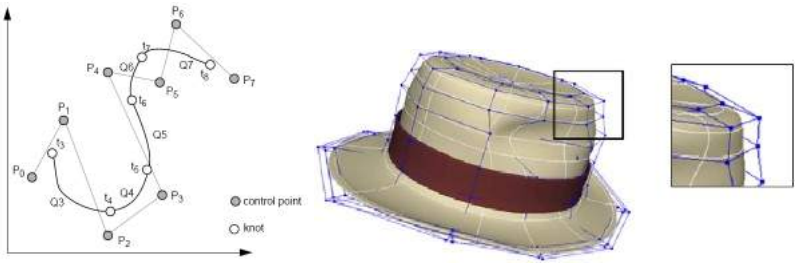

Figure 2.11: (a) B-Spline, www.pling.org.uk (b) NURBS surface, wiki.softimage.com

2.2.3 Non-Geometrical defined surfaces

Physical form finding

Physical form finding uses physical laws to determine a natural form, a model. The models make use of air pressure, gravity and material flow for designing a surface, which is determined based on equilibrium. The resulting surfaces are, therefore, also called 'experimental forms'.
Experimental methods include membranes under tension, pneumatic membranes, flowing forms and hanging reversed membranes, Ramm [40]. Three of these methods were described by Heinz Isler, one of the pioneers in experimental form finding, in his paper 'New Shapes for Shells' in 1959, Isler [21]. Here he describes three methods for creating a shell surface; freely shaped hill, membrane under pressure and hanging cloth reversed. His informed opinion states about the first method that it's 'prehistoric'. The second method creates shells that are 'statically reasonably good'. However, from structural point of view, especially Isler's shells based on gravity, created with the hanging cloth reversed, were very interesting and Isler called it 'the best method for design'. These shells behaved superior to

the geometrical defined surfaces, Huijben et al. [18], whereas analytical methods were merely approximations of these natural forms.
Other methods of physical form finding are for example soap films and biomimetics.

Hanging models Hanging wet cloth, hanging chains and hanging nets are models which make use of gravity in order to find its equilibrium. Due to the material that is used, bending is excluded from these models. Therefore, these models are in complete tension, and, if reversed they only contain compression. Thus, the material and therewith its stiffness is used to its optimum.
With these models gravity is the main load that is simulated with these models (Figure 2.12a). Point loads can be added by means of hanging weights at a specific point, like Gaudí did in his models (Figure 2.12b). Other dominant load cases, however, are difficult to simulate simultaneously.
For hanging membranes it should be noted that it has an additional ability to carry load by in-surface shear resistance. It can result in wrinkling of the membrane, where in compression buckling would occur (Figure 2.12c). Consequently, the material with its elastic properties and the cutting pattern play an important role in this form finding method. This makes comparing of the models difficult and certain phenomenons, like behavior at free edges, hard to explain, Mungan and Abel [31]

Figure 2.12: (a) hanging models Isler (b) hanging sandbags in model Gaudí (c) wrinkling hanging membrane

Pneumatic models Pneumatic models consist of a membrane which is loaded by an inside (air) pressure normal to its surface to find its equilibrium. In this way, only tension forces occur in the membrane (Figure 2.13a). By using this shape for a concrete shell compression forces will dominate the structure under its own distributed weight. But, because the own weight is not exactly normal to the surface, like the pressure, consequently, the structural behavior is not exact as well. But it should be noted that with shallow shells the influence is very small, Mungan and Abel [31].
A method more often used in form finding of tent structures is soap film modeling. With this method a equilibrium shape with a minimal surface is created between certain boundaries. For example, a soap film in a wire loop is free to minimize its surface, Hoogenboom [17]. Here, the air pressure is equal on both sides (Figure 2.13b).

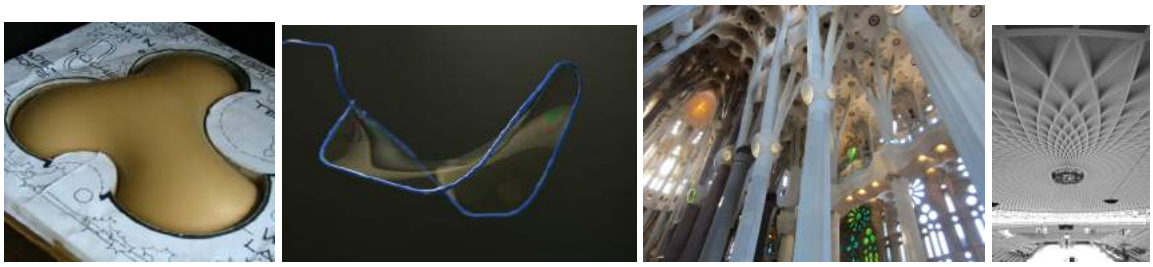

Figure 2.13: (a) pneumatic model, Isler (b) soap film wire loop (c) tree structure, Gaudí (d) ribbed shell, Nervi

Biomimetics In biomimetics the designer tries to learn from nature and imitates its structural behavior, since nature has its own optimizing law against the same natural forces. Here, the focus lies on the principles which form the basis of the natural structure, in order to use it to a designs full advantage. However, not only a structural reason underlies the imitation of natural structures, also the shape itself can be an inspiration to a designer. Structures that inspired designers are for example cellular structures like honeycombs, dragonfly wings, spider webs, bones and skeleton structures, sea shells, leaf structures and tree structures. Additionally, for concrete shell structures one can think of egg shells, fruit shells or indeed the ribbed stiffened 'plates' like leafs, dragonfly wings or bones. Famous designers who make use of natural examples are Gaudí, with for example the tree structures in his Sagrada Família, and Nervi, with his ribbed stiffened shell structures (Figure 2.13c and d).

Designing with experimental forms Designing through physical form finding has proven it's advantages over for example analytical methods. The models resemble the exact, natural, form which delivers a structural efficient shape (minimal material). Like analytical form finding the (direct) aesthetic appearance is good, just as the intuitive understanding of the structural shape. And, it can form the basis and deliver data for CAD models.
There are, however, some typical disadvantages regarding the design of these shells. For instance, the construction which is complex and difficult, like the calculations are. For construction, however, reusing of formwork is a possibility. Furthermore, the creation and measuring of the models is time consuming and results compared to computational modeling in limited variants. As mentioned, simulating the actual building material for the structure is complicated and with that the variation in thickness too. Besides, the buckling and nonlinear behavior can only indirectly be incorporated in the form finding methods. Finally, a great disadvantage is that the designer can not apply or experiment with multiple dominant load cases that easily, mainly with the load case gravity.
Despite the mentioned cons of this form finding methods a lot of shells are successfully completed in the past, these days and will be in the future. Although, nowadays these designs are more than often, always, backed up by finite element analysis, as to satisfy involving authorities (Peerdeman [35], Mungan and Abel [31], Huijben et al. [18], Ramm [39]).

Computational form finding

Computational form finding makes use of the possibilities that computers give, with their computational power, to solve algorithmic problems resulting from the non-linear behavior of structures. These methods are often used in combination with other form finding methods, described in previous sections.
Computational methods have as a main advantages that it offers precision/flexibility in form and calculation and interfacing possibilities with CAD, FEA and CAM programs, Oosterhuis [34]. This last benefit results in broader support by and access for designers. The drawback is, however, the bad intuitive understanding of the structural behavior, unlike with the physical form finding. And, unfortunately, the manufacturing aspects beneficial for the execution of the structure are not yet implemented in these form finding applications. Until this moment the most common computational methods used in practice are the force density method and the dynamic relaxation method. There are other methods, but not commonly used, and called therefore academic methods.

Force density method The force density method uses a linear system of equations to model static equilibrium of a pre-tensioned cable net under prescribed force/length ratios, Lewis [28]. Key assumption is that the ratio of tension force to length of each cable can be constant, which transforms a non-linear system of equations into a linear one. Force density ratios need to be specified for each element, where different ratios give different equilibrium shapes. When the force densities for a node are equal and evenly distributed around the node a minimal surface (equilibrium shape) is generated, Vambersky and Wagemans [49]. This method is suitable for the determining the shape of membrane structures, and when inverted it can be used for shells. The equilibrium shape is found easily, however, when applying its solution to load constraints or additional geometrical conditions it becomes non-linear, resulting in additional required iteration steps, Schek [41].
An example of an application of the force density method is the cable net structure created for the Olympic stadium in Munich (Figure 2.14a). The method was developed as a response to the need for a suitable computational modeling program for the stadium. It was then used in combination with experimental models and a finite element program.

Figure 2.14: (a) Olympic stadium Munich, www.muenchen.de (b) Great Court Yard roof British museum, blog.incipeindustries.com

Dynamic relaxation method The dynamic relaxation method is a method which lets the structure relax to a equilibrium situation. It, basically, calculates the dynamic behavior by Newton's second law of motion. The mass (M) of the structure is assumed to be concentrated at the joints and an additional viscous damping term (C), which is proportional to the velocity (V) of the joint, is included in the formulation. Hereby, the motion of the structure is followed, step by step, from the time of loading to when it reaches a position of equilibrium due to damping effects, Topping and Khan [48]. Here, the motion is fictitious making it suitable for static analysis. The simplified formula yields; R=M*V+C*V, where R is the residual force at time t in a certain direction in a certain joint. This method is particularly useful for form finding of nets and membrane structures. Not really for finding the shape, but, more for the structural calculations used for form finding purposes. The advantage of this method is that it doesn't solve matrices, which saves lots of calculation power, despite the iteration steps. Besides, this method can deal with local instabilities, like wrinkling of membranes.
An example of an application of the dynamic relaxation method is the Great Court Yard roof of the British museum (Figure 2.14b). Here, in combination with analytical methods, the dynamic relaxation method is used to 'relax' the grid for a more efficient structural load bearing behavior, Vambersky and Wagemans [49].

Academic methods Academic methods include for example the transient stiffness method, the updated reference strategy system, the particle spring method and the thrust network analysis.
The transient stiffness method was simultaneously developed with the force density method, for the form finding of the Olympic stadium in Munich, Lewis [28]. There are similarities with the numerical Newton-Raphson method when it comes to solving a system of non-linear equations. Lewis devotes a whole chapter comparing this method with dynamic relaxation method and concludes, even though the method is faster in solving single iterations and simple structures, the dynamic relaxation method is overall faster at solving complex shapes, Veenendaal [53].
The updated reference system is often seen as an extension of the force density method, Mungan and Abel [31]. It's consistently derived from continuum mechanics and can be applied to membranes and cable structures.
The particle string systems are based on lumped masses, called particles, connected by linear elastic strings. The strings have assigned properties like length, axial stiffness and damping coefficient. Forces can be applied to the particles and with a iterative Runga-Kutta method equilibrium is found, Kilian and Ochsendorf [24]. Where the dynamic relaxation is used for form finding of tension structures, this method can be used for shell structures, as it is an elaboration on the relaxation method, Kuijvenhove and Hoogenboom [27].
The thrust line analysis is a form finding method for compression-only structures such as unreinforced masonry structures, Block and Ochsendorf [9]. The thrust network analysis is a three-dimensional extension of this theory for compression-only surfaces and systems.

2.2.4 Analytical theories

This thesis is about thin (concrete) shells. Thin shells are like plates; they are defined by their material properties, middle plane and thickness. Furthermore, both structures have

two large dimensions and one smaller dimension (the thickness). However, shells have a curved middle plane. Therefore, they are able to resist out of plane forces by in plane forces, called membrane forces. This makes shells strong and economic structures.
The theory of the membrane behavior is the membrane theory. This theory holds for the largest part of the shell's surface, but in some regions the theory will not hold and compatibility moments will compensate the shortcomings of the membrane field. This disturbed zone should be analyzed with the more complete bending theory. Together these theories are very useful for initial design and analysis of thin shell structures (Blaauwendraad and Hoefakker [8]).

Membrane theory

The membrane theory holds for thin concrete shells, where the thickness of a certain element is much smaller compared to its length and width. Consequently, the flexural rigidity is much smaller than its extensional rigidity. Therefore, mainly membrane forces are developed when externally loaded. This forms the basis for the membrane theory, where it is assumed that a thin shell produces a pure membrane stress field and that no bending occurs.
In order to apply this theory the shell has to meet some loading and boundary conditions (Figure 2.15a):

- Boundary conditions and deformation constraints must be compatible with the requirements of the membrane field
- No concentrated load should be applied
- No (sudden) change in geometry is allowed

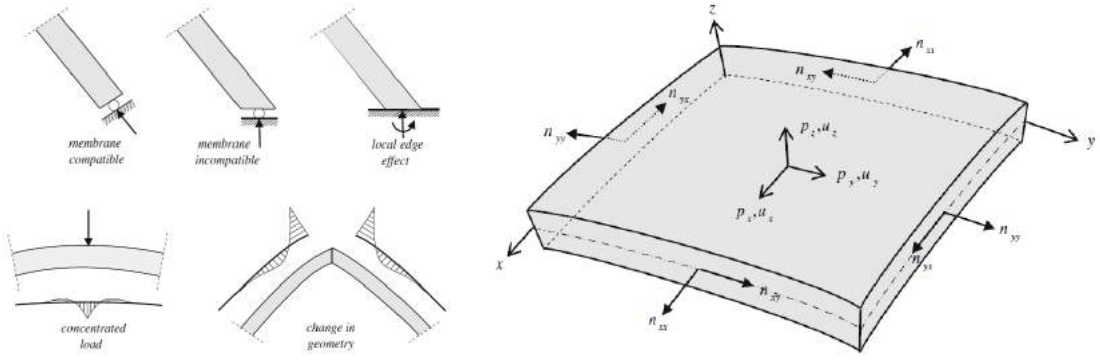

Figure 2.15: (a) Loading and boundary conditions (b) shell element: membrane forces and coordinate system

Due to shearing and stretching of the middle plane only in-plane and normal forces occur in the membrane stress field, no bending, torsion or transverse shear is produced. Figure 2.15b shows a shell element with its membrane forces and coordinate system which is placed in the middle surface in the direction of the principle curvatures.

The behavior of structures can be defined with the three basic relations: kinematic relation, constitutive relation and the equilibrium relation. They relate the vectors of displacements, strains, membrane forces and loads (Figure 2.16a).

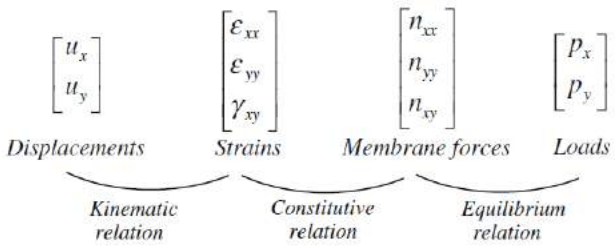

Figure 2.16: Relation between the different vectors

Kinematic relation The displacements u_x and u_y act in the direction of the principal curvatures k_x and k_y respectively. Normal to the middle surface, in the direction of the z-axis, is the displacement u_z. The strain vector due to the displacements u_x and u_y is the same as for a plate loaded in its plane. Displacement u_z contributes to both strains ε_{xx} and ε_{yy}, but not to the shear strain γ_{xy}. This leads to the kinematic relation:

$$\begin{bmatrix} \varepsilon_{xx} \\ \varepsilon_{yy} \\ \gamma_{xy} \end{bmatrix} = \begin{bmatrix} \frac{\delta}{\delta x} & 0 & -k_x \\ 0 & \frac{\delta}{\delta y} & -k_y \\ \frac{\delta}{\delta y} & \frac{\delta}{\delta x} & 0 \end{bmatrix} \begin{bmatrix} u_x \\ u_y \\ u_z \end{bmatrix}$$

$$e = Bu$$

Constitutive relation The membrane forces (or stress resultants) n_{xx}, n_{yy} and n_{xy} are obtained by integrating the stresses (σ) over the thicknesses (t) of the shell. Since the stresses are uniformly distributed over the thickness, pure membrane stress field, it comes down to multiplying the stresses by the thickness. By assumption, the shell material is linear elastic and obeys Hooke's law. Therefore, with Young's modulus E (elasticity) and Poisson's ratio ν (lateral contraction), the constitutive relation becomes:

$$\begin{bmatrix} n_{xx} \\ n_{yy} \\ n_{xy} \end{bmatrix} = \frac{Et}{1-\nu^2} \begin{bmatrix} 1 & \nu & 0 \\ \nu & 1 & 0 \\ 0 & 0 & \frac{1-\nu}{2} \end{bmatrix} \begin{bmatrix} \varepsilon_{xx} \\ \varepsilon_{yy} \\ \gamma_{xy} \end{bmatrix}$$

$$s = De$$

Equilibrium relation The load components p_x and p_y are tangential to the middle surface and the two equilibrium equations are the same as for a plate loaded in its plane. In order to get the equilibrium for the load component p_z, normal to the middle surface, the curvature of the middle surface is investigated. By doing this, the principle curvatures k_x and $k_y$are

determined and finally the equilibrium in x- and y-direction is obtained. This yields the equilibrium relation, where B^T is the adjoint of the differential operator matrix B:

$$\begin{bmatrix} p_x \\ p_y \\ p_z \end{bmatrix} = \begin{bmatrix} -\frac{\delta}{\delta x} & 0 & -\frac{\delta}{\delta y} \\ 0 & -\frac{\delta}{\delta y} & -\frac{\delta}{\delta x} \\ -k_x & -k_y & 0 \end{bmatrix} \begin{bmatrix} n_{xx} \\ n_{yy} \\ n_{xy} \end{bmatrix}$$

$$p = B^T s$$

Arbitrary curvatures The relations of the membrane theory that were obtained are applicable to thin shells related to a coordinate system determined according to the principal curvatures. In practice, it's more useful to be able to rotate the coordinate system in an arbitrary direction. For example along the edge of a shell. This results in slightly different relations.
For the kinematic relations an additional twist k_{xy} is introduced. Via this twist u_z will now contribute to the shear strain γ_{xy}. The kinematic relation for arbitrary curvatures is:

$$\begin{bmatrix} \varepsilon_{xx} \\ \varepsilon_{yy} \\ \gamma_{xy} \end{bmatrix} = \begin{bmatrix} \frac{\delta}{\delta x} & 0 & -k_x \\ 0 & \frac{\delta}{\delta y} & -k_y \\ \frac{\delta}{\delta y} & \frac{\delta}{\delta x} & -2k_{xy} \end{bmatrix} \begin{bmatrix} u_x \\ u_y \\ u_z \end{bmatrix}$$

The constitutive relation remains unchanged when using the coordinate system for arbitrary curvatures. The equilibrium relation, however, does change with the coordinate system. The consequence of the two curvatures k_x and k_y is solved first and then the effect of the twist k_{xy} is incorporated. The shear membrane force n_{xy} now contributes to the equilibrium in the z-direction. So, the equilibrium relation for an arbitrary placed coordinate is:

$$\begin{bmatrix} p_x \\ p_y \\ p_z \end{bmatrix} = \begin{bmatrix} -\frac{\delta}{\delta x} & 0 & -\frac{\delta}{\delta y} \\ 0 & -\frac{\delta}{\delta y} & -\frac{\delta}{\delta x} \\ -k_x & -k_y & -2k_{xy} \end{bmatrix} \begin{bmatrix} n_{xx} \\ n_{yy} \\ n_{xy} \end{bmatrix}$$

Bending theory

The bending theory is an extension of the membrane theory. It covers for example edge disturbances, where compatibility moments compensate the shortcomings of the pure membrane stress field, caused by the mentioned loading and boundary conditions. Bending moments, twisting couples and transverse shear forces are the driving forces behind the compensation, Peerdeman [35]. Therefore, some vectors are extended, see Figure 2.17.

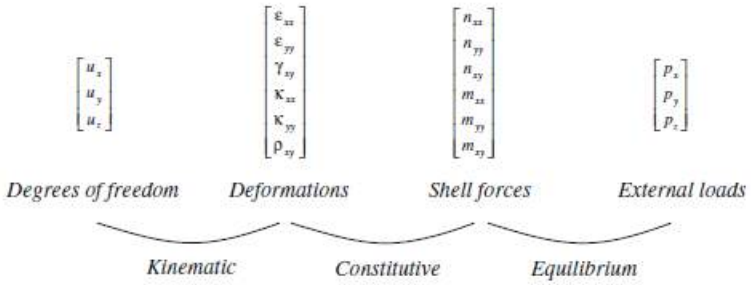

Figure 2.17: Relation between the different vectors

It can be noticed that the displacement vector and load vector are still the same. The other ones, however, are extended. For the bending moments the bending stress resultants $m_{xx}$and m_{yy} are added together with the twisting stress resultant m_{xy}. The shell is bent in the x- and y-direction which causes the curvatures k_x and k_y to change. The torsion deformation ρ_{xy} is a result of the twisted surface. The transverse shear forces, however, are neglected in this theory.
In fact the theory of flat plates is used, in combination with the membrane theory, to express the curvature change due to bending moments. In the end the relations for the bending theory yield as follows:

kinematic relation:

$$\begin{bmatrix} \varepsilon_{xx} \\ \varepsilon_{yy} \\ \gamma_{xy} \\ k_x \\ k_y \\ \rho_{xy} \end{bmatrix} = \begin{bmatrix} \frac{\delta}{\delta x} & 0 & -k_x \\ 0 & \frac{\delta}{\delta y} & -k_y \\ \frac{\delta}{\delta y} & \frac{\delta}{\delta x} & -2k_{xy} \\ 0 & 0 & -\frac{\delta^2}{\delta x^2} \\ 0 & 0 & -\frac{\delta^2}{\delta y^2} \\ 0 & 0 & -2\frac{\delta^2}{\delta x \delta y} \end{bmatrix} \begin{bmatrix} u_x \\ u_y \\ u_z \end{bmatrix}$$

Constitutive relation:

$$\begin{bmatrix} n_{xx} \\ n_{yy} \\ n_{xy} \\ m_{xx} \\ m_{yy} \\ m_{xy} \end{bmatrix} = \begin{bmatrix} D_m & \nu D_m & 0 & 0 & 0 & 0 \\ \nu D_m & D_m & 0 & 0 & 0 & 0 \\ 0 & 0 & D_m(\frac{1-\nu}{2}) & 0 & 0 & 0 \\ 0 & 0 & 0 & D_b & \nu D_b & 0 \\ 0 & 0 & 0 & \nu D_b & D_b & 0 \\ 0 & 0 & 0 & 0 & 0 & D_b(\frac{1-\nu}{2}) \end{bmatrix} \begin{bmatrix} \varepsilon_{xx} \\ \varepsilon_{yy} \\ \gamma_{xy} \\ k_x \\ k_y \\ \rho_{xy} \end{bmatrix}$$

Here D is the rigidity matrix, with the membrane rigidity $D_m = \frac{Et}{1-\nu^2}$ and the flexural rigidity $D_b = \frac{Et^3}{12(1-\nu^2)}$.

Equilibrium relation:

$$\begin{bmatrix} p_x \\ p_y \\ p_z \end{bmatrix} = \begin{bmatrix} -\frac{\delta}{\delta x} & 0 & -\frac{\delta}{\delta y} & 0 & 0 & 0 \\ 0 & -\frac{\delta}{\delta y} & -\frac{\delta}{\delta x} & 0 & 0 & 0 \\ -k_x & -k_y & -2k_{xy} & -\frac{\delta^2}{\delta x^2} & -\frac{\delta^2}{\delta y^2} & -2\frac{\delta^2}{\delta x \delta y} \end{bmatrix} \begin{bmatrix} n_{xx} \\ n_{yy} \\ n_{xy} \\ m_{xx} \\ m_{yy} \\ m_{xy} \end{bmatrix}$$

2.2.5 Specialized theories

The introduced theory is the classical theory for thin shells. There are quite a few types of thin shells to distinguish, for example: Circular cylindrical shells, hyperbolic- and elliptic-paraboloid shells and shells of revolution, and they all have their own extended and more specified theory. For this thesis the most interesting shells are the shells of revolution, since they represented the spherical shells. Additional information with detailed analytical theories on spherical shells or other types of shells can for instance be extracted from Blaauwendraad and Hoefakker [8], Ter Maten [46] or Peerdeman [35].

2.2.6 Finite element theory

For the structural analysis of structures one can choose between analytical methods, like explained in the previous section which concerns the deformation behavior on macroscopic scale, and numerical methods (Figure 2.18) which give analyzes the behavior by numerical approximation. The use of analytical methods is limited to rather simple structures with limited boundary conditions. For complex structures, like shell structures, numerical methods are strongly preferred. Numerical methods can be split into two distinct methods: numerical solutions of differential equations for displacements or stresses and matrix methods based on discrete element idealization, Przemieniecki [37]. The first method is mainly based on approximations of differential equations and due to practical limitations, this method is particularly useful for the analysis of rather simple structures too. The matrix method, however, is suitable to analyze complex structures and is therefore used to analyze the shell structure.

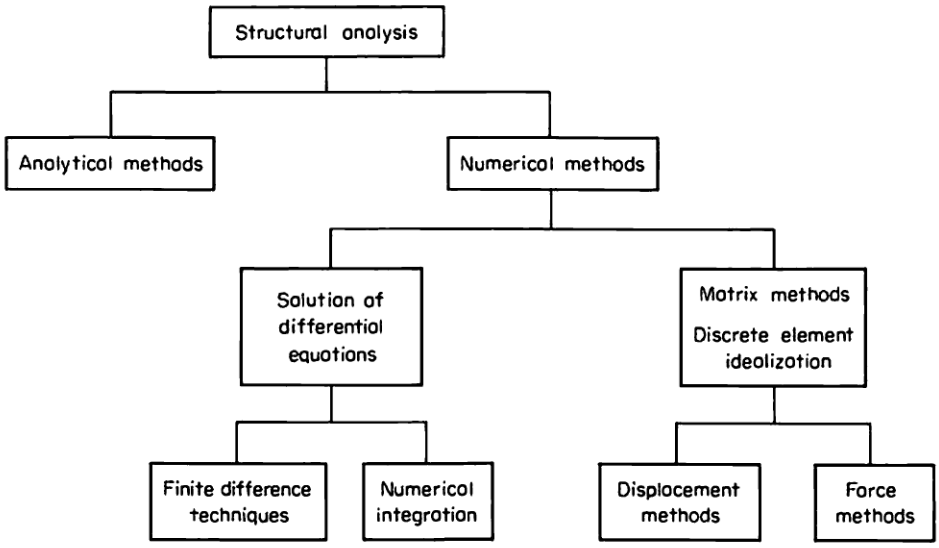

Figure 2.18: Overview structural analysis methods [37]

The concept behind matrix methods is that they replace the known elastic and internal properties (expressed in matrix form) of a continuous structure by a mathematical model consisting of finite size structural elements, therefore called finite element method. Moreover, for analyzing a structure it is first idealized into an assembly of discrete structural elements (with assumed displacements and stresses) and subsequently these elements are combined by relations which satisfy the force-equilibrium and displacement compatibility. These relations are applied on the boundary of the elements where the element connecting nodes lie. The systematic sequence of operations which needs to be performed is convenient because it prevents writing down full equations and it is in particular suited for a computer to solve.
There are two matrix methods. The first method chooses the displacements as unknowns and is therefore called the displacement method. The second method chooses the forces as unknowns and is therefore called the force method.

SCIA Engineer The finite element analysis (FEA) program that will be used for the research is SCIA Engineer, which is a well known and established commercial software package designed for structural engineers. For the calculation of membrane forces it includes, elaborating on the theory explanation of the previous text, a 3-node triangle and a 4-node quadrilateral with three degrees of freedom per node, see Figure 2.19a [15]. Those flat elements are based on a combination of a disc element (plane stress) and a plate element (bending), together they have six degrees of freedom, where the sixth (red Figure 2.19b) doesn't really contribute to the accuracy [17].
The program has a graphical system which adds to the input of the geometry and can be used to present and illustrate calculation results. Furthermore, the software offers the opportunity to calculate all 4-dimensional problems, where the fourth dimension implies the analysis of distribution of internal forces over time, Ter Maten [46].

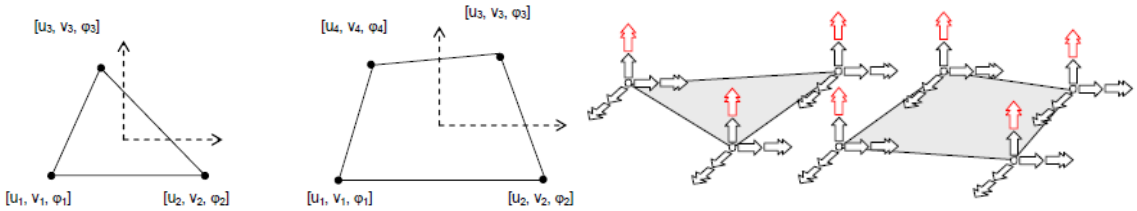

Figure 2.19: (a) Elements used in SCIA Engineer [15] (b) degrees of freedom of flat shell elements [17]

There is a lot more to say about the finite element method, several sources are, including the ones already mentioned: Hoogenboom [17], Peerdeman [35], Ter Maten [46], Przemieniecki [37], Blaauwendraad and Hoefakker [8], Engineer [15], Cook et al. [12] and Buchanan [10].

2.3 Adjustable formwork

2.3.1 Introduction

First, we look back to the examined precast structures covered in the first chapter. Those structures where structurally divided into panels for which no general mould method could be derived. On the other hand, however, this means a lot of methods have been developed over the years to make double curved elements. These moulds where made of all kind of material, like timber, steel, foam and fabric. To get an overview of the what the market offers some well known methods are discussed in existing moulds and techniques. Concluding remarks will be for the adjustable or flexible formwork, which will be used for the panels in this project. Thereafter an overview is given marking the development of the adjustable formwork, concluding with the most resent mould and its production process.

2.3.2 Existing moulds

There are multiple methods to produce double curved elements. Here the advantages and disadvantages of these methods are elaborated on.

Timber mould Formwork made out of timber dominates when it comes to in-situ casting of concrete. However, for double curved prefabrication this material is less suitable. Usually, plywood or particle board is used for the moulds. Those can be made through workmanship or accurately through CNC (computer numerical control) cutting. So, for making the curved moulds special knowledge and effort is required. Furthermore, the moulds are reusable when a good surface protection is applied but the moulds are not flexible making them suitable for repetition but not with various shapes.

Steel mould Steel is commonly used for casting curved concrete as well. Especially in the precasting industry, because steel moulds are too expensive for casting in-situ. Clearly, This is a disadvantage for the steel moulds too and this is why repetition of the mould is highly preferred. Advantages are that reuse is possible for many times, every shape is possible to create and the material surface doesn't need a lot of attention before casting. But, also for

the steel moulds hold that they are not flexible and therefore not suitable for making unique elements.

Foam mould A foam mould is mostly constructed out of expanded or extruded polystyrene (EPS/XPS), Janssen [23]. This material is easily sculpted into moulds through CNC cutting or wire cutting. Then, for reuse a durable special layer (coating) has to be constructed on the foam. The material is cheap and can be recycled entirely, Gelderman and Homan [16]. In some cases, however, special measures have to be taken in order to resist and control the heavy load of the cast concrete. For every different shaped element a new foam mould is needed, so it's not a practical material for creating multiple one-of-a-kind freeform panels.

Fabric mould With fabric it's possible to construct double curved concrete elements when stretching the fabric, through tension or applying air pressure. Where it must be noted that air pressure based shapes are limited to synclastic forms. Examples of curved cast elements using fixed points creating tension are the fabric moulds studied by Verhaegh [54] (Figure 2.20a) and Veenendaal [53] (Figure 2.20b).
The first research showed positive results, with good quality concrete elements. However, it was concluded that the mould is hard to control because only at points fixed to the supports the shape can be influenced. Also, limited shapes can be generated as the fabric used for the experiments deformed plastic. The latter research has the same conclusions for various other fabric methods (like flat sheet spline method, keel mould method and pinch mould method).

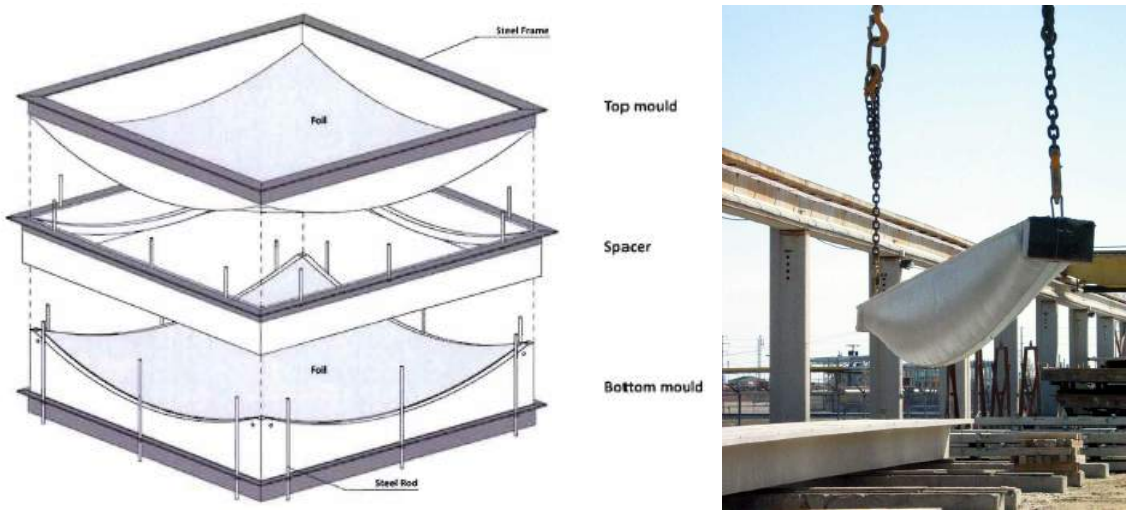

Figure 2.20: (a) Fabric mould (b) Fabric moulded beam

Print techniques Since decades designers speak about printing building components, like trivial objects have been printed lately with this technique. Once this technique is ready, it will eliminate the need for moulds. Developments are going fast and the race for the first 3d-printed house is ongoing. Double curved elements have been printed in 2012 [4], see

Figure 2.21a. However, as shown in the Figure, the surface quality is not very high at the moment, but the technique is still in development. Furthermore, the costs for such a printing machine are very high. Besides, a special concrete which is hardened almost instantly has to be used to keep the shape intact at the moment it is printed. At this moment there are disadvantages, but it is a promising method to create double curved elements of unlimited shapes.

Figure 2.21: (a) 3d-Printed double curved concrete elements (b) Flexible formwork [25]

Flexible mould The flexible mould consists generally of a base plate with actuators and a flexible layer (Figure 2.21b). The actuators are adjustable in height and deform the flexible layer which forms or carries the deformed mould. Unlike the methods mentioned before, this mould is suitable for casting multiple double curved elements of various shapes using the same mould. It's development, configuration, test results and production technique will be discussed in this chapter.

2.3.3 Evolution of the adjustable formwork

The concept of the adjustable formwork has its origin in the ideas of Renzo Piano. The original idea was to scale up a small element by measuring it with a machine which communicates the data to a flexible formwork system (Figure 2.22a). This flexible formwork consists of pistons deforming a flexible mat. Originally, it was the intention to produce curved polyester elements with this method, but retrospectively it can be used to make concrete elements as well. At that time (between 1960-1970) the force analysis for double curved elements was not advanced enough, so unfortunately the idea was never realized by Piano.
Subsequent ideas for a flexible formwork resembled Piano's idea. The main distinctions were the distance between the pistons and the material used for the flexible mat. Four patents in relation to the flexible formwork were given, two of them from mister H.Vidal [56] and F. Kosche [26] are not discussed here, because they don't add to much. What is discussed is a collection of concepts and the two other patents which did in a way contribute to the adjustable formwork in its present shape, based on the overviews presented by E. Den Hartog [13] and B. Janssen [23].

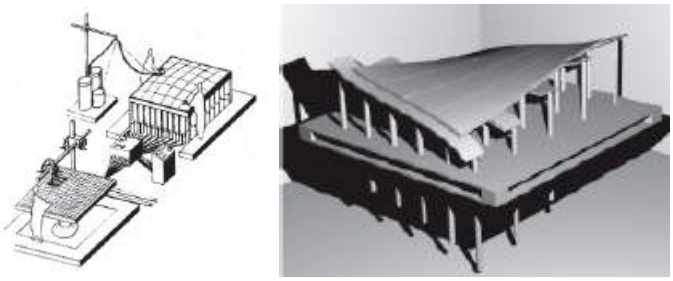

Figure 2.22: (a) Renzo Piano's adjustable formwork concept [14] (b) Strip mould

Strip mould The concept for the strip mould came from H. Jansen, Jansen [22]. The mould consisted of adjustable pistons which deformed a rubber mat by means of two wooden strips spanning in transverse and longitudinal direction (Figure 2.22b). Originally it was meant to cast double curved glass fibre reinforced plastic facade elements, but concrete is possible as well. Furthermore, Jansen concluded that it's possible to combine this kind of mould with a computer program which creates NURBS surfaces. Moreover, these NURBS surfaces use a collection of control points which can be linked to the supports of the mould, which can be seen as a collection of control points too. Problems that remained partly unsolved were the distance between the pistons and the stiffness of the strips.

Pin mould The pin mould is dominated by pins, they are placed against each other, carrying an elastic layer (Figure 2.23a). The thermoplastic layer was positioned directly on the pins. The concept was brought up by M. Quack [38] and M. Roosbroeck [52] tested the idea. The mould was intended as an open mould, but Roosbroeck suggested a closed mould. The results, however, were not really satisfactory. The surface of the elements was not smooth, the pins were visible. Another disadvantage was the uncontrollable thickness. Besides, a lot of pins were necessary in order to cast an element.

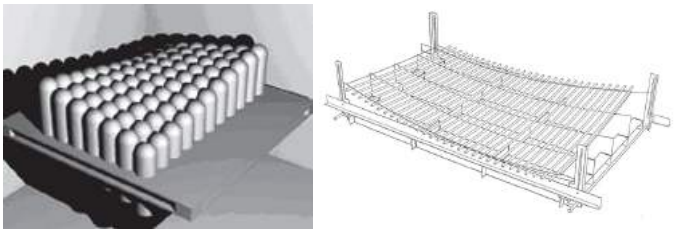

Figure 2.23: (a) Pin mould [52] (b) Adjustable mould by Vollers and Rietbergen [57]

Adjustable mould One form of the adjustable mould is developed by K. Vollers and D. Rietbergen and later patented, [57]. It describes a mould consisting of vertical curved wooden panels in the longitudinal and steel rods in the transverse direction (Figure 2.23b). The steel rods can be seen as the flexible layer, being supported by the panels. This system is intended to make double curved glass panes by deforming an initially flat pane into a double curved one. Therefore the glass is heated in order to let it deform plastic on the formwork. Another patent [58] described the same method while using a more viscous material. The difference is that the viscous material is heated and partly cooled in order to

deform the material in a more controlled way. Besides, for this last material an additional elastic layer was used.
The set-up for the described moulds, with the panels and steel rods, could be replaced by pistons or actuators. This idea belongs to Vollers and Rietbergen as well, and resulted in an adjustable mould with actuators and an elastic layer (Figure 2.24). The actuators are adjustable with a custom made script on the computer. Originally, this was also invented to curve glass facade elements. But K. Huyghe and A. Schoofs performed the experiments for this concept, using it for double curved concrete facade elements [19]. They, too, applied the technique where the concrete is poured on a horizontal surface and only when the material (concrete) was hardened enough it was deformed. Some problems were still not totally solved, like is illustrated in Figure 2.24, where some actuators actually don't touch the surface of the flexible layer. The necessary research on the behavior of the flexible plates was later performed by B. Janssen [23].

Figure 2.24: Adjustable mould used by Huyghe and Schoofs [19]

2.3.4 Adjustable formwork configuration

The adjustable formwork in its present shape consists of a base plate with on top of that the actuators and a flexible layer with a flexible edge to complete the mould (Figure 2.25a). These parts will be discussed here, based on the configuration of the flexible formwork explained by B. Janssen in his research, [23].

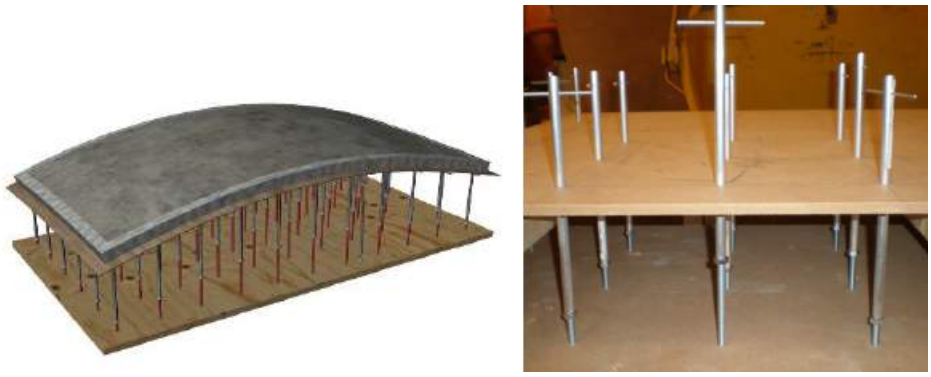

Figure 2.25: (a) Adjustable formwork (b) Actuators

Actuators The actuators serve as support points for the flexible layer and take care of its accurate deformation. They are adjustable in height by means of a hollow pipe in combination with screw-thread and nut (Figure 2.25b). These actuators could be connected with a computer in order to adjust them automatically. K. Huyghe and A. Schoofs did this for their research with the flexible formwork and were able to adjust the actuators fast and accurately [19]. It did show the possibilities for futuristic formworks, but for the many experimental works which are focused on other aspects of the formwork it's an expensive and vulnerable system.

Flexible layer In order to curve the mould smoothly, between the supports, the flexible layer needs proper elastic properties. Therefore, it can not be too stiff and not too flexible. At first, the right material had to be found. Secondly, the right configuration had to be chosen. A simple wooden plate with 3,8 mm thickness performed well according to tests. The resulting set-up was called the plate mould and experiments for double curved elements where performed on this. Then, the configuration was adjusted which resulted in two stripped layers of 3,8 mm thick of the same material. This was called the strip mould and the same tests as done with the plate mould where executed. A more extensive word about these moulds and the test results will follow in next sections.

Flexible edge The flexible edge completes the mould. It has to be flexible as well in order to be able to deform and follow the shape of the flexible layer after casting the concrete. Meanwhile, it has to be stiff enough to withstand horizontal forces resulting form the concrete. These requirements resulted in the choice for a foam, which was easily accessible, in every desirable format, and cheap. The porosity of the foam is a problem which was solved by covering it with a foil. This could also be covered with a permanent coating. The connection of the edge and the flexible layer should be strong but not permanent in order to make multiple unique elements with the same mould. A proposed solution is to make a permanent edge along the perimeter of the mould, glued to the elastic layer, and clamp temporary and custom shaped foam edges against the inside of the permanent edge (Figure 2.26a).
The position and placement of this inner edge should be studied carefully in advance, because the edge will deform, just like the concrete. Without taking care this leads,

probably, to an unwanted deformed shape in relation to the concrete. Figure 2.26b pictures this problem which can be prevented by considering it in advance.

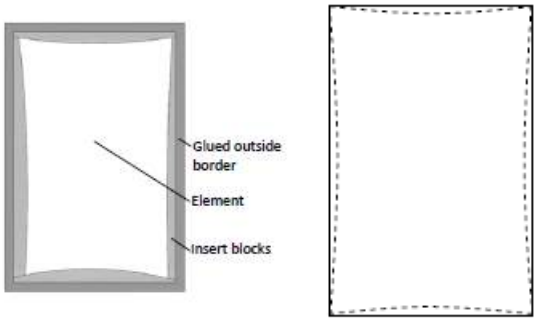

Figure 2.26: (a) Permanent and inserted edge (b) Initially straight edge curves when deformed

2.3.5 Plate mould

The plate mould casts the element making use of only a 3,8 mm wooden plate as flexible layer. On top of this plate a foam edge is placed, completing the boundaries for this open mould (Figure 2.27a and 2.27b). Additionally, a supporting wooden plate is introduced as a support for the flexible layer when it is positioned horizontally. Once the deforming will start the plate will be pushed down in order to let the pistons carry the weight of the concrete in the deformed state.

Figure 2.27: (a) Plate mould, horizontal casting position (b) deformed plate mould

Experiments were performed using a support point distance of 200 mm and the overall dimension of the mould is 2x1 m. The thickness of the element is 50 mm, and still was after deforming, and the curvature radii were between 1,5 and 2,5 m, 1,5 m can be considered the maximum.
Then the test results. The produced element came out in one piece, but the result was not perfect and satisfying. The reason is that the flexible plate buckled. Moreover, it showed discontinuities at the spots where the stresses became larger than the critical buckling stress and this was explained by the critical buckling stress being very low.
The other aspects from the mould that were tested for the first time, like the flexible edge and the moulding process with the pistons performed satisfactory. Also, the model which had to predict the plates behavior did this correct, it showed the tension forces on the exact positions were they occurred. There the plate wouldn't touch the supports.
The overall conclusion was that the plate mould would not be suitable to cast large double curved elements, due to the buckling of the plate.

2.3.6 Strip mould

The strip mould has a flexible layer consisting of transverse and longitudinal strips of 3,8 mm. Only in the middle they're simply connected by nails and to the supports for keeping their positions on the tubes and take care of horizontal displacements. Meanwhile, the top strips can still slide along each other and along the bottom strips, allowing the flexible layer to curve. Because of the seams between the top strips a foam mould is used on top of the flexible layer. It is made out of the same material as the edges and therefore flexible enough to curve, see Figure 2.28a and 2.28b.

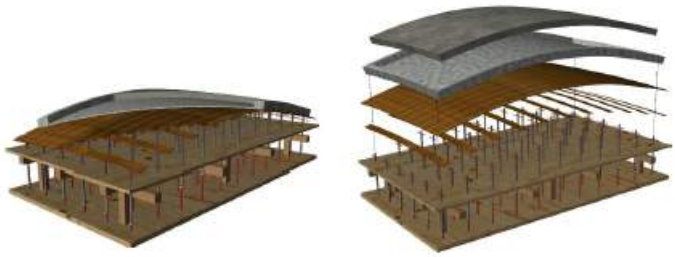

Figure 2.28: (a) Cross-section deformed strip mould (b) Configuration strip mould

Unlike the plate mould, the strip mould behaved satisfactory. Most important issue was the buckling of the plate and this did not occur using the strip mould. Although at some supports the tension in the layer was visible, this could easily be defused by locally tighten the strips with strings, this didn't cause any buckling. Furthermore, the model used for describing the behavior of the flexible layer predicted well.
The mould was also tested with reinforcement. This aspect was less satisfying because the reinforcement is not applicable if not weakened in advance, and even doing that the spacers of the reinforcement where compressed into the soft mould. Besides that, the foil, which seals the foam mould, caused a rough surface.
It was concluded that a solution has to be found for the reinforcement of the curved elements in order to increase its bearing capacities. Additionally, a suitable sealant for the foam mould has to be found in order to get a smooth surface. Finally, there are still some questions about increasing the thickness of the precast element, because then the strains will increase as well during deforming and this will result in bigger cracks.

2.3.7 Production of the elements

For the production of the double curved elements the strip mould is used. The casting procedure for the strip mould is presented shortly is this section. After that some important aspects are explained regarding the concrete mixture that is applied and some comments are placed about the reinforcement of the elements.

Casting procedure The casting procedure is illustrated in Figure 2.29. The procedure starts with the flexible mould, being the strip mould which is already described. Then the concrete is poured, for example self compacting concrete, together with the reinforcement, for instance textile reinforcement. Subsequently, the concrete hardens, increasing its yield

strength. After some time the mould is deformed into its final shape. Finally, after a day, the element can be demoulded. The mould can be used again for another (unique) element. The production process is also described and illustrated accurately by Janssen [23].

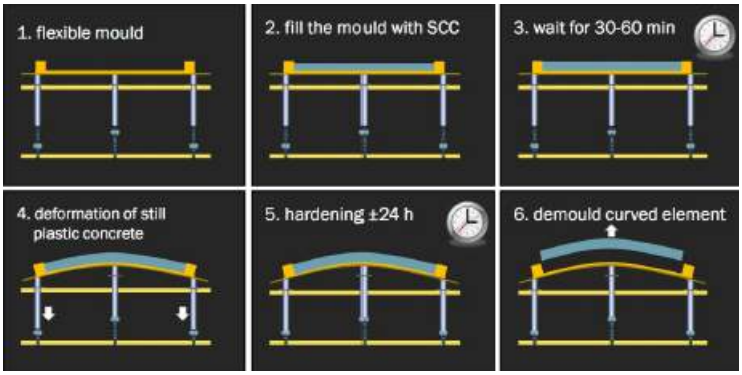

Figure 2.29: Casting procedure [43]

Important issues in this procedure are the concrete mixture, the type of reinforcement, the hardening time and the flowing of the concrete during the deforming and its effects on the final shape.

Concrete mixture

Several concrete mixtures were tested for the mould. Details can be found in the research reports of Janssen [23] and Kok [25] or articles like Schipper et al. [43]. Good results were obtained with two self compacting mixtures, their behavior concerning workability, yield strength and plastic behavior was satisfying [43].

Workability The workability is the ability of the concrete to easily fill up the mould while keeping a good quality. Experiments showed that the self compacting concrete provided a good workability: because of its high plastic viscosity the concrete stabilized quickly.

Yield strength The yield strength relates to the workability and plastic behavior. Preferably the yield strength is low in the beginning, for the workability. Then, with a fast increasing yield strength the plastic behavior of the concrete reduces, but the time until deforming can be reduced. The self compacting concrete provided this property regarding the yield strength. Another type of concrete that could be suitable is a high performance concrete in combination with fibres.

Plastic behavior The plastic behavior relates to the rheology of concrete. Rheology studies flowing properties of materials and does this by describing the relation between the induced stress on a material and its reaction by means of a deformation. Concrete rheology is an important factor with the described casting procedure because the concrete volume is deformed before it's fully hardened and therefore it can 'flow' plastically. That's because the strength of concrete is build up when it's at rest, a property of a thixotropic material, the low initial yield strength allows it to 'flow' and deform. So, the plastic behavior and the

deform time together form a potential problem deform effect on the strain in the concrete and the resulting cracks. In this case, however, not many cracks were spotted.

Reinforcement

For increasing its bearing strength the precast elements need reinforcement. Already mentioned is the effort to cast an element with weakened reinforcement. This experiment was partially a success, but this composition has no bright future regarding the production of bearing elements. Another study is performed, this time on textile reinforcement, by Kok [25]. These results were satisfying, although some movements of the textile reinforcement compared to its initial place in the concrete was observed. Another possibility is the application of fibre concrete in the concrete mixture for the flexible formwork. However, an experiment with this expensive option was not performed to present day.

Part II

Green Planet: design and optimization

Chapter 3

Dome analysis

3.1 Introduction

The analysis of the relative complex shell design of Green Planet requires an analysis of the force flow in similar shells. In addition, a certain confidence in the finite element analysis program (FEA program) needs to be build up, this goal can be accomplished by comparing results with the shell theory. The main goals of this analysis are:

1. Get familiar with the force and deformations in shells;
2. Show that the FEA program is reliable by comparing its results with results obtained by shell theory;
3. Analyze a simple dome with dimensions comparable to the design of Green Planet

Therefore, two models are analyzed, one representing the pure membrane theory and one model basically functioning as a reference for the design of Green Planet. The first model will be a roll supported hemisphere and the latter will be a hinged supported dome, called the reference dome, with the same dimensions as Green Planet. The hinged supports are applied to the reference dome in order to maintain the shape of the shell and to simulate the shell behavior. Normally, large horizontal forces will cause a great instability at the bottom of the shell when roll supports are applied. Furthermore, Green Planet is rather supported with hinges than with rolls. Because of necessary support measurements in horizontal direction, initially it will also be modeled with a hinge support, so choosing a hinge support makes the reference dome more comparable to the design of Green Planet.

3.2 Shell parameters

The main dimensions of the spherical dome are the dimensions that indicate the section of the sphere that is covered. In this chapter a hemispherical dome and a part of the top, under an angle φ of 28 (27,66) degrees, are discussed. The latter corresponds to the dimensions of Green Planet and is therefore called reference dome. It is illustrated with its dimensions in Figure 3.1 together with the dimensions of the hemispherical dome (in the background) to indicate the dimensions. Tables 3.1 and 3.2 provide an overview.

The concrete mixture that is chosen has a strength of C90/105. The reason for this choice is the final design which probably requires a high stiffness. By choosing this mixture the reference dome and the (concrete) Green Planet design can be compared in the end, if indeed this strength is deemed necessary. The thickness is chosen for the same reason. The main material properties and the boundary conditions are given in Table 3.3. The hemisphere will be able to move horizontally on the roller supports and therefore it resembles the membrane theory for shells as much as possible. The reference dome will have a hinged support, for it's horizontal forces are very high.

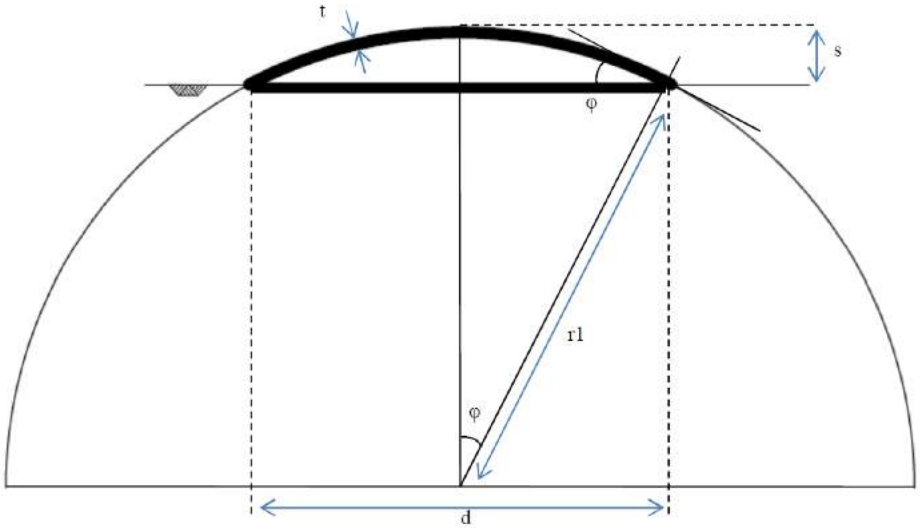

Figure 3.1: Geometrical dimensions spherical dome: the reference dome and hemisphere

Geometry hemispherical dome	Dimension
Angle (φ)	90 degrees
Sagitta (s)	79400 mm
Span (d)	158800 mm
Vertical radius of curvature (r1)	79400 mm
Thickness (t)	200 mm
Shell surface area	39611 m^2
r1/t	400
d/s	1

Table 3.1: Geometrical dimensions hemisphererical dome

Geometry reference dome	Dimension
Angle (φ)	27,66 degrees
Sagitta (s)	9080 mm
Span (d)	73730 mm
Vertical radius of curvature (r1)	79400 mm
Thickness (t)	200 mm
Shell surface area	4530 m^2
r1/t	400
d/s	8

Table 3.2: Geometrical dimensions reference dome

Parameter	Characteristic
E_{mod} (C90/105)	43600 N/mm^2
$f_{c;d}$ (C90/105)	60 N/mm^2
Density (C90/105)	2500 kg/m^3
Poisson's ratio (ν)	0 (0,2)
Loading	Deadweight
p (vertical load)	0,004905 N/mm^2
Supports Hemisphere	Roller
Supports Ref. dome	Hinged
Knockdown factor (C)	1/6
Meshsize	400 mm (2*t)

Table 3.3: Material properties and boundary conditions spherical domes

From Tables 3.1 and 3.2 it can be noted that the span to sagitta ratio (d/s = 1) is small for the hemispherical dome and the ratio (d/s = 8) for the reference dome is large. Shell structures with a ratio above 7 are considered to be flat shells. Shells with ratios above 10 are treated like plates because their resistance through curvature is negligible, but that rule is not applicable to these cases. Ideally, regarding the increase of normal forces and reduction of bending moments in the shell, the ratio should be 3,46 [17].

3.3 Linear elastic analysis: theory vs FEA

The main strength and stability results according to the shell theories are presented here. The theoretical values are determined and will instantly be compared to the finite element analysis results to verify the outcome of the program Scia Engineer.
For the sphere the coordinate system (φ, θ, z) is used instead of the conventional Cartesian coordinate system (x,y,z), see Figure 3.2. For hemispheres holds that the parameters r_1 (radius of curvature in the vertical plane) is equal to r_2 (radius of curvature in the latitude plane) unlike the reference dome, because r_2 is measured from the base. The radius in the horizontal plane is r and can be denoted as $r = r_1 * sin\varphi$

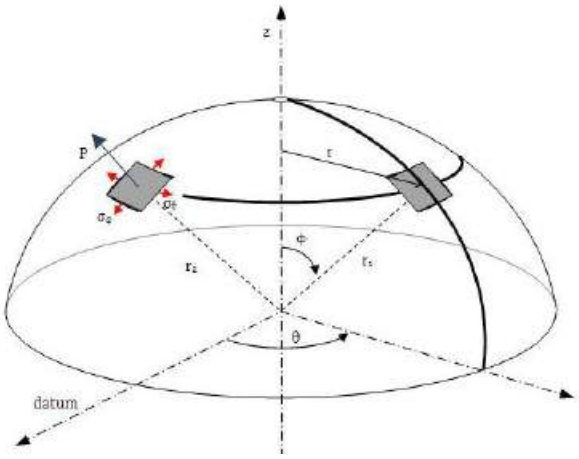

Figure 3.2: Sphere coordinate system (φ, θ, z) and parameters [46]

Resultant force check A first and simple check to verify FEA models is to compare the vertical and horizontal resultant forces. The theoretical value for the vertical resultant force (R_z) is given below. The resultant forces for the two models determined with the FEA program are summarized in Table 3.4 and considering the small difference with the theory it can be concluded that the program is accurate. The resultant of the horizontal force is zero which means that the horizontal forces are in equilibrium, as expected. More details about the vertical and horizontal forces will follow in the section 'Support reactions'.

$$R_z = \frac{1}{2} * \pi * r_1 * s * p$$

		Hemisphere	Reference dome
Theory	R_z[kN]	194292	22219
FEA	R_z[kN]	194288	22212
	ΔR_z [%]	0,002	0,03

Table 3.4: Resultant vertical force of the domes

Internal forces and stresses The internal forces and related membrane stresses can be calculated from the equilibrium equations from the membrane theory for a hemisphere. So, to clarify, the forces and stresses in the reference dome can be calculated with the formulas for the hemisphere, because the reference dome is a part of the hemisphere. For the hemisphere holds that $r_1 = r_2 = a$ and $r = a * sin\varphi$ and for the loads hold that $p_\varphi = p * sin\varphi$ and $p_z = -p * cos\varphi$. The load components and membrane forces are given in Figure 3.3. With the equilibrium equations the forces and stresses in the bottom and top of the shells are determined, see Table 3.5.

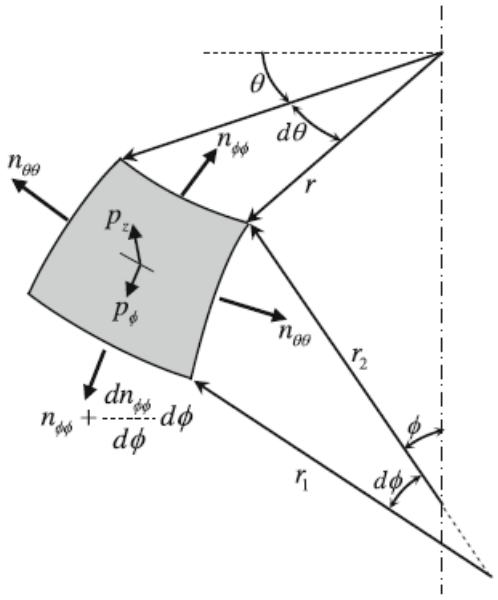

Figure 3.3: Load components and membrane forces on an infinitesimal element ($r_1 = r_2 = a$)[8]

$$n_{\varphi\varphi} = -p * a * \frac{1}{1+cos\varphi}$$

$$n_{\theta\theta} = p * a * (\frac{1}{1+cos\varphi} - cos\varphi)$$

$$\sigma_{\varphi\varphi} = n_{\varphi\varphi}/t$$

$$\sigma_{\theta\theta} = n_{\theta\theta}/t$$

	Hemisphere		Reference dome	
	top ($\varphi = 0$)	bottom ($\varphi = 90$)	top ($\varphi = 0$)	bottom ($\varphi = 28$)
$n_{\varphi\varphi}$[N/mm]	-194,7	-389,5	-194,7	-206,5
$n_{\theta\theta}$[N/mm]	-194,7	389,5	-194,7	-138,4
$\sigma_{\varphi\varphi}$[N/mm^2]	-0,97	-1,95	-0,97	-1,03
$\sigma_{\theta\theta}$[N/mm^2]	-0,97	1,95	-0,97	-0,69

Table 3.5: Internal forces and membrane stresses for hemispherical and reference domes

From these results it can be concluded that there is always a compressive force in the meridional direction of the spheres. In circumferential direction, however, arises a tensile force at some point of the sphere. This can easily be illustrated when the force distribution over a hemisphere is plotted, see Figure 3.4. At the angle of 52 degrees, the force in circumferential direction becomes a positive tensile force. For (concrete) domes it's therefore preferred to build the dome up to an angle of 52 degrees in order to avoid special (reinforcement) measures to deal with the (extra, in case of edge disturbance) tensile force. In case of the reference dome this requirement is met. The hemisphere however bears these

tensile forces, see Figure 3.6 where the circumferential force becomes a tensile force when the angle φ is around 52 degrees.

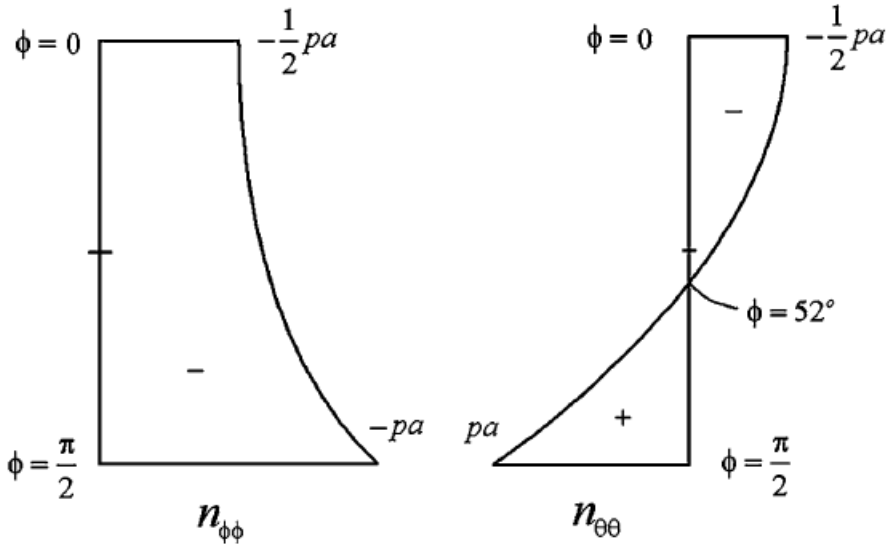

Figure 3.4: Distribution stress resultant over the theoretical hemisphere [8]

Internal forces and stresses by FEA The results of the FEA are presented and then compared with the theoretical solutions to form a conclusion. Table 3.6 shows the results of the FEA for the internal forces and stresses and Table 3.7 compares the deviations as a percentage of the theoretical values. Here, the average stress is taken from the positive and negative face of the shell, in this way representing the middle plane of the shell, to compare it with the theoretically determined stress. Figure 3.5 shows how the forces act in the reference dome, for both principal directions. From this illustration it can be clearly derived that the meridional forces transfer the self weight from the top to the support and that the circumferential forces act perpendicularly and correct the tangent forces to form an equilibrium.

	Hemisphere		Reference dome	
	top ($\varphi = 0$)	bottom ($\varphi = 90$)	top ($\varphi = 0$)	bottom ($\varphi = 28$)
$n_{\varphi\varphi}$[N/mm]	-194,9	-387,0	-194,7	-202,9
$n_{\theta\theta}$[N/mm]	-195,0	394,3	-194,7	-40,6
$\sigma^{-}_{\varphi\varphi}$[N/mm^2]	-0,97	-1,82	-0,97	-1,00
$\sigma^{-}_{\theta\theta}$[N/mm^2]	-0,96	1,99	-0,97	-0,16
$\sigma^{+}_{\varphi\varphi}$[N/mm^2]	-0,99	-2,05	-0,98	-1,02
$\sigma^{+}_{\theta\theta}$[N/mm^2]	-0,99	1,95	-0,98	-0,24
$\sigma_{\varphi\varphi;avg}$[N/mm^2]	-0,98	-1,94	-0,98	-1,01
$\sigma_{\theta\theta;avg}$[N/mm^2]	-0,98	1,97	-0,98	-0,20

Table 3.6: FEA internal forces and stresses

	Hemisphere		Reference dome	
	top ($\varphi = 0$)	bottom ($\varphi = 90$)	top ($\varphi = 0$)	bottom ($\varphi = 28$)
$\Delta n_{\varphi\varphi}$ [%]	0,10	0,65	0	1,74
$\Delta n_{\theta\theta}$ [%]	0,15	1,23	0	70,66
$\Delta \sigma_{\varphi\varphi;avg}$ [%]	1,03	0,52	1,03	1,94
$\Delta \sigma_{\theta\theta;avg}$ [%]	1,03	1,05	1,03	71,01

Table 3.7: Deviation between shell theory and FEA as percentage of the theoretical value

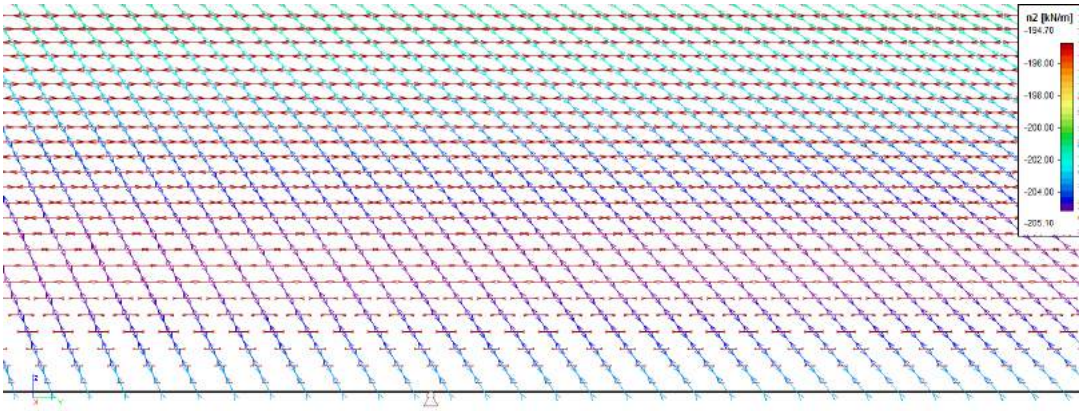

Figure 3.5: Trajectories of the meridional force (in color) and circumferential force (in dark red) for the reference dome

The results obtained by the finite element analysis show little deviation from the theoretical values (Table 3.7). The most remarkable results are those of the reference dome; above all the differences in stress in the circumferential direction. However, this is a direct consequence of the fact that the support, which is a hinge, can resist horizontal forces. That's why this large difference is not found for the roll supported hemisphere. So, if one wishes, this large difference in circumferential force can be avoided by replacing the hinge for a roller support, under an angle, in line with the membrane force. When the roll support is not placed under an angle, this is creating the same situation as for the hemisphere, the reference dome is unstable and the FEA program is not able to finish the calculations. When the value for the circumferential force/stress ($n_{\theta\theta}/\sigma_{\theta\theta}$) at it's peak value is checked, which is a few meters above the support, the exact value of the theoretical derived force and stress is obtained.
Figure 3.6 shows the distribution of the stress resultant $n_{\theta\theta}$ for both domes. Their shape is indeed sinusoidal like the one for the theoretical hemisphere (Figure 3.4). Although, the shape of the reference dome is a little divergent in the area of the edge, where the influence of the edge disturbance is noticed, the length of the disturbed area is the influence length. This length can be determined for cylinders and cones and depends on the angle φ at which the shell touches the ground [8]. This length is for (hemi) spherical shells equal to $l_i = 2,5 * \sqrt{(a * t)}$ (which is the same as for cylinders). For the reference dome, however, this length is determined differently because of the small angle φ at which the shell touches the ground. The comparison with a cone shape conforms better, this yields an influence

length of $l_i = 2,5 * \sqrt{(r_2 * t)} \backsimeq 7$m. This length corresponds with the influence length indicated in Figure 3.6. The edge disturbance is not an issue for the hemisphere because the roll supports allow horizontal movement. Interesting to note for optimization is that the influence length depends on the thickness of the shell.

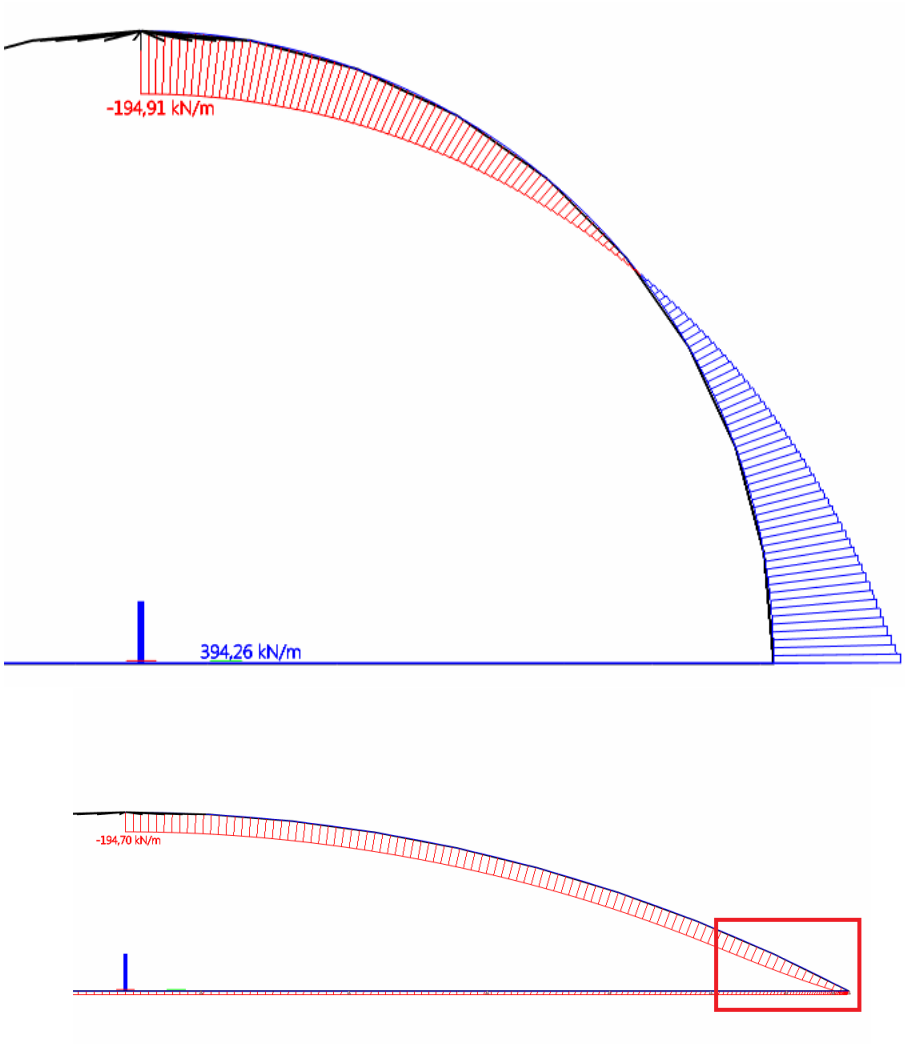

Figure 3.6: Distribution stress resultant $n_{\theta\theta}$ for hemisphere and reference dome (with marked influence length)

Support reactions After determination of the membrane forces it is possible to check the support reactions of the domes. At first the resultant vertical force is checked again, by summing all the vertical reactions distributed over the base circumference. Furthermore, the vertical and horizontal reaction forces are compared to the theoretical values, see Table 3.8. The conclusion is that the differences between theory and FEA are small. The difference with the horizontal force is due to the difference in meridional membrane force and that's caused by the small moments in the shell near the edge.

	Hemisphere			Reference dome		
	Theory	FEA	ΔR (%)	Theory	FEA	ΔR (%)
R_z[kN]	194292	193857	0,22	22219	22177	0,19
R_z[kN/m]	389,5	388,6	0,23	95,86	95,75	0,11
R_H[kN/m]	0	0	0	182,9	178,5	2,41

Table 3.8: Comparison of the support reactions

Displacements and rotations The displacements are derived from the strains in the shell which are directly related to the membrane forces. The rotations are small and therefore neglected. In contrast to the horizontal displacement at the bottom of the hemisphere, which is rather easy to determine with the strain, the top displacement is hard to determine. To calculate the theoretical top displacement, when determined with the strain contribution, it is required to sum all the local vertical displacements derived from the local strains. A second, and preferred, method is the use of potential energy of the dome. This is done in Appendix A where the top displacement is determined for the hemispherical dome using potential energy

The expression for the top displacement according to Appendix A is $u_z = -1,97\frac{pa^2}{Et}$. In addition to this value for u_z the FEA results can be compared to results from other FEA programs. In the exam mentioned in appendix 1 there was additional information about a check in a FEA program resulting in a value $u_z = -1,73\frac{pa^2}{Et}$. When results from a hemisphere made in DIANA are analyzed, found in [35] , a value of $u_z = -1,69\frac{pa^2}{Et}$ is obtained. These results were quite similar and therefore used for the comparison in Table 3.9 as well.

		Hemisphere	Reference dome
		top ($\varphi = 0$)	top ($\varphi = 0$)
Theory	$u_{z;top}$ [mm]	-6,99	-1,51
Other FEA	$u_{z;top}$ [mm]	-6,13	-1,32
FEA	$u_{z;top}$ [mm]	-6,50	-1,84
	$\Delta u_{z;top}$ [%]	7,54	21,85

Table 3.9: Top displacement comparison shell theory and FEA

For the hemisphere it can be concluded that the FEA was accurate enough because the value lies in between the theoretical value and the values derived from other FEA programs. The difference with the theoretical value is 8 percent which is not too much, and the value seems to be on the safe side compared to other FEA programs. However, the results for the reference dome differ almost three times as much as for the hemisphere. The explanation for this is that the theoretical value was derived with the potential energy method using a hemisphere and not the reference dome, because attempts to apply the method to the reference dome were not successful. But, it can be mentioned that the FEA value of the reference dome makes sense, being larger than the theoretical value, because the shape of the reference dome is more shallow than the hemisphere resulting (in average) in larger values for u_z.

The hemisphere is, because of its support conditions, the only dome (of the two mentioned here) moving horizontally. At the bottom it moves in radial direction, these results are compared in Table 3.10. From this table it can be concluded that the difference with the theory is small.

$$u_{r;bottom} = \varepsilon_{\theta\theta} * r_2$$

	Hemisphere	
Theory	$u_{r;bottom}$ [mm]	4,26
FEA	$u_{r;bottom}$ [mm]	4,38
	$\Delta u_{r;bottom}$ [%]	2,82

Table 3.10: Horizontal displacement of the hemisphere

Bending moments by FEA The membrane theory for shells holds when it is assumed that no bending moments occur, like in a perfect shell with supports in line with the meridional forces. In reality most shells deal with an edge disturbance, and to correct this compatibility moments are generated. In order to incorporate those bending moments the membrane theory is extended with the bending theory. It was tried to predict the size of the bending moments with this extended theory, but because the prediction is done with extensive approximating methods which are introduced in for example [47] the estimations were not accurate. It is, however, possible to check the obtained results from the FEA by an other theory, which is much simpler than the method mentioned before. Because the membrane forces and the stresses are already verified they can be used to compare the stresses with the contributions of the membrane force and bending moments.
As already mentioned the largest compatibility moments are required at the bottom edge of the shells. For the hemisphere they're expected at the bottom, if any, and for the reference dome a few meters above the hinged supports, dependent on the influence length. This is clearly illustrated in Figure 3.7 which shows the bending moments in the, normative, meridional direction. Table 3.11 gives an overview of the maximum moments.

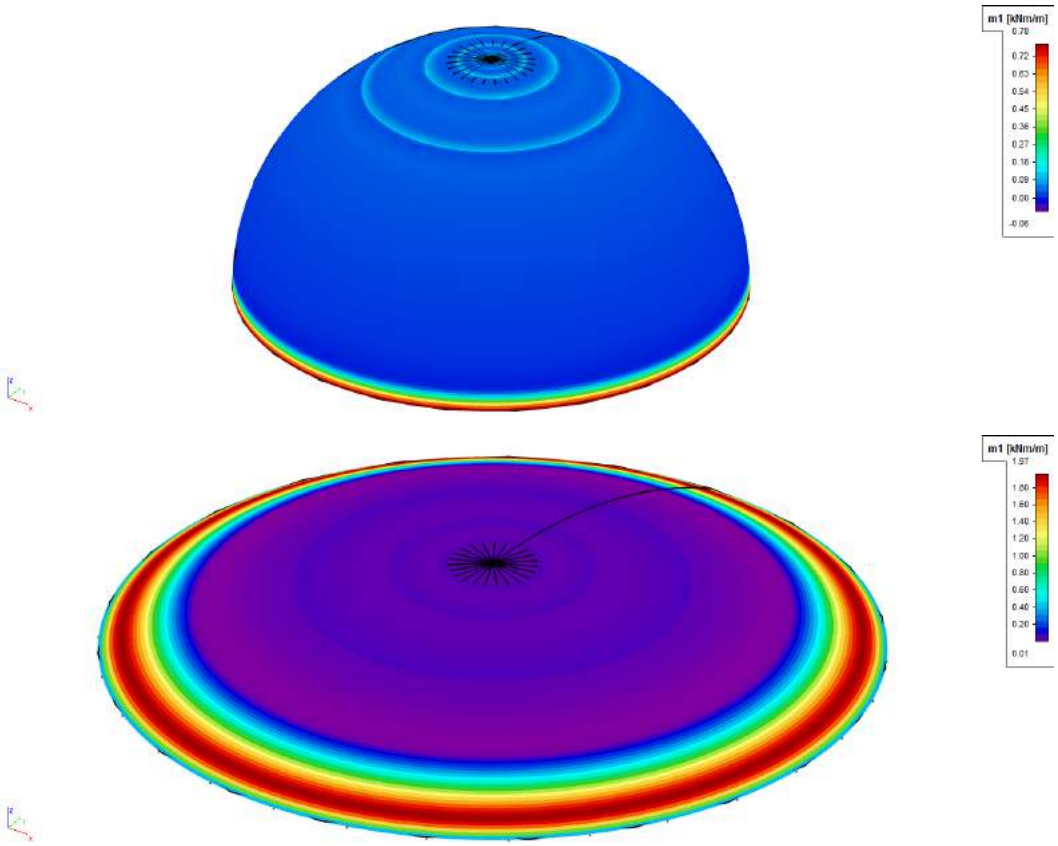

Figure 3.7: Bending moments in meridional direction

	Hemisphere	Reference dome
$m_{\varphi\varphi;max}$[kNm/m]	0,78	1,97
$m_{\theta\theta;max}$ [kNm/m]	0,16	0,58

Table 3.11: Maximum bending moments in the domes

The moments in the shell appear to be small. This is as expected because the difference between the stress on the negative and positive face of the shell was small, indicating that there's only a small moment working over the element's cross-section adding to the membrane force. This can be clarified with the following formulas for the stress in thin shells (where z is 0,5*t):

$$\sigma_{\varphi\varphi} = \frac{n_{\varphi\varphi}}{t} + z * \frac{12 * m_{\varphi\varphi}}{t^3}$$

$$\sigma_{\theta\theta} = \frac{n_{\theta\theta}}{t} + z * \frac{12 * m_{\theta\theta}}{t^3}$$

To check the bending moments of the hemisphere the stresses at the bottom of the hemisphere are gathered from Table 3.6. Those values are compared to the stress resulting from the predetermined membrane forces (same table) and maximum bending moments (Table 3.11), which are at the bottom. The comparison is made in Table 3.12.

In order to check the maximum bending moments in the reference dome extra information is needed from the finite element model. The stress at the position where the maximum bending moment occurs is checked and used for the comparison. Then the stress is determined with the formulas by determining the membrane force from the model at the position of the maximum moments from Table 3.11. The results for the reference dome are also gathered in Table 3.12.

	Hemisphere			Reference dome		
	FEA	Formula	$\Delta\sigma$ (%)	FEA	Formula	$\Delta\sigma$ (%)
$\sigma^{-}_{\varphi\varphi}$[N/mm^2]	-1,82	-1,82	0	-0,73	-0,73	0
$\sigma^{-}_{\theta\theta}$[N/mm^2]	1,99	2,00	0	-0,43	-0,43	0
$\sigma^{+}_{\varphi\varphi}$[N/mm^2]	-2,05	-2,05	0	-1,32	-1,32	0
$\sigma^{+}_{\theta\theta}$[N/mm^2]	1,95	1,95	0	-0,60	-0,60	0

Table 3.12: Comparison of the stresses with bending moment contribution

The results of the comparison show that there's no doubt about the validity of the program concerning the relation between the forces, stresses and moments. One last thing to notice is that the bending moments in the reference dome are say 3 times as high as those in the hemisphere. At the same time the deadweight of the reference dome is about 10% compared to the hemisphere. In fact for every load the compatibility moments in the reference dome are thirty times as high as those for the hemisphere. It can be concluded that regarding the bending moments the reference dome is a highly unfavorable structure compared to the hemisphere.

3.4 Linear buckling analysis: theory vs FEA

Shell structures are most likely to fail by buckling because of their relatively small thickness. Other failure causes could be material non-linearity (cracking or crushing) or a combination of geometrical and material non-linearity [46]. Thus, thin shell structures are very sensitive to imperfections (both in the shell geometry and in loading) which again influence the actual buckling load negatively. The factor which accounts for this influence, representing the difference between a perfect and an imperfect shell, is the knockdown factor. This factor is empirically determined to be C=1/6 and, so, happens to have a major influence on the critical load. The knockdown factor is applied after the critical load is determined. Table 3.13 compares the critical buckling loads of the domes. Figure 3.8 and Figure 3.9a illustrate the most critical failure modes of the shell structures. The critical buckling load is determined with the following equation:

$$p_{cr;lin} = \frac{-2}{\sqrt{3(1-\nu^2)}} * \frac{Et^2}{r1^2} = -1,16 * \frac{Et^2}{r1^2}$$

	Hemisphere				
	Theory	FEA (Roller)	Δp (%)	FEA (Hinge)	Δp (%)
$p_{cr;lin}$[kN/m^2]	-320	-84	73,75	-186	41,88

	Reference dome		
	Theory	FEA	Δp (%)
$p_{cr;lin}$[kN/m^2]	-320	-321	0,31

Table 3.13: Critical buckling load comparison

From the table it is clear that the theoretical and FEA buckling loads match very accurate for the reference dome. But, for the hemisphere there's a big difference. The reason for the difference lies in the fact that the chosen formula for $p_{cr;lin}$ determines the critical load perpendicular to the shell, whereas the FEA model determines the critical vertical load (a vertical load of 1 kN/m^2 is applied). Furthermore, the vertical load is in line with the vulnerable edge (Figure 3.8), which perpendicularly meets the ground, it adds to the buckling rather than the perpendicular load. This holds for the hinged hemisphere. For the roller supported hemisphere it is obvious that the support provides an increased buckling length and so reduces the strength of the shell even more. So, when the hemisphere is loaded with a perpendicular load and supported by hinges the FEA must match the theory. This hypothesis is tested and this resulted indeed in a critical buckling load of 333 kN/m^2, very close to theoretical value. The buckling mode is given in Figure 3.9b.

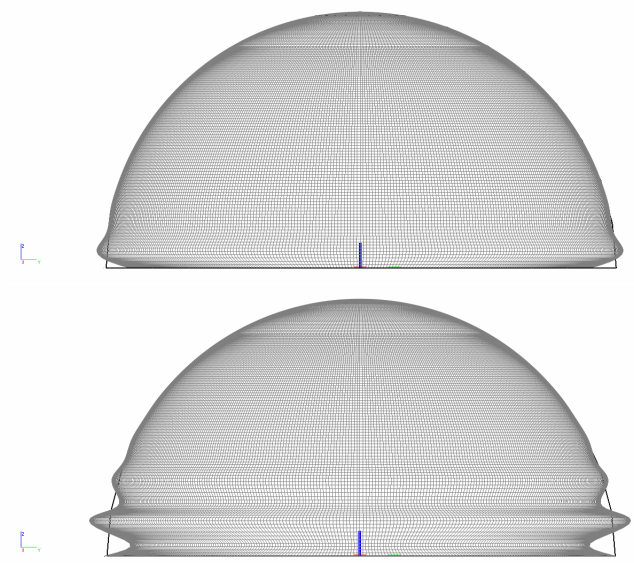

Figure 3.8: Buckling modes: (a) Roller supported hemisphere (8 times magnified) (b) Hinged supported hemisphere (8 times magnified)

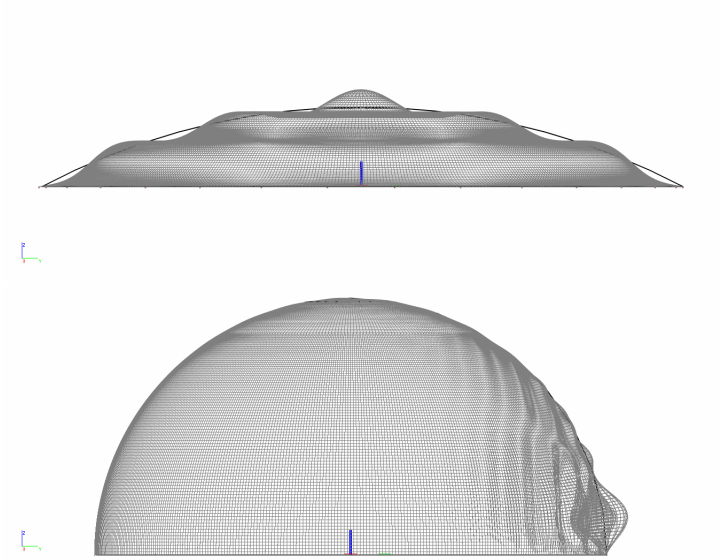

Figure 3.9: Buckling modes: (a) Hinged supported reference dome (2 times magnified) (b) Hinged supported perpendicular loaded hemisphere (8 times magnified)

Not addressed in the table are the second most critical buckling loads. Those loads are useful for measuring the sensitiveness of the shell for imperfections and therewith the possible occurrence of compound buckling or multi-mode buckling. Compound buckling is the failure mode where multiple buckling modes have the same critical load causing the modes to interact which results in a softening response after reaching the (critical) bifurcation point [17]. In this case all second critical buckling loads lie very close to the most critical loads (<2% difference) which means that the shells are very sensitive to imperfections, as was assumed.

3.5 Discussion

Some concluding words will be spend regarding the research which was performed with the hemisphere and the reference domes. Table 3.14 and Table 3.15 summarize the results. The main goals of this chapter (see Section 3.1) will be discussed.

Comparison theory and FEA The obtained results from both theory and FEA, which are listed in the tables, show little deviation. This holds for the hemisphere as well as for the reference dome. And, more importantly, in most cases where there was deviation between the results the FEA seems to be on the 'safe' side.
First for the hemisphere.

- Little deviation is found for the membrane forces and stresses at the bottom of the shell. The circumferential tensile forces are on the safe side. The meridional force however is a little bit lower than expected, but this difference is negligible compared to the safety factor.

- The displacements of the FEA are on the safe side as well, eight percent is an acceptable range for the deflection of the hemisphere.
- The bending moments are of course bigger than the membrane solution suggests. In this case they are rather small but proven to be in balance with the membrane forces and stresses in the shell.
- The buckling load is much smaller than the theoretically determined load. One of the reasons is the support condition which increases the buckling length. The second reason is the theoretically determined load which is designed for perpendicular loaded shells. In this case the vertical load is disadvantageous for the buckling resistance and results in a small critical buckling load.

		Hemisphere (roll supported)		
		Theory	FEA	Δ%
Resultant force	R_z[kN]	194292	194288	0
Membrane force	$n_{\varphi\varphi}$[N/mm]	-194,7	-194,9	0,10
($\varphi = 0$)	$n_{\theta\theta}$[N/mm]	-194,7	-195,0	0,15
Membrane stress	$\sigma_{\varphi\varphi}$[N/mm^2]	-0,97	-0,98	1,03
($\varphi = 0$)	$\sigma_{\theta\theta}$[N/mm^2]	-0,97	-0,98	1,03
Membrane force	$n_{\varphi\varphi}$[N/mm]	-389,5	-387,0	0,65
($\varphi = 90$)	$n_{\theta\theta}$[N/mm]	389,5	394,3	1,23
Membrane stress	$\sigma_{\varphi\varphi}$[N/mm^2]	-1,95	-1,94	0,52
($\varphi = 90$)	$\sigma_{\theta\theta}$[N/mm^2]	1,95	1,97	1,05
Total support reaction	R_z[kN]	194292	193857	0,22
Vertical support reaction	R_z[kN/m]	389,5	388,6	0,23
Horizontal support reaction	R_H[kN/m]	0	0	0
Vertical displacement	$u_{z;top}$ [mm]	-6,99	-6,50	7,54
Horizontal displacement	$u_{zr;bottom}$ [mm]	4,26	4,38	2,82
Meridional moments	$m_{\varphi\varphi;max}$[kNm/m]	0	0,78	-
Circumferential moments	$m_{\theta\theta;max}$ [kNm/m]	0	0,16	-
Critical buckling load	$p_{cr;lin}$[kN/m^2]	-320	-84	73,75

Table 3.14: Summary of the results of the finite element analysis validation for the hemisphere

Reference dome The conclusions drawn for the hemisphere are applicable to the reference dome as well. In addition, there are a few more things to add to the list that only hold for the hinged supported reference dome and therefore must be considered when analyzing the design for Green Planet:

- The membrane forces in the circumferential direction differ a lot. This is due to the supports which prevent the development of stress in this direction.
- The horizontal support reaction forces deviate little from the theoretical value, and can be considered accurate (also in relation to future safety factors).

- More research could be done concerning the deflection of the reference dome because the values are validated using equilibrium equations, while the deflection values of the hemisphere were validated with the potential energy method.
- The bending moments are large in comparison to the ones in the hemisphere (30 times as high when compared to the applied load). The reason is the way of supporting the shell which causes an edge disturbance with compatibility moments. However, this way of supporting is, at least, necessary for the reference dome because with a roller support it would have failed because of instability, the horizontal forces would be to large to handle. The moments are checked by comparing the stress with the generated stress by the sum of the membrane forces and the bending moments in a cross-section. This proved to be in good agreement with each other.
- The critical buckling load determined with the FEA matches the theory perfectly. On the one hand this is strange because the formula represents a perpendicular (to its surface) loaded shell, while the reference dome is loaded vertically. But, the dome is that shallow that, the vertical load can be taken for a perpendicular oriented load.

Based on these results it can be concluded that Scia Engineer is a reliable FEA program to work with for future research that is hard to back up by simple shell theories.

		Reference dome (hinge supported)		
		Theory	FEA	Δ%
Resultant force	R_z[kN]	22219	22212	0,03
Membrane force	$n_{\varphi\varphi}$[N/mm]	-194,7	-194,7	0
($\varphi = 0$)	$n_{\theta\theta}$[N/mm]	-194,7	-194,7	0
Membrane stress	$\sigma_{\varphi\varphi}$[N/mm^2]	-0,97	-0,98	1,03
($\varphi = 0$)	$\sigma_{\theta\theta}$[N/mm^2]	-0,97	-0,98	1,03
Membrane force	$n_{\varphi\varphi}$[N/mm]	-206,5	-202,9	1,74
($\varphi = 28$)	$n_{\theta\theta}$[N/mm]	-138,4	-40,6	70,66
Membrane stress	$\sigma_{\varphi\varphi}$[N/mm^2]	-1,03	-1,01	1,94
($\varphi = 28$)	$\sigma_{\theta\theta}$[N/mm^2]	-0,69	-0,20	71,01
Total support reaction	R_z[kN]	22219	22177	0,19
Vertical support reaction	R_z[kN/m]	95,86	95,75	0,11
Horizontal support reaction	R_H[kN/m]	182,9	178,5	2,41
Vertical displacement	$u_{z;top}$ [mm]	-1,51	-1,84	21,85
Meridional moments	$m_{\varphi\varphi;max}$[kNm/m]	0	1,97	-
Circumferential moments	$m_{\theta\theta;max}$ [kNm/m]	0	0,58	-
Critical buckling load	$p_{cr;lin}$[kN/m^2]	-320	-321	0,31

Table 3.15: Resume of the finite element analysis validation for the reference dome

Chapter 4

Shell structures comparison

4.1 Introduction

In the previous chapter the verification of the FEA program (Scia Engineer) was discussed and a preliminary analysis of a simple dome was carried out. The goal of this chapter is to decide which (simple) shell structure approximates the behavior of the Green Planet model (Figure 4.1) best. Besides, the behavior of the concrete Green Planet model is verified based on comparable but simpler shell structures. The main goals of this chapter are:

1. Decide which (simple) structure approximates the behavior of the Green Planet model best
2. Verify the behavior of the concrete Green Planet model

In order to accomplish these goals simple shell structures are analyzed and discussed first. In Chapter 3 the reference dome was discussed, in this chapter the weakened dome, arch, cylinder structure and asymmetrical loaded dome and weakened dome are covered. Subsequently, the Green Planet model is discussed and after it will be compared to the other models. The Green planet model is not yet fully analyzed (this will be done in Chapter 5) but only subjected to it's own weight, because this was (in Chapter 3) and will be done to compare it with other models as well. The thickness is 200 mm and the concrete class C90/105, for every model. The results follow from linear elastic and linear buckling analyzes.

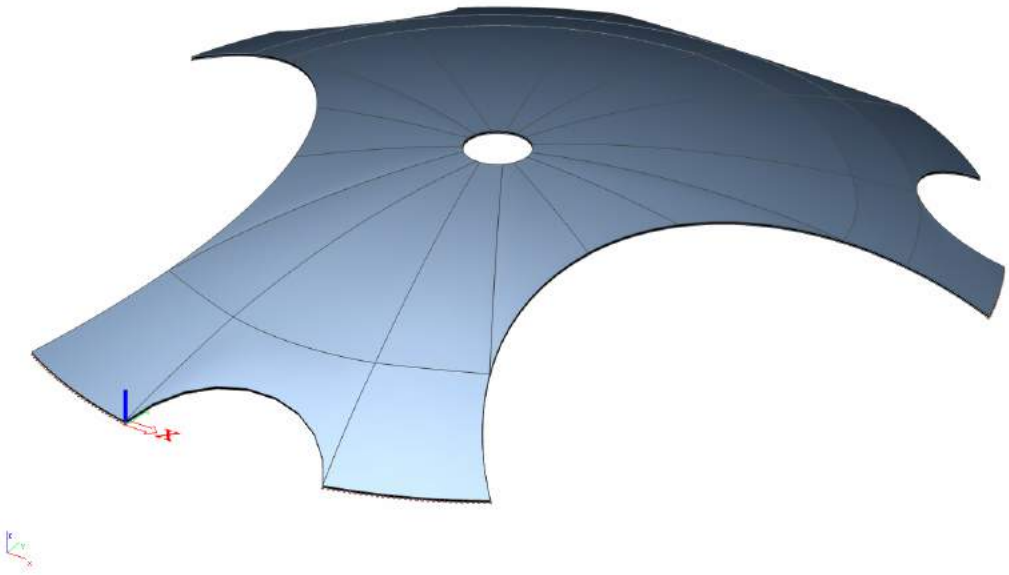

Figure 4.1: The Green Planet model that is used for analysis

4.2 Weakened dome analysis

In order to weaken the (reference) dome introduced in Chapter 3 an oculus with a diameter of 5 m is applied (same oculus as introduced in Green Planet). Figure 4.2 shows the model in Scia Engineer. When the top part is taken of the shell it requires a horizontal force to compensate it [49]. Because this horizontal force is pointing outwards large circumferential compressive forces are required to establish an equilibrium. This is the main consequence of the introduction of an oculus in a dome. Other consequences can be retrieved from Table 4.1 where the FEA results for the reference dome are compared to the results of the weakened dome with the oculus. In this table values are given for $\varphi = 0$, for the weakened dome this means the first point on the shell surface from the top (or: the highest point) which is approximately 2,5 meters from the top.

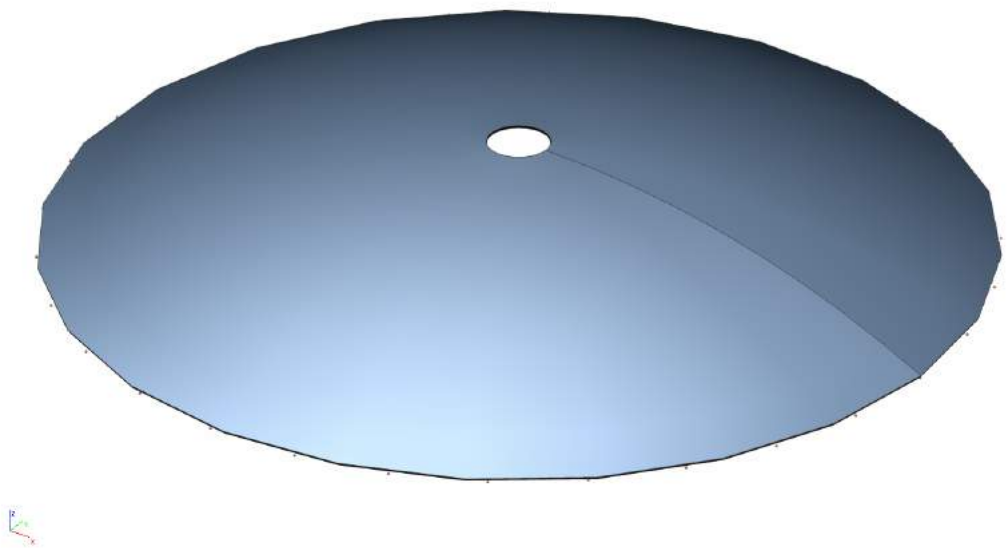

Figure 4.2: Model dome with oculus

		FEA Dome	FEA Weakened	Δ%
Resultant force	R_z[kN]	22212	22110	0,01
Membrane force	$n_{\varphi\varphi}$[N/mm]	-194,7	-8,66	95,55
($\varphi = 0$)	$n_{\theta\theta}$[N/mm]	-194,7	-388,5	99,54
Membrane stress	$\sigma_{\varphi\varphi}$[N/mm^2]	-0,98	-0,04	95,92
($\varphi = 0$)	$\sigma_{\theta\theta}$[N/mm^2]	-0,98	-1,94	97,96
Membrane force	$n_{\varphi\varphi}$[N/mm]	-202,9	-202,2	0,34
($\varphi = 28$)	$n_{\theta\theta}$[N/mm]	-40,6	-40,4	0,49
Membrane stress	$\sigma_{\varphi\varphi}$[N/mm^2]	-1,01	-1,01	0
($\varphi = 28$)	$\sigma_{\theta\theta}$[N/mm^2]	-0,20	-0,21	5,00
Total support reaction	R_z[kN]	22179	22468	1,30
Vertical support reaction	R_z[kN/m]	95,75	93,9	1,93
Horizontal support reaction	R_H[kN/m]	178,5	179,1	0,34
Vertical displacement	$u_{z;top}$ [mm]	-1,84	-1,84	0
Meridional moments	$m_{\varphi\varphi;max}$[kNm/m]	1,97	2,15	9,14
Circumferential moments	$m_{\theta\theta;max}$ [kNm/m]	0,58	0,63	8,62
Critical buckling load	$p_{cr;lin}$[kN/m^2]	-321	-226	29,60

Table 4.1: Comparison of the dome with the weakened dome with oculus

The table shows very clear that the circumferential forces ($n_{\theta\theta}$) are high indeed, they are doubled compared to the other case, which makes sense while the meridional forces ($n_{\varphi\varphi}$) are reduced to (almost) zero. Furthermore, there were some differences for the support reactions due to an inconsistency in the FEA program. The support reactions were expected to be more or less the same as for the reference dome, but the program's results were up to

five times higher as those reactions. This inconsistency is reported to Scia Engineer support and they admitted, eventually, that there is something wrong with the support reactions but that it will be fixed in the next version, which comes soon. It must be noted that this inconsistency in giving the support reactions is very important and must be considered in further research, until the next version is available. For now it is possible to use the support reactions derived from the internal forces at the bottom of the shell, which results in forces that are almost the same as the reference dome.
Also the moments increase a little, but the impact is not great. When the accuracy of the calculation of the weakened dome is increased, by decreasing the size of the mesh to 0,2 m, the moments get even smaller indicating that the influence of the oculus on the moments is small. Other consequences of the accuracy increase are very small, those include a membrane force increase in meridional direction (to zero) and decrease in circumferential direction, at the top.
The critical buckling load, however, happens to drop a lot. This is caused by the great circumferential force that has to be generated around the oculus to form an equilibrium. It is therefore no surprise that the first buckling mode occurs around the oculus, see Figure 4.3a. Even when a beam is installed to take up the ring forces and strengthen that part of the shell the first buckling mode occurs around the oculus, as could be seen in Figure 4.3b. But, the critical buckling load is improved to 292 kN/m^2, which depends on the strength of the ring beam. On the other hand, the consequences of the ring beam are an increased meridional force (this force tends to approach the value found for a dome without an oculus, when the ring beam strength increases) and an increased top displacement mainly due to the weight of the beam (this increase is about 10%).

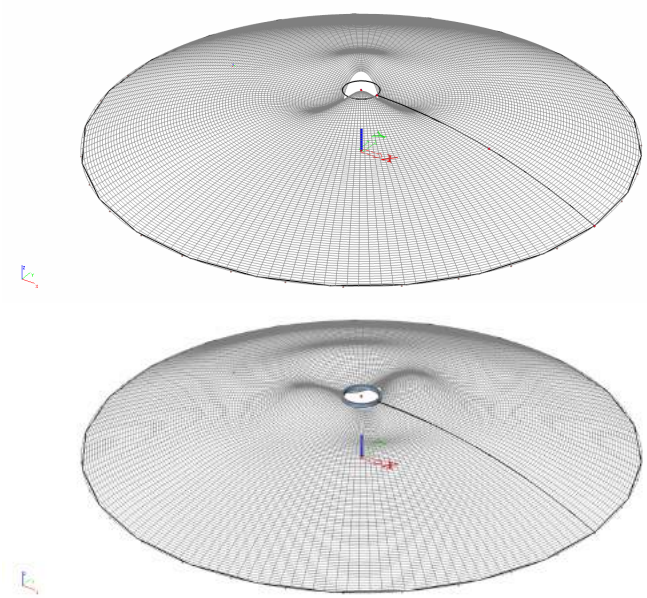

Figure 4.3: (a) First buckling mode of the dome with oculus (b) First buckling mode of the dome with oculus and ring beam

4.3 Arch analysis

In this section the mechanical schemes and results for an arch are presented. The focus will be on the deflection of the arch, because there's no membrane behavior to compare to the Green Planet design. The simplified 2d representation of the longitudinal and transverse cross-section of the Green Planet model that is introduced here, has the same dimensions (200 mm thick, but 1 m wide) and material properties (concrete C90/105) and is hinged in both supports.

Symmetrical loaded arch The first check for the mechanical scheme of the arch is performed with a symmetrical loading by its self weight. This yields the moment and deflection line given in Figure 4.4. The lines follow a similar symmetrical path and can be considered realistic mechanical schemes for a loaded arch.

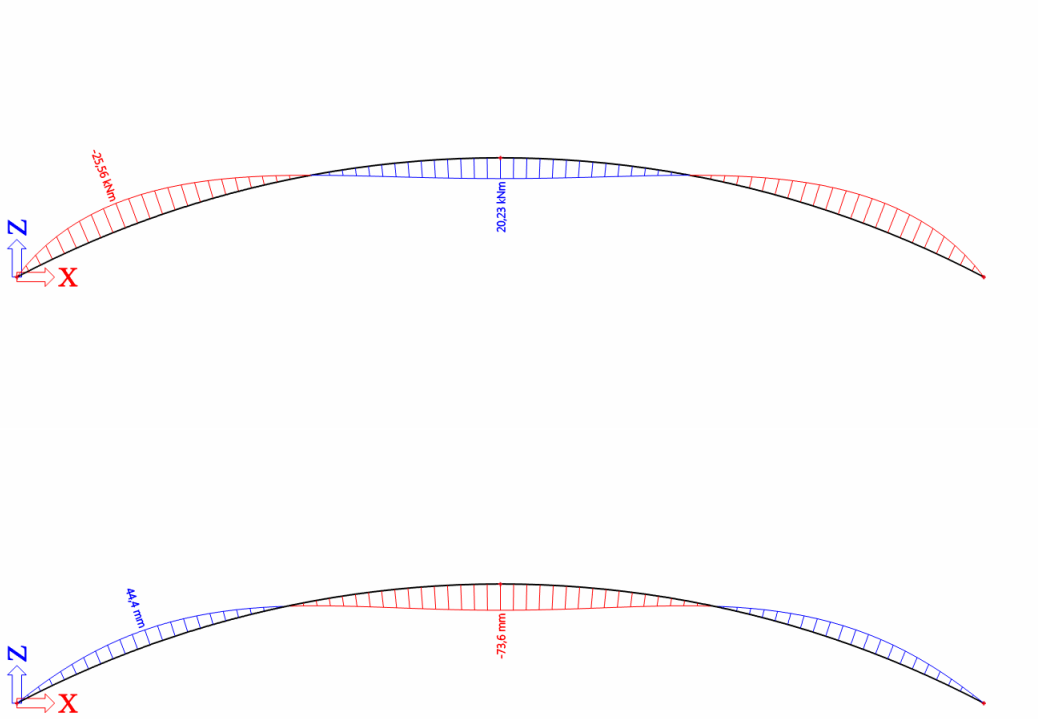

Figure 4.4: Moment line and deflection line in the arch (2 times magnified)

Asymmetrical loaded arch The arch is loaded by its self weight and on top of the right half a q-load (perpendicular to the arch) is added which is as great as the arches self weight. This simulates the situation of Green Planet, where the right part is approximately twice as large and heavy as the left part, see Figure 4.5a. This results in the given moment and deflection line, see Figure 4.5b.

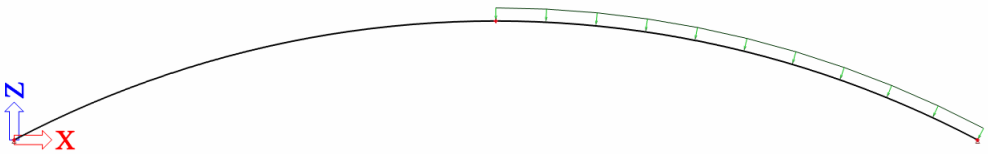
Z
X

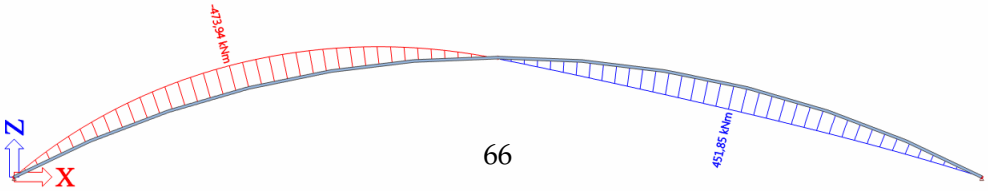
-473,94 kNm
451,85 kNm
Z
X

When this load case is compared to the symmetrical one it can be concluded that there's a large difference between those load cases. Table 4.2 illustrates this differences clearly. It can be concluded that for asymmetrically loaded arches the moments and displacements increase tremendously compared to symmetrical loading. The other parameters increase almost linear with the applied load.
To double check this conclusion the applied q-load is diminished to half its size in another experiment. This is not shown here, but it was concluded that in that case the moments and displacements drop by fifty percent too, as well as the other parameters. This proves that not the load but the asymmetrical placing of the load has a great effect on the moments and displacements of the arch.

parameter	Arch sym	Arch asym	Arch uneq	Δasym %	Δuneq %
M_{max}[kNm/m]	26	474	242	1723	831
$u_{z;max}$[mm]	74	2506	653	3286	782
$R_{z;left}$[kN/m]	188	236	281	26	50
$R_{z;right}$[kN/m]	188	321	281	71	50
$R_{h,left}$[kN/m]	372	567	633	52	70
$R_{h,right}$[kN/m]	372	522	633	40	70
N [kN/m]	417	611	691	47	66

Table 4.2: Difference between the symmetrical loaded arch and the asymmetrical and unequal loaded arches, where the latter two loaded arches have 50% more weight

Symmetrical but unequally loaded arch A q-load (perpendicular to the arch) is applied on the top half of the arch with a value equal to the self weight. This simulates the situation of Green Planet again, where the middle part is approximately twice as large and heavy as the parts at both sides, see Figure 4.6a. An overview of the important results is given in Figure 4.6b and in Table 4.2. To summarize, the load was increased by 50%, this resulted in a 831% increase for the maximum moment and a 782% increase for the vertical displacement in the middle of the arch, compared to the symmetrical loaded arch. The support reactions give results that were expected according to simple mechanics. The conclusion is that the symmetrical but unequally load has a significant (negative) effect on the moments and displacements in the arch, but the consequences are two or three times as large when the arch is loaded in an asymmetrical way.

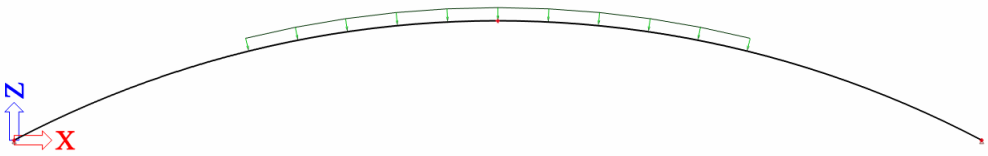
Z
X

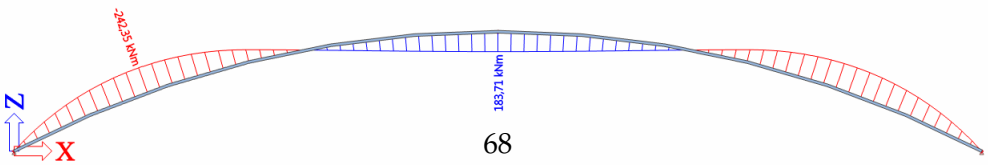
-242,25 kNm
183,71 kNm
Z
X

4.4 Cylinder structure analysis

Green planet is a shell structure and, while an arch isn't, it seems rational to compare it to a cylinder structure as well. However, it must be noted that the structure doesn't curve in two directions, like Green Planet, so it won't benefit as much from being a shell structure. The dimensions of the cylinder, a width of 30 m and a span of 70 m, are chosen to be more or less the same as Green Planet. The first goal is to check how the cylinder differs from the arch, regarding internal forces and deflection. Furthermore, the same data will be gathered for the cylinder as was done for the reference dome and the weakened dome. With these results it is possible to compare the shell structures with each other and discuss its weaknesses and strengths. Later, these results can be compared to Green Planet.
Three different load cases will be discussed, just like is done with the arch: a symmetrical load case with the self weight of the cylinder structure, an asymmetrical load case simulating the fact that the back of Green Planet contains twice as much weight and a symmetrical but unequally distributed load case simulating the top half of Green Planet having twice as much weight compared to the rest of the structure.

Symmetrical loaded cylinder When the cylinder structure (Figure 4.7a) is loaded by its self-weight it yields the maximum moment and deflection line given in Figure 4.7b. Actually, the given cross-section gives an indication of the maximum moment, because the maximum moment occurs in another cross-section, but it's a good indication as the maximum moment differs only 3% and the deflection line in the same cross-section does give the maximum deflection. These and more results are gathered in Table 4.3.

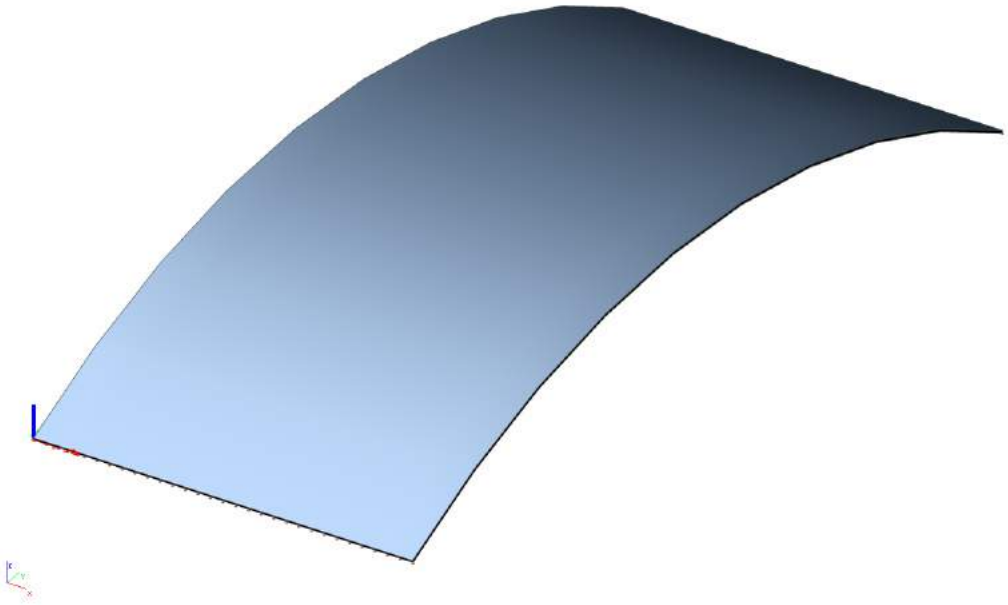

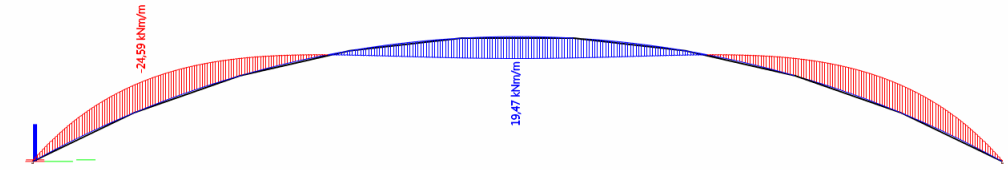
-24,59 kNm/m
19,47 kNm/m

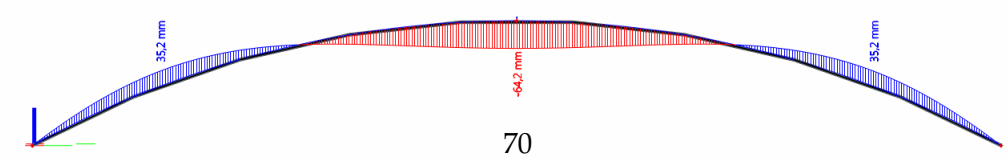
35,2 mm
-64,2 mm
35,2 mm

For the symmetrical (self weight) load case it can be concluded that the moment and deflection lines of the cylinder structure matches the lines of the arch structure. However, the maximums belonging to these lines differ a little bit. The maximum moment and deflection are smaller for the cylinder compared to the arch, due to the possibility to distribute the internal forces across the (larger) surface of the structure. For the normal force holds the opposite, it is smaller for the arch structure, but these forces are very local. On average the normal force of the cylinder structure matches the arch structures normal force. The support reactions are locally higher too, on average they are the same as for the arch.

Asymmetrical loaded cylinder The Cylinder structure is loaded by its self weight and a distributed load over the right half of the structure (perpendicular to its surface), again to simulate Green Planet (see Figure 4.5). This asymmetrical load gives the moment and deflection lines as given in Figure 4.8 and results given in Table 4.3.

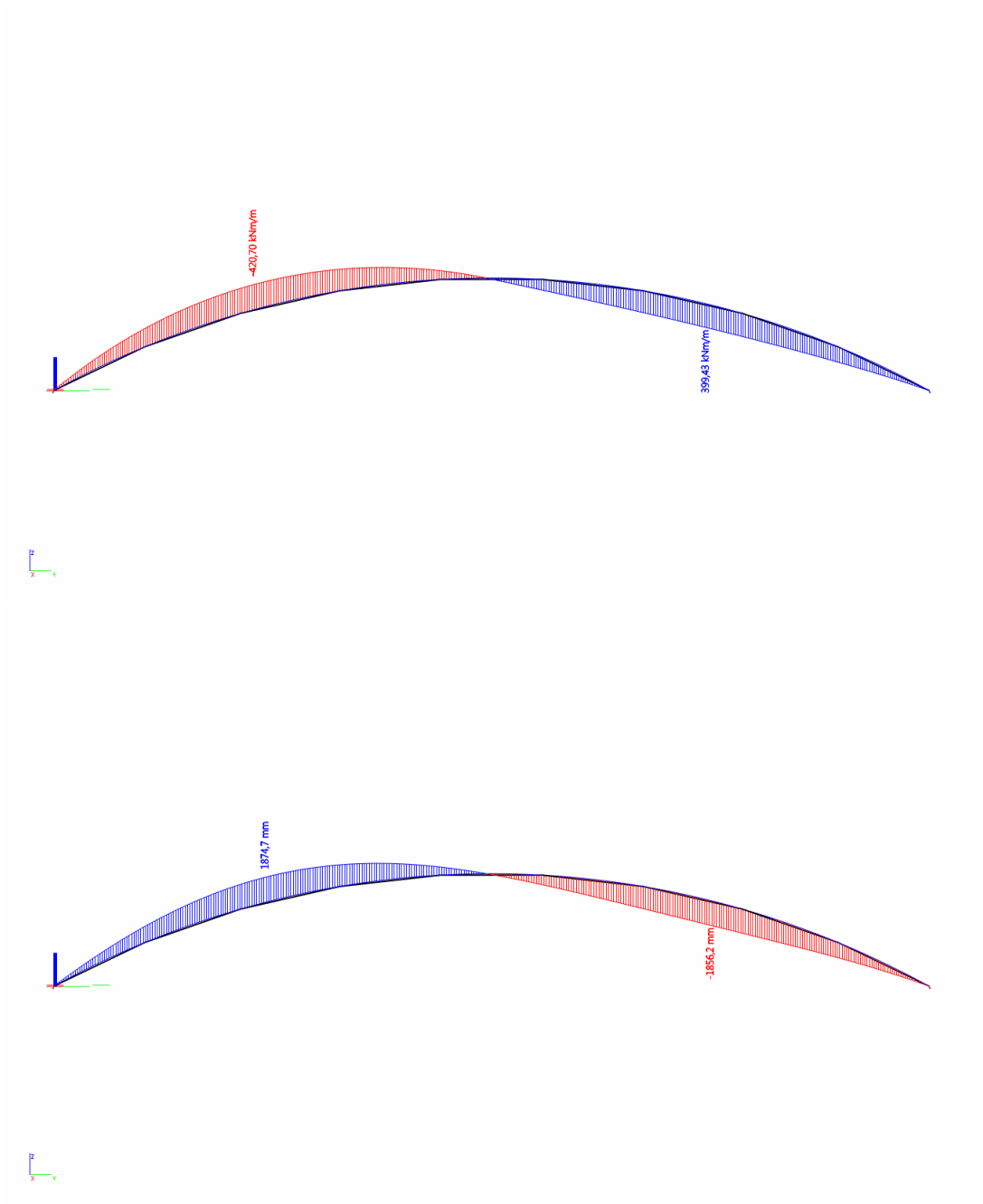

Figure 4.8: Moment and deflection lines of the asymmetrically loaded cylinder structure (2 times magnified)

parameter	Cylinder sym	Cylinder asym	Cylinder uneq	Δasym %	Δuneq %
M_{max}[kNm/m]	25	436	225	1644	800
$u_{z;max}$[mm]	64	1875	548	2830	756
$R_{z;left,max}$[kN/m]	255	245	305	-4	20
$R_{z;right,max}$[kN/m]	255	525	305	106	20
$R_{h,left,max}$[kN/m]	485	595	695	23	43
$R_{h,right,max}$[kN/m]	485	840	695	73	43
N_{max} [kN/m]	564	1784	1108	216	96

Table 4.3: Difference between the symmetrical loaded cylinder structure and the asymmetrical and unequal loaded structures, where the latter two have 50% more weight

The total load of the asymmetrical load is 50% larger compared to the symmetrical load case. From Table 4.3 it is derived that the results didn't increase linearly with this load increment. On the contrary, the maximum moment and deflection increase by more than a thousand percent, due to the asymmetrical loading. This situation is comparable with the arch structure. Furthermore, the normal force in the cylinder structure is the same as observed for the arch structure, except for a few unstable areas (at the edges of the structure) where the normal force is much larger. Also, the maximum results of the support reactions of the cylinder are misleading because they occur only very locally, on average the support situation matches the one of the arch structure.

Symmetrical loaded but unequally loaded cylinder The moment and deflection lines due to the extra loading on the top half of the cylinder are given in Figure 4.9. Table 4.3 contains an overview of the results of this load case and compares it to the symmetrical load case where only self weight is applied. It can be concluded that for this load case he same conclusions apply as for the unequally loaded arch structure, despite the (locally) higher maximum values for the cylinder structure.

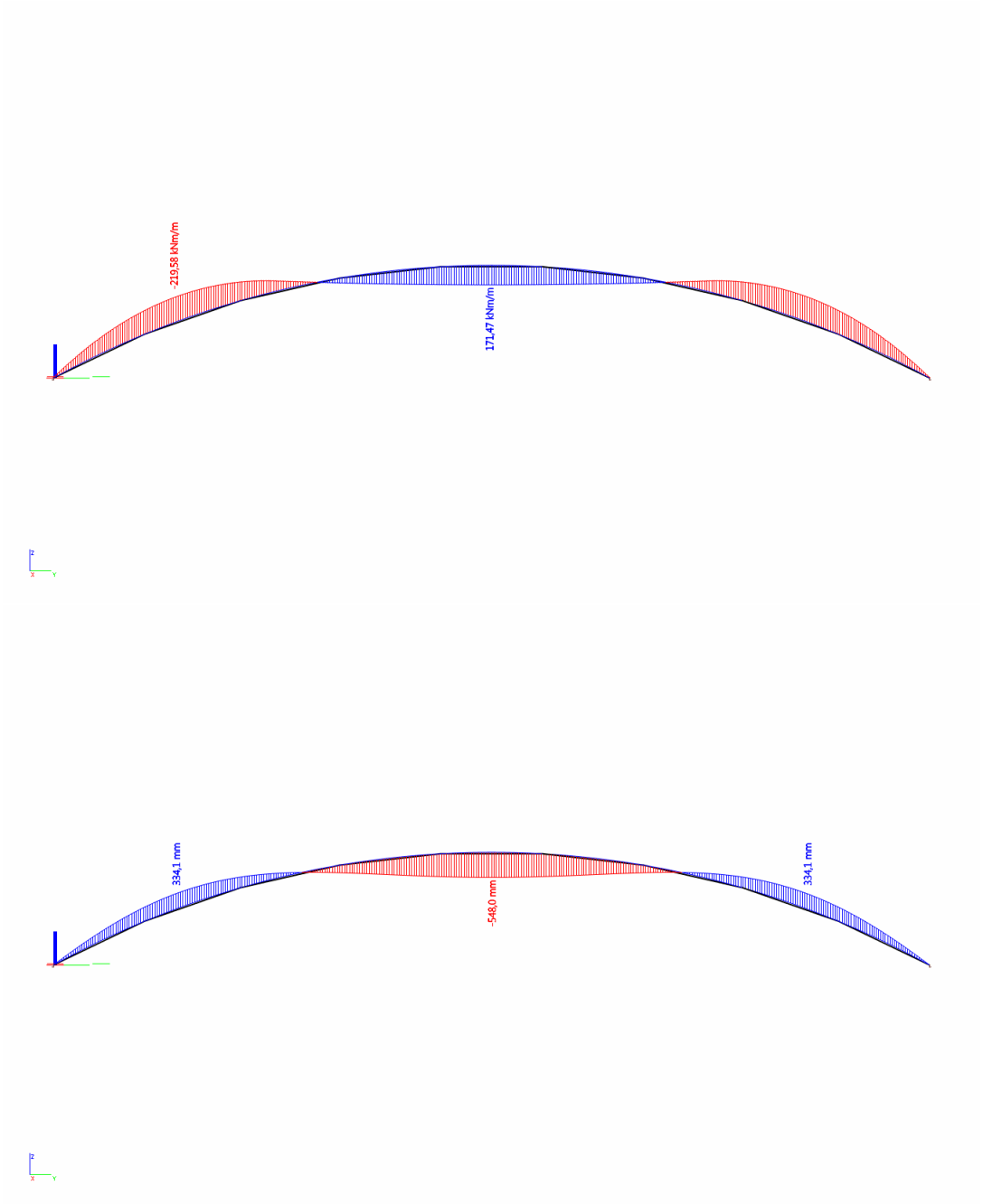

Figure 4.9: Moment line and deflection line of the cylinder structure (2 times magnified)

4.5 Asymmetrical loaded dome

In Chapter 3 a simple dome structure was analyzed (reference dome), this model can be used to compare its behavior with the Green Planet model. In order to make the comparison yet more realistic, the same reference dome is subjected to an asymmetrical

load. This simulates the load condition of Green Planet when it is only subjected to its self weight, because the back half of the model (see Figure 4.1) is approximately twice as heavy (maximum), as already mentioned. Therefore, an asymmetrical load of 4,91 kN/m^2(equal to the weight of 200 mm thick concrete) is subjected to an area covering about 500 m^2, see Figure 4.10a. Figure 4.10b shows the deformation of the reference dome after applying the asymmetrical load (and self weight).
The results are gathered in Table 4.4 (some aspects may be abbreviated because of a lack of space) and supplemented with results of the weakened dome which is loaded (asymmetrically) in exact the same way. The results are then compared to the situations without the extra load.

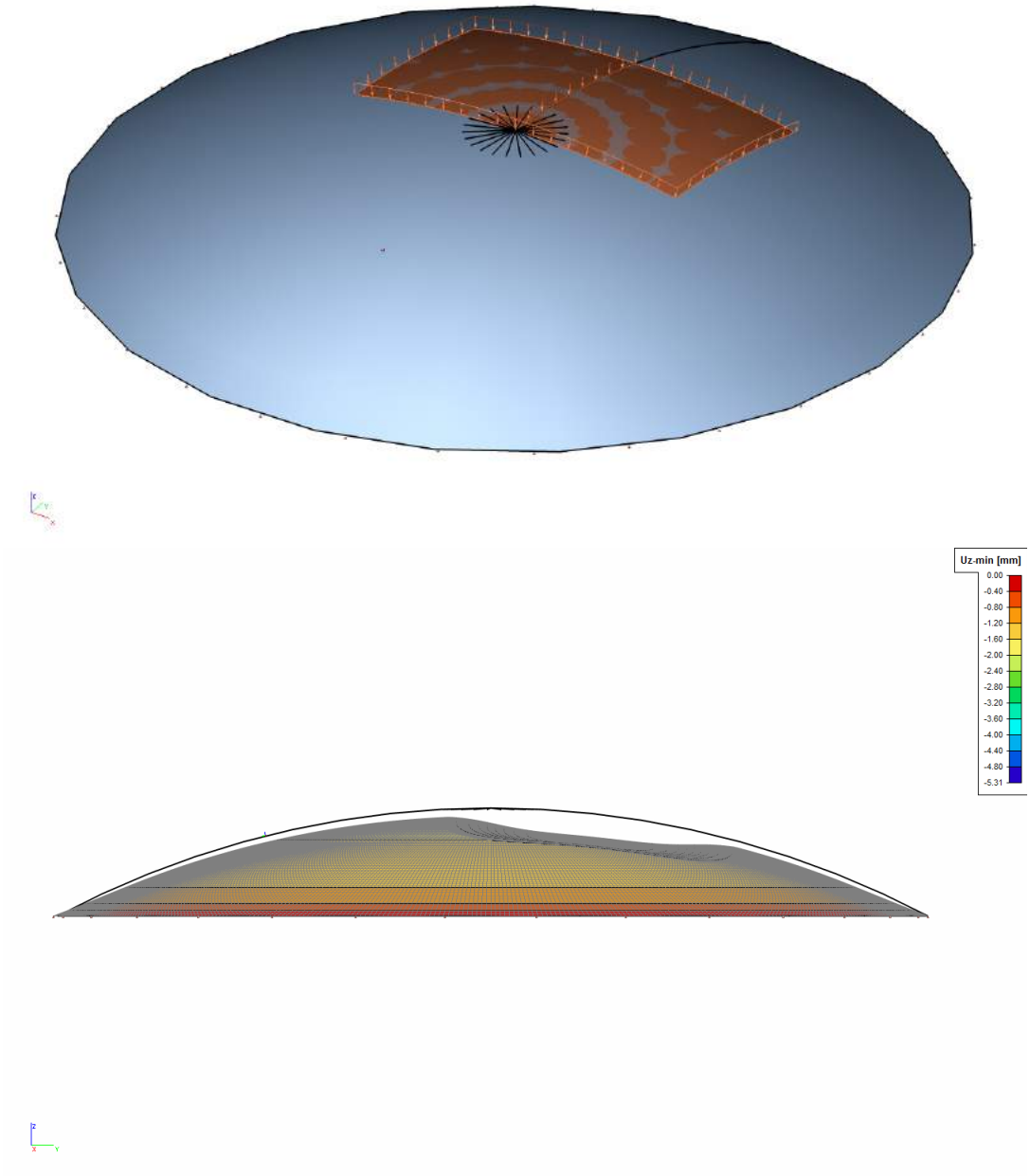

Figure 4.10: (a) The model of the reference dome subjected to an asymmetrical load (b) Deformation of the asymmetrical loaded reference dome (2 times magnified)

		Dome	Weak D	Dome AS	Weak AS	ΔDome %	ΔWeak %
Resultant force	R_z[kN]	22212	22110	24836	24412	12	10
Membrane force	$n_{\varphi\varphi}$[N/mm]	-194,7	-8,66	-302,31	-6,85	55	21
($\varphi = 0$)	$n_{\theta\theta}$[N/mm]	-194,7	-388,5	-306,45	-790,84	57	104
Membrane stress	$\sigma_{\varphi\varphi}$[N/mm^2]	-0,98	-0,04	-1,45	-0,08	48	100
($\varphi = 0$)	$\sigma_{\theta\theta}$[N/mm^2]	-0,98	-1,94	-1,47	-3,94	50	103
Membrane force	$n_{\varphi\varphi}$[N/mm]	-202,9	-202,2	-237,19	-231,97	17	15
($\varphi = 28$)	$n_{\theta\theta}$[N/mm]	-40,6	-40,4	-47,43	-46,39	17	15
Membrane stress	$\sigma_{\varphi\varphi}$[N/mm^2]	-1,01	-1,01	-1,17	-1,14	16	13
($\varphi = 28$)	$\sigma_{\theta\theta}$[N/mm^2]	-0,20	-0,21	-0,21	-0,20	1	1
Tot. supp react	R_z[kN]	22179	22468	-	-	-	-
Vert supp react	R_z[kN/m]	95,75	93,9	112,05	109,6	17	17
Horz supp react	R_H[kN/m]	178,5	179,1	209,2	206,2	17	15
Vert displacem	$u_{z;max}$ [mm]	-1,84	-1,84	-5,26	-5,39	186	193
Merid. moments	$m_{\varphi\varphi;max}$[kNm/m]	1,97	2,15	3,69	5,43	87	153
Circf. moments	$m_{\theta\theta;max}$ [kNm/m]	0,58	0,63	4,63	5,08	698	706
Crit buckl load	$p_{cr;lin}$[kN/m^2]	-321	-226	-48,58	-43,24	85	81

Table 4.4: Overview of the results of previously discussed models, including the asymmetrical loaded domes (FEA Dome AS and FEA Weak AS)

Firstly, some interesting conclusions can be drawn from Figure 4.10b. The large displacement of the structure appears to be very local, directly under the asymmetrical applied load, which indicates the stiff behavior of this shell. This, in contrast to the (single curved) arch and cylinder structure whose large displacements were noticeable over the whole surface area. The displacement (and behavior) of the asymmetrical loaded weakened dome, besides, is similar to the reference dome and the same Figure (Figure 4.10b) can be used.
Furthermore, there is a big difference in the maximum displacement between the dome and cylinder structures, as can be noticed when the $u_{z;max}$ is compared, see Table 4.5. Also the displacement increase of the dome and cylinder structures, when the asymmetrically load is applied, is very distinct being respectively $\pm$190 and $\pm$2800%.

		Dome	Weak D	Cylinder	Dome AS	Weak AS	Cylin AS
Resultant force	R_z[kN]	22212	22110	10749	24836	24412	15904
Membrane force	$n_{\varphi\varphi}$[N/mm]	-194,7	-8,66	-330	-302,31	-6,85	-600
($\varphi = 0$)	$n_{\theta\theta}$[N/mm]	-194,7	-388,5	9,89	-306,45	-790,84	48,58
Membrane stress	$\sigma_{\varphi\varphi}$[N/mm^2]	-0,98	-0,04	1,36	-1,45	-0,08	60,43
($\varphi = 0$)	$\sigma_{\theta\theta}$[N/mm^2]	-0,98	-1,94	0,64	-1,47	-3,94	13,05
Membrane force	$n_{\varphi\varphi}$[N/mm]	-202,9	-202,2	-564,38	-237,19	-231,97	-1784,28
($\varphi = 28$)	$n_{\theta\theta}$[N/mm]	-40,6	-40,4	-186,80	-47,43	-46,39	-320,76
Membrane stress	$\sigma_{\varphi\varphi}$[N/mm^2]	-1,01	-1,01	-5,68	-1,17	-1,14	-69,05
($\varphi = 28$)	$\sigma_{\theta\theta}$[N/mm^2]	-0,20	-0,21	-0,98	-0,21	-0,20	-13,73
Vert supp reaction	$R_{z,max}$[kN/m]	95,75	93,90	264,96	112,05	109,60	473,73
Horz supp reaction	$R_{H,max}$[kN/m]	178,50	179,10	498,32	209,20	206,20	890,96
Vert displacement	$u_{z;max}$ [mm]	-1,84	-1,84	-64,2	-5,26	-5,39	-1874,70
Merid. moments	$m_{\varphi\varphi;max}$[kNm/m]	1,97	2,15	25,47	3,69	5,43	436,31
Circumf. moments	$m_{\theta\theta;max}$ [kNm/m]	0,58	0,63	5,27	4,63	5,08	90,19
Crit buckling load	$p_{cr;lin}$[kN/m^2]	-321	-226	-3,05	-48,58	-43,24	0,88

Table 4.5: Overview of the results of previously discussed models, including the asymmetrical loaded domes (FEA Dome AS and FEA Weak AS)

Now the results (Table 4.5) of the asymmetrical loaded dome and weakened dome are discussed in comparison to the earlier calculated symmetrical ones. The most remarkable differences (where the increase is larger than the resultant force increase) when applying the asymmetrical load are the membrane forces/stresses at the top, the vertical displacement, the moments and the critical buckling load.
The results meet the expectations, for example the membrane forces and stresses increases which are around four times as high compared to the resultant force increase. The resultant force increase includes the applied load and compares it to the total load which is ten times larger, while these membrane forces increases happen locally around the applied load. So it's hard to compare these increases, but it makes sense that the membrane forces have a larger increase. Furthermore, the maximum vertical displacement increases with almost 200%, this is a large increase but not even close to the increase of 2830% which was found for the asymmetrical loaded cylinder (Table4.3). So, a major distinction is emerging here, between the two different asymmetrical loaded shell structures. Also, when a closer look is taken at the moments it can be concluded that the cylinder has larger increases. Where the increase for the domes is $\pm$700% it is $\pm$1650% for the cylinder structure. Again, the influence of the second curvature is well reflected in the results. Table 4.5, then, shows the difference in critical buckling load between the three asymmetrical loaded shell structures. It shows that the dome structures are much more stable, as expected, and that the difference in stability is very large.

4.6 Green Planet analysis

In the introduction of this chapter the Green Planet model was introduced, see Figure 4.1. In this section the behavior of the model is briefly discussed while in the next section it will

be compared to the previously treated shell structures. The dimensions of the model are given in Table 4.6a, those dimensions were tried to apply to all previous discussed shell structures as good as possible. This holds for the material properties and boundary conditions as well, see Table 4.6b.
In this analysis the Green Planet model is only subjected to its self weight. The results are determined by linear calculation and gathered in Table 4.7. Figures 4.11 and 4.12 provide an insight in the deformation of the shell structure loaded by its self weight.

Geometry Green Planet	Dimension
Angle (φ)	27,66 degrees
Sagitta (s)	9080 mm
Span (d)	73730 mm
Vertical radius of curvature (r1)	79400 mm
Thickness (t)	200 mm
Shell surface area	$\pm$2500 m^2
r1/t	400
d/s	8

Parameter	Characteristic
E_{mod} (C90/105)	43600 N/mm^2
$f_{c;d}$ (C90/105)	60 N/mm^2
Density (C90/105)	2500 kg/m^3
Poisson's ratio (ν)	0 (0,2)
Loading	Deadweight
p (vertical load)	0,004905 N/mm^2
Supports Green Planet	Hinged
Knockdown factor (C)	1/6
Meshsize	200 mm (t)

Table 4.6: Green Planet dimensions and characteristics: (a) Geometrical dimensions (b) Material properties and boundary conditions

		BG1
Resultant force	$R_{z;res}$[kN]	12230
First principal membrane force	$n_{1;max}$ [N/mm]	420
Second principal membrane force	$n_{2;min}$ [N/mm]	-1451
First principal moment	$m_{1;max}$ [kNm/m]	20,4
Second principal moment	$m_{2;min}$ [kNm/m]	-26,0
First principal membrane stress	$\sigma^{-}{}_{1;max}$ [N/mm^2]	4,55
Second principal membrane stress	$\sigma^{-}{}_{2;min}$ [N/mm^2]	-8,87
Vert. support reaction, z-direction	$R_{z;max;up}$ [kN/m]	573
Vert. support reaction, z-direction	$R_{z;max;down}$ [kN/m]	-90,3
Horiz. support reaction, y-direction	$R_{y;max}$ [kN/m]	1074
Horiz. support reaction, y-direction	$R_{y;min}$ [kN/m]	-139
Horiz. support reaction, x-direction	$R_{x;max}$ [kN/m]	607
Horiz. support reaction, x-direction	$R_{x;min}$ [kN/m]	-607
Vertical displacement	$u_{z;max;up}$ [mm]	10,9
Vertical displacement	$u_{z;max;down}$ [mm]	-20,5
Critical buckling load	$p_{cr;lin}$ [kN/m^2]	8,15
Second critical buckling load	$p_{cr;lin;2}$ [kN/m^2]	8,74
Difference between buckling loads	$\Delta p_{cr,lin}$[%]	7

Table 4.7: Results of the Green Planet model, loaded only by its self weight

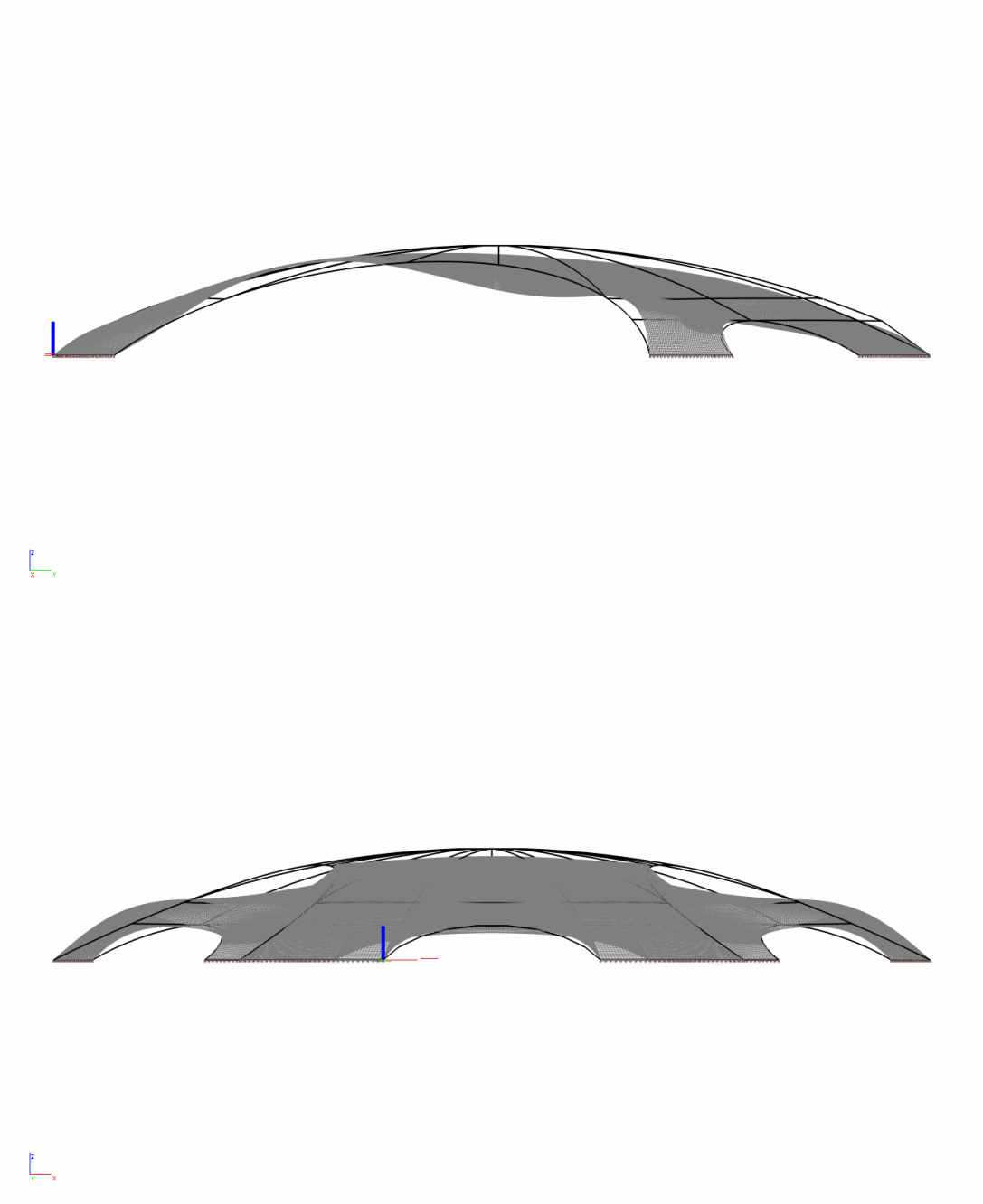

Figure 4.11: Deformation Green Planet, loaded only by its self weight, view from aside and from the back side (image is 2 times magnified)

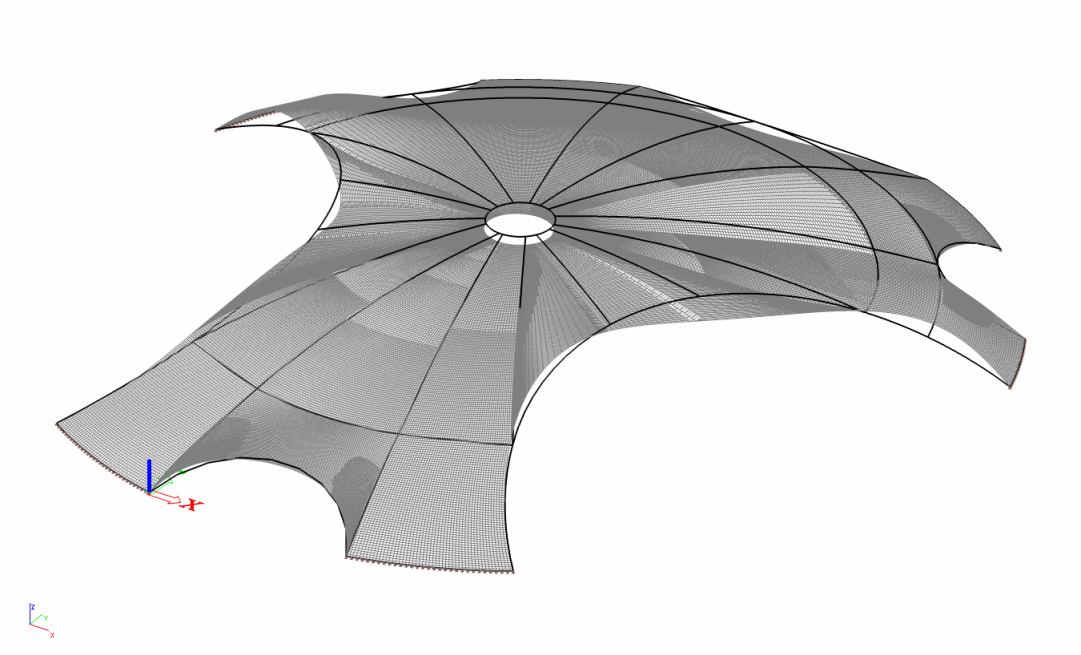

Figure 4.12: Deformation Green Planet, loaded only by its self weight, view from above (image is 2 times magnified)

Now, a brief comment on the results of Table 4.7 will be given, in the next chapter the results will be compared to the other discussed models. The principal membrane forces of the unloaded shell structure of Green Planet are not too large: when the maximum membrane (circumferential) force is compared to the compressive design strength of the concrete in combination with the thickness, it can be concluded that the shell can easily resist this force. The occurring moments, however, are quite large for a concrete shell which is (in this stage) not reinforced. Together with the membrane forces they yield a maximum membrane stress of 4,55 N/mm^2, this value approaches the average tensile strength of 5,10 N/mm^2 (C90/105). So, in a later stage adding reinforcement is a must for this concrete shell structure.
Furthermore, it can be noticed that the support reaction forces are large. The forces acting on the foundation are not equally spread over the width causing large peak forces. Additionally, the available foundation space is limited, compared to other discussed models, forcing the structure to transfer all the loads rather concentrated. The displacements, however, are surprisingly small for a structure which spans almost 75 meters.
The critical buckling load is small for a, yet, unloaded structure, because eventually a minimum critical buckling load of 6 is required (a factor for imperfections must be applied) . In next chapters the results and requirements of Green Planet will be discussed in detail. This chapter is about comparing results and in the next section the results of Green Planet will be compared to results of the other models.

4.7 Comparison

In previous sections the behavior and characteristics of the dome, weakened dome, arch, cylinder structure and asymmetrical loaded equivalents were discussed. In this section the Green Planet model will be compared to the three distinct models that simulate the behavior best: the asymmetrical loaded dome, weakened dome and cylinder structure. The results of those three models are gathered in Table 4.8 and compared to the results of Green Planet.

		Green Planet	Dome AS	Weak AS	Cylinder AS
Resultant force	R_z[kN]	12230	24836	24412	15904
Membrane force	$n_{\varphi\varphi}$[N/mm]	-771,56	-302,31	-6,85	-600
($\varphi = 0$)	$n_{\theta\theta}$[N/mm]	112,47	-306,45	-790,84	48,58
Membrane stress	$\sigma_{\varphi\varphi}$[N/mm^2]	-4,42	-1,45	-0,08	60,43
($\varphi = 0$)	$\sigma_{\theta\theta}$[N/mm^2]	1,11	-1,47	-3,94	13,05
Membrane force	$n_{\varphi\varphi}$[N/mm]	-1450,85	-237,19	-231,97	-1784,28
($\varphi = 28$)	$n_{\theta\theta}$[N/mm]	-445,33	-47,43	-46,39	-320,76
Membrane stress	$\sigma_{\varphi\varphi}$[N/mm^2]	-8,03	-1,17	-1,14	-69,05
($\varphi = 28$)	$\sigma_{\theta\theta}$[N/mm^2]	-2,10	-0,21	-0,20	-13,73
Max membrane force	$n_{1;max}$ [N/mm]	420,17	-43,83	8,87	9215,47
Min membrane force	$n_{2;min}$ [N/mm]	-1450,85	-476,60	-799,39	-18681,80
Max membrane stress	$\sigma^-{}_{1;max}$ [N/mm^2]	4,55	-0,13	0,12	60,24
Min membrane stress	$\sigma^-{}_{2;min}$ [N/mm^2]	-8,87	-2,38	-3,90	-80,64
Max meridional moments	$m_{\varphi\varphi;max}$[kNm/m]	26,33	3,69	5,43	436,31
Max circumf. moments	$m_{\theta\theta;max}$ [kNm/m]	20,42	4,63	5,08	90,19
Vert. support reaction	$R_{z,max}$[kN/m]	681,13	112,05	109,60	473,73
Horiz. support reaction	$R_{H,max}$[kN/m]	1281,02	209,20	206,20	890,96
Vert. displacement	$u_{z;max}$ [mm]	20,50	5,26	5,39	1874,70
Critical buckling load	$p_{cr;lin}$[kN/m^2]	8,10	31,42	26,21	0,42

Table 4.8: Overview of the results of previously discussed models, including the asymmetrical loaded dome (FEA Dome asymm)

		ΔDome %	ΔWeak %	ΔCylinder %
Resultant force	R_z[kN]	103	99,6	30,0
Membrane force	$n_{\varphi\varphi}$[N/mm]	-60,8	-99,1	-22,2
($\varphi = 0$)	$n_{\theta\theta}$[N/mm]	-172	-603	-56,8
Membrane stress	$\sigma_{\varphi\varphi}$[N/mm^2]	-67,2	-98,2	-1267
($\varphi = 0$)	$\sigma_{\theta\theta}$[N/mm^2]	-232	-455	1076
Membrane force	$n_{\varphi\varphi}$[N/mm]	-83,7	-84,0	23,0
($\varphi = 28$)	$n_{\theta\theta}$[N/mm]	-89,3	-89,6	-28,0
Membrane stress	$\sigma_{\varphi\varphi}$[N/mm^2]	-85,4	-85,8	760
($\varphi = 28$)	$\sigma_{\theta\theta}$[N/mm^2]	-90,0	-90,5	554
Max membrane force	$n_{1;max}$ [N/mm]	-110	-97,9	2093
Min membrane force	$n_{2;min}$ [N/mm]	-67,2	-44,9	1188
Max membrane stress	$\sigma^-{}_{1;max}$ [N/mm^2]	-103	-97,4	1224
Min membrane stress	$\sigma^-{}_{2;min}$ [N/mm^2]	-73,2	-56,0	809
Max meridional moments	$m_{\varphi\varphi;max}$[kNm/m]	-86,0	-79,4	1557
Max circumf. moments	$m_{\theta\theta;max}$ [kNm/m]	-77,3	-75,1	342
Vert. support reaction	$R_{z,max}$[kN/m]	-83,5	-83,9	-30,4
Horiz. support reaction	$R_{H,max}$[kN/m]	-83,7	-83,9	-30,4
Vert. displacement	$u_{z;max}$ [mm]	-74,3	-73,7	9045
Critical buckling load	$p_{cr;lin}$[kN/m^2]	-288	-224	94,8

Table 4.9: Overview of the results of previously discussed models, given is the difference between Green Planet and the indicated model

Among the resultant forces of the four different models Green Planet has the smallest. The expectation is, simply stated, that with a larger resultant force comes a larger value for whatever force, stress or moment is determined. When this expectation is not met for the difference between the result of Green Planet and another model, a minus is added to the percentage indicating the difference.
The first thing that can be noticed is that all values of the asymmetrical loaded dome and weakened dome are smaller compared to Green planet, despite their resultant force being twice as large. The opposite holds for the asymmetrical loaded cylinder, which resultant force is thirty percent higher but which results are often much higher compared to Green Planet. So, the first impression is that the results of Green Planet lie in between the results of the dome-type structures and the cylinder structure.
The hypothesis stated in last paragraph is supported by the results for the maximum and minimum membrane forces/stresses and moments of the models. The results of the dome and weakened dome are 44 to 110 % smaller compared to Green Planet. The results of the weakened dome approach the results of Green Planet best, which is logical. The results of the cylinder structure, however, are larger and in some occasions very large, compared to Green Planet. Also, the structure is not safe in strength and stability and therefore the cylinder structure is hard to compare to Green Planet. So, an asymmetrically loaded cylinder structure with dimensions and material strength comparable to Green Planet is very hard to realize.
Although the cylinder structure is loaded to its maximum its support reactions are still smaller than needed for Green planet. The reason is the load is transferred rather

concentrated and Green planet is prone to peak forces, more than the other models. Nevertheless, the foundation conditions of Green Planet are most comparable to the cylinder structure, not only because of the size of the support reactions but also because of the way the structure deforms and the effect of it on the foundation. This becomes clear when the deformations in Figure 4.8 and Figure 4.11 are compared, both structures deform downwards where the load is at its maximum and upwards on the other side to compensate large downward forces and deformation. Additionally, large (edge) moments are necessary to retain the structures shapes. Whereas for the domes the (largest) moments and deformations happen very locally, as pictured in Figure 4.10b. So, although the deformation of the weakened dome is closest to the maximum value of Green planet, it is the overall deformation behavior of the cylinder structure that matches the Green planet best.
Also for the stability of Green Planet holds that its value lies in between the other structure types. A closer look is taken at the buckling mode of the three shell structures. The weakest area of the weakened dome, where the shell buckles first, is around the oculus (Figure4.13a). The other buckling modes happen around the oculus as well or locally under the asymmetrically applied load (Figure4.13b). The cylinder structure buckles differently, in the three most critical cases the structure buckles over the whole width of the structure (Figure 4.14a). The fourth buckling mode of the cylinder structure, however, shows it buckles locally too (Figure 4.14b). It buckles near the edges and this mode is quite similar to the buckling modes of Green Planet (Figure 4.15a and 4.15b), where the first buckling mode tends to buckle over the whole width as well. So, in this case Green Planet behaves quite similar to the cylinder structure, but where the cylinder structure fails Green Planet doesn't because the double curvature adds a lot to the stiffness to the structure.

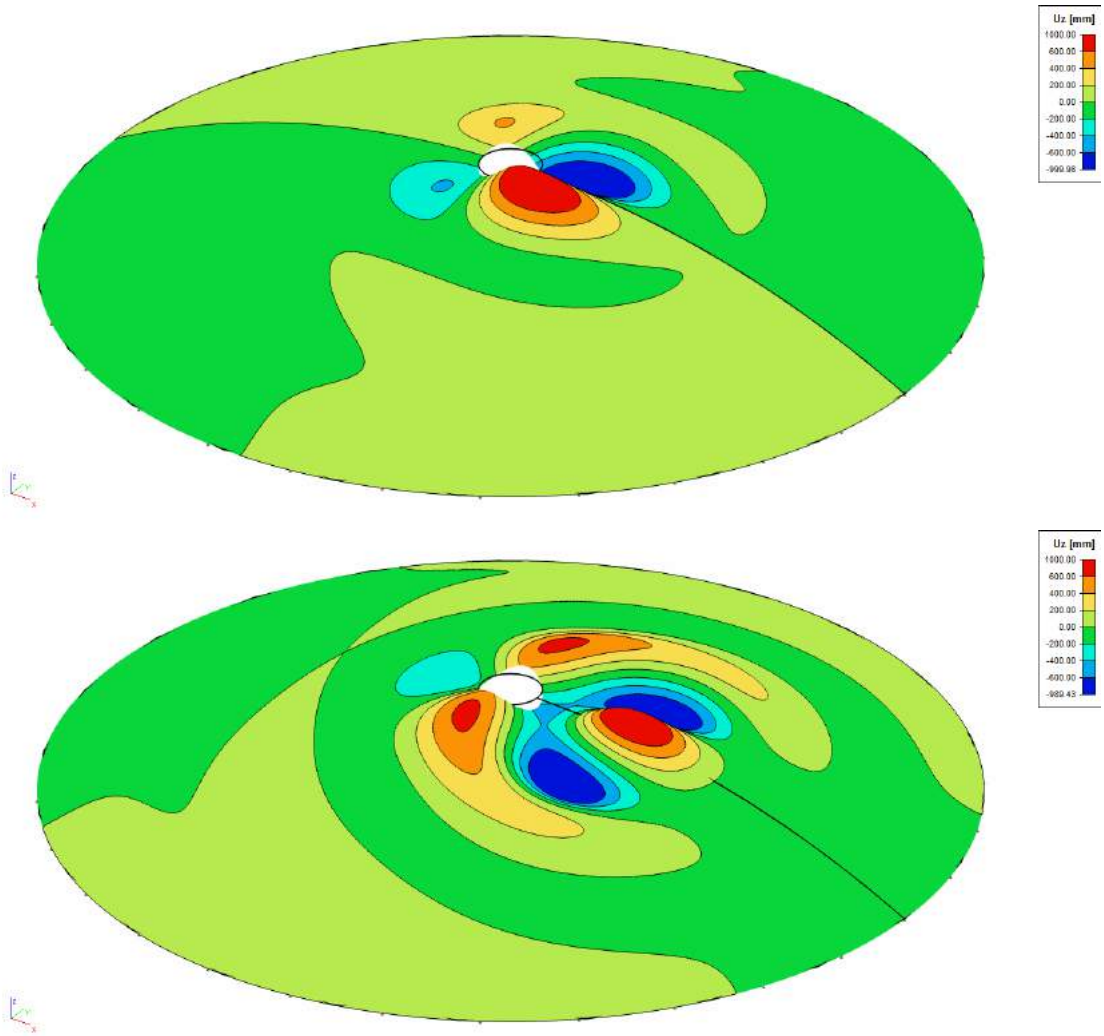

Figure 4.13: (a) First buckling mode weakened dome (b) Fourth buckling mode weakened dome

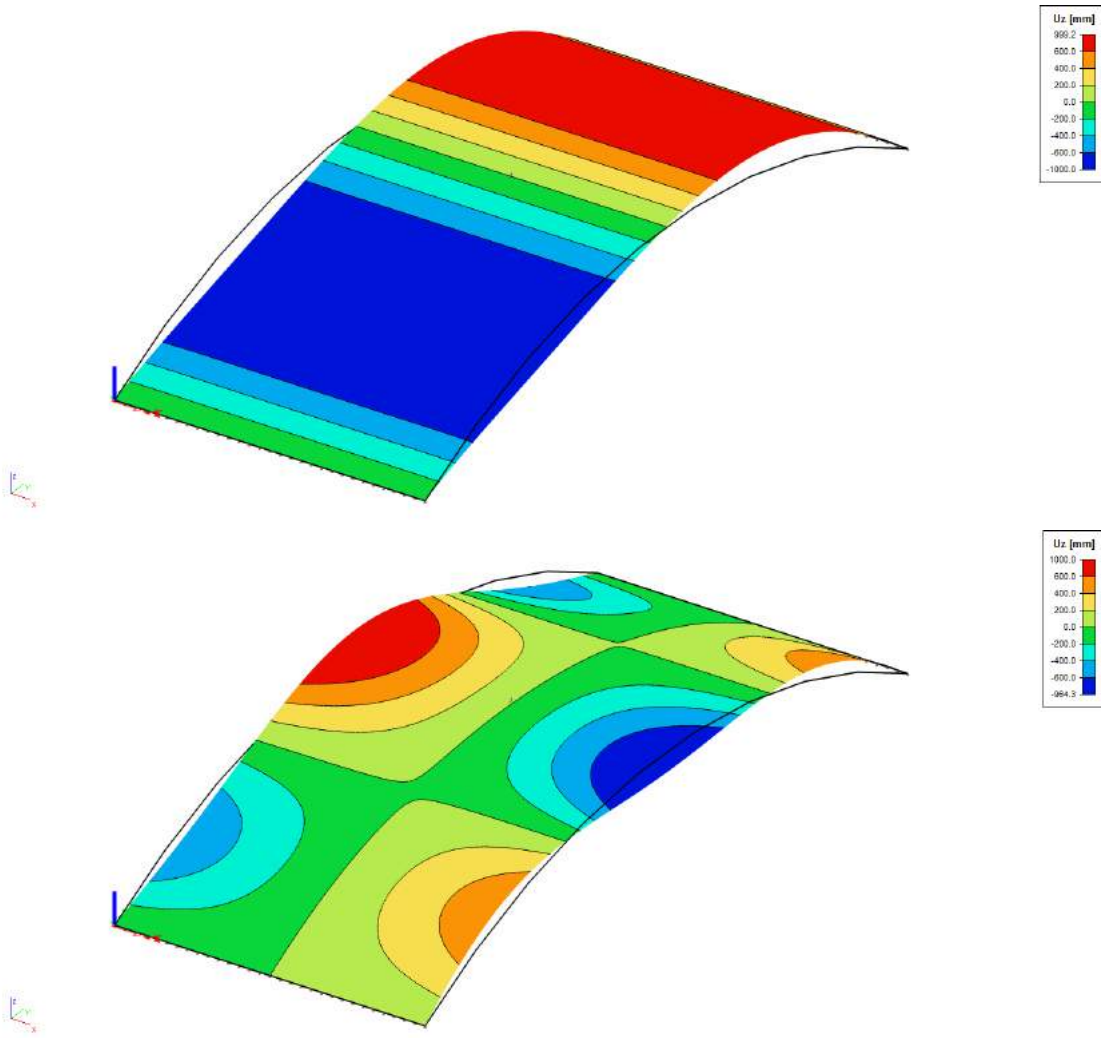

Figure 4.14: (a) First buckling mode cylinder structure (b) Fourth buckling mode cylinder structure

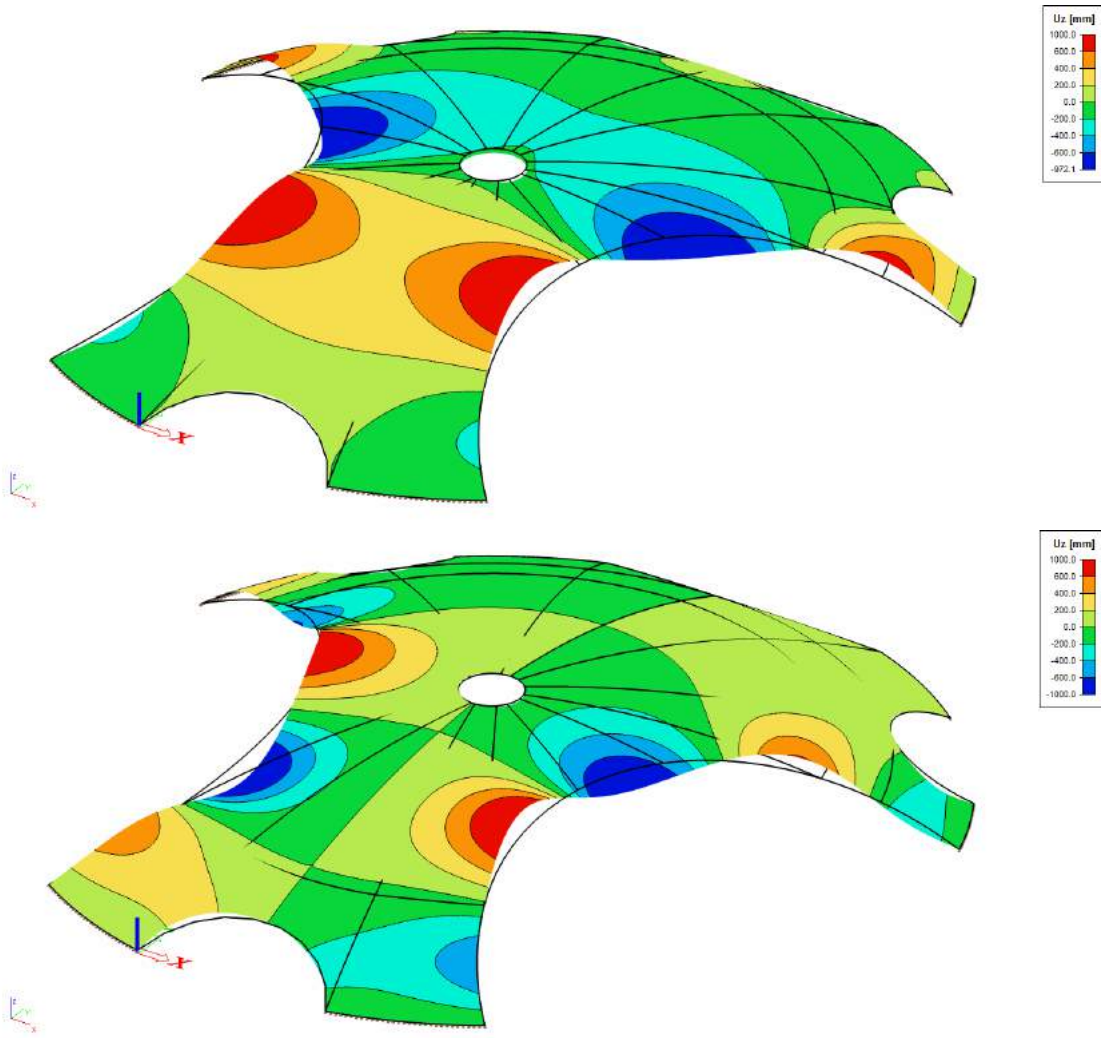

Figure 4.15: (a) First buckling mode Green Planet (b) Fourth buckling mode Green Planet

The results of Table 4.8 can also be used to investigate the behavior of Green Planet and see whether and how they relate to the results of simpler models. The conclusion is that they do relate to the other models. The meridional and circumferential forces and stresses at the top and bottom of Green Planet are most comparable to the values found for the cylinder structure. The size of the maximum moments, however, tend to be more like the weakened dome but the differences are not pronounced. This also holds for the maximum membrane forces and stresses, for which it must be noted that they happen very locally. The maximum support reactions of Green Planet and the cylinder structure match best, although the total length of the foundation has its influence here. Furthermore, the maximum displacement of Green Planet is rather small and is best compared with the weakened dome. The second curvature has a stiffening effect in this case, the differences with the cylinder structure are very large. This stiffness has a beneficial effect on the critical buckling load as well. Still the bending and buckling behavior of Green Planet matches the cylinder structure best as explained before. So the values of the bending and buckling behavior of Green Planet are

more similar to the weakened dome, while the actual bending and buckling behavior matches the cylinder structure best. Based on these observations it can really be concluded that Green Planet can best be identified as a cylinder structure with a second curvature which adds to the stiffness.

4.8 Discussion

Two goals were set in the first section of this chapter and these are briefly discussed in this section. The behavior of Green Planet can be judged upon a few typical properties it possesses: deformation, force distribution, moment distribution, support reactions and stability. Those properties were determined with the FEA program by linear analysis and this was also done for three other similar shell structures, the asymmetrically loaded dome, weakened dome and cylinder structure. The results were gathered in Table 4.8 and discussed in last section. The conclusion of Table 4.8 was that, mainly based upon the deformation and buckling behavior, Green Planet is best compared with the cylinder structure. However, due to the double curvature of Green Planet its values won't always agree with those of the single curved cylinder structure. Green Planet behaves stiffer, just like domes are much stiffer too.
The results of Table 4.8 point out that the values that represent Green Planet are in line with the results of other models that were examined. Also, the deformation and buckling behavior was comparable. So the FEA model is simulating an acceptable behavior of Green Planet.

Chapter 5

Design Green Planet analysis

5.1 Introduction

In this chapter the Green Planet model is analyzed and in the end optimized. First, the boundary conditions are set and the loads are determined. With a detailed analysis the normative loads for the Green Planet design are obtained.
The double-curved shell structure model is one of a kind and therefore general rules about applying a mesh might not suffice. A short study determines a suitable mesh for the model. Also, the influence of the thickness and the material strength is analyzed. Subsequently, a Green Planet model with optimized thickness and material strength is presented.
These analyzes give a good indication of the support reactions and it's possible to design a foundation. Several foundation options are considered and analyzed to present a suitable solution for Green Planet.

5.2 Loading

Supports Before going in detail on the loading it is important to set the boundary condition for the supports. For the support of the design there are two options left. A roller support is not an option because the shallow shell results in high thrust forces. That leaves the options clamped support and hinged support. Table 5.1 mentions the pros and cons of the two options.

	Clamped support	Hinged support
Pro	Reduction buckling length	Relatively easy to build
	Reduces the deformation in the shell	Forces on the support are not much higher
		Thrust forces can be taken by e.g. a tension ring
Con	Big forces and moments at the support	The buckling length is slightly larger
	A full inclination is hard to realize	
	Especially in Holland because of the soil	
	Settlements will provoke extra bending moments	

Table 5.1: Comparison clamped and hinged support [30]

It can be concluded that the hinged support is in favor over the clamped support. Simply because there are more disadvantages for the clamped support and the realization for the hinged support is easier.

5.2.1 Permanent loads

- Concrete: $q = 2500[kg/m^3] * 9,81[m/s^2] * 0,2[m] = 4,905[kN/m^2]$
- Roofing + Green roof is estimated on $1,0[kN/m^2]$ [51]. This source points out that an average sedum roof has a vegetation layer of 20 mm plus a drainage layer of 50 mm which together, when fully saturated, form a load of 90 kg/m^2. This value is backed up by a phone call with the people from Jalving, Emmen, the company which installed the sedum roof for Green Planet, they pointed out that the load of the vegetation is around 4,5 kg/m^2 and when saturated an extra 90 kg/m^2 is added, just as the research pointed out.

5.2.2 Variable loads

- Snow
- Wind
- Person for maintenance (yearly fertilizing and weeding of the sedum roof for example): point load with an approximate load of 1,0 kN/m^2 per 0,1[m]x0,1[m], for now not taken as governing load

Wind

- Basic wind velocity (Area III): $v_b = 24,5[m/s]$
- Exposure factor $C_e(z)$ (Area II): $C_e(9[m]) = 2,3$
- Peak velocity pressure:
  $q_p(9[m]) = 1,25[kg/m^3] * 0,5 * 2,3 * 24,5^2[m/s] = 0,86[kN/m^2]$
- External wind pressure: $w_e = q_p(z_e) * c_{pe,10}$
- Aerodynamic effects of the structure described by $c_{pe,10}$, incorporating depending on the geometry: internal/external pressure for buildings, nett pressure, friction and force.
- The sagitta/span (f/d) ratio is 0,123 and there's no 'base' for this shell (see image on top of 5.1) which means h/d is zero. These parameters are needed for the determination of the external pressure coefficient, see Figure 5.1, where the first light blue line marks 0,123 and the second can be ignored. Table 5.2 calculates the external wind pressure on the shell with the obtained pressure coefficient. The area indication for the model is clarified in Figure 5.2. For zone C half of the load of zone B is taken.

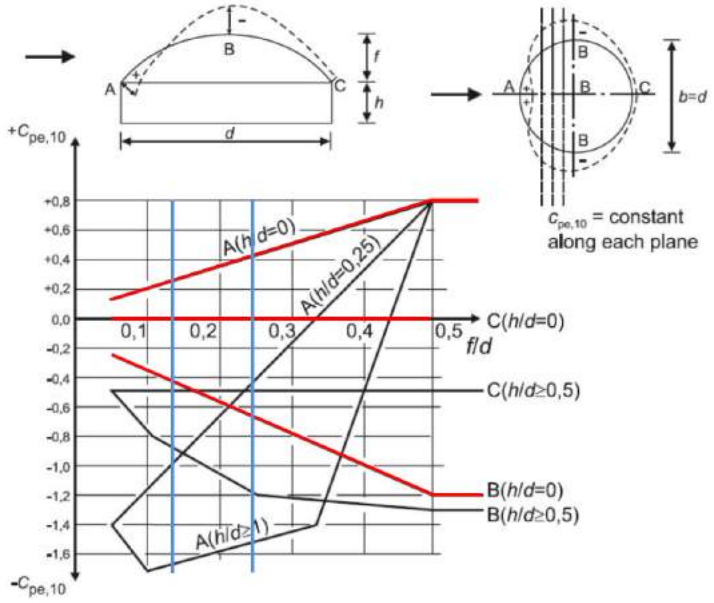

Figure 5.1: Recommended values for external wind pressure coefficients for spheres [46]

	$c_{pe,10}$	$w_e[kN/m^2]$
Zone A	0,26	0,23
Zone B	-0,41	-0,36
Zone C	-0,21	-0,18

Table 5.2: External pressure on the sphere

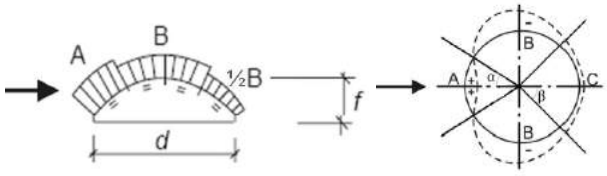

Figure 5.2: (a) External wind pressure schematized for cylindrical roofs and (b) top scheme for spheres[46]

The wind loads from the external pressure are rather small, because at the same time the shell with its openings can be considered a canopy, these values are determined. The following data is from Eurocode 2 EN 1991-1.4, wind actions. Duo pitched roofs/canopies are categorized in two groups, one where wind is blocked inside and one where this doesn't happen. In this case, for Green Planet, both cases apply. This yields the internal and external wind pressures as given in Table 5.3. It must be mentioned that these values apply to a pitched roof which isn't curved like the shell, this could be favorable for aerodynamics and with that the downward wind load, but for now these values are used. The load combinations are shown in Figure 5.3. Because the wind loads for the canopy are

unfavorable compared to the ones determined before with the external wind pressure, these values will be used for the design.

	c_f	$w_e[kN/m^2]$
Upward pressure (blocked)	-1,3	-1,12
Upward pressure (not blocked)	-1,0	-0,86
Downward pressure	+0,8	+0,69

Table 5.3: Internal and external pressure on the shell structure

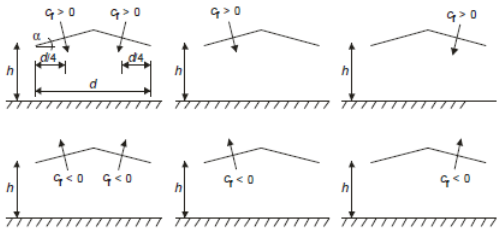

Figure 5.3: Possible windload combinations, from Eurocode 2 EN 1991-1.4

5.2.3 Snow

- Based on cylindrical roofs
- According to the code, snow load on ground level is $s_k = 0,70[kN/m^2]$
- For the roof load by snow the next formula holds: $s = \mu_i * C_e * C_t * s_k$
- The exposure factor C_e is 0,8 and the Thermal factor C_t is 1,0.
- The roof shape coefficient μ_i is 0,8 for case a, see Figure 5.4, and for the drifted snow (case b) μ_i is 1,2 (For an angle of 28 degrees, from Eurocode 2 EN 1991-1.3)
- On both sides the snow will be distributed like demonstrated in Figure 5.5. The largest load will be placed on the back since this is the most unfavorable distribution
- The results for the snow loads are gathered in Table 5.4

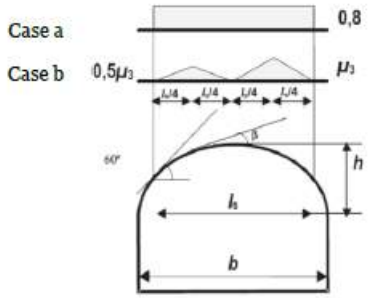

Figure 5.4: Shape coefficients for snow load on cylindrical roofs, from Eurocode 2 EN 1991-1.3

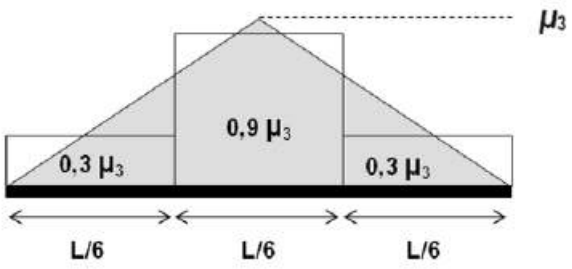

Figure 5.5: Shape coefficients for snow load on cylindrical roofs, from Eurocode 2 EN 1991-1.3

	$s[kN/m^2]$
Snow load (undrifted)	0,45
Snow load (drifted) front min/max	0,1/0,31
Snow load (drifted) back min/max	0,2/0,61

Table 5.4: Snow loads

5.2.4 Safety factors

The factors that guarantee the safety of the building are provided by NEN-EN 1990 (+A1+A1/C2-2011-nl). The consequence of a possible collapse is categorized by means of a consequence class and in this case a collapse of the roof of the gas station could have a significant economical and social impact, therefore it can be assigned to consequence class 2 (CC2). This class is related to the reliability class and therefore the building is assigned to reliability class 2 (RC2) as well. The associated safety factors are given in Table 5.5.

		permanent	variable
ULS	unfavorable	1,2	1,5
	favorable	0,9	0
SLS	unfavorable	1,0	1,0
	favorable	1,0	1,0

Table 5.5: Safety factors

5.2.5 Load combinations

The load combinations that will be applied are summed up in Table 5.6. All combinations will be calculated in the ultimate limit state (ULS), including the deflection. Normally the deflection is calculated in the serviceability limit state (for useability, SLS) but to reduce the amount of combinations they are now calculated in the ULS. The last combination considers merely the self weight of the structure, this load case is suitable to compare the model with the reference domes.

Combination	permanent	variable
Com1	self weight and roofing	snow (undrifted)
Com2	self weight and roofing	wind (upward)
Com3	self weight and roofing	wind (downward)
Com4	self weight and roofing	snow (drifted, large load on back half)
Com5	self weight and roofing	wind (downward, on back half)
Com6	self weight and roofing	wind (downward, on front half)
Com7	self weight and roofing	wind (upward, on back half)
Com8	self weight and roofing	wind (upward, on front half)
BG1	self weight (no safety factor)	

Table 5.6: Load combinations for the model of Green Planet

5.3 Analysis Green Planet

All mentioned load combinations together with their safety factors are applied to the Green Planet model. In this section the model is subjected to a geometrical and physical linear analysis. The mesh size is 0,2m, which was found to give good results. The material properties are the same as used for previous reference models (C90/105). The thickness is 200 mm (which was applied to the reference dome as well for comparison) which can be considered a minimum for the Green Planet model. The results of the analysis are shown in Table 5.7 where the most critical values are marked in red.

	Com1	Com2	Com3	Com4	Com5	Com6	Com7	Com8	BG1	Extreme
$R_{z;res}$[kN]	19351	13659	20138	18790	19201	18601	15174	16147	12230	20138
$n_{1;max}$ [N/mm]	665	607	674	661	739	607	607	845	420	845
$n_{2;min}$ [N/mm]	-2300	-2096	-2370	-2140	-2721	-2096	-2096	-2694	-1451	-2721
$m_{1;max}$ [kNm/m]	32,3	29,5	33,4	33,1	37,5	29,5	29,5	39,6	20,4	39,6
$m_{2;min}$ [kNm/m]	-41,7	-38,0	-43,0	-41,2	-51,4	-38,0	-38,0	-51,7	-26,3	-51,7
$\sigma^{-}{}_{1;max}$ [N/mm^2]	7,19	6,57	7,16	7,21	8,38	6,57	6,57	8,43	4,55	8,43
$\sigma^{-}{}_{2;min}$ [N/mm^2]	-14,3	-13,0	-14,8	-14,3	-16,6	-13,0	-13,0	-15,9	-9,0	-16,6
$R_{z;max;up}$ [kN]	181	165	186	170	195	165	165	187	115	195
$R_{z;max;down}$ [kN]	-28,7	-26,2	-31,3	-32,3	-47,4	-26,2	-26,2	-52,4	-18	-52,4
$R_{y;max}$ [kN]	340	310	349	319	366	310	310	338	215	366
$R_{y;min}$ [kN]	-246	-225	-260	-244	-309	-225	-225	-304	-155	-309
$R_{x;max}$ [kN]	192	175	198	184	243	175	175	242	121	243
$R_{x;min}$ [kN]	-192	-175	-198	-184	-243	-175	-175	-242	-121	-243
$u_{z;max;up}$ [mm]	17,1	15,6	17,5	16,5	23,7	15,6	15,6	27,1	10,8	27,1
$u_{z;max;down}$ [mm]	-32,3	-29,4	-33,1	-30,8	-42,0	-29,4	-29,4	-43,8	-20,4	-43,8
$p_{cr;lin}$ [kN/m^2]	5,15	7,46	4,91	5,29	5,02	5,37	6,57	5,78	8,15	4,91
$p_{cr;lin;2}$ [kN/m^2]	5,52	7,99	5,26	5,72	5,50	5,62	6,75	6,43	8,74	5,26
$\Delta p_{cr,lin}$[%]	7	7	7	8	10	5	3	11	7	5

Table 5.7: Results for all the different load combinations

In the next figures all the extreme values are gathered to form the most unfavorable situation for the particular unknown that is calculated.

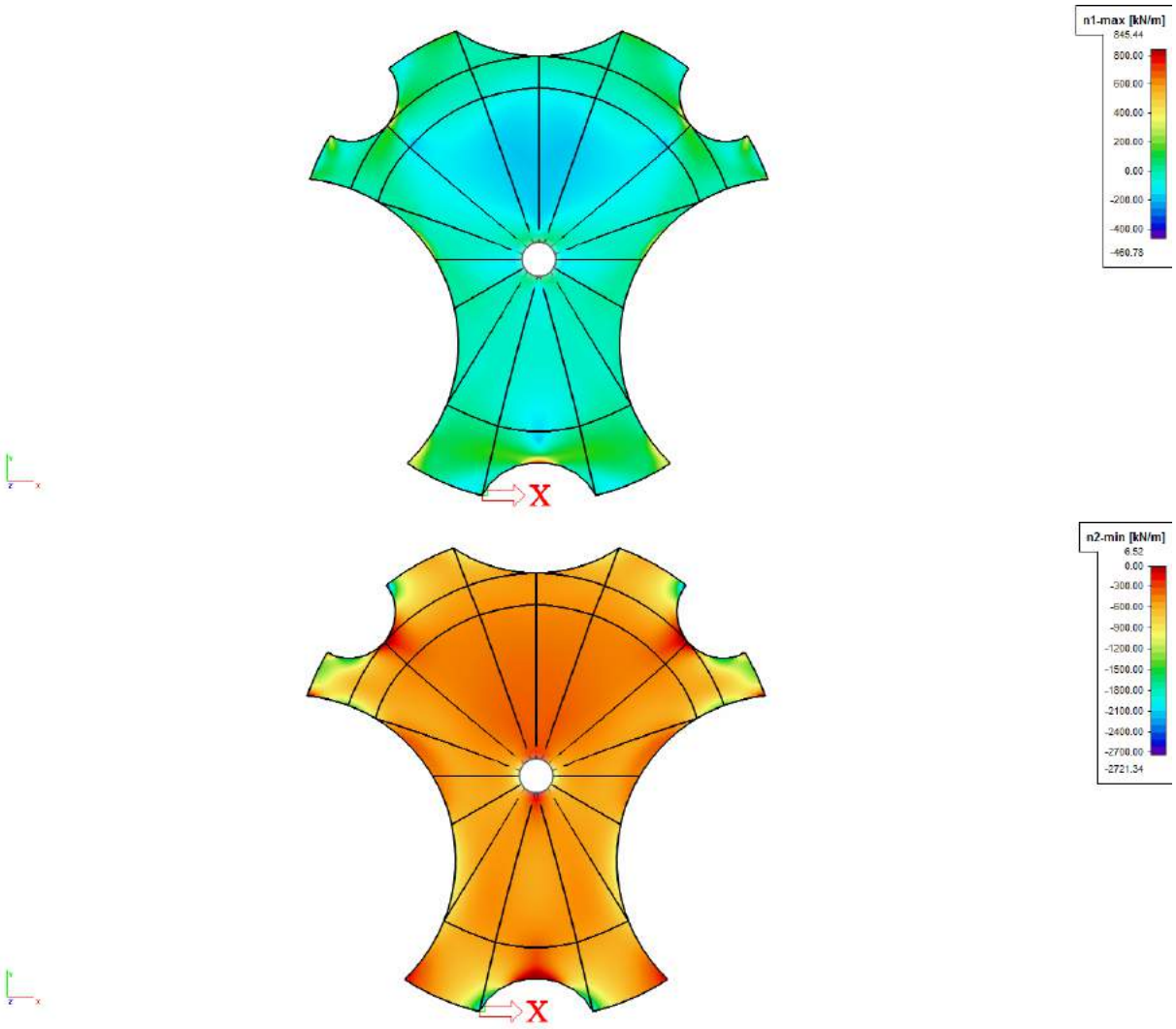

Figure 5.6: Extreme values membrane forces n1 and n2 [kN/m]

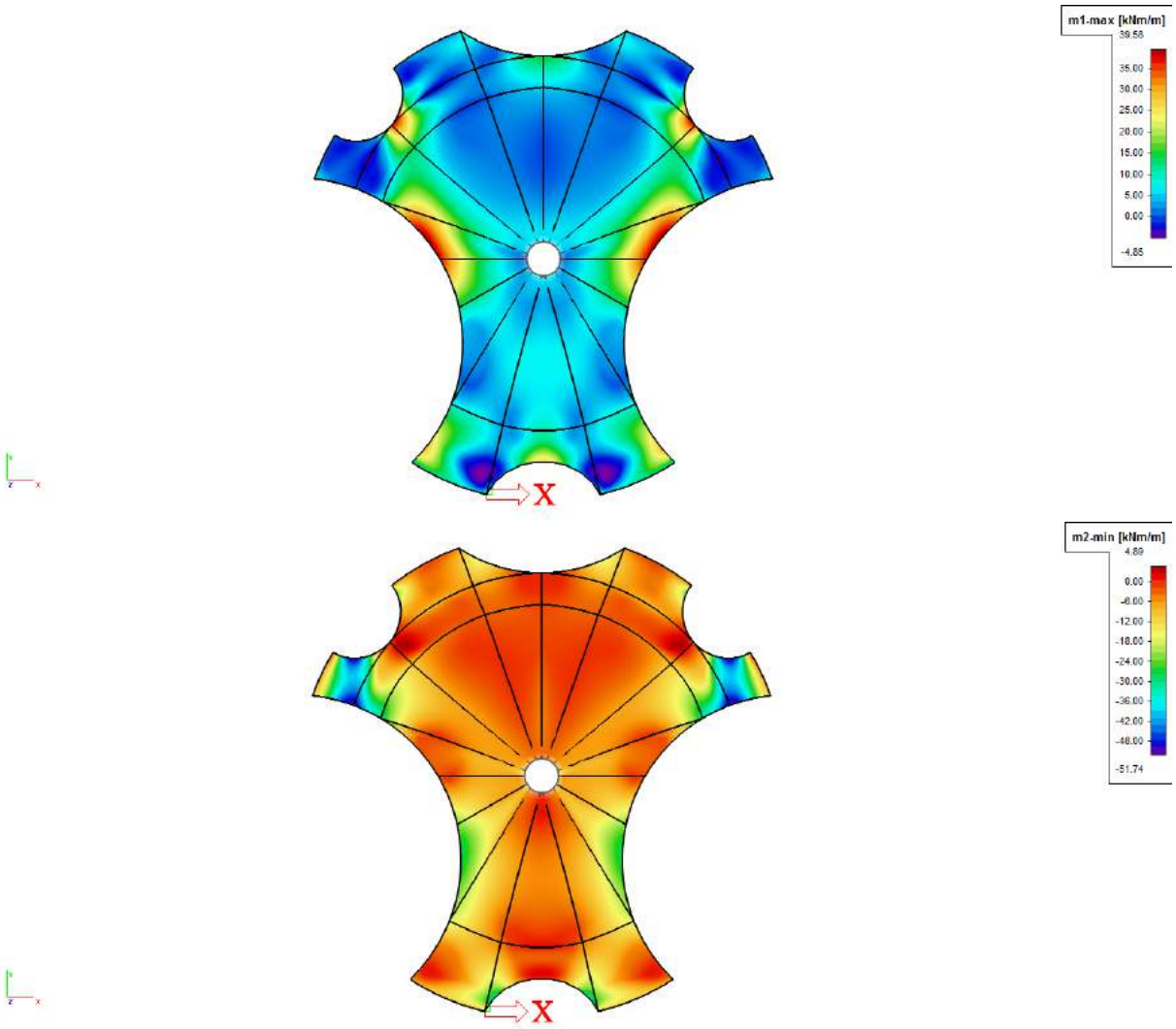

Figure 5.7: Extreme values bending moments m1 and m2 [kNm/m]

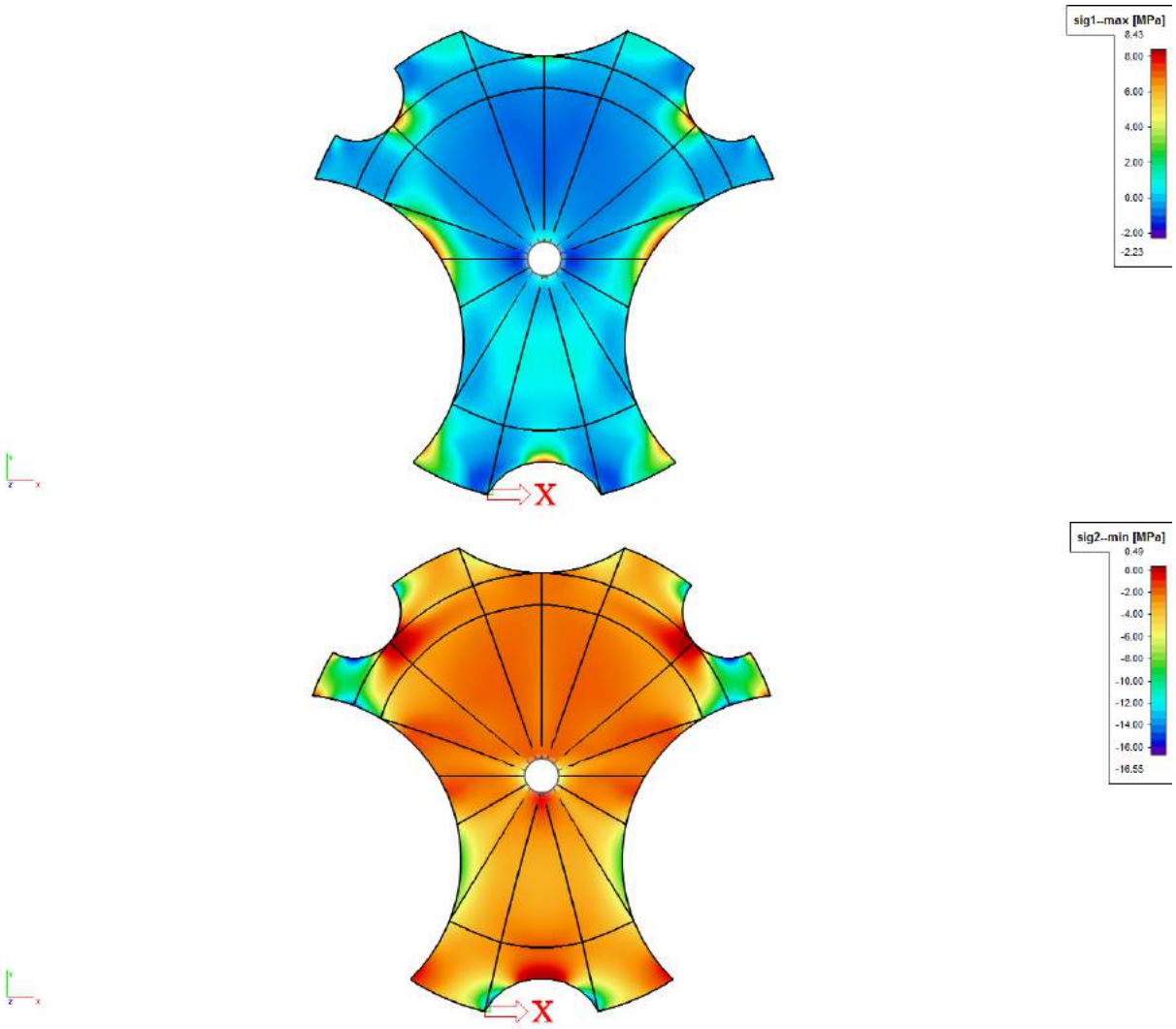

Figure 5.8: Extreme values membrane stresses s1 and s2 [MPa]

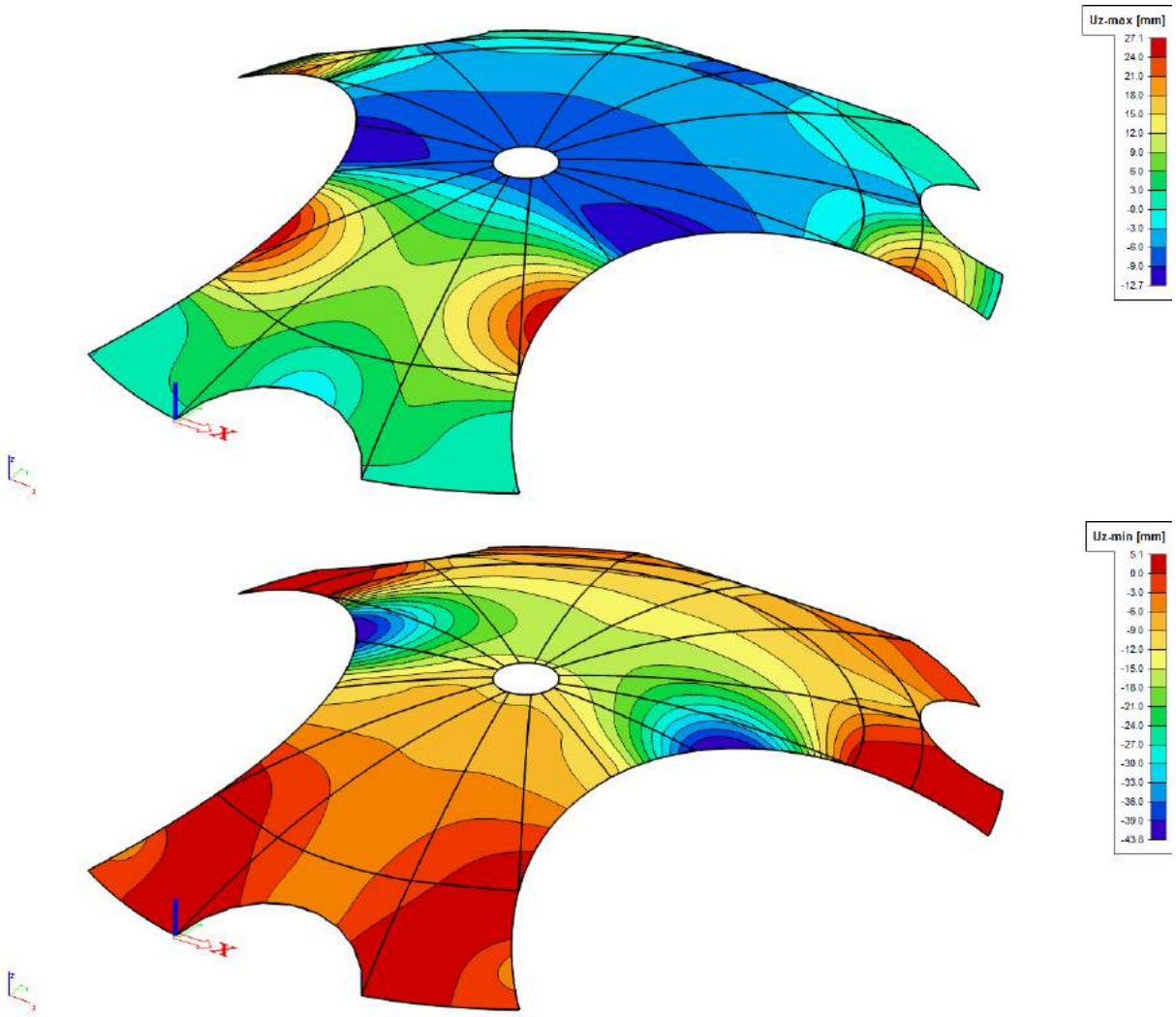

Figure 5.9: Extreme values vertical displacements u_{max} and u_{min} [mm]

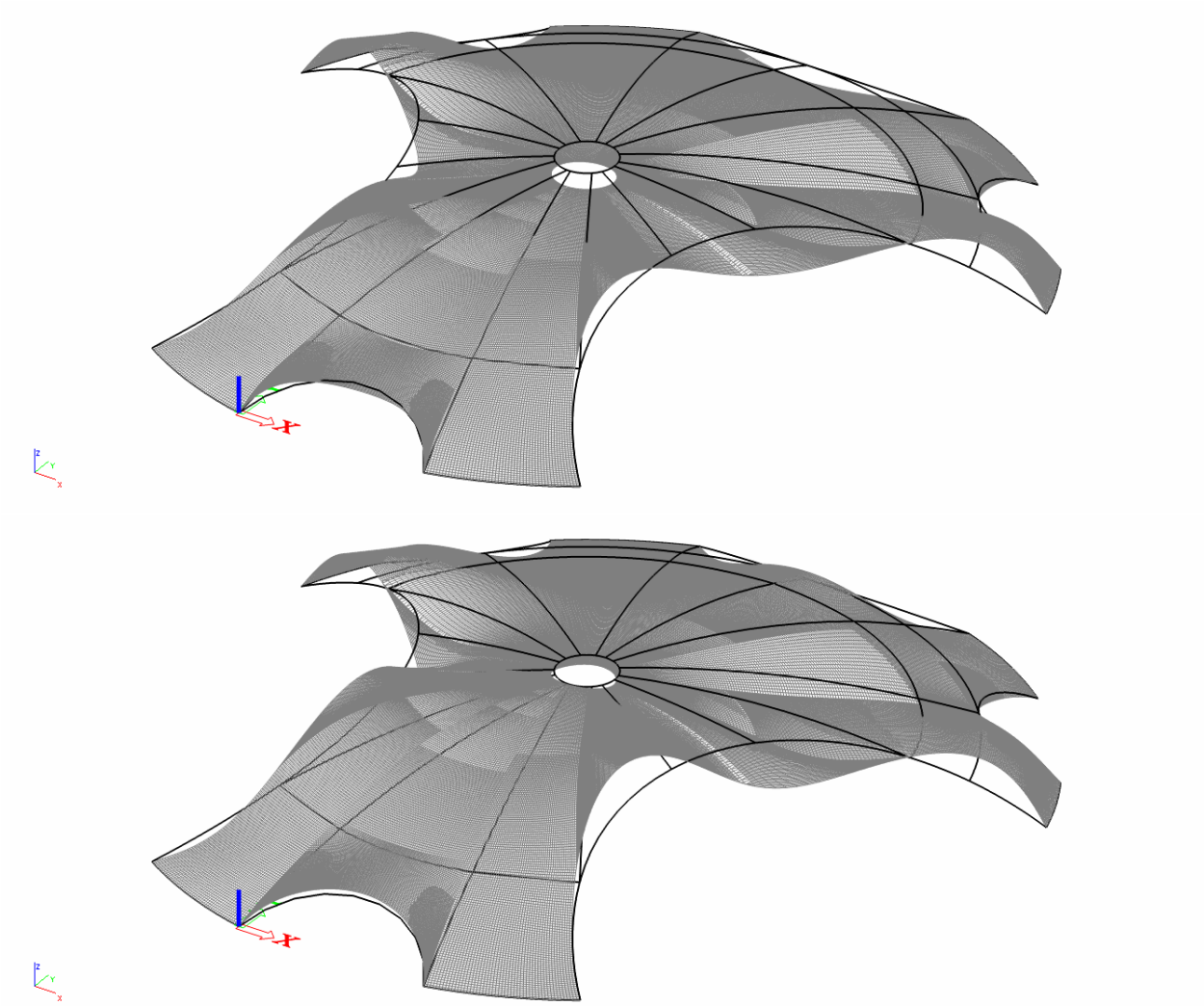

Figure 5.10: Deformation of the shell structure due to permanent load and most unfavorable variable load

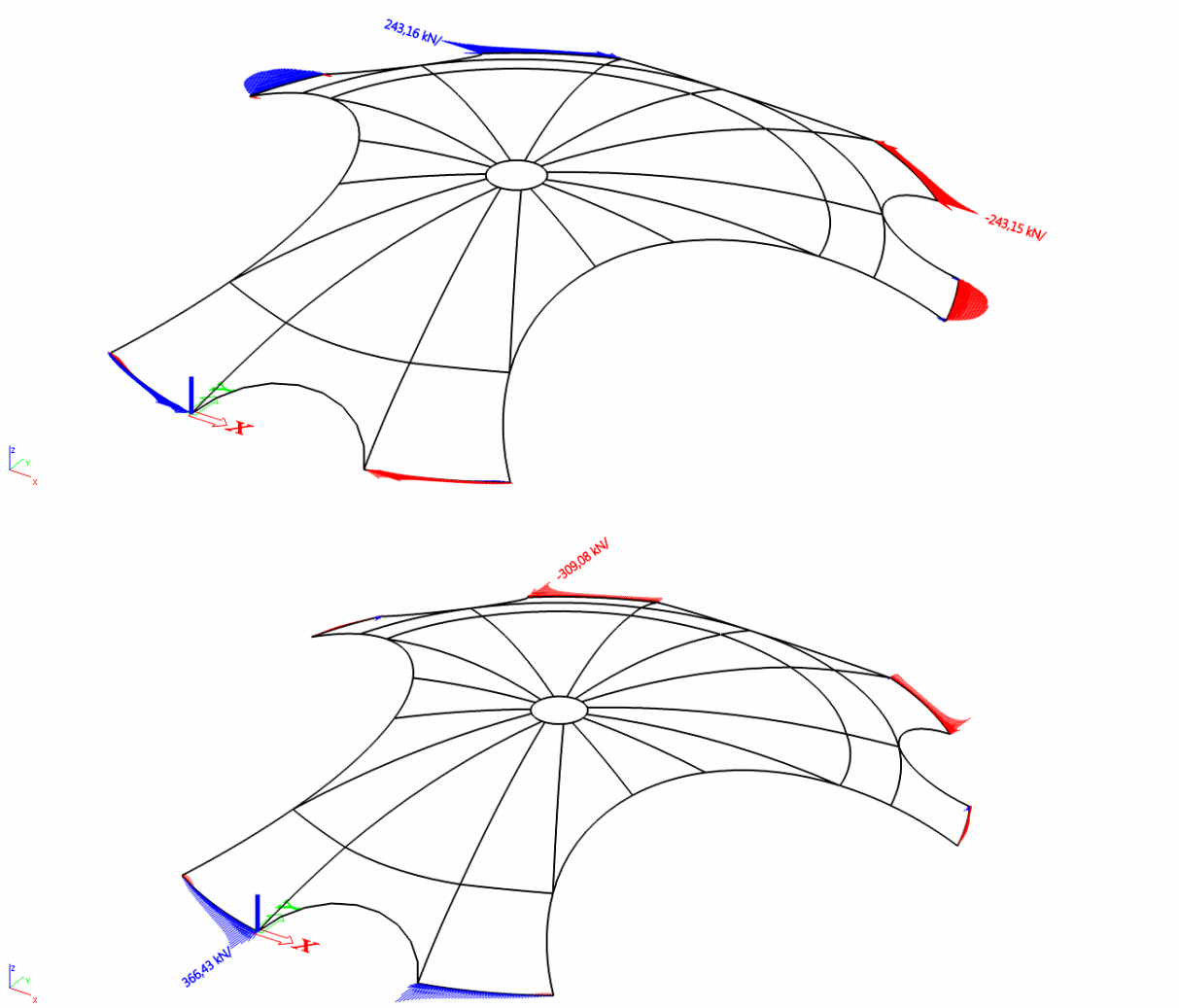

Figure 5.11: Extreme values horizontal support reactions Rx and Ry [kN]

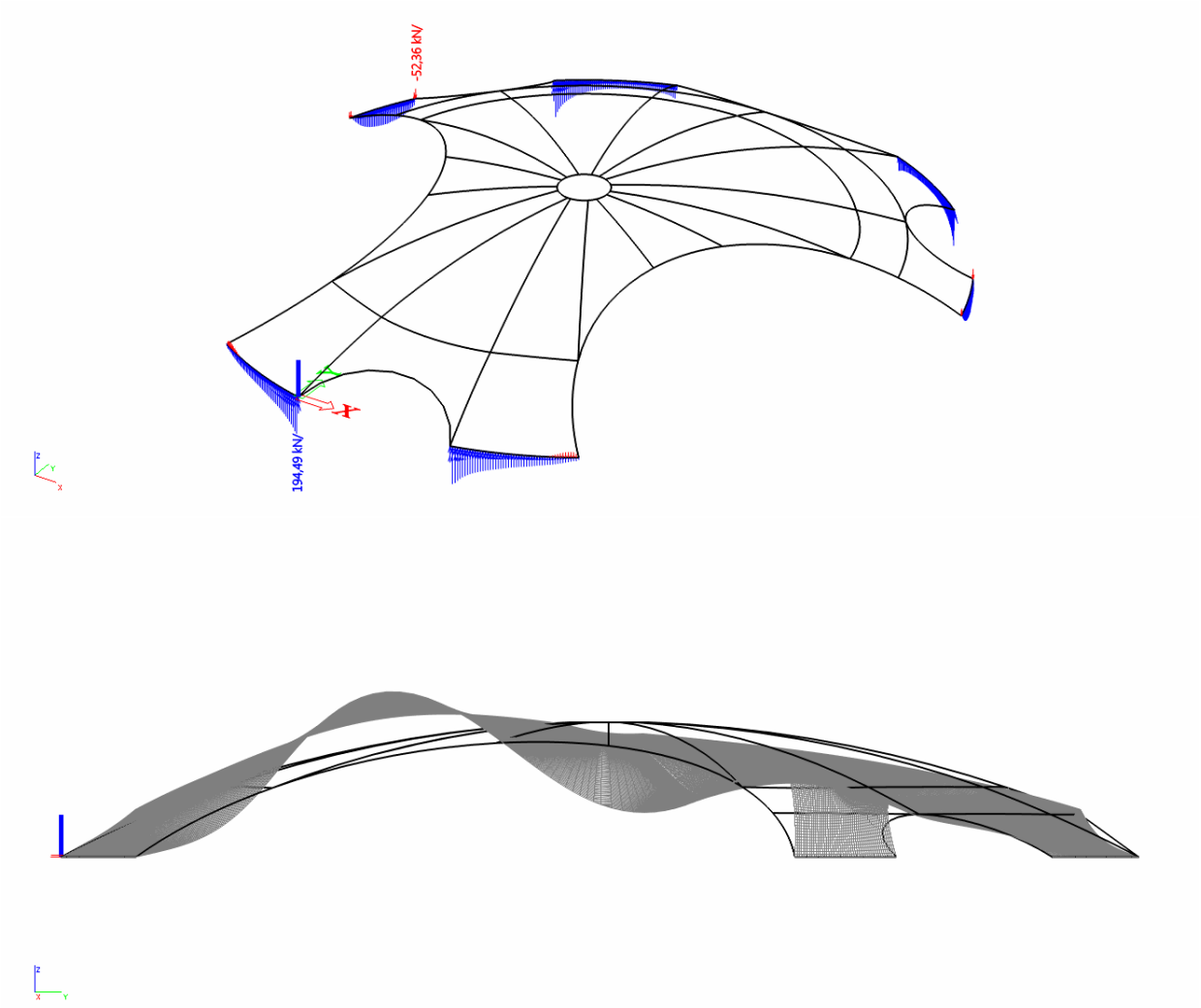

Figure 5.12: Extreme values vertical support reaction Rz [kN] and the (smallest) first buckling mode (Com3)

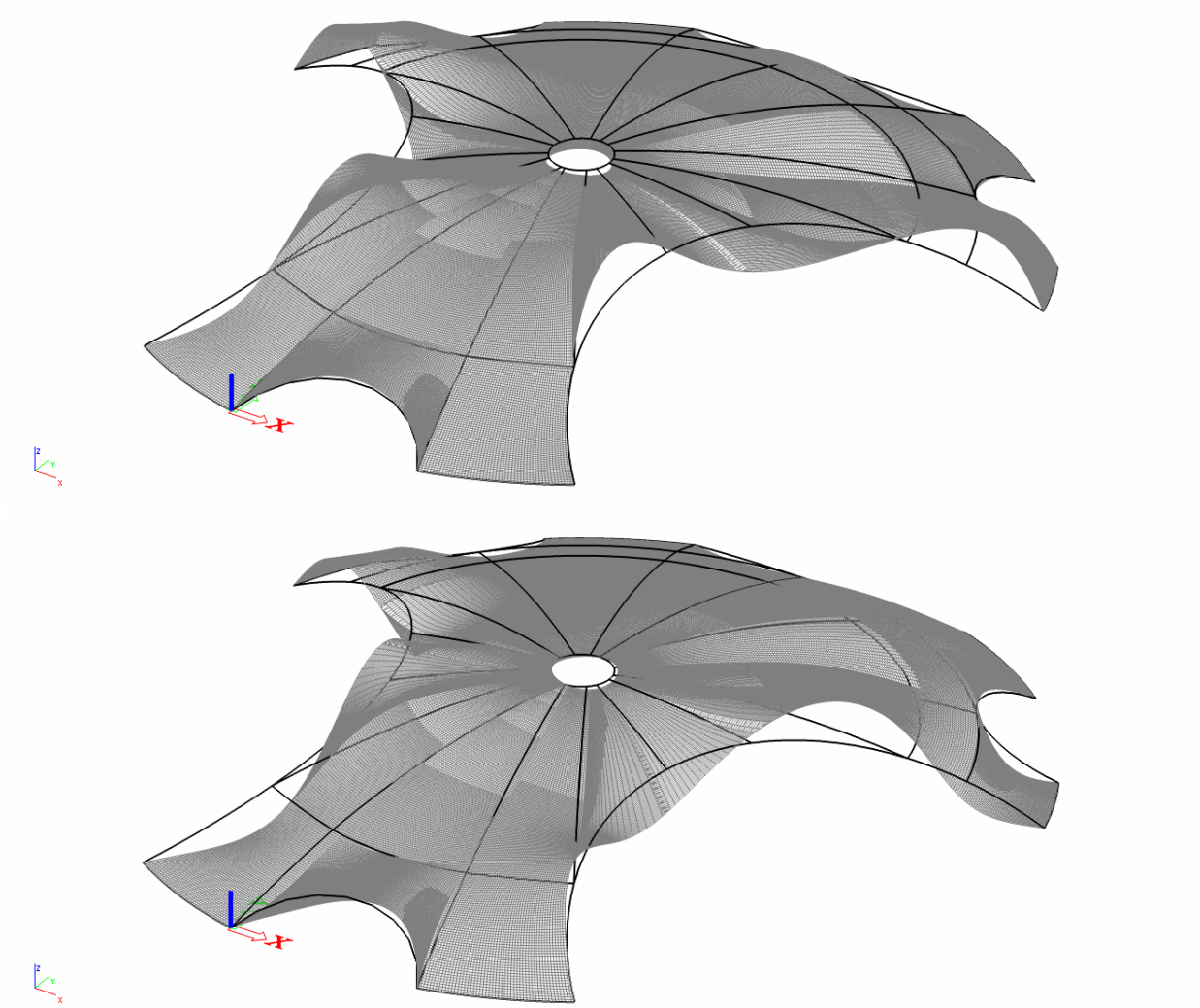

Figure 5.13: The (smallest) first buckling mode and the second buckling mode (Com3)

Conclusions Load combinations:

1. The snow load of combination 1 is always smaller compared to the equally distributed maximum wind load of combination 3. The fact that this wind load is applied perpendicular tot the surface instead of vertically didn't have a large influence and can be attributed to the shallow shape of the shell.

2. The upward wind load of combination 2 has a favorable effect on the resultant load consisting of two permanent downward loads. This conclusion can be drawn based on the results in the table as well, where these permanent loads appear to be the only loads responsible for the extreme values of this combination.

3. The third combination encompasses the distributed wind load acting downward. This results in the highest downward resultant load. As this resultant load is one of the

main factors for the critical buckling load this combination must be considered in future calculations.

4. The drifted snow load of combination 4 can be considered one of the critical load cases. But, because the roof is a canopy the wind load plays a larger role than expected. The load of combination 4 is asymmetrical and so its extreme values almost match the other (combinations) extreme values at some points, but they never exceed them. It can be concluded that the vertical load effect is smaller compared to combination 3 and the asymmetrical load contribution is smaller than that of combinations 5 and 8. Therefore, this load combination is not discussed in further research.

5. Combination 5 which is asymmetrical, with only wind load on the back half of the shell, has a major share of extreme values for the shell. This combination results in the largest compressive forces and stresses in the shell and the largest forces on the foundation.

6. For the sixth combination holds the same as combination 2, in fact their extreme values are the same. This means that the permanent load, because of the weight of the building and the roof, is unfavorable above the combination with the downward wind load acting on the front. The reason is that the permanent load apart is already an asymmetrical load, the heavy back is pushed down while the lighter front consequently moves up. Both aforementioned combinations have a favorable effect on this situation. That's why these combinations can be omitted in further research.

7. For the seventh combination holds exactly the same as for combination six, the upward wind load on the back has a favorable effect on the dead load of the construction and the combination can therefore be omitted in further research.

8. The last combination, com8, representing the upward wind load acting on the front part, can not be ignored. It causes the front part of the shell to stretch even higher in the air which has the largest tensile forces and stresses, bending moments and deformations as a result. Therefore it is one of the most critical loads.

- For further investigation and while improving the structure only the loads of combinations 3, 5 and 8 need to be taken into account, for they are the most critical loads for this shell structure.

strength and stability:

- From the difference between the buckling loads it can be concluded that the shell is sensitive to imperfections (difference between first and second buckling load is greater than 4 %) but not highly sensitive (applies to cases where the difference is smaller than 2%) for the combinations that have a buckling load that is too low ($p_{cr;lin} < 6$ kN/m^2). One can argue that the buckling loads of the different load cases are within the 2% boundary, but it is unlikely that these load cases happen at the same time or shortly after each other (wind load for example).

- The thrust forces on the foundation are large, also compared to the vertical forces. For future calculations (foundation) it's necessary to know the size of the thrust forces per meter width of the foundation. Therefore, it must be mentioned that the values for the support reactions in Table 5.7 are in fact per 0,2 meter width (not per meter), because of the mesh size, this means that the largest horizontal (distributed) load is (366/0,2) 1830 kN/m. On the other hand, this value is a peak value which means that the average distributed load is smaller, namely around 1250 kN/m at its maximum. The aforementioned maximum load (1830 kN/m) is smaller than the maximum internal force of the shell, the situation however is different because this force actually has to be transferred to and resisted by the foundation.

- The trajectories are examined. First n2, which represents (in most cases) the meridional force in the shell. The force is a compressive force, except for a few points which are clearly marked (dark red) in Figure 5.6 for extreme values of n2. The trajectories seem to flow very naturally for this shell and it agrees more or less with the trajectory pattern which occurred in the reference dome (Figure 3.5) and weakened dome. The only remarkable point is where the downward displacement reaches its extreme value (Figure 5.14a), there the membrane force (n2) curves very early towards the shell edge, in this way it is shown that a weak spot is present. Furthermore, it can be concluded that large forces occur very locally. When n1, which is the circumferential force, in Figure 5.6 is considered an edge disturbance can be observed. The green areas around the bottom of the shell mark the tension forces in the shell. Also the weak point that was highlighted for n2 produces tensile circumferential forces which compensate the downward displacement by pulling the shell back in place. This is also clearly seen in the front arch (Figure 5.14b) where large circumferential forces (red arrows) are generated in order to compensate for the compressive forces in meridional direction which cannot be transferred directly to the foundation at this location.

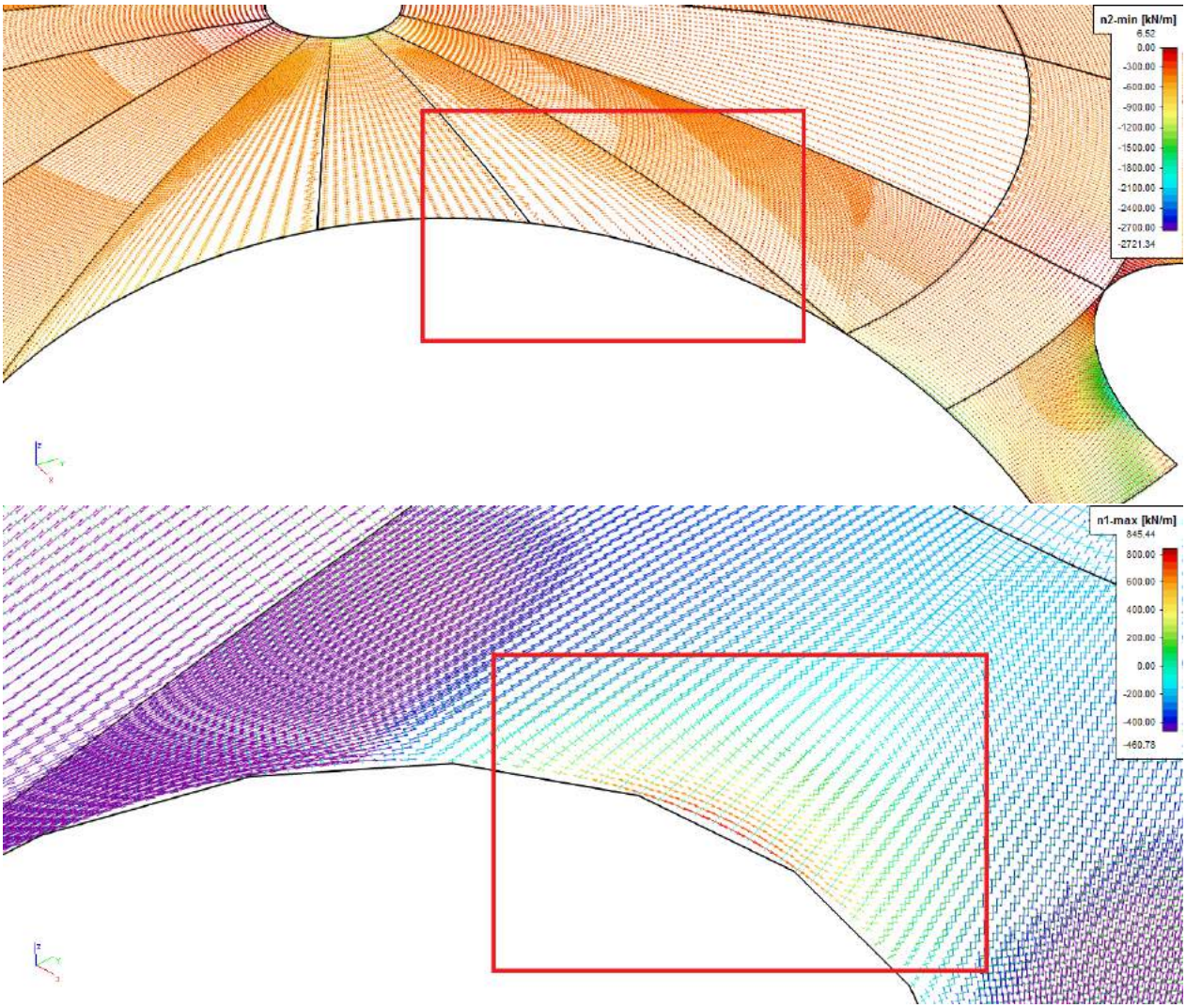

Figure 5.14: Irregularity in force trajectory (a) meridional force n2 (b) circumferential force n1

5.4 Mesh study

In the last section it was explained that the use of a mesh size of 0,2 meter is good enough for the calculations of the Green Planet shell structure. In order to prove this a small mesh study is performed where the extreme values, resulting from the three most critical loads, are calculated while using different mesh sizes. The results are collected in Table 5.8 together with the necessary calculation time for the linear analysis and linear buckling analysis. The extreme values are subsequently compared to each other by giving the increase (or decrease) as a percentage of the first value, see Figure 5.15. So, the difference in extreme values between for example mesh size 1,0 m and 0,4 m is denoted by the percentage captured under mesh size 0,4 m, where the difference is given as a percentage of the extreme value for mesh size 1,0 m. A series is colored green when the differences are small.

Extreme values	mesh 1,0m	mesh 0,4m	mesh 0,2m	mesh 0,15m	mesh 0,1m
$R_{z;res}$[kN]	20159	20143	20138	20137	20136
$n_{1;max}$ [N/mm]	596	715	845	974	1155
$n_{2;min}$ [N/mm]	-2286	-2412	-2721	-2824	-2999
$m_{1;max}$ [kNm/m]	40,2	40,9	39,6	39,7	39,8
$m_{2;min}$ [kNm/m]	-49,4	-51,3	-51,7	-51,7	-51,7
$\sigma^{-}{}_{1;max}$ [N/mm^2]	7,93	8,34	8,43	8,43	8,42
$\sigma^{-}{}_{2;min}$ [N/mm^2]	-15,9	-16,4	-16,6	-16,6	-16,6
$R_{z;max;up}$ [kN/m]	717	881	975	1013	1063
$R_{z;max;down}$ [kN/m]	-145	-198	-262	-293	-337
$R_{y;max}$ [kN/m]	1298	1615	1830	1873	1980
$R_{y;min}$ [kN/m]	-1074	-1468	-1545	-1647	-1718
$R_{x;max}$ [kN/m]	1040	1150	1215	1300	1384
$R_{x;min}$ [kN/m]	-1039	-1148	-1215	-1300	-1384
$u_{z;max;up}$ [mm]	23,3	26,0	27,1	27,2	27,3
$u_{z;max;down}$ [mm]	-42,2	-43,0	-43,8	-44,0	-44,1
$p_{cr;lin}$ [kN/m^2]	5,16	5,02	4,91	4,89	4,88
$p_{cr;lin;2}$ [kN/m^2]	5,61	5,42	5,26	5,24	5,23
$\Delta p_{cr,lin}$[%]	9	8	7	7	7
Computation time L.A.[min]	0	0,5	2	4	18
Computation time B.A.[min]	0	1	4	10	35

Table 5.8: Extreme values of the Green Planet model with varying mesh size

	mesh [m]				
	1	0,4	0,2	0,15	0,1
Extreme units					
Rz [kN]	20159	20143	20138	20137	20136
		-0,08%	-0,02%	0,00%	0,00%
N1 [N/mm]	596	715	845	974	1155
		19,97%	18,18%	15,27%	18,58%
N2 [N/mm]	-2286	-2412	-2721	-2824	-2999
		5,51%	12,81%	3,79%	6,20%
M1 [kNm/m]	40,2	40,9	39,6	39,7	39,8
		1,74%	-3,18%	0,25%	0,25%
M1 [kNm/m]	-49,4	-51,3	-51,7	-51,7	-51,7
		3,85%	0,78%	0,00%	0,00%
S1 [N/mm2]	7,93	8,34	8,43	8,43	8,42
		5,17%	1,08%	0,00%	-0,12%
S2 [N/mm2]	-15,9	-16,4	-16,6	-16,6	-16,6
		3,14%	1,22%	0,00%	0,00%
Rz up [kN/m]	717	881	975	1013	1063
		22,87%	10,67%	3,90%	4,94%
Rz down [kN/m]	-145	-198	-262	-293	-337
		36,55%	32,32%	11,83%	15,02%
Ry max [kN/m]	1298	1615	1830	1873	1980
		24,42%	13,31%	2,35%	5,71%
Ry min [kN/m]	-1074	-1468	-1545	-1647	-1718
		36,69%	5,25%	6,60%	4,31%
Rx max [kN/m]	1040	1150	1215	1300	1384
		10,58%	5,65%	7,00%	6,46%
Rx min [kN/m]	-1039	-1148	-1215	-1300	-1384
		10,49%	5,84%	7,00%	6,46%
Uz up [mm]	23,3	26	27,1	27,2	27,3
		11,59%	4,23%	0,37%	0,37%
Uz down [mm]	-42,2	-43	-43,8	-44	-44,1
		1,90%	1,86%	0,46%	0,23%
Pcr lin1 [kN/m2]	5,16	5,02	4,91	4,89	4,88
		-2,71%	-2,19%	-0,41%	-0,20%
Pcr lin2 [kN/m2]	5,61	5,42	5,26	5,24	5,23
		-3,39%	-2,95%	-0,38%	-0,19%
Delta Pcr [%]	9	8	7	7	7
Computation time linear analysis [min]	0	0,5	2	4	18
Computation time buckling analysis [min]	0	1	4	10	35

Figure 5.15: Comparing the extreme values with varying mesh size

Figure 5.15 shows that with a mesh size below 0,2 m the difference between two consecutive values is often less than 0,5%. The only exceptions are the extreme meridional and circumferential forces in the shell, their differences seem to grow independent of the mesh size. The consequence is that the support reactions increase as well. However, these extreme forces (n_1 and n_2) are local and on top of that they don't seem to influence the differences for the largest stresses (s_1 and s_2). So, because the increase of the membrane forces is more or less independent of the mesh size and because this increase doesn't influence the stresses too much, these differences can be omitted when choosing a mesh size. And because the other differences are below 0,5% a mesh size of 0,2 m is good enough for the calculations of the Green Planet model. But, extra attention should be paid to local internal forces. The calculation time was not selected as a decision tool but it can be noted that calculations up to a mesh size as small as 0,15 m can be performed rather easily.

5.5 Thickness study

The thickness of the shell has an influence on the strength of the shell through its inertia while at the same time it influences the (self) weight. It is required to find a balance between these factors to minimize costs and effort to build the shell. Therefore the extreme results of three thicknesses are compared, by applying load combinations 3, 5 and 8 to the three models. In this way it is decided whether the thickness should be increased or decreased (compared to the proposed 200 mm) and what the influence will be. A mesh size of 0,2 m is

used, the type of concrete is again C90/105. The results are shown in Table 5.9. A short note on $\Delta p_{cr,lin}$: this value is set to 7 for the case where the thickness is 200 mm, because this makes the values comparable, in reality (as seen in Table 5.7) this value is smaller but this was derived from a load combination that is not discussed here.

Extreme values	thickness 250mm	thickness 200mm	thickness 150mm
$R_{z;res}$[kN]	23807	20138	16469
$n_{1;max}$ [N/mm]	838	845	1275
$n_{2;min}$ [N/mm]	-3050	-2721	-2481
$m_{1;max}$ [kNm/m]	48,5	39,6	30,9
$m_{2;min}$ [kNm/m]	-64,8	-51,7	-40,0
$\sigma^{-}{}_{1;max}$ [N/mm^2]	6,3	8,43	12,6
$\sigma^{-}{}_{2;min}$ [N/mm^2]	-13,8	-16,6	-21,6
$R_{z;max;up}$ [kN/m]	1135	975	866
$R_{z;max;down}$ [kN/m]	-196	-262	-387
$R_{y;max}$ [kN/m]	2161	1830	1471
$R_{y;min}$ [kN/m]	-1649	-1545	-1423
$R_{x;max}$ [kN/m]	1310	1215	1107
$R_{x;min}$ [kN/m]	-1310	-1215	-1107
$u_{z;max;up}$ [mm]	16,7	27,1	50,4
$u_{z;max;down}$ [mm]	-30,2	-43,8	-73,4
$p_{cr;lin}$ [kN/m^2]	7,28	4,91	2,92
$p_{cr;lin;2}$ [kN/m^2]	7,41	5,26	3,02
$\Delta p_{cr,lin}$[%]	9	7	5

Table 5.9: Extreme values of the Green Planet model with varying thickness

Table 5.9 indicates that it is indeed interesting to think about the thickness of the shell. When the thickness is increased it has a small positive influence on the internal tension force and downward reaction force, besides it proportionally has a pronounced influence on the stresses (reduction of 17 and 25 percent because of larger cross-section), displacements and critical buckling load (increase of almost 50 percent because of stiffer behavior). Even though the moments and the compressive force in the shell increase a large reduction in the stresses is obtained. The negative consequence, on the other hand, is the increase of the load on the foundation with approximately 10 percent. When the thickness is reduced to 150 mm, the consequences for the forces in the shell and on the foundation are exactly the opposite. For the critical buckling load this means its critical value becomes higher compared to a 200mm thick shell: the shell doesn't meet the requirements. Another remarkable result of reducing the thickness is an increase of the internal tensional force by 50 percent. Furthermore, it has a pronounced influence on the tensile and compressive stresses which increase by approximately 50 and 30 percent. But, the compressive force, moments and resulting forces on the foundation are reduced as well as the building costs. From this research it can be concluded that both situations, increasing and reducing the thickness (of 200 mm), have their advantages and disadvantages. Therefore, it is preferred to vary the thickness based on the magnitude of the internal force and thus benefit from the advantages of both situations.

5.6 Material strength study

The stiffness of the shell depends strongly on the E-modulus of the concrete, before it cracks. On the other hand, the building costs increase with increasing E-modulus. So, this is another important parameter to study, especially the size of the impact when the E-modulus is varied. An overview of the results of the study is given in Table 5.10.

Extreme values	C35/45	C60/75	C80/95	C90/105
$R_{z;res}$[kN]	20138	20138	20138	20138
$n_{1;max}$ [N/mm]	845	845	845	845
$n_{2;min}$ [N/mm]	-2721	-2721	-2721	-2721
$m_{1;max}$ [kNm/m]	39,6	39,6	39,6	39,6
$m_{2;min}$ [kNm/m]	-51,7	-51,7	-51,7	-51,7
$\sigma^{-}{}_{1;max}$ [N/mm^2]	8,43	8,43	8,43	8,43
$\sigma^{-}{}_{2;min}$ [N/mm^2]	-16,6	-16,6	-16,6	-16,6
$R_{z;max;up}$ [kN/m]	975	975	975	975
$R_{z;max;down}$ [kN/m]	-262	-262	-262	-262
$R_{y;max}$ [kN/m]	1830	1830	1830	1830
$R_{y;min}$ [kN/m]	-1545	-1545	-1545	-1545
$R_{x;max}$ [kN/m]	1215	1215	1215	1215
$R_{x;min}$ [kN/m]	-1215	-1215	-1215	-1215
$u_{z;max;up}$ [mm]	34,7	30.3	28.0	27,1
$u_{z;max;down}$ [mm]	-56,0	-48,9	-45,3	-43,8
$p_{cr;lin}$ [kN/m^2]	3,84	4,40	4,75	4,91
$p_{cr;lin;2}$ [kN/m^2]	3,92	4,50	4,85	5,26
$\Delta p_{cr,lin}$[%]	7	7	7	7

Table 5.10: Extreme values of the Green Planet model with varying material strength

From the results it can be derived very clearly that the material strength only influences the stiffness of the shell, because reducing the E-modulus resulted only in larger deflections and lower critical buckling loads. An interesting conclusion is that reducing the material strength (for example from C90/105 to C35/45) decreases the critical buckling load by 22 percent. At the same time an increase of thickness (by 50mm) improves the same (reference) critical buckling load by 50 percent, as was concluded from the thickness study. Therefore, it would be interesting to combine the optimization option to vary the thickness with a reduction of concrete strength. Of course the building costs have to be included in the consideration.

5.7 Optimizing thickness and material strength

With the knowledge that is obtained in the previous sections an optimization study is executed to prove that the measures are effective and beneficial for the future design of the shell. First of all it is tried to stabilize the shell by improving the linear buckling load. No buckling will occur when the smallest critical load is at least 6 kN/m^2, as explained before.

Therefore, the thickness of the Green Planet model (originally concrete quality C90/105 with thickness 200 mm) is increased to 250mm, as was done in the thickness study. At the same time, to save costs, the material strength is lowered to C35/45. The result of this optimization step was almost satisfactory, but the buckling load was now a little too small. In order to improve the design of the shell the material strength was increased to C45/55. This improvement resulted in a linear determined critical buckling load of at least 6 kN/m^2, see Table 5.11.

Extreme values	C90/105, 200mm	C45/55, 250mm	C45/55, 150-300mm
$R_{z;res}$[kN]	20138	23807	21170
$n_{1;max}$ [N/mm]	845	838	244
$n_{2;min}$ [N/mm]	-2721	-3050	-3777
$m_{1;max}$ [kNm/m]	39,6	48.5	41,1
$m_{2;min}$ [kNm/m]	-51,7	-64.8	-26,8
$\sigma^-{}_{1;max}$ [N/mm^2]	8,43	6.3	2,98
$\sigma^-{}_{2;min}$ [N/mm^2]	-16,6	-13.8	-16,4
$R_{z;max;up}$ [kN/m]	975	1135	737
$R_{z;max;down}$ [kN/m]	-262	-196	-
$R_{y;max}$ [kN/m]	1830	2161	1375
$R_{y;min}$ [kN/m]	-1545	-1649	-860
$R_{x;max}$ [kN/m]	1215	1310	995
$R_{x;min}$ [kN/m]	-1215	-1310	-995
$u_{z;max;up}$ [mm]	27,1	20.1	2,7
$u_{z;max;down}$ [mm]	-43,8	-36.3	-13,8
$p_{cr;lin}$ [kN/m^2]	4,91	6.06	6.55
$p_{cr;lin;2}$ [kN/m^2]	5,26	6.17	6,93
$\Delta p_{cr,lin}$[%]	7	9	6

Table 5.11: Extreme values of the Green Planet model with varying material strength and concrete thickness

A drawback of the increased thickness is the increased load on the foundation of the shell. In order to reduce this load the thickness has to be reduced in strategic places on the shell. It was chosen to keep the same material strength, also for comparison, but to lower the thickness of the shell to 150 mm. Then, after a stability calculation, the weak spots were marked and their thickness was doubled to 300 mm thickness. These operations were repeated a couple of times (process of iteration) until the critical buckling load reached the value of six again. This resulted in the thickness distribution of Figure 5.16, where the self weight distribution indicate the local thickness of the shell, varying linearly between 150 and 300 mm. The thicknesses had to be increased especially along the (weak) arches (purple area in the figure), and in the front of the shell where there's initially less weight. The results are gathered in Table 5.11 as well.

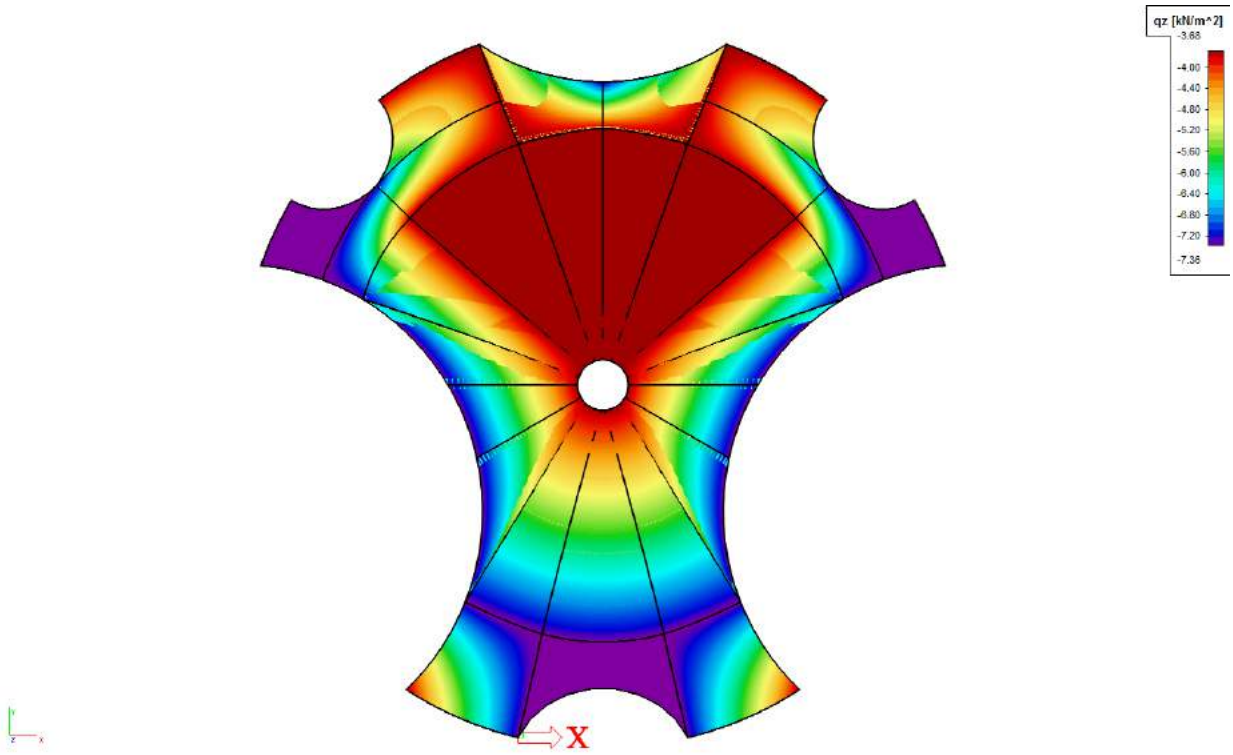

Figure 5.16: Self weight distribution of the shell indicating the local thickness

It's interesting to compare the extreme values (in red) of the Green Planet model with a constant thickness (200 mm) with the optimized model (150-200 mm thickness). The aspects that didn't improve during the optimization are the resultant force, the internal compressive force in the shell and the internal moment (although minor differences were observed). Apparently, the weight has increased a bit and the compressive forces have shifted. However, this shift of compressive forces can be seen as a positive consequence of the optimization, as the compressive stress has remained the same which means the concrete of the shell is used more effectively. Furthermore, all other aspects have improved, like the tension forces and stresses, the required support reactions, the deflections and the critical buckling load. The improved situation ensured that no downward vertical reaction force is needed anymore. Besides, the foundation, which is treated in the next section, will benefit largely from the great reduction in horizontal forces. Not only will it benefit from the reduction of the maximum load, also the distribution over the shell edge has improved slightly, see Figure 5.17 and 5.18, the distributions are now more evenly.

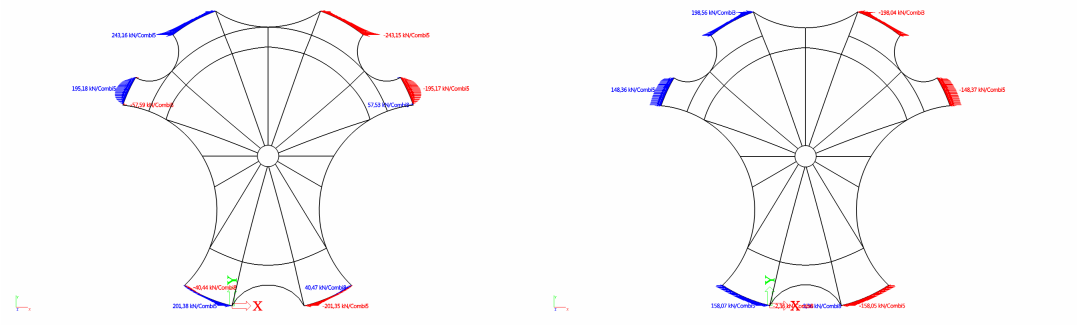

Figure 5.17: Horizontal support reactions (Rx) a) before situation and b) optimized situation

Figure 5.18: Horizontal support reactions (Ry) a) before situation and b) optimized situation

The optimization of the shell by varying the thickness has a great influence on the different forces and design aspects. But, it also comes at a cost, as it will make the production of the double curved concrete elements more difficult. It is also possible that the execution at the site will suffer from this decision.
There are a lot of possibilities to optimize the shell, this was only one (quick) possibility to show the possible impact. It is good to bear in mind what kind of improvements are possible but also what the limits are, when decisions are made.

5.8 Foundation

In reality the hinge supports are not infinitely strong in each direction, as was assumed in previous cases. In order to simulate the behavior of the loaded shell structure in cooperation with the foundation, use is made of the finite element program. The foundation solutions fitting the structure best are examined and elaborated on. First, the research is restricted to the horizontal directions of the foundation rather than the vertical direction, which is assumed to have a smaller effect on the stiffness of the shell.

Foundation plan There are several ways to support the shell construction of Green Planet. Before, the structure was compared to a dome structure and a cylinder structure and it therefore makes sense to seek for a foundation solution which is often applied to those kind of structures. First of all, a ring beam could be applied as a support, like is done for a lot of

domes. Another solution is the use of tie rods or cables, like is often done in arch construction (bridges).
In order to make a good decision the resultant horizontal forces are examined, by using Figure 5.17 (a and b) and 5.18 (a and b). When combining these horizontal forces (Rx and Ry) it is clear that the resultant forces act more or less towards the middle of the shell (this is done in Figure 5.19). Another observation is that large forces are generated from the load transferred through the arches directly to the foundation, causing peak loads at both ends.

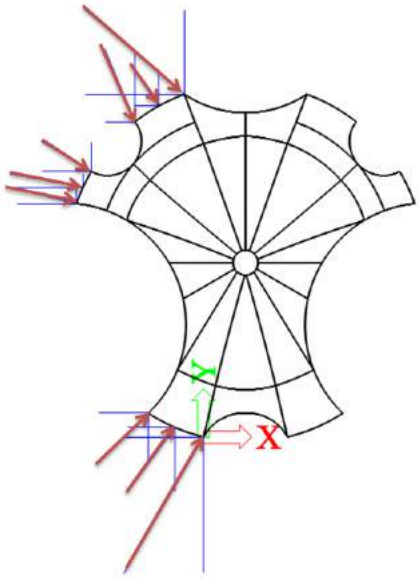

Figure 5.19: The resultant reaction forces (in red) from the horizontal reaction forces (Rx and Ry) on the foundation of Green Planet

Furthermore, use can be made of the fact that the support of the shell covers only a small part of the circumference. Since a ring beam is often applied to buildings like domes, which transfer their loads evenly to the support, which is slightly in contrast to this case, it seems illogical to chose the ring beam as a foundation method. This will cause huge deformations and consequently, quickly calculated, a huge ring beam of multiple meters thick (because of the amount of steel that is required) will be necessary. Even when prestressed cables are applied a very large ring beam is required. For those reasons a ring beam is not effective to serve as a foundation for this shell. Therefore, in this case, the preferred method is to use tie rods or cables to deal with the horizontal thrust forces.

Cable supported structure options It was argued that a foundation with cables suits Green Planet best. Basically, this still leaves two configurations that may serve as the best solution (see Figure 5.20a and b). The first option is to connect the 'arches' that can be recognized in the structure, spanning from south to north and west to east, with cables. Another option is to follow the resultant forces (see Figure 5.19), this means the cables still span from west to east, but cables cross to fix the two 'arches' in south-north direction.

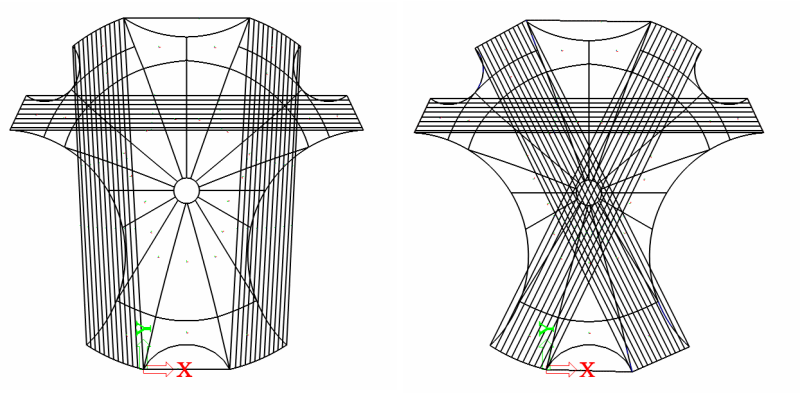

Figure 5.20: Green Planet with tension cable foundation (a) Option 1 (b) Option 2

In earlier discussed cases the stability was the largest obstacle for getting a stable and strong shell structure, because of that the focus will be on the stability of Green Planet. The stability strongly depends on how and how much the shell can displace after loading. This again depends on the elongation of the cables, which will allow the shell to displace a little bit (this, in contrast to earlier cases where hinges prevented horizontal movement). The elongation, then, depends linearly on the tension force in the cable, the cross-section and the modulus of elasticity. Therefore, initially, it is chosen to use a cable every meter and a (over dimensioned) cable diameter of 200 mm, to keep it simple and safe. Later on, depending on the results, a better solution is developed (varying for example the number of cables and the cross-section (for increased/reduced forces)). The cable is modeled like it is embedded in a concrete foundation block.
The optimized model from the previous section is used as a basis for this model. For this case the model is even further optimized, because of the high stress the new foundation induces on the 'arch' at the back and locally at the front. There, the thickness is increased from 150 to 300 mm as well. Those changes were made after some experimenting with the model and the impact of the transformation is pictured in Figure 5.21.

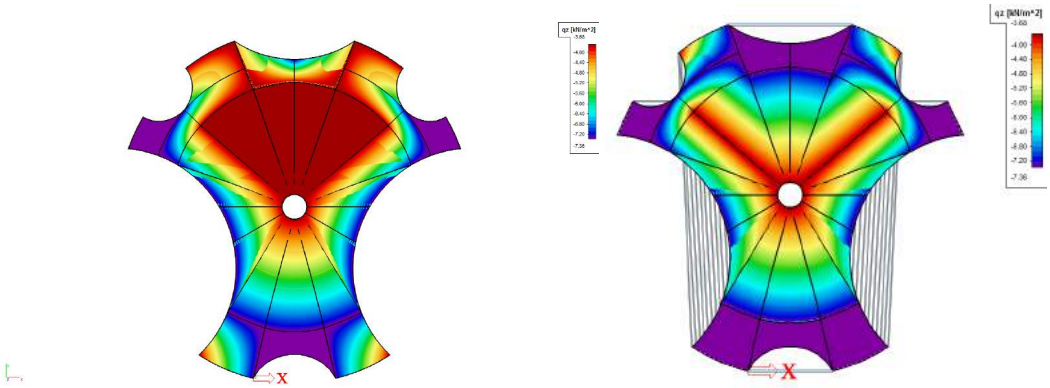

Figure 5.21: Self weight of the structure as an indication for the thickness (a) optimized model (b) model used for Green Planet with cable foundation

In order to model the cables properly the resistance of the soil around it is modeled as a line

load in two directions, taking a low value of 1 MPa for resistance (in fact the local soil-type is sand, the value should be on the safe side). In order to model the crossing cables the structure is locally lowered 250 mm. For option one this means only the west and east foundations are lowered. The model of option two had to be lowered a second time as well to let all three cable groups pass. The structures are loaded with the three most critical load cases (downward wind, downward wind on the back, upward wind on the front of the shell) which were found in 'Analysis Green Planet' a few sections before this. The results together with the results from the optimized Green Planet structure from previous section are given in Table 5.12.

Extreme values	Optimized GP (C45/55, 150-300mm)	Option 1	Option 2
$R_{z;res}$[kN]	21170	31712	32923
$n_{1;max}$ [N/mm]	244	21192 (400)	19486 (400)
$n_{2;min}$ [N/mm]	-3777	-38868 (-2000)	-17970 (-2000)
$m_{1;max}$ [kNm/m]	41,1	168,6 (90)	406,4 (170)
$m_{2;min}$ [kNm/m]	-26,8	-295,8 (-90)	-1998 (-250)
$\sigma^{-}{}_{1;max}$ [N/mm^2]	2,98	50,4 (8)	71,7 (20)
$\sigma^{-}{}_{2;min}$ [N/mm^2]	-16,4	-124 (-15)	-153 (-20)
$R_{z;max;up}$ [kN/m]	737	3620	4285
$R_{z;max;down}$ [kN/m]	-	-110	-1915
$R_{y;max}$ [kN/m] and N [kN]	1375	793	957
$R_{y;min}$ [kN/m]	-860		
$R_{x;max}$ [kN/m] and N [kN]	995	4537	2049
$R_{x;min}$ [kN/m]	-995		
$u_{z;max;up}$ [mm]	2,70	13,0	111
$u_{z;max;down}$ [mm]	-13,8	-47,9	231
$u_{x;max}$ [mm] (cables)		5,2	6,6
$p_{cr;lin}$ [kN/m^2]	6.55	3,87	4,28
$p_{cr;lin;2}$ [kN/m^2]	6,93	3,91	4,46
$\Delta p_{cr,lin}$[%]	6	1	4

Table 5.12: Results of the optimized Green Planet structure, foundation option 1 and foundation option 2

The first aspect of Table 5.12 that has to be clarified is the increased resultant vertical force. Because of the optimization of the shell and the installation of the new foundation a lot of weight is added. Two-third of the increase, however, is due to the weight of the cables, which has no influence on the load that has to be transferred through the shell. Still, when comparing, an increase of about 3500-4000 kN has to be considered.
Secondly, the extreme values of the forces, moments and stresses are very deceiving in these models. The reason for this is that some nodes where hard to model correctly and this will cause some unnecessary moments and peak stresses (see for example vertical support reaction $R_{z;max;up}$ [kN/m] which value is locally very large). For example the node in the front arch where two cables come together: preferably this cable in 'x' direction, 5.21b, is split up in several cables and distributed over the foundation as well, but due to required height difference it's hard to model and check this node to be correctly. Besides that it

appeared that less than one percent of the concrete surface (weak spots) endures a far much larger stress than the rest of the surface. Therefore, the peak stresses are mentioned in the table and also the values that hold for about one percent of the shell (between brackets). But, for the majority of the shell applies a much lower value, as is the case for the optimized Green Planet (although to a lesser extent).
When the model with hinges is compared to option 1 and 2 with a cable foundation, and the attention is focused on the differences between the forces/moments/stresses, it appears that particularly the tension forces and moments have increased. While the load didn't change much, this has to be a direct consequence of the fact that the shell is able to displace a little more (see $u_{x;max}$ [mm] (cables) in Table 5.12). Before examining the model with the cable foundation it was already clear that the displacements had to be kept to a minimum, but this observation proves it once more. Also, the vertical displacement of the shell suffers from the horizontal displacement (which is logical) and the critical buckling load as well. Finally, because of the small differences between the critical buckling loads ($\Delta p_{cr,lin}$[%]), it could be stated that the shell has become highly sensitive for imperfections, especially in case of option one.
Now, just to see if it might be possible to improve this particular foundation solutions, so that the shell won't buckle, the number of steel cables is doubled. For option one this resulted in a shell that behaves slightly stiffer, but the critical buckling load was still low with a value of 4,30 (compared to 3,87 in Table 5.12). This can be interpreted as a very small improvement given the very drastic attempt to improve the foundation. This means that the small displacements due to the elongation of the cables is fatal for this shell, unless other measures are taken.
Bases on the results two measurements are proposed. The first is the implementation of an edge beam along the big and weak 'arch', because earlier attempts (not documented) promised a lot of improvement with this measurement. The second measurement is the use of post-tension-cables to reduce the elongation of the cables to a minimum and keep the shell in it's position during installation of the shell (assumed possible because the self weight of the shell is the largest part of the load). These solutions will probably improve the design, but these are not examined with the FEA program in this study because this will be too time consuming and expertise on the subject will be required, they will be mentioned as recommendations.

5.9 Geometrical non-linear analysis

The results derived from geometrical non-linear analysis differ very little from the results obtained with linear calculation, due to small displacements. So, for now the safety of the shell structure is judged upon the linear buckling analysis results multiplied with a factor $\frac{1}{6}$. This factor accounts for imperfections and cracking of the concrete. As a recommendation, more expertise is necessary to interpret the geometrical non-linear analysis results and to add imperfections to the shell structure and assess these results.

Part III

Green Planet: segmentation and detailing

Chapter 6

Segmentation

6.1 Introduction

The segmentation of Green Planet is an important aspect of the design as it can influence the shells behavior, the production phase and the erection phase of the structure. In the end all the elements must be connected and the number of connections and the position of those connections will be determined with this segmentation. The connection of the elements can be a weak link in the structure and therefore this segmentation can have a great influence on the behavior of Green Planet.
But, more important perhaps is the erection phase, because it's a certainty that the segmentation will have an influence on that. In the erection phase the contractor needs to deal with the positioning of the formwork, the temporary supports, the positioning of the elements and the connecting of the elements and all that preferably in the quickest and least labor-intensive way. Important factors herein are the element pattern, the repetition of elements, the accessibility, the size of the elements, the number of elements and the shape of the elements. All will be determined by the segmentation choice.
At last, the production phase is influenced by the segmentation. For this phase it holds too that preferably the elements are produced in the quickest and least labor-intensive way. This case is special because of the use of the flexible formwork, so it is not a requirement that the elements are restricted by a certain curvature, but still the repetition is an issue as well as the size and number of elements for example.
The segmentation is an important design aspect and will be covered in the sections 'Segmentation options', 'Finite element modeling' and 'Effect of segmentation'. First, the segmentation options are explored and a final choice is made based on the grid options available and the boundary conditions. In FE modeling the grid that was chosen is applied to the Green Planet model in Scia Engineer and based on the grid the segments are modeled. This chapter ends with a comparison to find out if there is an effect on the shells behavior due to the segmentation. There shouldn't be a difference because the connections are still solid, but small inaccuracies were found before in connecting the three-dimensional elements.

6.2 Segmentation options

6.2.1 Grids

Basically, there are two fundamental grid types, the structured and unstructured [13][29]. The difference lies in the form of the segments and the organization of the grid points. When they are independent of their positions but based on a general rule then the grid is called structured. When the organization or connection of the grid points is different from point to point the grid is called unstructured. So, for unstructured grids the connectivity should be described explicitly while for the structured grid it is implicitly taken into account.
Unstructured grids offer an appropriate grid solution for structures with complex shapes. While structured grids are suited for structures that can be defined by one general rule, examples are Boundary confirming grids, Translational grids and the Isotope technique. But there are also grids that more or less combine the structured and unstructured grids, the so called composite grids. The main challenge of those grids is the connection between the different regions of the structure or between the grids. Examples of composite grids are Block-structured grids, Overset grids and Hybrid grids, see Figure 6.1.

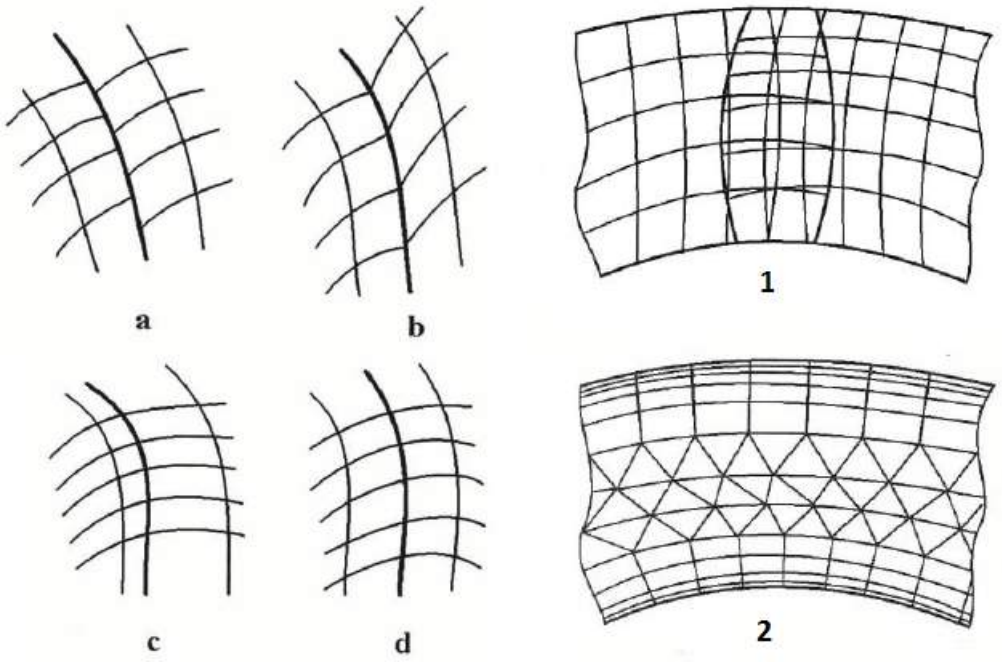

Figure 6.1: A) The connection of two adjacent blocks in block-structured grids with a connection that is (a) discontinuous, (b) non-smooth, (c) non-smooth and (d) smooth, B) A fragment of (1) an Overset grid, (2) a Hybrid grid [29]

The Green Planet design is not an extremely complex shape and therefore an unstructured grid is considered an excessive segmentation choice. But the design is not suitable to be subjected to a grid that is described by only one general rule as well. Because there are too many different interests and variables involved in the segmentation, as indicated in the introduction of this chapter, and the shape is a little too complex for this. On the other hand,

for the benefit of the erection phase a segmentation based on a structured grid is probably preferred, as this will make the structure a logical design for everyone to understand and would probably simplify the supporting, connecting and formwork conditions. So, in the end a grid is preferred to be a composite grid which is as structured as possible. Besides, the block-structured grids are preferable for the purpose of the erection phase, as the Overset grid is too complicated to execute. The Hybrid grid uses both structured grids and unstructured grids, the latter one to overcome overlap regions. The Hybrid grid is deemed to become too complex because the curvature of the construction is the same in all directions. So, for the Green Planet shell the block-structured grids will have the preference, using as little blocks as possible.

6.2.2 Boundary conditions

Before a mesh is chosen for the final segmentation it is important to know the boundary conditions, they will narrow down the options. The most important boundary conditions are:

- The Green Planet design. The boundaries are based on specified grid points from the original design in combination with the predetermined (and in both directions the same) curvatures. Figure 6.2a presents the intended outline of the structure and Figure 6.2b presents all specified grid points of the original design together with the segmentation plan for the original design.
- The maximum size of elements. The production of the elements with the adjustable formwork determines the boundaries of the maximum element sizes. In Chapter 2 the adjustable formwork was discussed and it was mentioned that the size of the rectangular elements were at a maximum 1 by 2 meters. For the production of precast elements for this building the estimation is that elements could measure up to a maximum of 2,5 by 5 meters. These element sizes would be strong enough for transportation as well.
- The minimum size of elements. In this case there is no minimum element size, because all kinds of sizes can be produced. But, bearing in mind that the use of as little elements as possible is preferredthe minimum sizes of the elements should always be as large as possible. Shortly, the elements sizes should always be as large as possible.
- The FE boundaries. Scia Engineer only allows elements to have 3 or 4 corner points/sides, so the grid must adapt in local situations where the general applied rule of the grid doesn't fit.

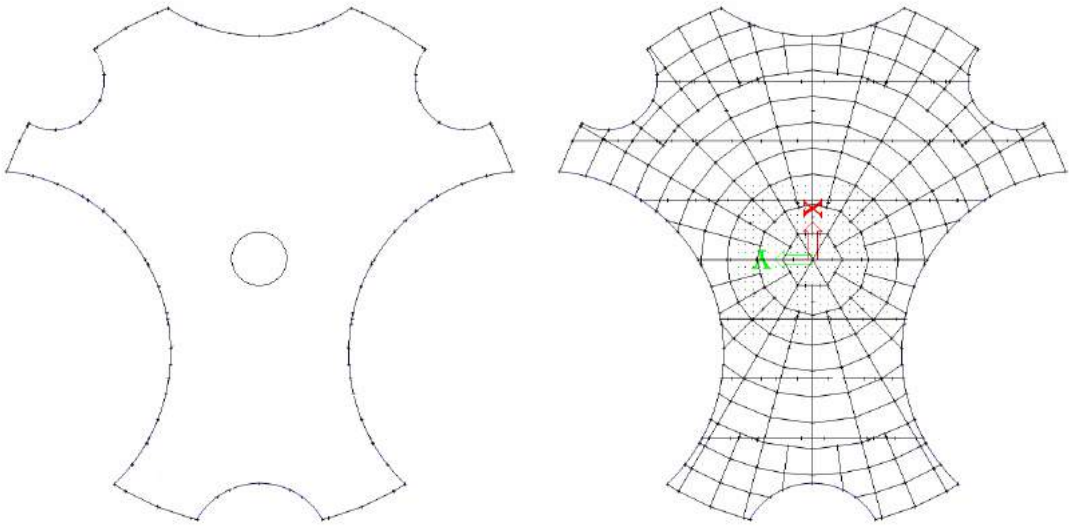

Figure 6.2: a) Boundaries of the Green Planet design b) Original segmentation design Green Planet

Besides these boundary conditions use can be made of the only symmetry line that is available in the structure, just like in the original design (Figure 6.2b). Also, it makes sense to position the elements in such a way that form follows force. In this case that would mean a form which follows the curved lines starting from the top and ending at the supports and (possible) edge beams. In theory this means that the connections will be positioned parallel with the normal forces. An advantage is that the main curves of the structure will be parallel to the (middle) length and width of the precast elements, which will rationalize the element production and building processes. So, the basic division of the original segmentation (Figure 6.2b) would be a feasible solution for the new design as well. A few adjustments will suffice, like the size of the elements, the shape of the concentric circles and the straight lines indicating the transverse beams.

6.2.3 Final segmentation design

The final segmentation design will be based on the original design, but there are still a few challenges left as mentioned before. The general rule of the design is that the grid lines start at the top of the structure in the middle of the oculus and follow the curve to the supports. The boundaries of the structure are respected no matter what happens, so when the grid lines bump into a design boundary they stop.
The space between the grid lines is getting wider from top to bottom. How wide the elements get is based on the boundary condition of the maximum element size, the element will be 5 meters wide at the supports. This means that the height of the bottom elements is allowed to be 2,5 meters. Therefore, the concentric circles of the grid will have a spacing of 2,5 meters and the width of the top to bottom grid lines will be from 0 to 5 meters.
There is no minimum size given, but the elements are supposed to be as large as possible. Therefore, from the point the width between the grid lines becomes 2,5 meters, the distance between the concentric circles is increased to 5 meters. So, at the top the elements will be 5

meters long and max 2,5 meters wide, at the bottom the elements will be 2,5 meters long and max 5 meters wide.
The grids will deviate from the stated rules if there's an unwanted clash with the outline of the design and the elements need to be adjusted to elements with 3 or 4 sides. The result is the segmentation plan in Figure 6.3.

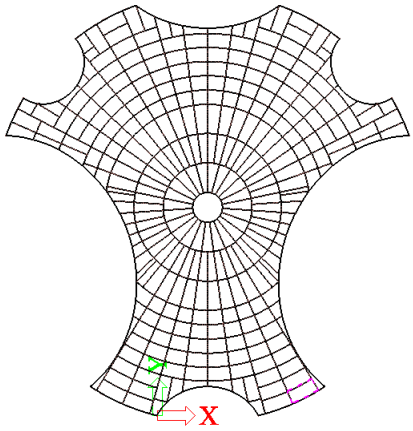

Figure 6.3: The final segmentation plan for Green Planet

6.3 Finite element modeling

Modeling the grid and subsequently the elements is a time-consuming thing if you want to segment a double curved structure in a FEA program like Scia Engineer. Therefore, a few steps are described how to come to the final segmented model. The available design points of Green Planet are those which were meant to serve as grid points for the original Green Planet design. The only useful points for this model are a few points on the symmetry curve and of course the points marking the outline of the structure. Figure 6.4 illustrates the segmentation in a late stage and Figure 6.5 presents the segmented Green Planet model. The steps that were taken to enhance the available grid points into the new segmented model are described below:

1. The first step was to create the symmetry line with the available grid points. The top of the curved symmetry line serves as the midpoint of the oculus and the starting point of many grid lines. The grid points that form the outline are connected with circular lines. Of course, only one side of the symmetry line is segmented, the other half will be mirrored in the end.

2. The second step is to create the concentric circle lines of the grid. The oculus ring is the first concentric circle and is based on the original dimensions. For the other concentric circles the curved symmetry line must be subdivided in such a way that it yields parts that measure at a maximum 5 meters. The midpoints are used for the 2,5 meter concentric circles. Because the created outline must match the concentric circles of the grid and, of course, they never do. This is very important because the grid lines, that will eventually form the elements center lines, must be flawless for the elements

to link correctly in the end. If only a slight angle presents itself this doesn't necessarily mean that the center lines of the elements will not link in the end, but the 3d elements will indicate the flaw in the angle. And this will influence the behavior of the shell. So, the outline must be adjusted in a way it fits the outline best and connect the grid line at the same time. In Figure 6.5 there are a bunch of circled grid lines close to each other, near the bottom, those were meant for experiments to connect the grid and the outer lines of the shell design.

3. The bottom concentric circle is divided into parts which measure not more than 5 meters and subsequently those parts are halved. The created grid points are the basis of the curved grid lines that will link the oculus midpoint to the bottom circle. But, this is easier said than done because besides the concentric circles and outline there isn't a grid point to ensure the curvature of these lines. The curved lines now have a starting point at the bottom and a point to end, a point on the oculus circle line that is subdivided into a predetermined number of parts too, but no intermediate point that will direct the curve. Because of this the other concentric circles must be subdivided into the predetermined number of parts as well, like the oculus ring. In this way it is possible to connect every curved line individually.

4. In this stage, the majority of the elements can be modeled and then copied along the concentric circle, see Figure 6.5. But there are a lot of elements along the outline that need to be modeled individually. In some cases the combination grid line and outline yields an element with 5 sides. In that case often an element is extended or cut in smaller parts. As long as the size is not exceeding the boundary conditions and it doesn't influence the elements that do follow the grid.

5. The last step involves checking all the connections between the elements, they have to be flawless. This check is very important because of so many proceedings that were required and several elements had to be revised. In the end, when every connection was deemed smooth, the segments could be mirrored, supports are added, all grid lines are removed and all loads could be applied again.

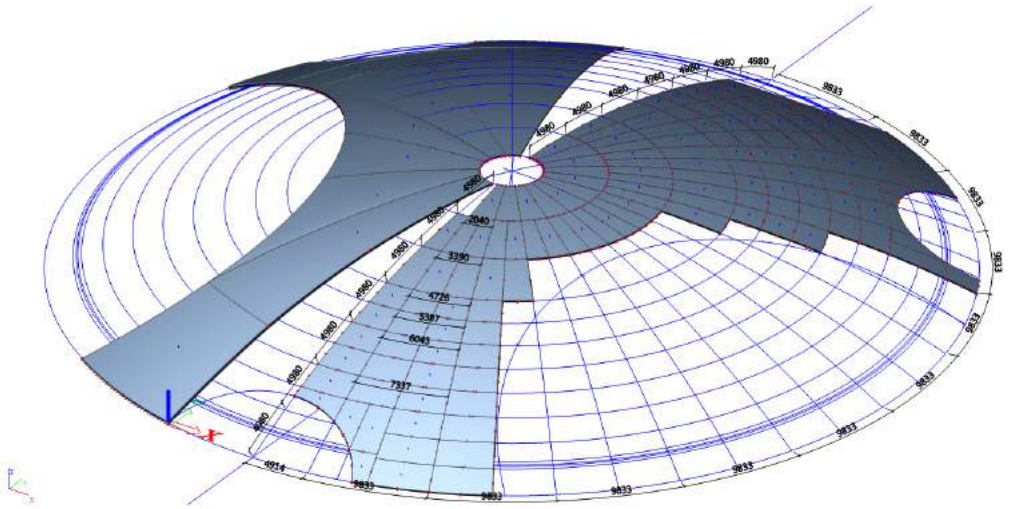

Figure 6.4: The new Green Planet model in the end phase of the segmentation

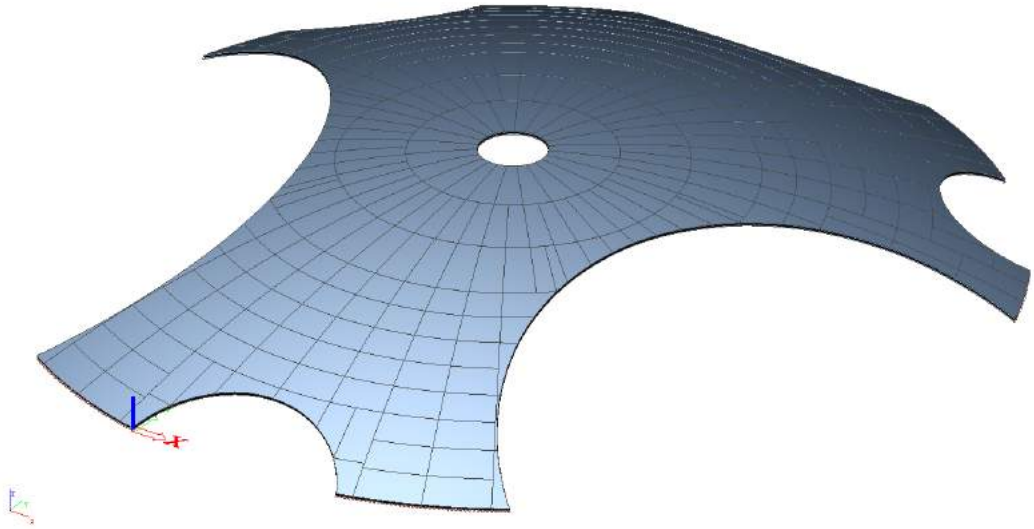

Figure 6.5: The new Green Planet model segmented

6.4 Effect of segmentation

The shell structure of Green Planet is subdivided into smaller elements with great accuracy. Besides the size and number of the elements nothing has changed compared to the Green Planet model that was used before.
The conditions for both models are: they have the same geometry, load condition (most unfavorable load combinations (3,5 and 8) determined in Chapter 5), thickness (150 mm), material properties (C45/55, which is chosen after the material strength study in Chapter

5), support condition (hinged) and connection (solid concrete). Hypothetically, there will be a small difference between the extreme values of the two designs due to the limitations of the FEA program. Moreover, the program fails to connect curved elements perfectly, as the upper and lower sides of the elements tend to flair out a little from time to time. Table 6.1 presents the differences between the models.

Extreme values	Green Planet	Segmented, 150mm	Δ%	Segmented, 250mm
$R_{z;res}$[kN]	16468	16356	-0,7	23644
$n_{1;max}$ [N/mm]	2422	2501	3,3	1336
$n_{2;min}$ [N/mm]	-3271	-2767	-15,4	-3264
$m_{1;max}$ [kNm/m]	50,0	43,1	-13,8	62,0
$m_{2;min}$ [kNm/m]	-43,8	-48,8	11,4	-77,4
$\sigma^{-}{}_{1;max}$ [N/mm^2]	16,9	17,3	2,4	7,62
$\sigma^{-}{}_{2;min}$ [N/mm^2]	-22,7	-27,0	18,9	-16,4
$R_{z;max;up}$ [kN/m]	877	850	-3,1	1002
$R_{z;max;down}$ [kN/m]	-394	-626	58,9	-528
$R_{y;max}$ [kN/m]	1474	993	-32,6	1377
$R_{y;min}$ [kN/m]	-1443	-1408	-2,4	-1631
$R_{x;max}$ [kN/m]	1120	1231	9,9	1610
$R_{x;min}$ [kN/m]	-1120	-1231	9,9	-1610
$u_{z;max;up}$ [mm]	61,4	65,4	6,5	21,7
$u_{z;max;down}$ [mm]	89,2	94,2	5,6	38,3
$p_{cr;lin}$ [kN/m^2]	2,41	2,40	-0,4	6,02
$p_{cr;lin;2}$ [kN/m^2]	2,50	2,48	-0,8	6,12
$\Delta p_{cr,lin}$[%]	4	3	-25.0	2

Table 6.1: Result comparison between Green Planet with large and small (segmented) elements, the last column suggests a segmented Green Planet which has a safe critical load factor

The deviation between the models is about 10% on average if the internal forces are considered. Besides that the distribution of the foundation force in vertical direction, which has its resultant working upwards, tends to get worse. The Ry (horizontal reaction force) however is distributed more evenly over the support as this value drops substantially. But these reaction forces are peak loads that occur theoretically, in reality these forces will be distributed more evenly trough the concrete. The displacements and the critical load factors differ too, a little, this is probably caused by a slightly increased maximum compressive stress. Overall, the results of both designs agree with each other quite well if one considers the amount of elements (327) and thus the amount of potential weak spots that were added. The last column of Table 6.1 suggests a thickness of 250 mm to ensure the safety of the shell with respect to the critical load factor and therefore the safety against buckling. This model of Green Planet will be used in the next Chapter 7.

Chapter 7

Detailing

7.1 Introduction

The previous chapter discussed the subdivision of the double-curved elements. Together those elements could make the bearing and stabilizing shell structure of Green Planet. To ensure the shell's stability, stiffness and strength the elements require a connection that provides the necessary stiffness.
In this chapter the stiffness of the connection is determined. This means, the axial, rotational and shear stiffness of the connection is determined and subsequently verified with basic mechanical models. In the subsection 'Theory' the basic model will be introduced as well as the calculation of the relevant connection stiffness. Next, the subsection 'FEA model' discusses the basic model which is simulated in Scia Engineer, the results are compared to the theory. At last, the relevant stiffness is applied to a suitable FEA model and the results are compared with the results of the other two models. When all results correspond with each other it can be concluded that the relevant stiffness is valid. When the stiffness is valid for those basic models it doesn't necessarily mean the calculation method will be valid for (more complicated) shell structures too. Therefore, the application of the design formulas is discussed in the following section. Ultimately, the stiffness values for the connections of Green Planet are determined and applied in the Green Planet FEA model. After that, the influence of the connection on the behavior of Green Planet will be discussed.

7.2 Axial connection

7.2.1 Theory

Mechanical models For the calculation of the axial stiffness of the connection it is practical to start with a simple mechanical scheme. Therefore, in the mechanical scheme the normal force must be constant and all other forces left out. Figure 7.1a is the basic model which will be used to calculate the axial stiffness of the connection. The model consists of two concrete (C45/55) plates with a length of 3,5 meters and a height of 30 mm, connected by a 500 mm thick connection.

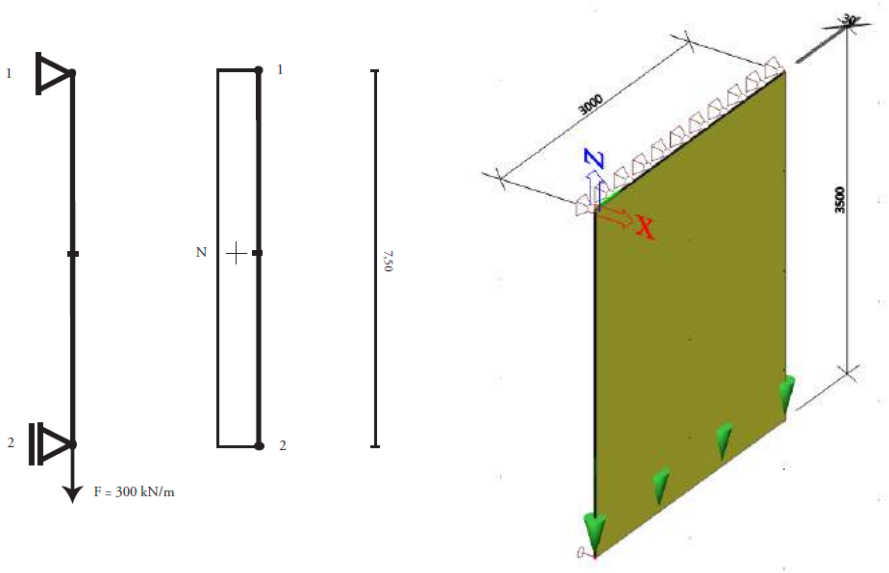

Figure 7.1: a) Simple mechanical scheme for the calculation of the axial stiffness with measurements in meters b) One simply supported concrete slab

But, first the axial deformation of a separate slab is investigated to develop trust in the upcoming FEA results, see Figure 7.1b. When a load $F = 300kN/m$ is applied to the slab it's deformation is theoretically determined with $u_z = \frac{L}{E} * \frac{F}{h} = \frac{3500}{36300} * \frac{300}{30} = 0.964$ mm. The elongation of the full model (7.1a) is determined in the same way and results in $u_z = 2.066$ mm. Furthermore, a connection is tested using only half the width of the model and thus simulating a connection with 50% of it's original stiffness. This connection yields a larger deformation, because the stress in the connection doubles, which is $u_z = 2.20$ mm. Previous results hold for the connection which is 500 mm thick and they're determined for a small connection thickness of 10 mm as well. The length of the structure becomes 7,01 meters when a connection thickness of 10 mm is applied. The critical loads and deformations of the slab and both connection types are gathered in Table 7.1.

	Slab	500 mm	500/2 mm	10 mm
	Theory	Theory	Theory	Theory
F [kN/m]	300	300	300	300
σ [MPa]	10	10	10	10
u_z [mm]	0.964	2.066	2.200	1.931

Table 7.1: Critical loads and deformation for the slab and the two connection types

Axial stiffness The axial spring stiffness is determined using Hooke's law. A line force (F) is applied to the structure to induce an axial displacement (u), the quotient of both is the axial stiffness (k). The width (b) is taken out of the formula because the stiffness is the characteristic of a line connection (see Figure 7.2). Therefore, the unity of the k becomes MN/m^2. The axial stiffness of the connection is determined with the mechanical properties of concrete (C45/55) and it is assumed that the connection behaves like it's part of a

continuous slab. The relation for the axial stiffness, using the dimensions given in Figure 7.2, becomes:

$$k = \frac{F}{u} = \frac{F}{\frac{\sigma * d}{E}} = \frac{EA}{d} = \frac{E*h*b}{d}$$

$$\frac{k}{b} = \frac{Eh}{d}$$

The three connections discussed in the previous section are now tested for their stiffness as well, see Table 7.2, with this formula.

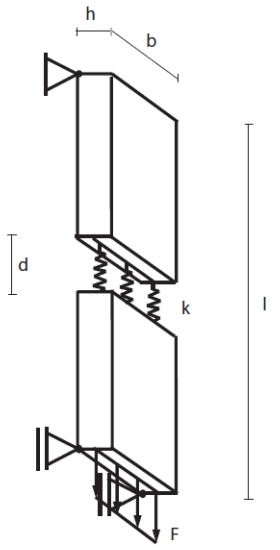

Figure 7.2: Axial stiffness model and dimensions

	500 mm	500/2 mm	10 mm
$k\ [MN/m^2]$	2178	1089	108900

Table 7.2: Rotational stiffness for two connection types

7.2.2 FEA model

The basic test model discussed in the previous section (Figure 7.1) is constructed in Scia Engineer. Again, four models are distinguished: the simple supported slab and the three models in which two slabs are connected while having a connection thickness of 500 mm, 500/2 mm (half the width is taken) and 10 mm, see Figure 7.3 and 7.4. All other conditions are the same as in the theoretical model in order to compare the results. The results of the FEA model are gathered in Table 7.3 and compared to the theoretical values. The comparison shows that the results deviate only a little and it can be concluded that the models agree with each other.

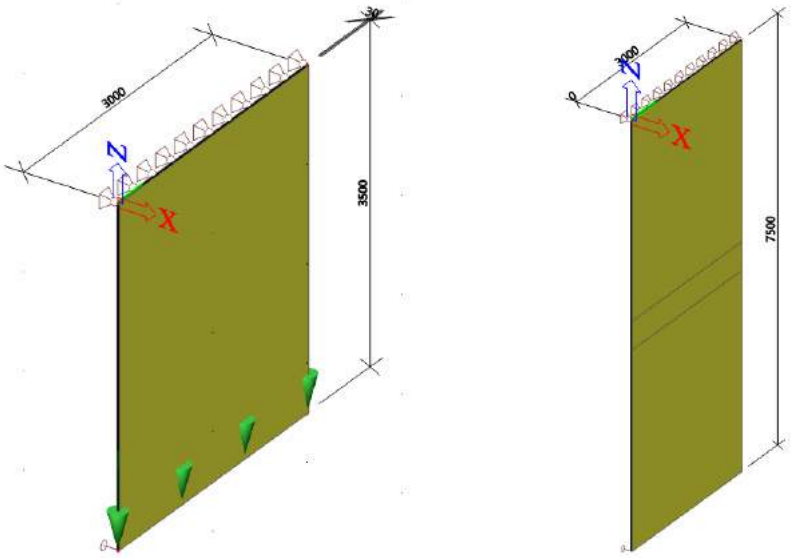

Figure 7.3: a) one simply supported concrete slab b) two connected slabs with connection thickness 500 mm

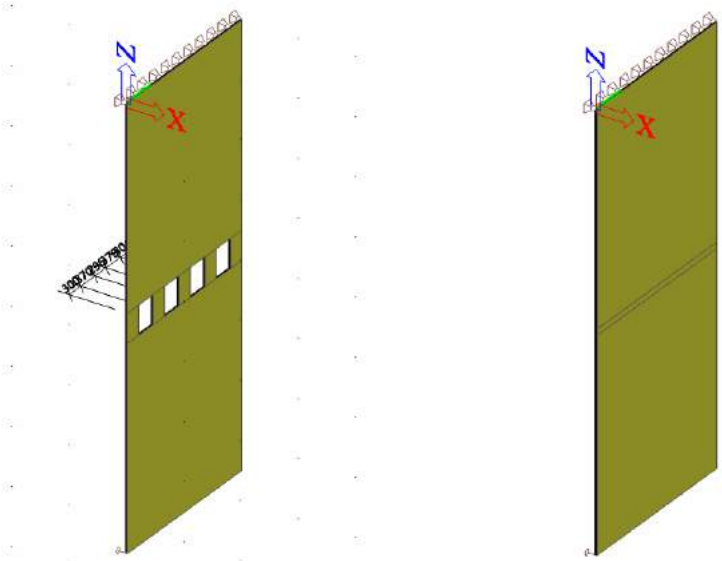

Figure 7.4: a) two connected slabs with connection thickness 500/2 mm and b) 10 mm

	Slab		
	Theory	FEA	Δ%
F [kN/m]	300	300	0
σ [MPa]	10	10	0
u_z [mm]	0.964	0.961	0.3

	500 mm		
	Theory	FEA	Δ%
F [kN/m]	300	300	0
σ [MPa]	10	10	0
u_z [mm]	2.066	2.062	0.2

	500/2 mm		
	Theory	FEA	Δ%
F [kN/m]	300	300	0
σ [MPa]	20	20	0
u_z [mm]	2.200	2.321	5

	10 mm		
	Theory	FEA	Δ%
F [kN/m]	300	300	0
σ [MPa]	10	10	0
u_z [mm]	1.931	1.952	1.1

Table 7.3: Comparison of two calculation methods (theory and FEA) for a) the slab and three connection thicknesses b) 500 mm c) 500/2 mm (half the width) d) 10 mm

7.2.3 Application and verification

The last step in the process, determining the (axial) stiffness of the connection simulating a continuous slab, is to apply the theoretically obtained stiffness in a new FEA model. The results of this model should correspond with the results of the other two calculations. The axial stiffness (2178 MN/m^2, 1089 MN/m^2 and 108900 MN/m^2) is assigned to a spring which connects the slabs. The spring is a substitute for the connection and its thickness, therefore it will reduce the height of the structure (Figure 7.5a) to the length of the two slabs. The results of all connection thicknesses are compared with the theoretical values in Table 7.4 and the first FEA model results in Table 7.5.

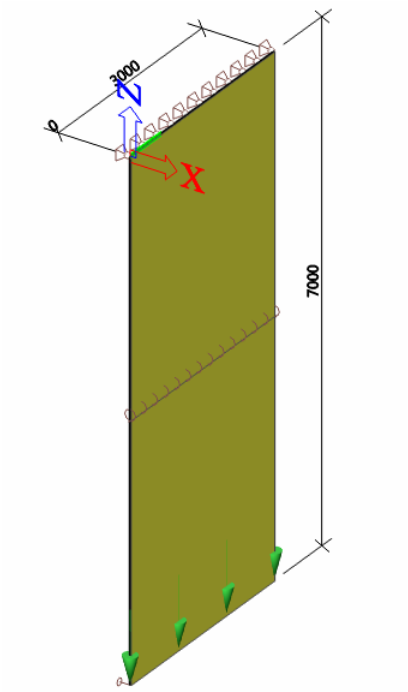

Figure 7.5: The basic test model in Scia Engineer, the connection modeled with an axial spring

	500 mm		
	Theory	FEA Spring	Δ%
F [kN/m]	300	300	0
σ [MPa]	10	10	0
u_z [mm]	2.066	2.078	0.6

	500/2 mm		
	Theory	FEA Spring	Δ%
F [kN/m]	300	300	0
σ [MPa]	20	20	0
u_z [mm]	2.200	2.216	0.7

	10 mm		
	Theory	FEA Spring	Δ%
F [kN/m]	300	300	0
σ [MPa]	10	10	0
u_z [mm]	1.931	1.943	0.6

Table 7.4: Comparison of two calculation methods (theory and FEA spring) for three connection thicknesses a) 500 mm b) 500/2 mm c) 10 mm

	500 mm		
	FEA	FEA Spring	Δ%
F [kN/m]	300	300	0
σ [MPa]	10	10	0
u_z [mm]	2.062	2.078	0.8

	500/2 mm		
	FEA	FEA Spring	Δ%
F [kN/m]	300	300	0
σ [MPa]	20	20	0
u_z [mm]	2.321	2.216	4.7

	10 mm		
	FEA	FEA Spring	Δ%
F [kN/m]	300	300	0
σ [MPa]	10	10	0
u_z [mm]	1.952	1.943	0.5

Table 7.5: Comparison of two calculation methods (FEA and FEA spring) for three connection thicknesses a) 500 mm b) 500/2 mm c) 10 mm

After the comparison it's clear that the FEA spring model results match the theory results perfectly (Table 7.4). There's, however, a little deviation in the outcome of both FEA model results regarding the 500/2 mm connection. But, this difference is easy to explain. Both theory and FEA spring model have a connection that distributes the stress evenly along the connection. In the FEA model the stress distribution is a little disturbed and this causes the peak deformation to be a little larger. In the end it can be concluded that the calculation method for the axial stiffness, representing the stiffness of a connection that simulates a continuous slab, is valid.

7.3 Rotational connection

7.3.1 Theory

Mechanical model For the calculation of the rotational stiffness it is practical to start with a simple mechanical scheme. Therefore, in the mechanical scheme the moment must be constant and all other forces left out. Figure 7.6 is the basic model which will be used to calculate the rotational stiffness.

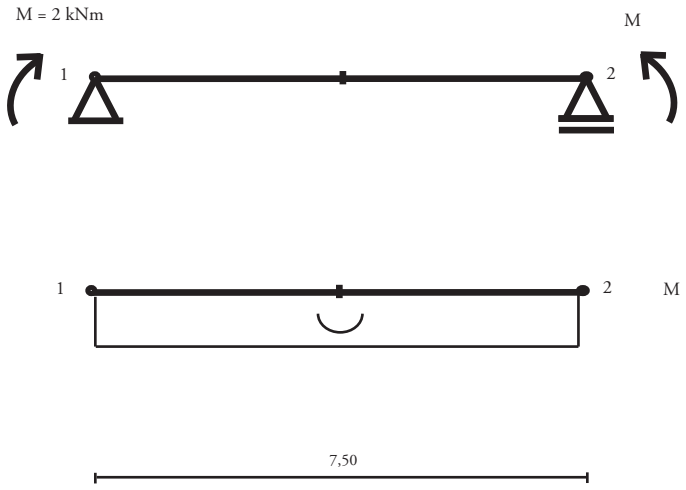

Figure 7.6: Simple mechanical scheme for the calculation of the rotational stiffness with measurements in meters

The rotational stiffness of the connection is determined with the mechanical properties of concrete (C45/55) and it is assumed that the connection behaves like it's part of a continuous slab. The thickness of the connection is 0,5 meter in this example, together with the length of the slab the structure spans 7,5 meters (Figure 7.6). For the height of the concrete slab a value of 75 mm is chosen, this is comparable to the height of the double curved concrete elements. With the given information the critical loads and the deflection of the described model are determined:

$$M = 2kNm$$

$$\sigma = \frac{M*y}{I} = 2,13MPa$$

$$u_z = \frac{1}{8} * \frac{M*(l)^2}{E*I} = 11,02mm$$

These values hold for the connection which is 500 mm thick and they're determined for a small connection thickness of 10 mm as well. The length of the structure becomes 7,01 meters when a connection thickness of 10 mm is applied. The critical loads and deflection of both connection types are gathered in Table 7.6.

	500 mm	10 mm
	Theory	Theory
M [kNm/m]	2	2
σ [MPa]	2,13	2,13
u_z [mm]	11,02	9,63

Table 7.6: Critical loads and deflection for two connection types

Rotational stiffness When a moment is applied to a structure it induces a rotation. The rotational stiffness of a connection equals the quotient of this moment and rotation. Figure 7.7 shows how the current problem is tackled: by duplicating the mechanical scheme and applying superposition it is possible to determine the rotation (φ_1 and φ_2) which is caused by the moment.

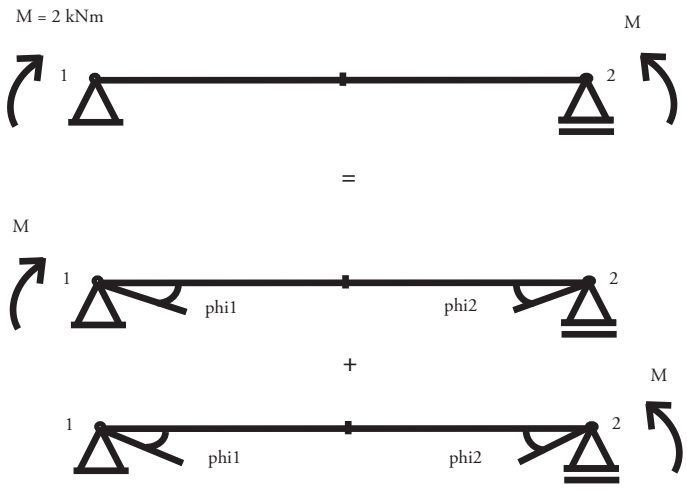

Figure 7.7: Breaking up the system previous to the calculation of the stiffness

So, theoretically, the rotational stiffness can be calculated in the following manner:

$$\varphi_1 = \varphi_2 = \frac{1}{2} * \frac{Ml}{EI}$$

$$k = \frac{M}{\varphi_{tot}}$$

$$\varphi_{tot} = \varphi_1 + \varphi_2$$

$$k = \frac{EI}{l}$$

Here, the unity of the rotational stiffness k is $MNm/m/rad$ and φ_{tot} is the rotation located at the connection. Table 7.7 presents the stiffness of the connections for thicknesses of 500 and 10 mm. The stiffness is linearly dependent on the thickness of the connection. So, as both connections have the same inertia because of the same height (75 mm) and width (per meter), the rotational stiffness must be fifty times as large (thickness ratio 1/50). To compare, the stiffness of both connections is (per meter) as large as that of a HE 120 A beam would be, if loaded in its strongest axis. However, the steel beam will be able to resist both compression and tension whereas the concrete is only able to withstand the compression part that goes along with the rotational stiffness, the tension part must be covered by for example steel (reinforcement).

	500 mm	10 mm
$k\ [MNm/m/rad]$	2,552	127,6

Table 7.7: Rotational stiffness for two connection types

7.3.2 FEA model

The basic test model discussed in the previous section (Figure 7.11) is constructed in Scia Engineer. Again, two models are distinguished, they have a connection thickness of 500 mm and 10 mm (Figure 7.8). All other conditions are the same as in the theoretical model in order to compare the results. The results of the FEA model are gathered in Table 7.8 and compared to the theoretical values. The comparison shows that the results deviate only a little and it can be concluded that the models agree with each other.

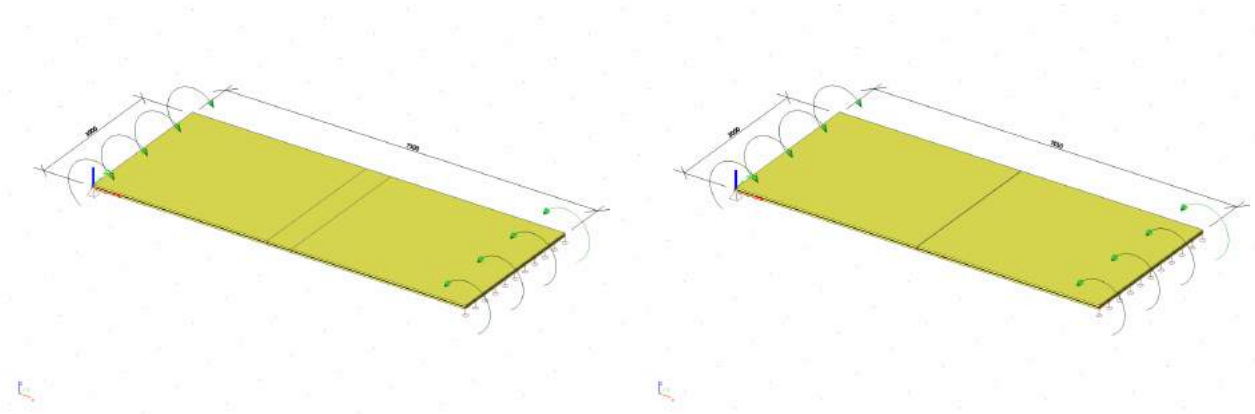

Figure 7.8: The basic test model in Scia Engineer a) connection thickness 500 mm b) connection thickness 10 mm

	500 mm		
	Theory	FEA	Δ%
M [kNm/m]	2	2	0
σ [MPa]	2,13	2,14	0,5
u_z [mm]	11,02	11,17	1,4
	10 mm		
	Theory	FEA	Δ%
M [kNm/m]	2	2	0
σ [MPa]	2,13	2,14	0,5
u_z [mm]	9,63	9,77	1,5

Table 7.8: Comparison of two calculation methods (theory and FEA) for two connection thicknesses a) 500 mm b) 10 mm

7.3.3 Application and verification

The last step in the process, determining the (rotational) stiffness of the connection simulating a continuous slab, is to apply the theoretically obtained stiffness in a new FEA model. The results of this model should correspond with the results of the other two calculations.
The shear stiffness (2,552 $MNm/m/rad$ and 127,6 $MNm/m/rad$) is assigned to a spring which connects the slab. The spring is a substitute for the connection and its thickness and will therefore reduce the span of the structure (Figure 7.9a). The results of both connection thicknesses are compared with the theoretical values in Table 7.9 and the first FEA model results in Table 7.10.

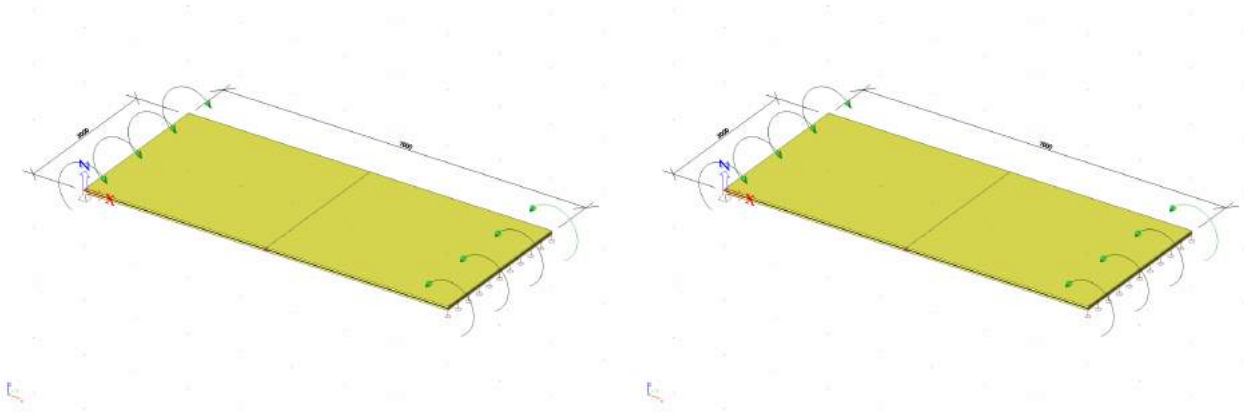

Figure 7.9: The basic test model in Scia Engineer, the connection modeled with a rotational spring a) connection thickness 500 mm b) connection thickness 10 mm

	500 mm		
	Theory	FEA Spring	Δ%
M [kNm/m]	2	2	0
σ [MPa]	2,13	2.12	0.5
u_z [mm]	11,02	11.11	0.8
	10 mm		
	Theory	FEA Spring	Δ%
M [kNm/m]	2	2	0
σ [MPa]	2,13	2,14	0,5
u_z [mm]	9,63	9,77	1,5

Table 7.9: Comparison of two calculation methods (theory and FEA spring) for two connection thicknesses a) 500 mm b) 10 mm

	500 mm		
	FEA	FEA Spring	Δ%
M [kNm/m]	2	2	0
σ [MPa]	2,14	2.12	0.9
u_z [mm]	11,17	11.11	0.5
	10 mm		
	FEA	FEA Spring	Δ%
M [kNm/m]	2	2	0
σ [MPa]	2,14	2,14	0
u_z [mm]	9,77	9,77	0

Table 7.10: Comparison of two calculation methods (FEA and FEA spring) for two connection thicknesses a) 500 mm b) 10 mm

After the comparison it's clear that the FEA model results match (Table 7.10). There's little deviation in the outcome of both theoretical and FEA spring results as well. Therefore, it can be concluded that the calculation method for the rotational stiffness, representing the stiffness of a connection that simulates a continuous slab, is valid.

7.4 Shear connection

7.4.1 Theory

Mechanical model First of all, a basic mechanical model is prepared for which the shear force in the connection is constant and where there are no other forces present, see Figure 7.10. In this way it's sufficient to add a shear (spring) stiffness to the connection and investigate its influence on the model.
The shear stiffness of the connection is determined with the mechanical properties of concrete (C45/55) and it is assumed that the connection behaves like a part of a continuous slab. The thickness of the connection is 0,5 meter in this example, the slab spans 7,5 meters (Figure 7.10).

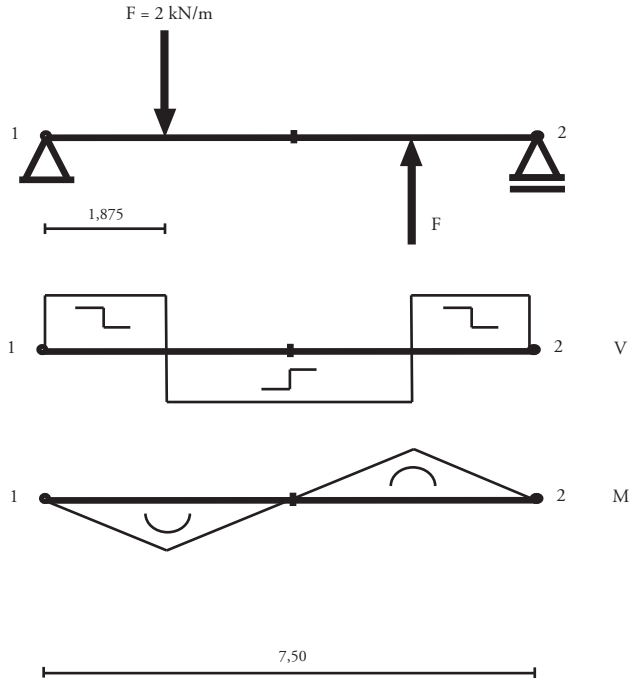

Figure 7.10: Mechanical model with measurements in meters

The applied forces F are positioned at 1/4th of the length, thus a system of two simple models is available for the purpose of calculation. For the height of the concrete slab a value of 75 mm is chosen, this is comparable to the height of the double curved concrete elements. With the given information the critical loads and the deflection of the described model (Figure 7.10) are determined:

$$V = \frac{1}{2} * F = 1kN$$

$$M = \frac{1}{4} * F * (\frac{1}{2}l) = 1,88kNm$$

$$\sigma = \frac{M*y}{I} = 2MPa$$

$$u_z = \frac{1}{48} * \frac{F*(\frac{1}{2}l)^3}{E*I} = 1,72mm$$

These values hold for the connection which is 500 mm thick and they're determined for a small connection thickness of 10 mm as well. The length of the structure becomes 7,01 meters when a connection thickness of 10 mm is applied. The critical loads and deflection of both connection types are gathered in Table 7.11.

	500 mm	10 mm
	Theory	Theory
V [kN/m]	1,00	1,00
M [kNm/m]	1,88	1,75
σ [MPa]	2,00	1,87
u_z [mm]	1,72	1,40

Table 7.11: Critical loads and deflection for two connection types

Shear stiffness When a shearforce is applied to a linear elastic structure (or a small element) it induces a shear distortion (γ), see Figure 7.11a. This value relates to the quotient of the deflection (v) and the thickness (d) of the element. The stiffness of the loaded element is equal to the quotient of the shearforce and the deflection. Besides, when considering a 3d element, the stiffness is divided by the width (b) of the element. Figure 7.11b shows the 3d test model with its dimensions, the slabs are connected by means of a connection with a thickness d, height h and width b, which is simulated using springs with a stiffness of k.

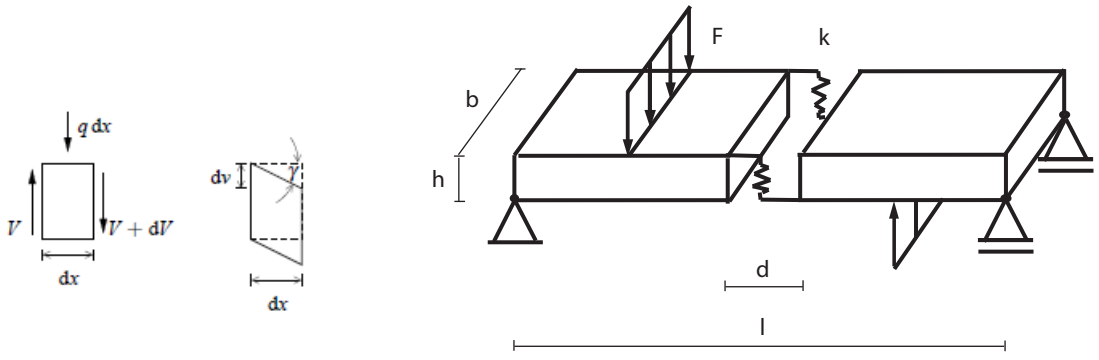

Figure 7.11: a) Shear distortion of an element b) The basic test model with dimensions

Finally, incorporating the relation for rectangular cross-sections loaded by shearforce, the expression for the (spring) stiffness k of the connection is determined:

$$\gamma = \frac{v}{d}$$

$$\frac{k}{b} = \frac{V}{v}$$

$$V = \frac{5}{6} * A * G * \gamma$$

$$G = \frac{E}{2(1+\nu)}$$

$$k = \frac{5}{12} * \frac{E*A}{d(1+\nu)}$$

$$\frac{k}{b} = \frac{5}{12} * \frac{E*h}{d(1+\nu)}$$

In these equations material constant G is the shear modulus, ν the poisson's ratio (which is 0,2 for concrete) and A the cross-section of the connection $(b * h)$. The stiffness $(\frac{k}{b})$ is, like the loads, determined per meter width and therefore has a unity MN/m^2. The shear stiffness of both connection types is determined with the formula and the values are gathered in Table 7.12.
The stiffness of the connection with the largest thickness is the smallest, this corresponds with the fact that the shear distortion is smaller for a larger element. Another remarkable thing is the magnitude of the stiffness, which appears to be high in both cases, but when considering the size of the connection it seems right there's need for a load of 1891 kN to deform the connection 1 mm in vertical direction. This, however, holds for the connection when it's part of a continuous slab, which was stated in the beginning of this section.

	500 mm	10 mm
$k\ [MN/m^2]$	1891	94531

Table 7.12: shear stiffness for two connection types

7.4.2 FEA model

The basic test model discussed in the previous section (Figure 7.11) is modeled in Scia Engineer. Again, two models are distinguished, they have a connection thickness of 500 mm and 10 mm (Figure 7.12). All other conditions are the same as in the theoretical model in order to compare the results. The results of the FEA model are gathered in Table 7.13 and compared to the theoretical values. The comparison shows that the results deviate only a little and it can be concluded that the models agree with each other.

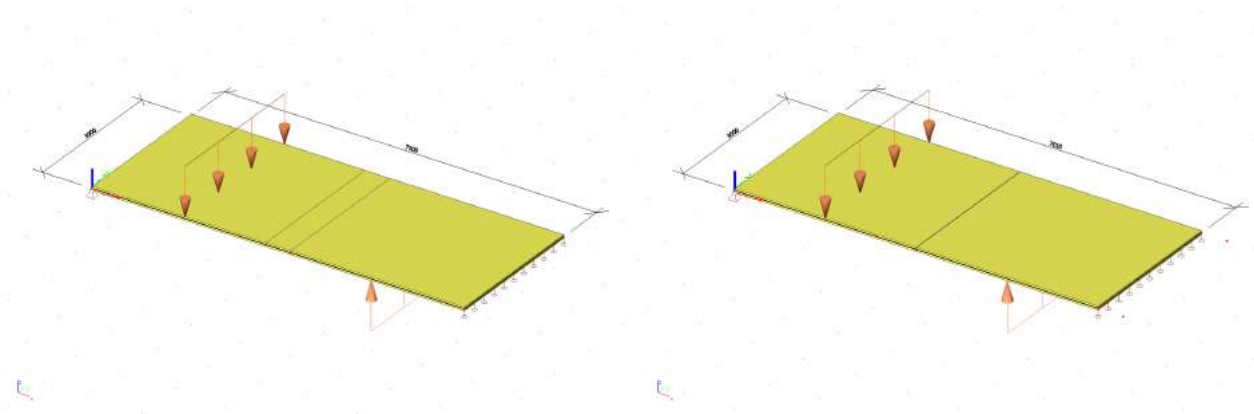

Figure 7.12: The basic test model in Scia Engineer a) connection thickness 500 mm b) connection thickness 10 mm

	500 mm		
	Theory	FEA	Δ%
V [kN/m]	1,00	1,00	0
M [kNm/m]	1,88	1,91	1,6
σ [MPa]	2,00	2,00	0
u_z [mm]	1,72	1,78	3,5
	10 mm		
	Theory	FEA	Δ%
V [kN/m]	1,00	1,00	0
M [kNm/m]	1,75	1,80	2,9
σ [MPa]	1,87	1,92	2,7
u_z [mm]	1,40	1,46	4,3

Table 7.13: Comparison of two calculation methods (theory and FEA) for two connection thicknesses a) 500 mm b) 10 mm

7.4.3 Application and verification

The last step in the process, determining the (shear) stiffness of the connection simulating a continuous slab, is to apply the theoretically obtained stiffness in a new FEA model. The results of this model should correspond with the results of the other two calculations. The shear stiffness (1891 MN/m^2 or 94531 MN/m^2) is assigned to a spring which connects the slab. The thickness of the connection is added to the length of the structure's span (Figure 7.13a). So, in contrast to the case of the rotational spring, the thickness of the connection must be incorporated. The reason for this is the way in which the structure is loaded and the position the load is applied. In the case of the rotational spring the applied load had a global effect on the structure, influencing the rotation as well as the deflection of the plate. In this case the spring adds shear stiffness to the plate at the center, thus influencing almost nothing because there's a very small shear force and shear deformation. The results of both connection thicknesses are compared with the theoretical values in Table 7.14 and the first FEA model results in Table 7.15.

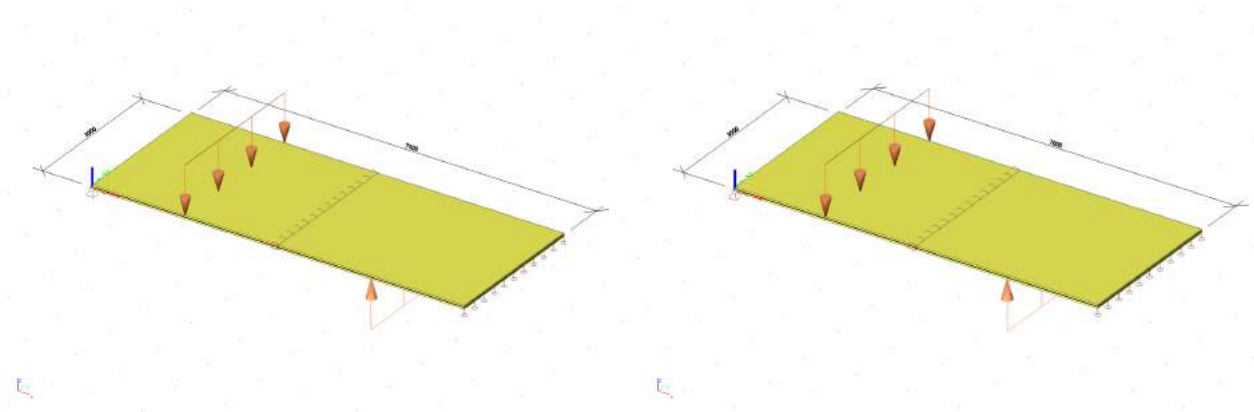

Figure 7.13: The basic test model in Scia Engineer, the connection modeled with a spring in vertical direction only a) connection thickness 500 mm b) connection thickness 10 mm

	500 mm		
	Theory	FEA Spring	Δ%
V [kN/m]	1,00	1,00	0
M [kNm/m]	1,88	1,91	1,6
σ [MPa]	2,00	2,00	0
u_z [mm]	1,72	1,78	3,5
	10 mm		
	Theory	FEA Spring	Δ%
V [kN/m]	1,00	1,00	0
M [kNm/m]	1,75	1,79	2,3
σ [MPa]	1,87	1,91	2,1
u_z [mm]	1,40	1,45	3,6

Table 7.14: Comparison of two calculation methods (theory and FEA spring) for two connection thicknesses a) 500 mm b) 10 mm

	500 mm		
	FEA	FEA Spring	Δ%
V [kN/m]	1,00	1,00	0
M [kNm/m]	1,91	1,91	0
σ [MPa]	2,00	2,00	0
u_z [mm]	1,78	1,78	0
	10 mm		
	FEA	FEA Spring	Δ%
V [kN/m]	1,00	1,00	0
M [kNm/m]	1,80	1,79	0,6
σ [MPa]	1,92	1,91	0,5
u_z [mm]	1,46	1,45	0,7

Table 7.15: Comparison of two calculation methods (FEA and FEA spring) for two connection thicknesses a) 500 mm b) 10 mm

After the comparison it's evident that the FEA model results are very much alike (Table 7.15). Of course, this also means that the results of the spring stiffness are simular to the theoretical values, like they did for the other FEA model. Therefore, it can be concluded that the calculation method for the shear stiffness, representing the stiffness of a connection that simulates a continuous slab, is valid.

7.4.4 Conclusion

The most reliable comparison value, when comparing the influence of the connection on the slabs behavior, was the deflection. Table 7.16 gives an overview of the differences between the models deflection.

Connection type	Comparison	Value	Connection 500mm (%)	Connection 10mm (%)
Axial	Theory vs FEA	u_z	0.2	1.1
	Theory vs Spring	u_z	0.6	0.6
	FEA vs Spring	u_z	0.8	0.5
Rotational	Theory vs FEA	u_z	1.4	1.5
	Theory vs Spring	u_z	0.8	1.5
	FEA vs Spring	u_z	0.5	0
Shear	Theory vs FEA	u_z	3.5	4.3
	Theory vs Spring	u_z	3.5	3.6
	FEA vs Spring	u_z	0	0.7

Table 7.16: Summary of connection comparisons

The most important comparison of either connection type is the third one (FEA vs Spring), because this is the only comparison executed in the same digital environment using (almost) the same boundary conditions. Based on these comparisons, with a maximum deviation of 0,8%, it can be concluded that the applied formulas (for axial stiffness:$\frac{k}{b} = \frac{Eh}{d}$, for rotational stiffness: $k = \frac{EI}{l}$ and for shear stiffness:$\frac{k}{b} = \frac{5}{12} * \frac{E*h}{d(1+\nu)}$) are trustworthy. Nonetheless, the comparison with theoretical results, with a maximum deviation of 4,3%, indicates that a skeptical approach is required when applying these formulas.

7.5 Application connection design

7.5.1 Introduction

This section discusses up to what extent it is possible to design a connection for a shell structure, using a finite element program. In the previous three sections formulas were derived for the determination of the axial, rotational and shear connection stiffness by means of simple structures. By combining these formulas a 3D (3 directions) stiffness is obtained, for one connection. In this way, the formulas of the connections, designed in previous sections, can be applied for connecting Green Planet and to investigate its influence on the stiffness of the shell structure.
To determine whether the formulas are indeed suitable for a combination into one connection, two shell structures are tested with this connection. First a single curved shell structure, a cylinder structure, is connected using a stiffness determined with the formulas. And after that a double-curved structure, a dome, is examined.

7.5.2 Cylinder structure

Set up

The conditions and boundary conditions of the cylinder structure are in proportion to the Green Planet structure. The length is 7 m, the width 3 m and its height 0,9 m, see Figure 7.14.

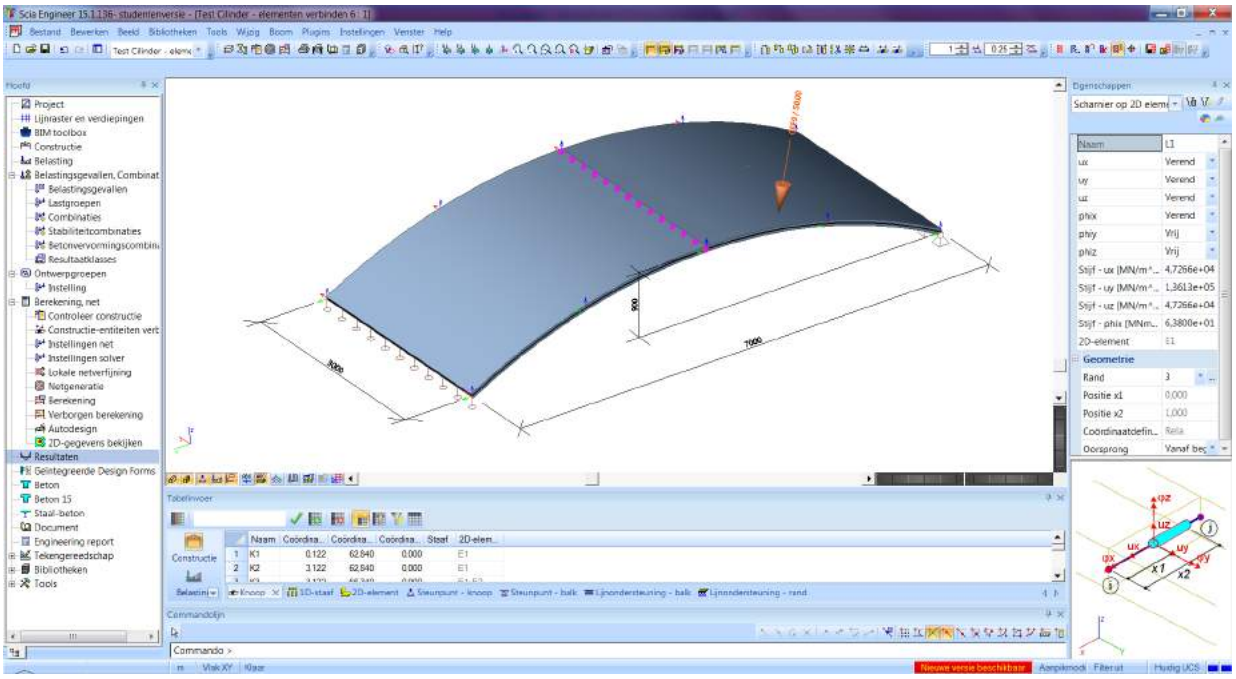

Figure 7.14: Cylinder structure dimensions (mm) and boundary conditions in Scia Engineer

In this figure the boundary conditions are given as well, in the windows along the right edge. Those are determined with a shell thickness 75 mm, a material (Concrete 45/55) stiffness of 36 300 MPa and a connection thickness of 10 mm. The formulas derived for the three directions were:

$$K_{axial}: \frac{k}{b} = \frac{Eh}{d}$$

$$K_{rotational}: k = \frac{EI}{l}$$

$$K_{shear}: \frac{k}{b} = \frac{5}{12} * \frac{E*h}{d(1+\nu)}$$

By filling in the constants we obtain the stiffness for this connection, see Table 7.17.

Stiffness	Value	Unit
K_{axial}	272 250	MN/m^2
$K_{rotational}$	127.6	MNm/m/rad
K_{shear}	42 266	MN/m^2

Table 7.17: Connection stiffness

At first the cylinder will be tested being a statically determinate structure (Figure 7.14), later on it will be tested as a statically indeterminate structure to investigate the shells susceptibility to buckling.

Statically determinate structure

The set ups in Figure 7.15, 7.16 and 7.17 are used for this test, in combination with the calculated stiffness of Table 7.17. The loads applied are (1) an evenly distributed load downwards (1 kN/m^2), (2) an evenly distributed load upwards (0,69 kN/m^2), (3) an asymmetrical distributed load upwards (0,69 kN/m^2), (4) an asymmetrical load downwards covering only half the surface (1 kN/m^2), (5) an asymmetrical load downwards covering only half the surface increased by a factor ten (10 kN/m^2), (6) an asymmetrical placed point load (15 kN), (7) an asymmetrical placed point load increased by a factor three (50 kN). The values are partly based on the critical loads determined for Green Planet. The displacement at the top of the cylinder is used for comparison, the model with the spring stiffness (springmodel) is compared with values derived from a model simulating a solid concrete cylinder structure (basemodel). Table 7.18 shows the results of the comparisons.

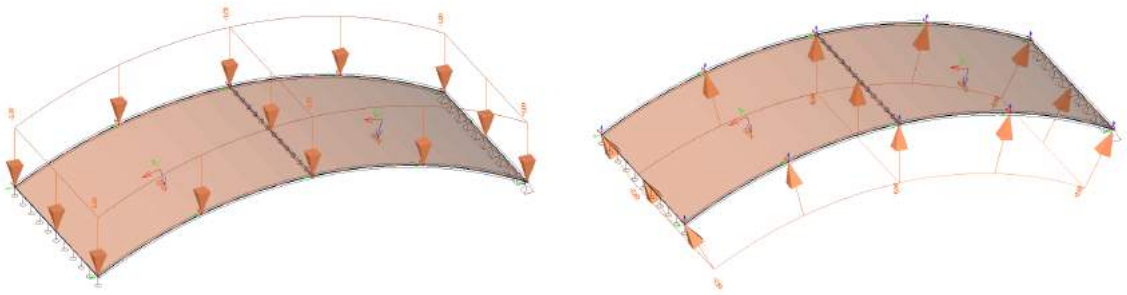

Figure 7.15: Loaded cylinder structure, load 1 and 2

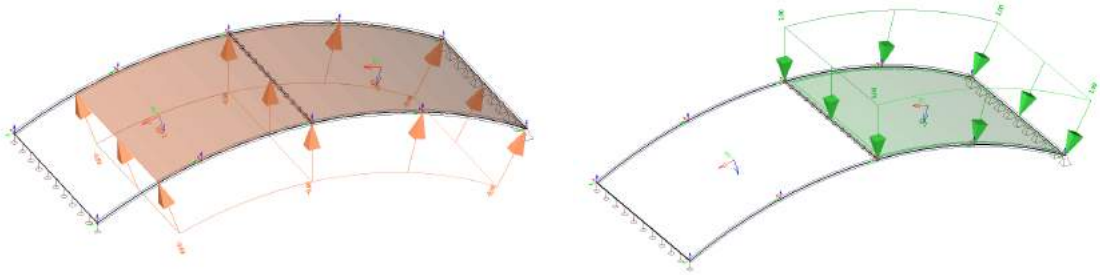

Figure 7.16: Loaded cylinder structure, load 3 and 4

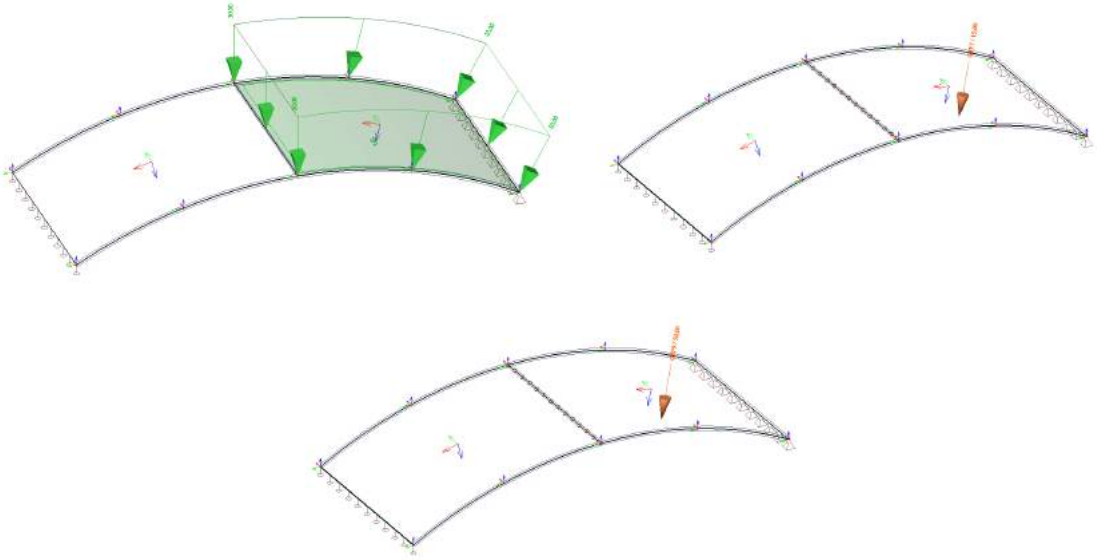

Figure 7.17: Loaded cylinder structure, load 5 to 7

Load 1		
Base model	u_z[mm]	24.95
Cylinder + spring	u_z[mm]	25.05
	Δu_z[%]	0.40

Load 2		
Base model	u_z[mm]	15.83
Cylinder + spring	u_z[mm]	15.90
	Δu_z[%]	0.44

Load 3		
Base model	u_z[mm]	15.98
Cylinder + spring	u_z[mm]	16.05
	Δu_z[%]	0.44

Load 4		
Base model	u_z[mm]	13.21
Cylinder + spring	u_z[mm]	13.27
	Δu_z[%]	0.45

Load 5		
Base model	u_z[mm]	132.1
Cylinder + spring	u_z[mm]	132.7
	Δu_z[%]	0.45

Load 6		
Base model	u_z[mm]	28.52
Cylinder + spring	u_z[mm]	28.62
	Δu_z[%]	0.35

Load 7		
Base model	u_z[mm]	95.08
Cylinder + spring	u_z[mm]	95.41
	Δu_z[%]	0.35

Table 7.18: Comparison between the basemodel and springmodel displacements, from left to right: load 1 to 7

The differences between the basemodel and springmodel are small, even smaller than expected when compared with the summary results of previous chapter, in Table 7.16. Besides the load variation the stiffness is varied too, see Table 7.19, where variation A is the stiffness calculated in Table 7.17. At first only the stiffness variations A to E are applied to the springmodel. Comparisons have been made with the basemodel, like in Table 7.18, and the results are gathered in Table 7.20.

Variation	A (K)	B (K/2)	C (K*2)	D (K/10)	E (K*10)	F (K/100)	G (K*100)
Thickness [mm]	75	75	75	75	75	75	75
E (C45/55) [MPa]	36 300	36 300	36 300	36 000	36 300	36 300	36 300
K_{axial} [MN/m^2]	272 250	136 130	544 500	27 225	2 722 500	2 722.5	2 7 225 000
$K_{rotation}$ [MNm/m/rad]	127.6	63.8	255.2	12.76	1 276	1.276	12 760
K_{shear} [MN/m^2]	94 531	42 266	189 062	9 553	945 310	945.3	9 453 100

Table 7.19: Variation of the connection stiffness

	Differences (Δu_z[%])					Differences (amplification factor)			
Load	A (K)	B (K/2)	C (K*2)	D (K/10)	E (K*10)	B (K/2)	C (K*2)	D (K/10)	E (K*10)
1	0.40	0.76	0.24	3.53	0.08	1.9	0.6	8.4	0.2
2	0.44								
3	0.44								
4	0.45	0.76	0.30	3.26	0.15	1.7	0.7	7.2	0.3
5	0.35	0.60	0.25	2.52	0.14	1.7	0.7	7.2	0.4
6	0.35	0.59	0.22	2.50	0.13	1.7	0.6	7.1	0.4
7	0.45			3.26	0.15			7.2	0.3

Table 7.20: Comparison between the basemodel and springmodel with varying stiffness, given are the displacement differences and the amplification factor between the differences of A and the other situations

Not only the displacement difference is given in Table 7.20, but also the difference between the displacement differences (amplification factor). This amplification factor must be compared with the initial amplification factor, which is applied to the stiffness K, to get an idea up to what extend the displacement is influenced by the initially applied amplification factor. From this experiment a few conclusions can be adopted.

- The maximum difference for situation A is 0,45%, this is an acceptable percentage and provides trust in the use of the formulas
- Both symmetrical and asymmetrical load appear to have a similar deflection difference, no big differences between these two different ways of loading are found
- Both large and small load appear to have a similar deflection difference, no big differences between these two different ways of loading are found
- Both distributed and point load appear to have a similar deflection difference, no big differences between these two different ways of loading are found
- Increasing or lowering the stiffness has influence on the difference between the basemodels and the springmodels displacement. But a lot of effort is required to improve the difference between the models (K*2 and K*10)
- This also means, however, it can be concluded that the calculated stiffness is not a divergence point of the stiffness, because making the connection even stiffer helps to

lower the displacement difference between the models. The exact output of the models is not presented, for this is too much information, but checking the numbers learns that the stiffness (K*10) didn't cause the occurring displacement of the springmodel to be less than the basemodels displacement. So making the spring ten times stiffer is actually making the differences between the models displacements thrice as small (see the amplification factor), making the results of the springmodel diverge to the results of the basemodel. Whilst making the connection ten times weaker makes the differences in displacements seven to eight times larger. When the stiffness is doubled or halved this results in both situations to a difference that differs around 1,7 times the original difference between the displacements. So, what this means is that the calculated stiffness is not the best simulation for the stiffness of a cross-section of a continuous slab, although 0,45% is an acceptable difference, since there are stiffness values with better results. Therefore, more research is required to understand the value of the calculated stiffness.

Internal forces

Besides the displacement it might be interesting to see how the spring stiffness influences the internal forces of the cylinder compared to a continuous cylinder. When the cylinder is loaded the edges will suffer some edge disturbance with peak stresses in a very small area, a common reaction for a shell structure. The values derived from the edge disturbance are filtered out when comparing the results between the base- and springmodel. But the fact that more edge disturbance appears when applying a spring stiffness is reason for some caution when it comes to interpreting the results (and the differences). Table 7.21 presents the comparison results for load 1 and 3 to 7 (load 1 and 2 are comparable).

Load 1	Basemodel	Springmodel	Δ[%]	Load 3	Basemodel	Springmodel	Δ[%]
M_x[kNm/m]	-1.32	-1.33	0.8	M_x[kNm/m]	0.85	0.85	0
M_y[kNm/m]	-6.35	-6.36	0.2	M_y[kNm/m]	4.09	4.09	0
V_x[kN/m]	2.00	2.00	0	V_x[kN/m]	1.00	1.00	0
V_y[kN/m]	4.00	4.00	0	V_y[kN/m]	3.00	3.00	0
N_x[kN/m]	-12.2	-12.0	1.7	N_x[kN/m]	7.29	8.00	9.7
N_y[kN/m]	11.9	12.1	1.7	N_y[kN/m]	-7.31	-7.43	1.6
Load 4	Basemodel	Springmodel	Δ[%]	Load 5	Basemodel	Springmodel	Δ[%]
M_x[kNm/m]	-0.77	-0.77	0	M_x[kNm/m]	-7.75	-7.74	0.1
M_y[kNm/m]	-3.75	-3.75	0	M_y[kNm/m]	-37.5	-37.5	0
V_x[kN/m]	1.00	1.00	0	V_x[kN/m]	10.0	10.0	0
V_y[kN/m]	-3.00	-3.00	0	V_y[kN/m]	-30.0	-30.0	0
N_x[kN/m]	-3.92	-4.00	2.0	N_x[kN/m]	-39.2	-40.0	2.0
N_y[kN/m]	6.71	6.63	1.2	N_y[kN/m]	67.1	66.3	1.2
Load 6	Basemodel	Springmodel	Δ[%]	Load 7	Basemodel	Springmodel	Δ[%]
M_x[kNm/m]	-4.19	-4.09	2.4	M_x[kNm/m]	-14.0	-13.6	2.9
M_y[kNm/m]	-13.0	-12.8	1.6	M_y[kNm/m]	-43.2	-42.5	1.6
V_x[kN/m]	-51.4	-42.8	20	V_x[kN/m]	-171	-143	20
V_y[kN/m]	50.0	50.0	0	V_y[kN/m]	-180	-150	20
N_x[kN/m]	11.6	14.6	26	N_x[kN/m]	38.5	48.7	26
N_y[kN/m]	26.1	26.0	0.4	N_y[kN/m]	87.0	86.6	0.5

Table 7.21: Comparison between the basemodel and springmodel internal forces, from left to right: load 1 and 3 to 7

From these results a few conclusions are derived.

- It's characteristic to notice how the results of load 6 and 7 differ from each other and how the results of load 4 and 5 don't differ, except for the factor that is applied to the load (10). That means the distributed load is indeed affecting the whole structure and the point load mainly locally.
- Another difference between those load pairs is that the difference between the basemodel and springmodel is quite large for load 6 and 7, in contrast to the other loads. The large difference is caused by local forces around the point load, comparable with the edge disturbance but not negligible. So, the introduction of the spring causes the normal force along the surface of the cylinder to increase by 26%, this means that it has a direct effect on the local (in) stability of the cylinder structure. Whereas it doesn't occur for the distributed load, because the cylinder structure is statically determinate and deforming into a new equilibrium. It is, however, interesting to examine the instability a little more in depth as it is one of the main failure loads of shell structures. Therefore, the cylinders behavior is investigated in a statically indeterminate state, in the next section "statically indeterminate structure".
- Overall, the result is acceptable. The results for load 6 and 7 are local results that actually don't differ too much for being peak stresses, but it must be taken into

consideration. The other loads differ 9,7% and 2,0% at most. Preferably, a difference of 1% or less is found. But there is a reason why the difference is larger, the N_x values that apply to this situation are maximum values adopted because there were edge disturbances involved that had to be filtered out. So, taking load 3 as an example, the value 8,00 kN/m is actually somewhere in between 6,00 and 8,00 kN/m and that value comes a lot closer to the original value of 7,29 kN/m. So, the internal forces comparison is acceptable and so far the results of the springmodel are in line with the results of the basemodel.

Two way connection

The concrete elements of Green Planet will be connected on all four sides, that means the spring will be applied in longitudinal and transverse direction of the structure. Therefore, a short experiment is executed to see what happens if the cylinder is split in half by applying a spring along the length of the shell structure. Figure 7.18 presents one of the loads applied to the shell with connection springs applied in two directions.

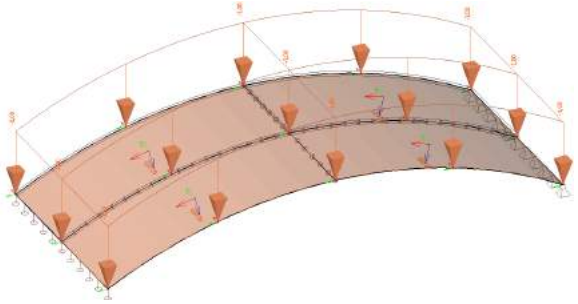

Figure 7.18: The spring connection applied in two directions

	Displacement differences (%)	
Load	A(K) one-way	A(K) two-way
1	0.40	1.52
2	0.44	1.52
3	0.44	1.56
4	0.45	1.51
5	0.35	1.59
6	0.35	1.51
7	0.45	1.49

Table 7.22: The displacement difference between the basemodel and the springmodels (one way and two way connection)

Now, this experiment is carried out just like the first cylinder experiment, using the same loads, and hence it can be compared, see Table 7.22. The results show a clear difference of three to four times the values of the first experiment. Still, 1,5% difference is not much but this is a large increase. The reason for the increase is mainly the shape of the cylinder, it is

single curved whereas the Green Planet shell is double-curved and in this situation transverse normal forces would resist the load better. This is underlined by the results of the internal forces, see Table 7.23, where values N_y and their differences have increased compared to the previous springmodel. It can also be noticed that this increase only happens when a distributed load is applied to the structure, the point load situation isn't influenced much which underlines again it has a local influence on the shells behavior. The pattern of the internal forces is the same as generated by the (same) loads in the basemodel. So there is a strong resemblance between the basemodel and the springmodels, but the difference of 5,5% (N_y, load 3) calls for more proof that the calculated stiffness is the actual stiffness that simulates a continuous concrete slab. A model that matches the Green Planet model better, and actually has a curved surface in two directions, is a dome structure and will be covered in a new section.

Load 1	Basemodel	Springmodel	Δ[%]	Load 3	Basemodel	Springmodel	Δ[%]
M_x[kNm/m]	-1.32	-1.30	1.5	M_x[kNm/m]	0.85	0.84	1.2
M_y[kNm/m]	-6.35	-6.42	1.1	M_y[kNm/m]	4.09	4.13	1.0
V_x[kN/m]	2.00	2.00	0	V_x[kN/m]	1.00	1.00	0
V_y[kN/m]	4.00	4.00	0	V_y[kN/m]	3.00	3.00	0
N_x[kN/m]	-12.2	-12.0	1.7	N_x[kN/m]	7.29	8.00	9.7
N_y[kN/m]	11.9	12.5	5.0	N_y[kN/m]	-7.31	-7.71	5.5
Load 4	Basemodel	Springmodel	Δ[%]	Load 5	Basemodel	Springmodel	Δ[%]
M_x[kNm/m]	-0.77	-0.76	1.3	M_x[kNm/m]	-7.75	-7.56	1.6
M_y[kNm/m]	-3.75	-3.79	1.1	M_y[kNm/m]	-37.5	-37.9	1.1
V_x[kN/m]	1.00	1.00	0	V_x[kN/m]	10.0	10.0	0
V_y[kN/m]	-3.00	-3.00	0	V_y[kN/m]	-30.0	-30.0	0
N_x[kN/m]	-3.92	-4.00	2.0	N_x[kN/m]	-39.2	-40.0	2.0
N_y[kN/m]	6.71	6.88	2.5	N_y[kN/m]	67.1	68.8	2.5
Load 6	Basemodel	Springmodel	Δ[%]	Load 7	Basemodel	Springmodel	Δ[%]
M_x[kNm/m]	-4.19	-4.10	2.2	M_x[kNm/m]	-14.0	-13.7	2.2
M_y[kNm/m]	-13.0	-12.9	0.8	M_y[kNm/m]	-43.2	-42.9	0.7
V_x[kN/m]	-51.4	-42.8	20	V_x[kN/m]	-171	-143	20
V_y[kN/m]	50.0	50.0	0	V_y[kN/m]	-180	-160	20
N_x[kN/m]	11.6	14.8	28	N_x[kN/m]	38.5	49.2	28
N_y[kN/m]	26.1	26.2	0.4	N_y[kN/m]	87.0	87.3	0.3

Table 7.23: Comparison between the basemodel and springmodel (two way connection) internal forces, from left to right: load 1 and 3 to 7

Statically indeterminate structure

The previous part of the cylinder analysis considered the statical determinate situation which gave a good insight into the behavior of the shell and offered a simple way to determine the worth of the calculated spring stiffness that was applied. But, the cylinder shell is deforming into equilibrium (and failing) mainly due to moments rather than normal forces while most shell structures fail because of buckling. This failure mode is applicable to

Green Planet too. Therefore, the emphasis of this section will be on the critical buckling load of the cylinder. Besides, the spring is now allocated at a quarter of the distance instead of in the middle of the structure to prevent the creation of a symmetrical arch with three hinges. Figure 7.19 illustrates the statically indeterminate cylinder structure of this experiment. This structure is loaded with the same loads as before. The comparison that will be made is based on the critical load factors. These load factors are numbers that need to be multiplied to the applied load to get the actual load that will cause the shell structure to buckle. The results of the experiment are presented in Figure 7.20 together with the comparison in Table 7.24.

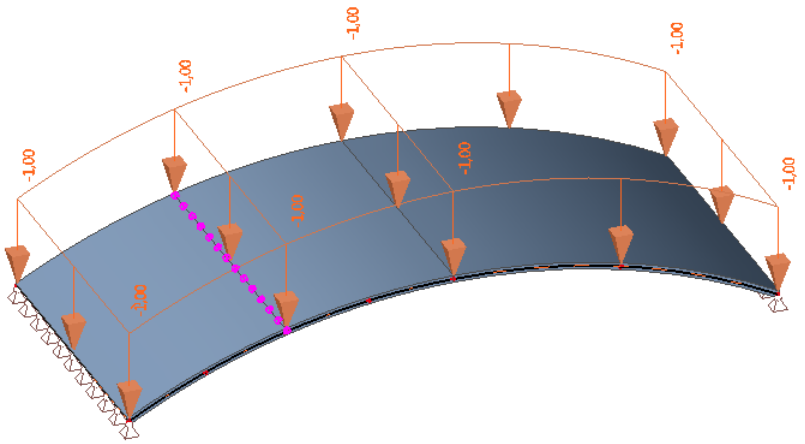

Figure 7.19: The spring connection applied to the statically indeterminate cylinder structure

Stabiliteitcombinatie : S1	
1	133,06
2	300,71
3	537,13
4	654,84
Stabiliteitcombinatie : S2	
1	-940,22
2	-774,62
3	-431,89
4	-193,43
Stabiliteitcombinatie : S3	
1	-997,04
2	-819,56
3	-457,09
4	-204,65
Stabiliteitcombinatie : S4	
1	266,35
2	592,03
3	1046,17
4	1209,94
Stabiliteitcombinatie : S6	
1	125,64
2	161,29
3	249,39
4	355,76
Stabiliteitcombinatie : S7	
1	37,69
2	48,39
3	74,82
4	106,73
Stabiliteitcombinatie : S5	
1	26,63
2	59,20
3	104,62
4	120,99

Stabiliteitcombinatie : S1	
1	132,66
2	300,31
3	537,05
4	642,23
Stabiliteitcombinatie : S2	
1	-921,43
2	-774,51
3	-431,28
4	-192,85
Stabiliteitcombinatie : S3	
1	-977,19
2	-819,41
3	-456,42
4	-204,03
Stabiliteitcombinatie : S4	
1	265,46
2	590,98
3	1045,68
4	1192,39
Stabiliteitcombinatie : S6	
1	124,19
2	160,48
3	244,82
4	353,89
Stabiliteitcombinatie : S7	
1	37,26
2	48,14
3	73,44
4	106,17
Stabiliteitcombinatie : S5	
1	26,55
2	59,10
3	104,57
4	119,24

Figure 7.20: Critical load factors of the basemodel and springmodel, note that the set ends with load 5

Load 1	Δ[%]	Load 2	Δ[%]	Load 3	Δ[%]
1	0.3	1	2.0	1	2.0
2	0.1	2	0.0	2	0.0
3	0.0	3	0.1	3	0.1
4	2.0	4	0.3	4	0.3

Load 4	Δ[%]	Load 5	Δ[%]	Load 6	Δ[%]	Load 7	Δ[%]
1	0.3	1	0.3	1	1.2	1	1.2
2	0.2	2	0.2	2	0.5	2	0.5
3	0.0	3	0.0	3	1.9	3	1.9
4	1.5	4	1.5	4	0.5	4	0.5

Table 7.24: The difference between the critical load factors

The first buckling mode shows the largest deviation when load 2 and 3 are applied, 2.0%. But, these loads act upwards and the critical load factor is very large, because of the minus sign the factors are mixed up and should be in the same order as load 1, this yields exactly the same deviation set. There are also no differences between the deviations of load 4 and 5 and between those of load 6 and 7. The way of loading appears to determine the factor deviation, but there is an explanation for it; the only difference is the size of the load. However, the absence of difference between the deviations of load 1 and 3 is a special one, but one that is taken for true for now. So, the maximum deviation is 2% (in mode 4 of load 1 to 3) and the average deviation is a little less than 1%. This means the springmodel is quite accurate, but there's still a reason to be skeptical about it.
The internal forces and displacements of the statically indeterminate structure are given in Table 7.25. First, the difference with the statical determinate structure is obvious, the displacements and internal moments have become much smaller, whilst the normal forces increased or remained (approximately) the same. Then, the difference between the displacement of the basemodel and springmodel is very similar to earlier results; very small. This holds for the internal forces too, the difference between the models remains small. This means a trend presents itself; apparently the change in support (boundary condition) and spring position doesn't influence the accuracy of the model compared to the basemodel. Here, the max difference is 3,5% (difference of 5,9% (load 4) is because of rounding numbers) but that difference is derived from an area subjected to peak stresses, as is the case with almost all V_x, V_y, N_x and N_y for this statically indeterminate structure. So, considering that observation it can be concluded that the models agree with each other quite well, as they did before for the statically determinate structure. At least, this holds for the internal forces and the displacements.

Load 1	Basemodel	Springmodel	Δ[%]	Load 3	Basemodel	Springmodel	Δ[%]
u_z[mm]	0.06	0.06	0	u_z[mm]	0.13	0.13	0
M_x[kNm/m]	-0.01	-0.01	0	M_x[kNm/m]	-0.05	-0.05	0
M_y[kNm/m]	0.05	0.05	0	M_y[kNm/m]	-0.25	-0.25	0
V_x[kN/m]	0.19	0.19	0	V_x[kN/m]	0.90	0.90	0
V_y[kN/m]	0.39	0.40	2.6	V_y[kN/m]	1.71	1.72	0.6
N_x[kN/m]	-8.22	-8.42	2.4	N_x[kN/m]	5.20	5.34	2.7
N_y[kN/m]	-13.1	-13.1	0	N_y[kN/m]	8.28	8.24	0.5
Load 4	Basemodel	Springmodel	Δ[%]	Load 5	Basemodel	Springmodel	Δ[%]
u_z[mm]	0.90	0.90	0	u_z[mm]	8.97	9.01	0.4
M_x[kNm/m]	0.17	0.18	5.9	M_x[kNm/m]	1.75	1.75	0
M_y[kNm/m]	-0.87	-0.87	0	M_y[kNm/m]	-8.66	-8.65	0.1
V_x[kN/m]	2.03	2.06	1.5	V_x[kN/m]	20.3	20.6	1.5
V_y[kN/m]	3.38	3.41	0.9	V_y[kN/m]	33.8	34.1	0.9
N_x[kN/m]	-5.06	-5.20	2.8	N_x[kN/m]	-50.6	-52.0	2.8
N_y[kN/m]	-10.1	-9.76	3.5	N_y[kN/m]	-101	-97.6	3.5
Load 6	Basemodel	Springmodel	Δ[%]	Load 7	Basemodel	Springmodel	Δ[%]
u_z[mm]	2.40	2.41	0.4	u_z[mm]	7.99	8.04	0.6
M_x[kNm/m]	-3.53	-3.55	0.6	M_x[kNm/m]	-11.8	-11.8	0
M_y[kNm/m]	6.79	-6.84	0.7	M_y[kNm/m]	-22.6	-22.8	0.9
V_x[kN/m]	-51.9	-52.5	1.2	V_x[kN/m]	-173	-175	1.2
V_y[kN/m]	-46.8	48.0	2.6	V_y[kN/m]	-156	160	2.6
N_x[kN/m]	-48.1	-49.2	2.3	N_x[kN/m]	-160	-164	2.5
N_y[kN/m]	-76.5	-75.8	0.9	N_y[kN/m]	-255	-253	0.8

Table 7.25: Comparison between the basemodel and springmodel displacement and internal forces, from left to right: load 1 and 3 to 7

For the statically indeterminate structure it's not really interesting to alter the stiffness (use situation B, C etc.) and elaborate on it extensively. The internal forces will not change very much because the normal forces will be transferred through the connection easily, and since the connection is pretty stiff. The resistance against failure is indicated by the displacement, but mainly by the buckling resistance. Now, to see the actual influence of the stiffness a short research is carried out, in the same way as the one before but now with a connection stiffness that is divided by ten. The research pointed out that that the displacement difference (Δ[%]) increased by a factor 8. The critical load factor however increased with factors varying between 0,5 and 10. The conclusion from this is that the calculated stiffness is not just a stiffness but one that actually makes sense regarding the small differences with the basemodel results and the bigger differences that arise when a weaker spring is applied.

Multiple springs

Besides the position change of the spring it's useful to see what happens if the cylinder is weakened by multiple springs (Figure 7.21). The question is whether this will effect the difference between the continuous concrete shell and the shell stiffened by springs that is

supposed to behave accordingly. The conditions are the same as for the statically indeterminate structure and the standard (situation A, calculated stiffness) is applied. Figure 7.22 presents the critical load factors as a result of this experiment and Table 7.26 indicates the differences between the load factors.

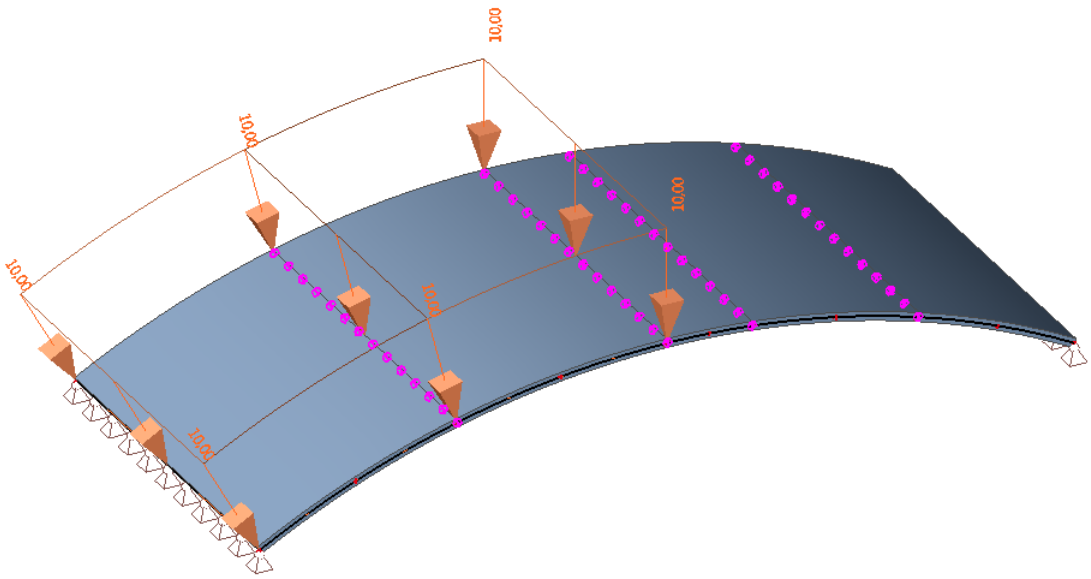

Figure 7.21: Multiple spring connections applied to the statically indeterminate cylinder structure

Stabiliteitcombinatie : S1	
1	133,06
2	300,71
3	537,13
4	654,84
Stabiliteitcombinatie : S2	
1	-940,22
2	-774,62
3	-431,89
4	-193,43
Stabiliteitcombinatie : S3	
1	-997,04
2	-819,56
3	-457,09
4	-204,65
Stabiliteitcombinatie : S4	
1	266,35
2	592,03
3	1046,17
4	1209,94
Stabiliteitcombinatie : S6	
1	125,64
2	161,29
3	249,39
4	355,76
Stabiliteitcombinatie : S7	
1	37,69
2	48,39
3	74,82
4	106,73
Stabiliteitcombinatie : S5	
1	26,63
2	59,20
3	104,62
4	120,99

Stabiliteitcombinatie : S1	
1	132,15
2	298,26
3	459,39
4	535,09
Stabiliteitcombinatie : S2	
1	-771,50
2	-656,39
3	-428,28
4	-192,11
Stabiliteitcombinatie : S3	
1	-816,25
2	-698,57
3	-453,25
4	-203,25
Stabiliteitcombinatie : S4	
1	264,64
2	587,24
3	900,09
4	1042,21
Stabiliteitcombinatie : S6	
1	116,92
2	152,41
3	234,28
4	346,88
Stabiliteitcombinatie : S7	
1	35,08
2	45,72
3	70,28
4	104,06
Stabiliteitcombinatie : S5	
1	26,46
2	58,72
3	90,01
4	104,22

Figure 7.22: Critical load factors of the basemodel and springmodel, note that the set ends with load 5

Load 1	Δ[%]	Load 2	Δ[%]	Load 3	Δ[%]
1	0.7	1	0.4	1	0.4
2	0.8	2	43	2	43
3	43	3	0.8	3	0.8
4	0.4	4	0.7	4	0.7

Load 4	Δ[%]	Load 5	Δ[%]	Load 6	Δ[%]	Load 7	Δ[%]
1	0.6	1	0.6	1	7.5	1	7.5
2	0.8	2	0.8	2	5.8	2	5.8
3	34	3	34	3	6.5	3	6.5
4	0.4	4	0.4	4	2.6	4	2.6

Table 7.26: The difference between the critical load factors of the basemodel and springmodel

First of all, a note should be made for Table 7.26, because the differences that are given are not for all modes the differences derived from the original springmodel table in Figure 7.22. For loads 1, 4 and 5 the last two modes (3 and 4) exchanged position in the springmodel, this was recognized from the deformation pattern in the FEA program. This exchanging of position was applicable to the first two modes of load 2 and 3 as well, which results are essentially the same as load 1, as already explained in the previous section.
Now, after evaluating the results it can be concluded that the differences are inconsistent. But, a closer look on the actual deformation patterns of the buckled shell learns that there is a link between all modes that differ more than 0,8%; edge instability. So, the edge is the weakest part of the shell, causing more instability in the springmodel compared to the basemodel. It seems as if the connections weaken the edge of the shell, making little cuts so it can buckle more easily. Then however, the reverse should be true too: if the point load is moved more closely to the center of the structure it must reduce the critical load factor difference. This experiment was carried out and indeed the difference reduced a lot. So the conclusion is that the applied stiffness is a good substitute for a continuous connection considering the max 0,8% difference, but the edge instability should be taken care of because this is an uncertain factor.
Looking back at earlier results from the statically indeterminate structure it appears that the maximum difference between the factors would have been 0,3% if the edge instability results would have been omitted there too. That would be a very accurate result. However, this also means that using multiple springs actually makes a big difference. Every spring that is applied reduces the accuracy of the springmodel compared to the basemodel because every spring adds a little weakness that adds to the total.
In the end it's important to know how many connections will be applied per meter structure and the expected difference (with the basemodel) this will yield. In this example the number of springs applied is four and the structure is 7 meters long. These dimensions are comparable to the rectangular Green Planet elements that will have maximum dimensions of 2,5 and 5 meters. In this example the maximum difference (edge instability excluded) was 0,8%, this will be an acceptable difference for Green Planet.

7.5.3 Dome structure

In the chapter 'Shell structures comparison' it was investigated which shell structure was best compared to the Green Planet design. The conclusion was that the cylinder represented Green Planet best, amongst others because the deformation pattern of the cylinder and Green Planet agree. Most of the other Green Planet results, however, appeared to be somewhere in between the ones from the cylinder and the dome structure. So, why is it interesting to investigate the dome structure with connection springs? Because there will be no edge disturbance or instability and the prediction is that there will be more similarity between the results because of that. Furthermore, this will allow an investigation where the stiffness of the springs is varied to see the influence on the buckling behavior and determine which stiffness gives the best results.
A perfectly continuous concrete dome is modeled in Scia Engineer and is again called the 'basemodel'. A model with exactly the same dimensions and specifications but subdivided with elements is called the 'springmodel', see Figure 7.23, because springs will be added in concentric circles around the midpoint at the element edges (marked in purple in Figure 7.23). The value of the spring is varied using the same values as for the cylinder structure, see Table 7.27, which is possible because the element thickness (75 mm) has not changed. The applied loads will be the same too and no further introduction, they will be called load 1 to 7 again, see Figure 7.15 to 7.17, Figure 7.23 presents load 5 for example. There is one difference however and that is load 3, this distributed load will act downwards on the shell in this case.
The basemodel versus springmodel comparison will be based on the buckling load again which is expressed with the critical load factor. The results are presented in Figure 7.24 and Table 7.28.

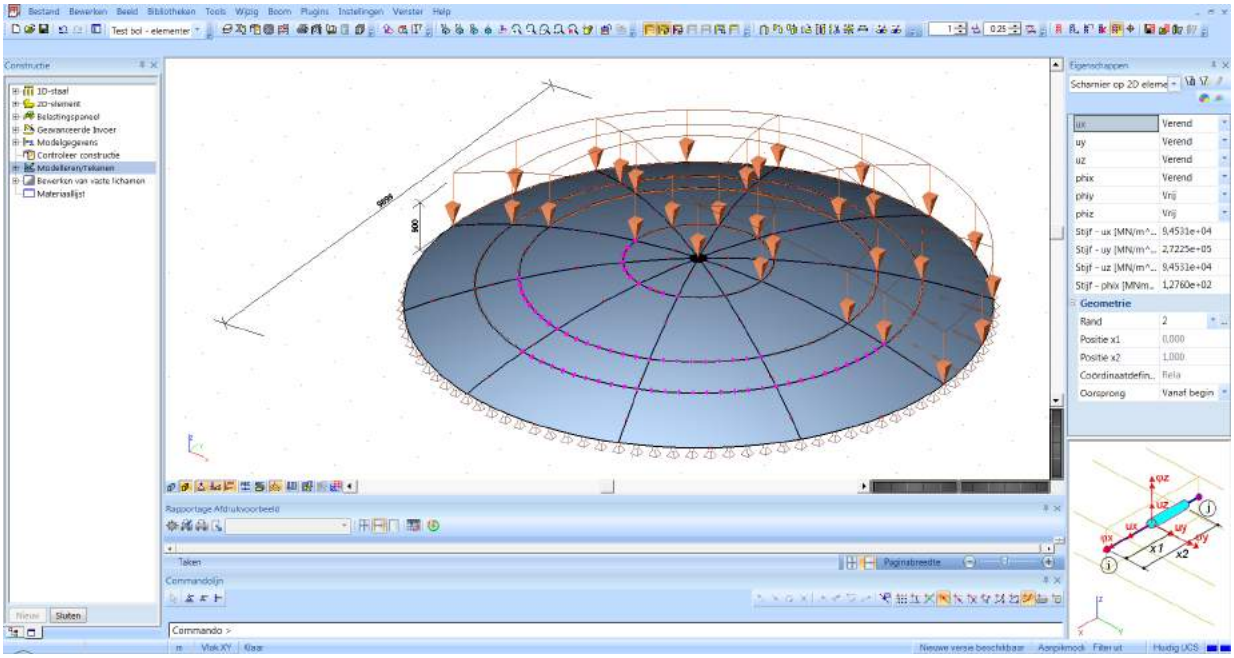

Figure 7.23: Dome structure dimensions (diameter 10 m, height 0,9 m) and boundary conditions in Scia Engineer

Variation	A (K)	B (K/2)	C (K*2)	D (K/10)	E (K*10)	F (K/100)	G (K*100)
Thickness [mm]	75	75	75	75	75	75	75
E (C45/55) [MPa]	36 300	36 300	36 300	36 000	36 300	36 300	36 300
K_{axial} [MN/m^2]	272 250	136 130	544 500	27 225	2 722 500	2 722.5	2 7 225 000
$K_{rotation}$ [MNm/m/rad]	127.6	63.8	255.2	12.76	1 276	1.276	12 760
K_{shear} [MN/m^2]	94 531	42 266	189 062	9 553	945 310	945.3	9 453 100

Table 7.27: Connection stiffness variations

Stabiliteitcombinatie : S1	
1	1217,62
2	1233,19
3	1233,34
4	1242,97
Stabiliteitcombinatie : S2	
1	-1801,40
2	-1787,45
3	-1787,24
4	-1764,67
Stabiliteitcombinatie : S3	
1	1557,97
2	1567,91
3	1672,64
4	1713,88
Stabiliteitcombinatie : S4	
1	1049,49
2	1052,17
3	1198,24
4	1199,66
Stabiliteitcombinatie : S6	
1	405,15
2	519,80
3	544,01
4	814,59
Stabiliteitcombinatie : S7	
1	121,54
2	155,94
3	163,20
4	244,38
Stabiliteitcombinatie : S5	
1	104,95
2	105,22
3	119,82
4	119,97

Stabiliteitcombinatie : S1	
1	1203,47
2	1213,07
3	1213,09
4	1216,72
Stabiliteitcombinatie : S2	
1	-1763,36
2	-1758,10
3	-1758,07
4	-1744,15
Stabiliteitcombinatie : S3	
1	1527,61
2	1546,75
3	1640,78
4	1676,23
Stabiliteitcombinatie : S4	
1	1026,62
2	1028,98
3	1170,73
4	1172,43
Stabiliteitcombinatie : S6	
1	394,77
2	506,62
3	528,49
4	794,07
Stabiliteitcombinatie : S7	
1	118,43
2	151,99
3	158,55
4	238,22
Stabiliteitcombinatie : S5	
1	102,66
2	102,90
3	117,07
4	117,24

Figure 7.24: Critical load factors of the basemodel and springmodel, note that the set ends with load 5

Load 1	Δ[%]	Load 2	Δ[%]	Load 3	Δ[%]
1	1.2	1	2.2	1	2.0
2	1.7	2	1.7	2	1.4
3	1.7	3	1.7	3	1.9
4	2.2	4	1.2	4	2.2

Load 4	Δ[%]	Load 5	Δ[%]	Load 6	Δ[%]	Load 7	Δ[%]
1	2.2	1	2.2	1	2.6	1	2.6
2	2.3	2	2.3	2	2.6	2	2.6
3	2.3	3	2.3	3	2.9	3	2.9
4	2.3	4	2.3	4	2.6	4	2.6

Table 7.28: The difference between the critical load factors of the basemodel and springmodel

The first thing to note in Table 7.28 is the lack of extreme differences, all load factors are more or less the same. This is a direct consequence of eliminating the edge instability. So, it is true that the differences between basemodel and springmodel are large because of the edge instability, and those differences should be considered but in the end left out because they don't represent the behavior of the spring in combination with Green Planet.
Now the experiment is carried out for stiffness variation D, E, F and G as well, so the stiffness is reduced or increased a lot in the springmodel. Without going into detail, the same results are gathered from these models and the same critical load factor difference tables are obtained. Subsequently, a line chart is made of the average critical load factor differences of each stiffness variation, see Figure 7.25. The exact differences are in sequence 30,7%, 5,7%, 2,0%, 1,5% and 1,5%. Interpreting the graphics, this means that when the calculated stiffness is reduced by a factor 100 the average deviation of the springmodel compared to the basemodel is (only) 31%. At the same time, there is very little difference between the situations the stiffness is increased by a factor 10 and factor 100. So, these data suggest that the actual stiffness of a continuous concrete must be somewhere in between the calculated stiffness and this stiffness reduced by a factor 10.
Because of this conclusion we zoom in on the 'factor 10 area' with another line chart. Now variation B and C from Table 7.27 are used and these results are gathered in the line chart as well, resulting in the line chart of Figure 7.26.

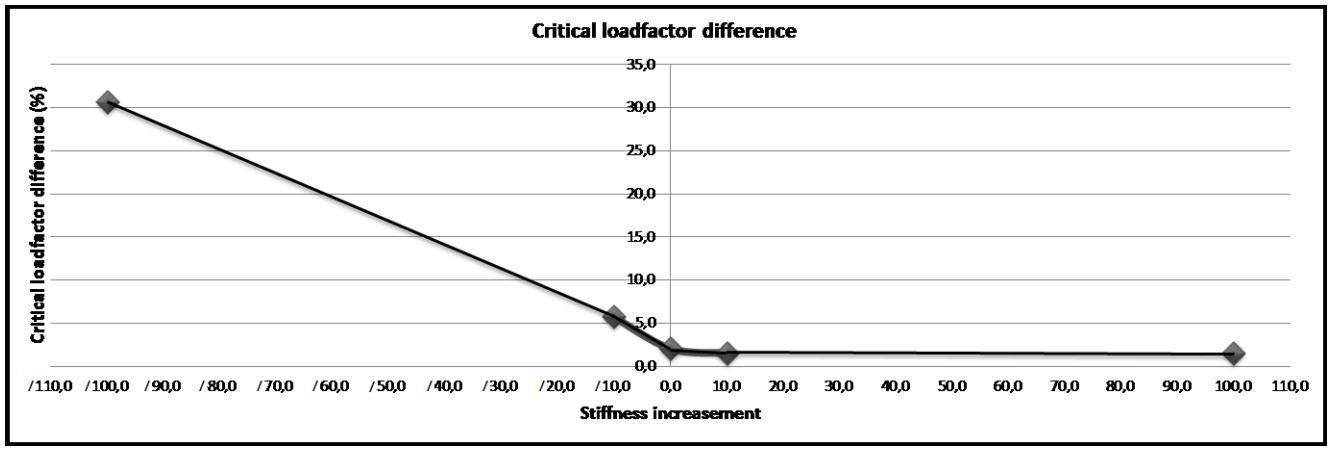

Figure 7.25: Line chart of the average critical load factor difference when the stiffness is reduced/increased up to a factor 100

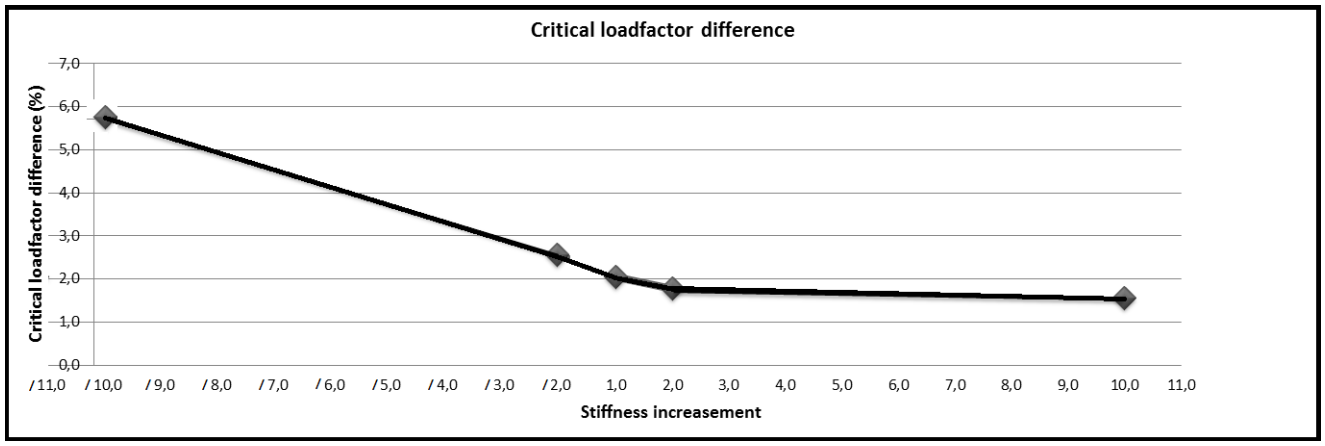

Figure 7.26: Line chart of the average critical load factor difference when the stiffness is reduced/increased up to a factor 10

In the last chart the factor 2 is introduced and now the exact differences are in sequence 5,7%, 2,6%, 2,0%, 1,8% and 1,5%. If it wasn't clear already, it is now, the factor 2 area seems to be the turning point for the critical load difference. The true stiffness must be somewhere in this area and this means that the calculated stiffness is close to the actual stiffness that this research is meant to yield, based on the critical buckling load. Yes, 2,0% is a considerable difference, but it doesn't get much better when the stiffness is increased tremendously. Therefore, the formulas of the calculated stiffness are accepted to use in the Green Planet experiments.
An observation that remains surprising is the low critical load factor difference (6%) while the stiffness is as many as ten times weaker compared to the starting point. For example, if the quality of the concrete is reduced tremendously in a way that the stiffness of the concrete is reduced by a factor ten, this will only cause the buckle load to be 6% smaller. In that case it would not really be rewarding to design a stiff connection, so more research is needed to figure out the value of this findings.

A suggestion would be to perform a research on the behavior of the shell with a non-linear analysis and/or using imperfections. Up to this point all calculations were performed with linear stability analysis making use of a reduction factor 6 that will be applied in the end to account for non-linearity's and imperfections.

7.5.4 Conclusions

In this section the axial, rotational and shear connection stiffness, which were determined individually in the previous section, are combined to form a connection applicable to a shell structure. The question was if this combination would result in a realistic behavior and if therefore these formulas can provide a reliable connection stiffness. To answer these questions there was a constant comparison between a continuous concrete structure model and a model that was supposed to simulate the first model by means of springs with a stiffness determined with the presented formulas. A cylinder structure and a dome structure were investigated. Firstly, the conclusions of the cylinder:

- The displacement of the models is very similar. A difference of max 0,45% is even better than the max 0,8% that was found for the simple models which served the determination of the stiffness formulas. The displacement patterns match with each other.
- The displacement difference, however, is improvable when more stiffness is applied to the spring. This means the formulas might be wrong and present values that are too low.
- The internal forces of the models are very similar. A difference of max 1,7% is found, provided that values as a result of peak stresses are omitted. The internal forces patterns match with each other.
- Once a spring is applied in both longitudinal and transverse direction the displacement difference increases a lot, with a factor 3 to 4. The internal forces generated by the distributed loads (not the point loads) show a little more deviation too. The patterns, however, remain similar. The increase in difference is attributed to adding more springs (the first and third conclusions prove this) and the lack of curve in the therefore weak transverse direction of the cylinder structure.
- The buckling loads of the models (now statically indeterminate) are very similar. The maximum difference is 2% and the average is 1%. The displacement of the models remains similar too (max 0,6%). The internal forces are a bit susceptible to peak stresses causing the differences to reach max 3,5%, but when ignored the max difference is 0,9%.
- When multiple springs are applied to the model there is more edge instability in the buckling modes, causing the differences to increase. Omitting the edge instability will lead to a max difference of 0,8% and would have lead to a max difference of 0,3% for the statically indeterminate model with only one spring applied.

- The cylinder with multiple springs has more springs applied per meter than Green Planet will have. The 0,8% difference in buckling behavior would be an acceptable result

Now, the conclusions of the dome structure will follow:

- The buckling loads of the comparing models are very similar. Besides, the results are very consistent, which means that the edge instability is ruled out. The max difference is 2,9% and the average is 2%.
- The critical load factors (indicators for the buckling load) of alternative models with increased and reduced spring stiffness are gathered and compared. The comparison demonstrates that a large increase in stiffness will only improve the difference with the initial model to an average value of 1,5%. A stiffness reduction however could mean a difference average of 30%. Therefore, the conclusion is that the 2% difference is actually a great result for the applied stiffness.
- However, an observation that remains surprising is the low critical load factor difference (6%) when the stiffness is reduced by a factor ten. And a low critical load factor difference of 31% is found when the stiffness is reduced by a factor hundred. More research is required to determine whether this is comparable with practical experiments.

With these conclusions the questions stated above can be answered. Yes, the formula combination does yield a realistic behavior and the results are actually quite accurate if peak stresses and instabilities are left out. In the end the buckling behavior will differ up to 1 or 2% it seems, with these deviations the formulas can provide a reliable connection stiffness. But, practical experiments are required to determine whether the ratio between the buckling reduction and the stiffness reduction is realistic.

7.6 Connecting Green Planet

7.6.1 Introduction

In this chapter the aim is to understand the influence of a connection on the internal forces and resistance of the Green Planet shell. The structure was segmented in Chapter 6 and the the influence of the segmentation was investigated in Section 6.4. Besides the segmentation discussion there was a variation of the segmented Green Planet presented, one that has enough buckling resistance. This Green Planet shell has a constant thickness of 250 mm and will be used in this experiment were it's compared with the same model connected with a predetermined stiffness. The first section explains the conditions of the model including the connection stiffness and the second section discusses the results of both models and the differences. The section before last will discuss the influence of the connection stiffness by comparing the model that is supposed to simulate the continuous concrete shell with a model were the stiffness is reduced by half. The last section will propose a final Green Planet design and includes some recommendations.

7.6.2 Conditions

In the beginning of this chapter the axial, rotational and shear stiffness formulas were determined based on simple models. They were tested on these simple models and on shell models thereafter and in both cases the formulas resulted in acceptable differences compared with their solid concrete parent models. The conditions remained a constant factor throughout these tests: the concrete quality C45/55 with a stiffness of 36 300 MPa and the connection thickness of 10 mm. These conditions will be applied to the springs of connected Green Planet model as well. Furthermore, both models are supported by hinges and therefore statically indeterminate. The thickness of the elements is however increased to 250 mm as mentioned in the introduction. The formulas derived for the three directions were:

$$K_{axial}: \frac{k}{b} = \frac{Eh}{d}$$

$$K_{rotational}: k = \frac{EI}{l}$$

$$K_{shear}: \frac{k}{b} = \frac{5}{12} * \frac{E*h}{d(1+\nu)}$$

By filling in the conditions we obtain the stiffness for the connection, see Table 7.29. The stiffness of model B, which has half the stiffness of model A, is added to the table because this value will be used in the last section of this chapter.

Stiffness	model A (K)	model B (K/2)	Unit
K_{axial}	907 500	453 750	MN/m^2
$K_{rotational}$	4 727	2 363	MNm/m/rad
K_{shear}	315 104	157 552	MN/m^2

Table 7.29: The applied connection stiffness for model A and B

7.6.3 Connection influence on Green Planet

In this chapter the segmented continuous concrete shell of Green Planet is compared with the same segmented shell that has a connection with the predetermined spring stiffness between every element. The latter is supposed to simulate the behavior of the first model. Table 7.30 presents the results of the segmented model X (see Section 6.4) and model A with the spring stiffness connections, the last column indicates the difference.

Extreme values	model X	model A	Δ[%]
$R_{z;res}$[kN]	23644	23644	0
$n_{1;max}$ [N/mm]	1336	2730	104
$n_{2;min}$ [N/mm]	-3264	-4198	28,6
$m_{1;max}$ [kNm/m]	62,0	63,2	1,9
$m_{2;min}$ [kNm/m]	-77,4	-82,9	7,1
$\sigma^{-}{}_{1;max}$ [N/mm^2]	7,62	10,5	37,8
$\sigma^{-}{}_{2;min}$ [N/mm^2]	-16,4	-21,7	32,3
$R_{z;max;up}$ [kN/m]	1002	1036	3,4
$R_{z;max;down}$ [kN/m]	-528	-560	6,1
$R_{y;max}$ [kN/m]	1377	1430	3,8
$R_{y;min}$ [kN/m]	-1631	-1688	3,5
$R_{x;max}$ [kN/m]	1610	1700	5,6
$R_{x;min}$ [kN/m]	-1610	-1700	5,6
$u_{z;max;up}$ [mm]	21,7	23,1	6,5
$u_{z;max;down}$ [mm]	38,3	40,9	6,8
$p_{cr;lin}$ [kN/m^2]	6,02	5,66	6,4
$p_{cr;lin;2}$ [kN/m^2]	6,12	5,76	6,3
$\Delta p_{cr,lin}$[%]	2	2	0

Table 7.30: Results of the segmented model X and model A with the spring stiffness connections, the last column indicates the difference

At first sight the difference between the models is about 6% with four outliers with 30 and 100% difference. In the previous section where the dome structure was used as an experiment, see Table 7.28, the maximum difference between the critical load factors was 3%. This difference was a result of a segmented model where only the concentric circles were connected by springs with an appointed stiffness. So, with that in mind, the difference of 6% lies perfectly in line with the expectations.
The normal forces and stresses are the results that differ most and require more attention. When the force pattern of both models is observed there is no difference recognizable, see Figure 7.27 were $n_{1;max}$is illustrated. Only the peak forces differ and they are so small they're not even visible in this overview. The same holds for the maximum main normal forces of $n_{2;min}$, See Figure 7.28. The stresses are derived from these normal forces and therefore give the same deviation and give the same patterns too. So, these peak forces and stresses should be considered but no real conclusions can be drawn based on these results. The overall result is acceptable since a great amount (591) of connections is applied, which means almost 600 potential weak spots. In the end, a difference of about 6% is deemed good enough for these models that are intended to behave the same.

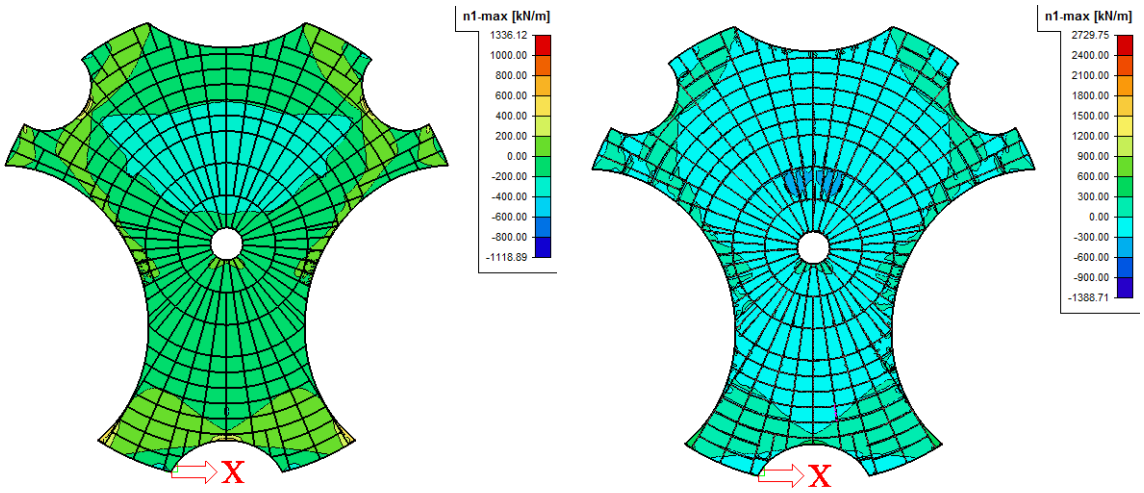

Figure 7.27: Normal force pattern $n_{1;max}$ of a) model X and b) model A

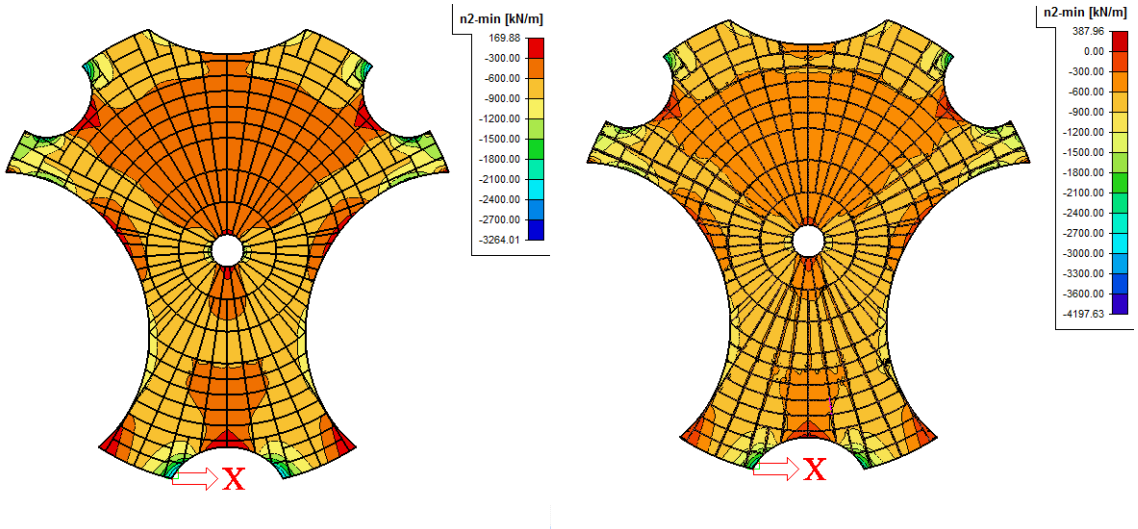

Figure 7.28: Normal force pattern $n_{2;min}$ of a) model X and b) model A

7.6.4 Connection stiffness influence on Green Planet

This last section discusses the connection stiffness and its influence on the internal forces and failure mode. Model A is supposed to simulate a continuous concrete shell and model B in its way is supposed to simulate a realistic design which has connections weakening the structure. The assumption in this case is that the connections will have a stiffness that is half the stiffness of the (imaginary) connection of the continuous concrete shell structure. The results are given in Table 7.31.

Extreme values	model A	model B	Δ[%]
$R_{z;res}$[kN]	23644	23644	0
$n_{1;max}$ [N/mm]	2730	2684	1,7
$n_{2;min}$ [N/mm]	-4198	-4579	9,1
$m_{1;max}$ [kNm/m]	63,2	63,7	0,8
$m_{2;min}$ [kNm/m]	-82,9	-82,9	0
$\sigma^{-}{}_{1;max}$ [N/mm^2]	10,5	10,4	1,0
$\sigma^{-}{}_{2;min}$ [N/mm^2]	-21,7	-23,5	8,3
$R_{z;max;up}$ [kN/m]	1036	1037	0
$R_{z;max;down}$ [kN/m]	-560	-561	0
$R_{y;max}$ [kN/m]	1430	1429	0
$R_{y;min}$ [kN/m]	-1688	-1689	0
$R_{x;max}$ [kN/m]	1700	1705	0
$R_{x;min}$ [kN/m]	-1700	-1705	0
$u_{z;max;up}$ [mm]	23,1	23,2	0,4
$u_{z;max;down}$ [mm]	40,9	41,1	0,5
$p_{cr;lin}$ [kN/m^2]	5,66	5,63	0,5
$p_{cr;lin;2}$ [kN/m^2]	5,76	5,74	0.3
$\Delta p_{cr,lin}$[%]	2	2	0

Table 7.31: Results of the model A with connection stiffness K and model B with connection stiffness K/2, the last column indicates the difference

The result of this experiment is surprising at first sight, the difference between the models is very small. Besides the peak stresses, which were already mentioned and treated in Section 7.6.3, the maximum difference is 0,5%. So, if the stiffness of all the connections is halved it will only result in a displacement that increases 0,5% and a buckling load that is 0,5% smaller. When looking back at the results of the dome structure the small differences are actually not surprising at all because this was the exact difference between two models with half the stiffness as well. So, the FEA calculations agree with each other and at least the outcomes are consistent. But, whether they are realistic is arguable because it's hard to accept the fact the stiffness of the connection has such a small influence on the stability of the shell structure. Practical tests could and should bring clarification in this case.

7.6.5 Final Green Planet design

Model B which is introduced in Section 7.6.2 and discussed in Section 7.6.4 is regarded as the final design for Green Planet, see Figure 7.29. This model fulfills the boundary conditions set up for the design, has a segmentation designed accordingly and it is supposed to have realistic connections. Still some intelligence could be added to this design, both in optimizing the FEA design and in practical design.

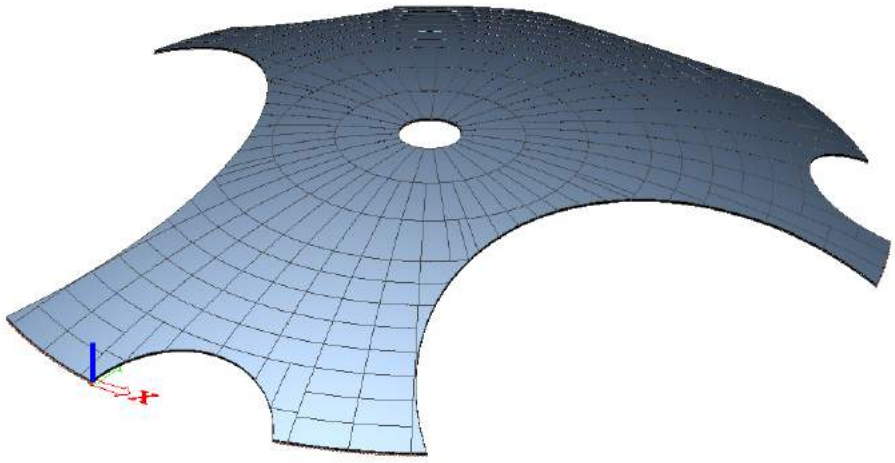

Figure 7.29: The final FEA model of Green Planet

Apart from practical concerns, which will follow in the next chapter, a few recommendations will be summed up regarding the optimization of the FEA design:

- Optimization of the element thickness. In Chapter 5 some methods were introduced to optimize the FEA design, one of them was the optimization of the element thickness. It was shown that by optimizing the thickness the buckling load and the displacement could be improved substantially. The thickness along the edges of the shell was increased whilst the thickness of the center portion of the shell was reduced. Such a study could be performed for this model as well, in combination with a practical feasibility study

- Adding edge beams. Shell structures without edge beams are prone to inextensible deformations or instabilities around the edges. These failure modes were often encountered during this research. Several attempts have been made to introduce a proper edge beam to the concrete shell, but these attempts were not satisfactory and could not be relied upon. So, this option is open for future research. The expectation is that this will have a major influence on the resistance of the shell structure because practically all failure modes were due to instabilities along the edges.

- Post tension foundation cables. For the foundation a few options were investigated consisting of steel tension cables. Due to small settlements that will always occur because of the elongation of the cables this foundation method has a destructive influence on the stability of the shell. Therefore, it was not suitable. With more resistance to buckling, possibly with adding edge beams, it might work out. But another option is applying post tension cables to compensate the elongation. This is worth the research, perhaps by an FEA program expert.

- Geometrical non-linear analysis. The stability problems that were addressed were always based on the linear stability analysis in combination with a conservative knock down factor. It would be interesting to perform a study with a geometrical non-linear analysis including imperfections to find out the real boundaries of the stability of the

shell. Hypothetically, the results must improve compared to the results determined with the conservative knock down factor. This was the conclusion in earlier attempts, but in those experiments the difference between the linear stability analysis and the non-linear analysis was remarkably small.

Part IV

Green Planet: execution and costs

Chapter 8

Execution and costs

8.1 Introduction

This final chapter addresses the execution of the Green Planet design and the challenges that have to be met. First, the feasibility of the proposed design is discussed and some important results are retrieved. The connection design is an important aspect of the execution of this shell structure and will be covered subsequently. Then, the execution method is discussed as well as the production of the elements. The design of the foundation is the last part of the execution that is discussed. The final section of this chapter will compare the costs of the new design with the original Green Planet design.

8.2 Feasibility

In Section 7.6.4 the connection stiffness influence on Green Planet was discussed and results were presented of a model with a connection stiffness which is half the value compared with a continuous concrete connection. Besides, as a boundary condition, the supports were all hinges, which means no settlements could influence the shell behavior. Hypothetically, if these results were correct, would this shell structure be feasible? That is the question that will be answered in this section. Table 8.1 presents the results of the model that was mentioned.

Extreme values	model B
$R_{z;res}$[kN]	23644
$n_{1;max}$ [N/mm]	2684
$n_{2;min}$ [N/mm]	-4579
$m_{1;max}$ [kNm/m]	63,7
$m_{2;min}$ [kNm/m]	-82,9
$\sigma^{-}{}_{1;max}$ [N/mm^2]	10,4
$\sigma^{-}{}_{2;min}$ [N/mm^2]	-23,5
$R_{z;max;up}$ [kN/m]	1037
$R_{z;max;down}$ [kN/m]	-561
$R_{y;max}$ [kN/m]	1429
$R_{y;min}$ [kN/m]	-1689
$R_{x;max}$ [kN/m]	1705
$R_{x;min}$ [kN/m]	-1705
$u_{z;max;up}$ [mm]	23,2
$u_{z;max;down}$ [mm]	41,1
$p_{cr;lin}$ [kN/m^2]	5,63
$p_{cr;lin;2}$ [kN/m^2]	5,74
$\Delta p_{cr,lin}$[%]	2

Table 8.1: Final Green Planet model results

The compressive and tension forces seem to have large maximum values, but those values are peak stresses and the majority of the results are a lot smaller. For instance, the tension force, which is interesting to address with regard to the reinforcement of the shell structure, see Figure 8.1. The largest tension force that occurs (99% of the shell surface) is maximum 300 kN/m, in the edge disturbance areas of the shell. Therefore, only 4 bars ϕ16mm per meter are required to transfer the tension forces, or 6 bars ϕ12mm (see Table 8.2). Apart from the edge disturbance areas and support areas, there is no tension in the shell. So, theoretically these bars are only required for half the surface of the shell, for the remaining part of the surface suffices a basic reinforcement mesh. The direct support areas, however, need a lot more reinforcement to cover and distribute the peak forces.

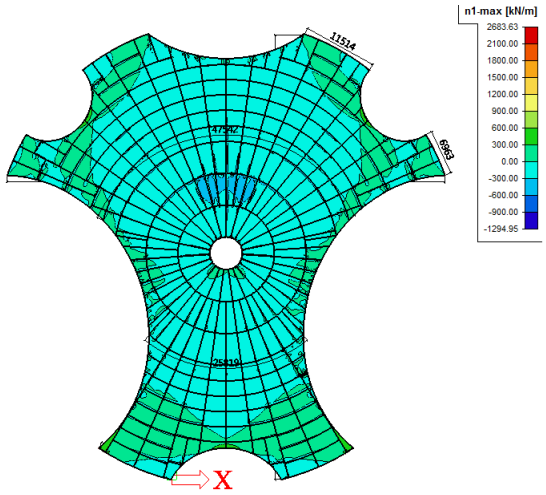

Figure 8.1: Tension forces Green Planet

Bar diameter [mm]	8	10	12	16	20	25	32	40
$F_{t;u}$ [kN]	22	34	49	88	137	214	350	547

Table 8.2: Tension force per reinforcement bar in kN (FeB 500, f_s= 435 N/mm^2), [46]

Figure 8.2 presents the overviews of the maximum tension and compressive stresses that occur in the Green Planet design. When peak stresses are omitted it leaves a maximum tension stress of 8 MPa and maximum compressive stress of 15 MPa. The compressive stress is low and can be handled by the concrete very easily. But, the tension stresses are too large, a reinforcement mesh would be required. Another interesting possibility, since the maximum tension stress is only 8 MPa, is the use of fiber concrete.

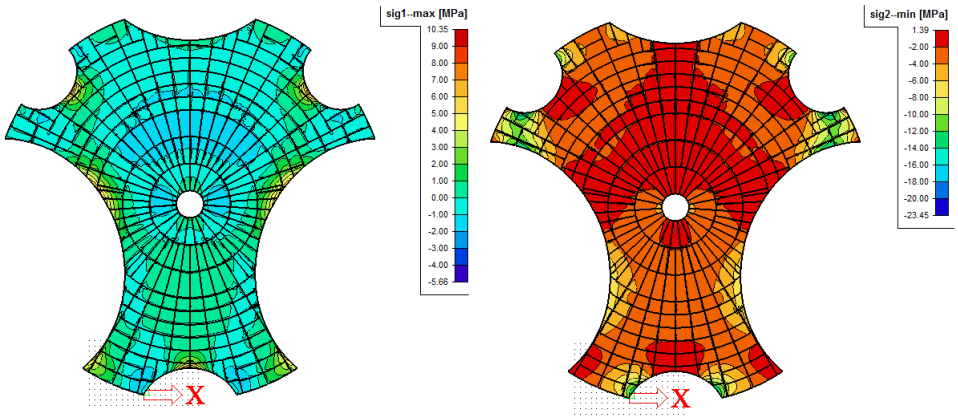

Figure 8.2: a) Overview of tension stresses and b) compressive stresses

The forces acting on the foundation are given in kN/m but in fact they have a maximum total value of approximately 10000 kN per support 'foot' (maximum of 12 meters wide) in

horizontal direction. Vertically a load with a maximum of 6000 kN is possible. In the section 'Foundation' these forces will be discussed in relation to the foundation solution.
The displacements of the shell are relatively small compared to the span, which is about 70 meters in both directions. Also, with an element thickness of 250 mm the required buckling load is almost met, being 5,63 while 6 is required, and with a few optimizations the shell could be safe with respect to buckling too.

8.3 Connections

Two interesting researches were performed with regard to connections for shell structures, [13, 46]. The different types of connections that were mentioned were a wet connection, bolted connection, post-tensioning connection, welded connection, glued connection and fiber joint connection. They all have their advantages and disadvantages, but for the precast double-curved elements it would serve to choose one of the most simple and established methods. Those would be the wet connection, bolted connection or welded connection.
In this shell structure the requirements for the stiffness of the connection are not very strict as was concluded in Chapter 7. This offers the opportunity to select from a wide range of connection options. Additionally, this might allow the prefabrication of the whole structure. The initial purpose of the curved concrete elements was to serve as a structural useful formwork and to cast the rest of the required concrete layer on top of it. But, the prefabrication of the structure is a very interesting option too. Therefore two connection designs are discussed, one for a prefabricated structure and one for the cast in-situ structure.

The wet connection The most easy connection for the cast in-situ design is the wet connection, Figure 8.3 shows the proposed connection. The total height of the final concrete layer will be 250 mm, 200 mm is deemed feasible but for now the 250 mm is selected because this is the thickness applied in the model depicted in Section 8.2. The curved elements will have a base layer of 50 mm, on top of that a reinforcement mesh is placed, and on top of that a new layer of 50 mm. The last layer will be smaller in width and in length, to leave a space of approximately 100 mm around the element. This width will be used for the bond between the reinforcement mesh and the in-situ concrete. In case the load on the structure acts upwards it's possible that extra reinforcement is required in the top part of the cross-section. This will only happen locally. On top of the elements it's possible to place (in-situ) the extra reinforcement bars with space holders.

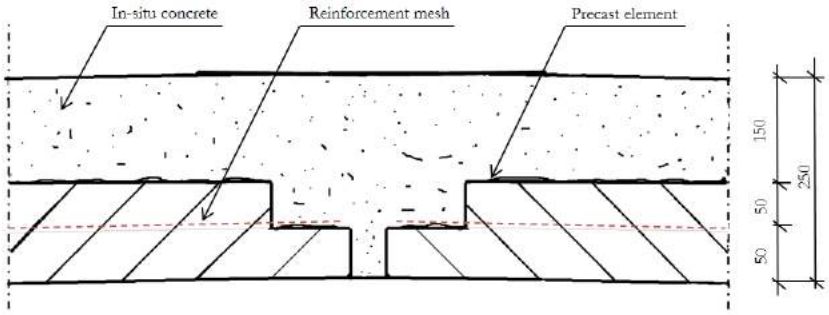

Figure 8.3: A cross-section of the proposed wet connection

The prefabricated connection There are a few possibilities for the prefabricated connection, but the most interesting one is illustrated in Figure 8.4. The concept is invented by R.N. ter Maten [46] and slightly adjusted for this case. Basically, the curved element consists of a reinforcement bar connected with a bolt at the end. When the bolt is tightened it induces a certain prestress on the connection which assures the connection maintains under compression.

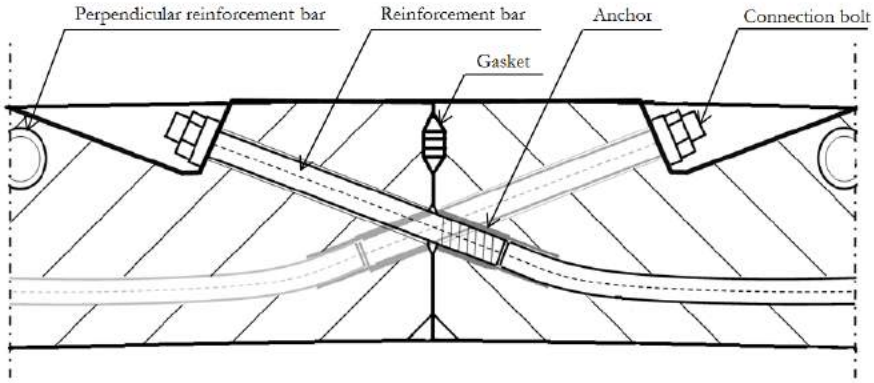

Figure 8.4: A cross-section of the proposed fully precast connection

8.4 Execution method

There are several methods to properly construct a segmented shell structure. A study on the execution methods for a dome structure was performed by R.N. ter Maten [46] and since the Green Planet design is related to this type of structure it is useful to present these various execution options. The execution methods for a dome structure are the Igloo method (Figure 8.5), the Igloo method II (Figure 8.6), the Top-down method (Figure 8.7), the Frame method (Figure 8.8) and the Segmental method (Figure 8.9).

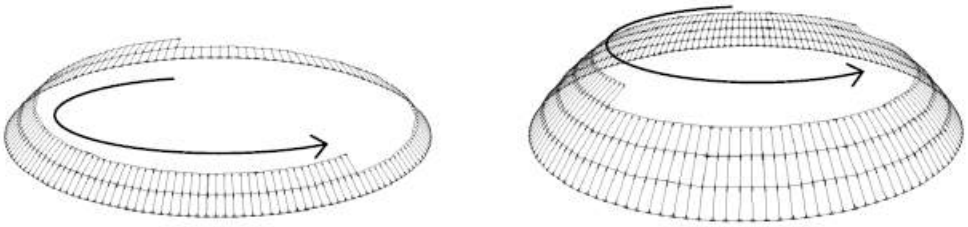

Figure 8.5: The Igloo method [46]

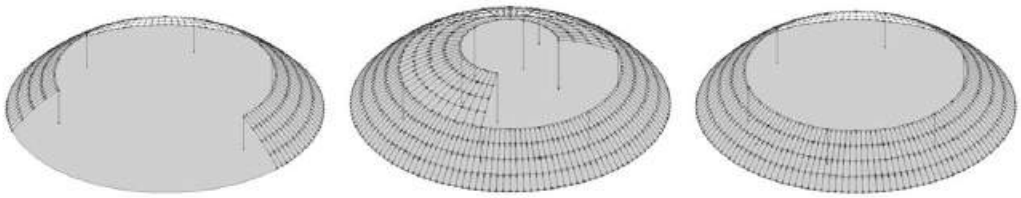

Figure 8.6: The Igloo method II [46]

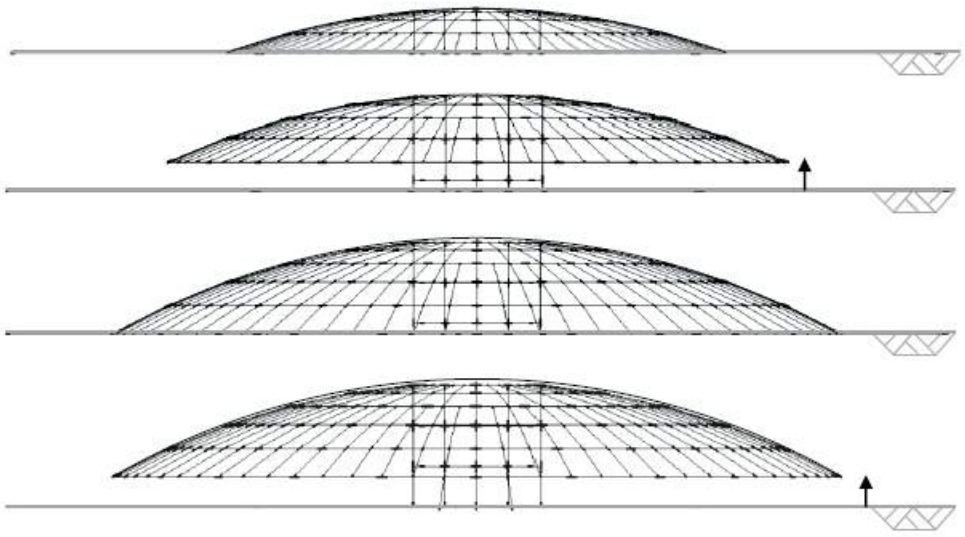

Figure 8.7: The Top-down method [46]

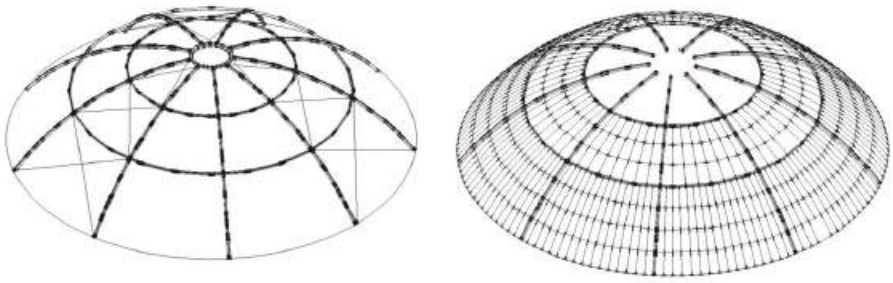

Figure 8.8: The Frame method [46]

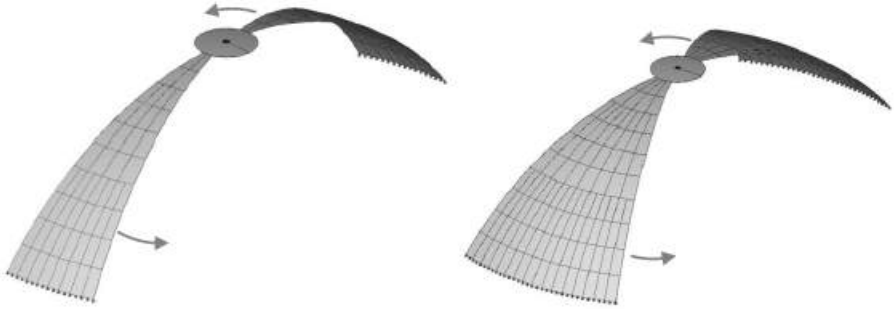

Figure 8.9: The Segmental method [46]

8.4.1 Proposed execution method

The advantages of the double-curved concrete elements produced with the adjustable formwork is that they can serve as formwork and are part of the permanent structure and it's behavior. This will save a lot of temporary formwork during the execution of the structure compared to other concrete designs where the concrete is applied in-situ. Still, some temporary formwork remains required: the scaffolding and formwork that will support the double-curved elements. The formwork planks have a double function as they serve as formwork for the wet connections as well. The proposal is to make use of the concentric circles that were created together with the segmentation. These 'lines' have a constant height along the circle and would serve as support lines in between which the elements can span. After the concrete is hardened they can be removed.
Another interesting option is to make use of the segmental method, illustrated in Figure 8.9. This method is particularly suitable for a fully prefabricated Green Planet design where the sections can be installed on the ground and subsequently hoisted in place. But since there are few supports in the Green Planet design and it's hard to find a real equilibrium situation between the segments, this method will not significantly reduce the amount of scaffolding that is needed.
For the Green Planet design where the concrete is applied in-situ it might be a good solution to combine the frame method and segmental method too. Figure 8.10 shows the final segmentation plan in the FEA program discussed in Chapter 6. Besides the concentric

circles it is useful to address the single curved lines perpendicular to the circles as well. These lines run from the top to the supports or edges. The scaffolding and formwork could be placed directly under these lines, like with the frame method, the precast elements spanning between the created support lines. Confirm the segmental method it is then possible to work around the structure in sections were the elements are positioned and the concrete is poured.

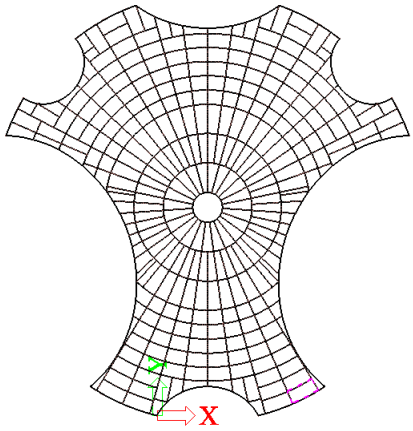

Figure 8.10: The final segmentation plan

8.5 Production of the elements

In Chapter 2 the production of the double-curved concrete elements was covered and this process needs to be scaled up for the required element sizes for the project Green Planet. As already mentioned in Chapter 6, the estimation is that elements could measure up to a maximum of 2,5 by 5 meters and the design agrees with these dimensions.
In Figures 8.3 and 8.4 the cross-sections of two element configurations is given. In Section 8.3 the production process for the first configuration was already described and this option is considered feasible. Difficulties are expected with applying and holding the reinforcement mesh in place. But, when the mesh is weakened a little bit it might be possible to produce the reinforced double-curved elements. Another solution would be to make use of steel reinforcement bars rather than the reinforcement mesh.
The second element configuration with the bolted reinforcement bars offers a bigger casting challenge. There are several anchors that need to be cast with the curved concrete element and several notches must be created (for the bolts). A separate study for the feasibility for the prefabrication of this double-curved element configuration is required.

8.6 Foundation

The foundation has to limit settlements as much as possible, because in Chapter 5 the effects of settlements in the shell were presented and it was concluded that it has a large influence on the (in)stability of the shell structure. Still, the maximum forces that the

foundation is subjected to are very large. The (horizontal) thrust forces are approximately 10000 kN for each 'foot' and the vertical load is approximately 6000 kN for each foot. Several foundation options are discussed in Chapter 5, for example the ring beam. This option would result in a concrete beam with very large dimensions. Also, the foundation cables were not suitable. But, post-tensioned cables are still a good option. However, this is a very expensive option. Another, maybe better, option could be prestressing the ground around a solid concrete foundation with grouted anchors. For the vertical support use can be made of normal concrete foundation piles, approximately 2 or 3 of those will be necessary for each 'foot'. To transfer the remaining thrust forces it is possible to position extra foundation piles under an angle approximating the angle of the concrete shell.

8.7 Costs

The costs of the original design and the new design of Green Planet will be compared and the construction parts that are being compared must be expressed in terms of €/m^2. The parts of the design that are involved in the comparison are the foundation, the formwork, the roof construction elements and other cost factors like transportation, hoisting and storage. The other structural parts are the same for both designs. The original design cost an estimated amount of 700 €/m^2 for the mentioned parts (source of this information is ABT, the engineering consultancy responsible for the structural design of Green Planet). For the new design it's interesting to see what the production of the double-curved elements will cost:
It was mentioned in [42] that the costs for one adjustable formwork are estimated on €3500 per m^2. With elements having maximum dimensions of 5x2,5 meters this would yield a price of €50000,- per adjustable formwork. Furthermore, there are additional costs because some parts of the adjustable formwork are not yet reusable, this will be 10%. These additional costs are applicable to all 327 elements, resulting in a total cost of approximately €1650000,- for the formwork. Besides that there are the labor and concrete costs, about 500 for every m^2, based on an element with a maximum thickness of 50 mm, but leaving the thickness out this part will still cost an estimated 500x2500 = €1250000,-. In total this would be €2950000/2500m^2= 1180 €/m^2. That is already more than the original design and the foundation will be a major cost item too.

Part V

Final remarks

Chapter 9

Conclusions and recommendations

9.1 Introduction

The aim of this master thesis was to investigate the application of double-curved elements produced with the adjustable formwork. The selected structure is the project Green Planet. There are a lot of aspects that need to be considered to come to a balanced design. In the end the main question will be if the final design is economically competitive with the original design. Therefore, the main research question of this thesis is:

> Is it possible to design an economically competitive and technically feasible alternative for project Green Planet, making use of a concrete shell structure consisting of double-curved precast concrete elements?

To answer this research question several sub-goals were set in Section 1.1, they are presented below. These goals were all covered in Parts II, III and IV, two goals per part. For a great deal the conclusions are based on the research and findings that served the goals, so this section is subdivided in the parts that were mentioned. The last section will cover the recommendations based on this study.

- Validate a suitable finite element analysis program;
- Design a suitable model for the Green Planet structure, analyze and optimize it;
- Find a good segment distribution;
- Design a suitable connection;
- Find the best execution method;
- Provide a cost indication;

9.2 Conclusions

Part II Green Planet: Design and optimization

- It was demonstrated that the results of theoretical models match the results of the finite element analysis software (Scia Engineer). Not all results corresponded perfectly which is mainly caused by inevitable differences in the loading and supporting conditions. It was interesting to observe how well the FEA software reflected these minor differences. The conclusion was that the software is suitable for shell structure modeling.
- The deformation and buckling behavior of Green Planet is best compared with a cylinder shaped structure. It was demonstrated that the deformed shape of both models matches in most circumstances.
- It was demonstrated that the results of the Green Planet model matches the results of comparable but more traditional shell structures. The Green Planet model was compared to a cylinder structure, a regular dome structure and a weakened (by an oculus in the top) dome structure with comparable dimensions and boundary conditions. The assessment was based on the structural behavior aspects deformation, force distribution, moment distribution, support reactions and stability determined by linear (stability) analysis. All results lie in between the results of the cylinder structure and the dome structures. The conclusion was that the Green Planet shell is best defined as a very stiff cylinder structure.
- The Green Planet model is simulating an acceptable and realistic behavior. The results of the model lie in between the results of theoretical substantiated models like the cylinder and dome structures. The only exceptions were the support reactions, those were biggest for the Green Planet shell, which is a consequence of limited supports.
- The Green Planet model was analyzed being loaded with realistic loads. It was found that load combinations 3, 5 and 8 are the most critical loads, being in sequence the distributed wind load acting downwards, the asymmetrically distributed wind load acting downwards on the back (large) half of the shell and the asymmetrically distributed wind load acting upwards on the front (small) half of the shell.
- It can be concluded that the shell is sensitive to imperfections, based on the difference between the buckling loads. The difference between the first and second buckling loads is greater than 4%. The structure is, however, not highly sensitive, this applies to cases where the difference is smaller than 2%.
- The thrust forces on the foundation of Green Planet are large, being 1250 kN/m when distributed.
- The Green Planet shell is mainly subjected to compressive forces. Tension forces only arise along the edges of the shell and in the areas subjected to edge disturbance, this is the area near the supports.
- It was demonstrated with a short mesh study that a mesh size of 0,2 m is sufficient for the calculations of the Green Planet model. The result differences with consecutive mesh sizes are below 0,5% and therefore this mesh size will give results which are accurate. However, extra attention should be paid to local internal forces. The

calculation time was not selected as a decision instrument but it can be noted that calculations up to a mesh size as small as 0,15 m can be performed rather easily.

- For the purpose of optimization the thickness of the shell was varied in order to investigate its influence on the internal forces and behavior of the shell. From this research it can be concluded that both situations, increasing and reducing the thickness (of 200 mm), have their advantages and disadvantages. Increasing the thickness will have many structural advantages because the forces will be distributed. Disadvantages are the increase of forces acting on the foundation and the costs. A balance need to be found for the applied thickness.

- The material strength only influences the stiffness of the shell. Reducing the E-modulus resulted only in larger deflections and lower critical buckling loads.

- It was demonstrated that optimizing the thickness in strategic positions of the Green Planet structure of the shell (at the edge or/and near the supports) can have a major influence on the shell's behavior. For example, it can have a positive influence on the internal forces, support reactions, deformation and buckling. The drawback, however, is that this will induce a project cost rise as well as a smooth thickness variation is hard to realize in a concrete shell structure. But, another advantage for example is the material strength which can be reduced significantly.

- The option to use cables as a foundation method was investigated. The conclusion was that the small displacements due to the elongation of the cables are always fatal for this shell.

Part III Green Planet: Segmentation and detailing

- The segmented Green Planet model is simulating an acceptable and realistic behavior. The Green Planet design is segmented and compared to the old model to check for modeling inaccuracies. With an average deviation of 10% the results of both designs agree with each other quite well, considering the amount of elements (327) and thus the amount of potential weak spots that were added.

- Three formulas were composed for calculating with the axial, rotational and shear stiffness of a connection in Scia Engineer. In the FEA program the connection is simulated by means of a spring with a certain stiffness that needs to be determined by the engineer. These formulas were tested by comparing basic FEA models consisting of one particular connection type with theoretical models and (other) FEA models. The maximum difference between the results of the models was 4,3% and this was considered a proper result. It was concluded that the formulas are appropriate to simulate a connection stiffness in Scia Engineer.

- It was demonstrated that combining the three formulas for the axial, rotational and shear stiffness of a connection in Scia Engineer results in a realistic (three-dimensional) connection behavior. The combined formula was tested by applying it to connections of single and double-curved FEA models. Those models were supposed to simulate a continuous concrete shell and were compared to FEA models of a continuous concrete

shell with the same boundary conditions. The maximum difference between the results of the models was 2,9%, unrealistic peak stresses and edge disturbances omitted, and this was considered a proper result. It was concluded that the combined formula is appropriate to simulate a connection stiffness in Scia Engineer.

- It was demonstrated that the connection stiffness has a small influence on the buckling behavior of a concrete dome structure. The critical load factors (indicators for the buckling load) of various models with increased and reduced spring stiffness were gathered and compared to the FEA model simulating a continuous concrete structure. The stiffness determined with the combined connection formula resulted in a difference of 2,0% with the solid concrete structure. It was shown that a large stiffness increase (combined formula stiffness multiplied by 10 and 100) only improved the difference with the initial model to a difference of 1,5%. A large stiffness reduction (combined formula stiffness divided by 10 and 100) resulted in a difference of 6% and 31% compared to the solid concrete structure model. This research indicates that a large connection stiffness reduction has a relatively small influence on the buckling behavior of the concrete dome.
- The segmented and connected Green Planet model is simulating an acceptable and realistic behavior. The segmented Green Planet model is connected by using the combined formula for the connection stiffness. This applied stiffness is simulating a continuous concrete shell and compared with the segmented continuous concrete shell. With an average deviation of 6% the results of both designs agree with each other quite well, considering the amount of connections (591) and thus the amount of potential weak spots that were added. Unrealistic peak stresses and edge disturbances were omitted in this deviation. The force pattern of both models agree with each other too and the connected Green Planet model is simulating a realistic behavior.
- It was proved that it's possible to design a suitable and realistic connection for Green Planet. The connection stiffness which is applied to the segmented and connected Green Planet model simulates a continuous concrete shell structure. When the stiffness of all connections is halved it would simulate a construction that's weakened considerably because of the connections. Connections that cause the stiffness of a continuous concrete section to halve are deemed straightforward to design. The comparison results showed that there is a small maximum difference of 0,5% between the Green Planet models if the stiffness of the connections is halved.

Part IV Green Planet: Execution and costs

- The Green Planet structure is not subjected to high tension forces. The maximum required tension strength is 8 MPa and, therefore, the amount of required reinforcement is relatively low. This is beneficial for the costs of the production process as well as the building process.
- It was demonstrated that there are multiple options for the structural connection of the double-curved concrete elements of the Green Planet design.

- Several options for the building process were given. The most appropriate execution method is probably a combination of the given methods, a combination of the frame method and the segmental method is deemed to be the optimal building method for the Green Planet structure.
- It was demonstrated that the concrete shell structure can be build with limited formwork and scaffolding due to the application of precast double-curved elements. In other cases, when building a concrete shell structure cast in-situ the whole surface must be supported by formwork and scaffolding.
- The proposed production process with the adjustable formwork producing the double-curved concrete elements is suitable for the project Green Planet. This is based on the structural requirements of the structure in combination with the suggested connection type which requires only a slight adjustment to the elements and thus the precasting process.
- A special solution for the foundation of Green Planet is required. The two options that are left and considered best feasible are the use of post-tension cables and the use of a large concrete base supported by piles and grouted anchors.
- A comparison of the costs between the original Green Planet design and the concrete Green Planet design indicates that there's a large cost difference. The costs of the new design are much higher. The production of the double-curved concrete elements is already more expensive than the total original Green Planet design.

The overall conclusion is that it's technically feasible to design an alternative for project Green Planet, making use of a concrete shell structure consisting of double-curved precast concrete elements. The economically competitiveness of this alternative, however, is not achieved and it is questionable if this possible at all since the original design is very economic. But, it must be noted that the original Green Planet design is supported by columns while the alternative concrete structure offers a column free space, structurally and in the end economically this makes a big difference.

9.3 Recommendations

This study primarily considered the feasibility of the project Green Planet and its economical competitiveness. Unfortunately, this means that lots of interesting optimization possibilities were not addressed due to a lack of time. Besides, such optimization steps could increase the economic competitiveness. However, some of these optimizations could have been carried out if modeling a double-curved structure in a FEA program would be more easily. The following recommendations are proposed:

Part II Green Planet: Design and optimization

- The behavior of Green Planet model was verified using theoretical and FEA models. Before finalizing the design it is recommended to build a physical scale model which confirms the behavior of the complex shell structure as well.

- The structural analysis resulted in the normative load combinations for the Green Planet design. These combinations can be supplemented with an analysis of the accidental and collision loads, especially since the design concerns a (gas) service station. But also the temperature load of the structure and the dynamic behavior can be investigated.
- In this thesis some methods were introduced to optimize the FEA design, one of them was the optimization of the element thickness. It was shown that by optimizing the thickness the resistance to buckling and the displacement could be improved substantially. The thickness along the edges of the shell was increased whilst the thickness of middle parts of the shell was reduced. A similar but more extensive study could be performed for the final design as well to improve it's structural behavior while making the material use more efficient.
- The optimization of the element thickness is mainly a theoretical study, but it would be interesting to investigate the impact on the production and building processes as well. The elements must probably be load bearing, because controlling an in-situ concrete pouring process in this case is likely to be too labor and cost intensive. Adjusting the production process, however, is an interesting option and this could bring the element production process again to a higher level. The thickness of the double-curved elements must vary, which will make the use of an adjustable counter or top mould obligatory in most cases. But, large structures with the dimensions of Green Planet may already benefit from a subtle element thickness change which might be feasible with the flexible formwork. This possibility could contribute to the architectural freedom of large load bearing free-form structures in general as well.
- It was shown that the material strength influences the most important failure mode buckling. An interesting option is the use of high-performance concrete or Ultra-high-performance concrete in the precast elements. This will reduce the required thickness of the concrete layer, the internal forces and therefore the loads on the foundation.
- For the foundation a few options with steel tension cables were investigated. Due to small settlements, which will always occur because of the elongation of the cables, this foundation method has a destructive influence on the stability of the shell. Therefore, it was not suitable. But, another option is applying post-tensioned cables to compensate the elongation. Those cables would eliminate the high thrust forces on the foundation to a great extent and this would be worth the research, perhaps supported with a FEA expert.
- The stability problems that were addressed were based on a linear stability analysis in combination with a conservative knock down factor. It would be interesting to perform a study with a non-linear analysis including imperfections and geometrical and physical nonlinearities to find out the real influence on the failure mode of the shell. Hypothetically, the results must improve compared to the results determined with the conservative knock down factor.

Part III Green Planet: Segmentation and detailing

- The segmentation of the shell structure in the FEA program (Scia Engineer) appeared to be a time consuming process. An interesting improvement would be the implementation of a segmentation tool. The development of such a tool would make an interesting research.
- The presented segmentation solution was the best modeling solution for the Green Planet shell. But, due to the limitations of the FEA program the user is restricted to use three or four corner points to model the elements. In reality, however, the use of a greater variety of element configurations is possible and this would improve the segmentation plan. It would be interesting to study the improvement of the FEA program at this matter. Additionally, when finalizing the Green Planet design, it is recommended to improve the segmentation plan at certain points. Especially along the edges and near the supports of the shell there's room for improvement. The elements with four corner points must be transformed into elements with five corner points in order to extend and agree with the overall configuration.
- Based on the results of the FEA program it was concluded that a large reduction (50%) in connection stiffness does not necessarily mean a large effect on the failure mode buckling. Practical research is required to confirm the conclusions that were drawn from digital results. In order to support the results found in this research a great follow-up study would be to model the required connection in a specialized FEA program and relate this model to laboratory experiments.

Part IV Green Planet: Execution and costs

- It was concluded that the required amount of reinforcement for the Green Planet design is relatively low, because the shell is not subjected to high tension forces. Therefore, a very interesting option is the application of fibre reinforced concrete or ultra-high-performance concrete. The tensile strength of this material matches the maximum required tension strength of the design (8 N/mm^2). This could mean that no reinforcement is required which could result in a reduction of labor costs.
- The bearing capacity of the double-curved concrete elements was not yet determined. For a final design it is necessary to calculate the capacity and preferably a study is performed upon the optimum thickness of the elements in relation to the required concrete layer thickness.
- The two connection proposals are based on the assumption that not a lot of stiffness is required. But, for the continuation of this research it would be valuable to know the exact connection stiffness they represent.
- The prefabricated elements are connected with a special bolt connection. This configuration seems complex to cast in a adjustable formwork. A separate study for the feasibility of the prefabrication of this double-curved element configuration is required.

- A large part of the costs involved in the new Green Planet design is on the account of non-reusable parts of the adjustable formwork. It is really worth an investigation to make the flexible formwork more sustainable and reusable.
- The double-curved concrete elements manufactured with the adjustable formwork were a lot smaller than the elements designed for the Green Planet design. It would make a valuable experiment to investigate whether this requires a different rheological behavior and mixture design.
- Besides the concrete elements an in-situ concrete layer is poured during construction. For this concrete the necessary rheological behavior and mixture design should be determined too, to control the pouring process on site.
- Transportation costs are an issue for both designs. To reduce these costs for the new design it might be beneficial to produce the concrete elements on site. A semi-controlled environment is required for the prefabrication but this might be a more cost efficient alternative.
- The original design of Green Planet is very economic compared to the presented alternative design. An important factor in this comparison is the column-free space the new design offers. For the cost comparison it's interesting to investigate what the original design will cost if it would offer a column-free space as well. Also, an alternative concrete shell structure with columns and supporting beams/ribs would make a better comparison. This would, however, detract the fairness of the shell structures structural integrity derived from its curvature.

Bibliography

[1] "www.edu.vrmmp.it/vep/debouw.html," Construction movie Philips pavilion, date 10/01/2014.

[2] "www.buildipedia.com," Heydar Aliyev cultural center, date 10/01/2014.

[3] "www.structurae.net," date 10/01/2014.

[4] "www.constructiondigital.com," 3d printing, the future of concrete, date 10/01/2014.

[5] "Azerbaijan's amazing transformation," Discovery Channel, Extreme engineering, April 2011.

[6] S. K. Bekiroglu, "Assembling freefree bbuilding in precast concrete," in *Precast 2010*, 2010.

[7] D. Billington, *The art of Structural Design, a Swiss legacy*. Princeton University Art Museum, 2003.

[8] J. Blaauwendraad and H. Hoefakker, *Structural shell analysis*. Springer, 2014.

[9] P. Block and J. Ochsendorf, "Thrust network analysis: a new methomethod for three-dimensional equilibrium," *IASS journal*, vol. 48, pp. 167–173, 2007.

[10] G. Buchanan, *Finite element analysis*. MC Graw Hill Book Company, 1995.

[11] I. Bucur-Horvath and R. Saplacan, "Force lines embodied in the building: Palezzetto dello sport," *IASS journal*, vol. 54, pp. 179–187, 2013.

[12] R. Cook, D. S. Malkus, M. Plesha, and R. Witt, *Concept and application of finite element analysis*. John Wiley & Sons, 2002.

[13] E. Den Hartog, "Prefabrication of concrete shells," Master's thesis, TUDelft, 2008.

[14] M. Diks, "Translucent sandwichsystem voor dubbel gekromde toepassingen," Master's thesis, TU Delft, 2005.

[15] S. Engineer, *Advanced concept training - FEM*, 2011.

[16] S. Gelderman and R. Homan, "Dubbelgekromde betonmallen," *Cement*, vol. 5, pp. 42–46, 2009.

[17] P. Hoogenboom, *Shell analysis, theory and application, course CIE4143*. TU Delft, 2013.

[18] F. Huijben, F. v. Herwijnen, and R. Nijsse, "Concrete shell structures revisited: introducing a new and low-tech construction method using vacuumatics formwork," in *Structural membranes 2011: V International Conference on Textile Composites and Inflatable Structures*, 2011.

[19] K. Huyghe and A. Schoofs, "Precast double curved concrete panels," Master's thesis, TU Delft, 2009.

[20] T. Iori and S. Poretti, "Pier luigi nervi: his construction system for shell and spatial structures," *IASS journal*, vol. 54, pp. 117–126, 2013.

[21] H. Isler, "New shapes for shells," in *Bulletin of the IASS*, 1961.

[22] H. Jansen, "Prefabricage bij blobconstructies, een civiele kijk op blobarchitectuur," Master's thesis, TU Delft, 2004.

[23] B. Janssen, "Double curved precast load bearing concrete elements," Master's thesis, TUDelft, 2011.

[24] A. Kilian and J. Ochsendorf, "Particle-spring systems for structural form finding," *IASS journal*, vol. 46, pp. 139–147, 2005.

[25] M. Kok, "Textile reinforced double curved concrete elements," Master's thesis, TUDelft, 2013.

[26] F. Kosche, "Schaltisch und verfahren zur herstellung von doppelt gekrummten bauteilen," German Patent DE 19 823 610 B4, 2005.

[27] M. Kuijvenhove and P. Hoogenboom, "Particle-spring method for form finding of grid shell structures consisting of flexible members," *IASS journal*, vol. 53, pp. 31–38, 2012.

[28] W. Lewis, *Tension structures: form and behaviour*. Thomas Telford, 2003.

[29] V. Liseikin, *Grid generation methods*. Springer, 2010.

[30] A. Middeldorp, "Een constructief ontwerp voor het ministerie van sociale zaken en werkgelegenheid in groningen," Master's thesis, Betonvereniging, opleiding Betonconstructeur PMSE, 2013.

[31] I. Mungan and J. F. Abel, *Fifty years of progress for shell and spatial structures*. IASS, 2011.

[32] P. L. Nervi, *Aesthetics and technology in building*, R. t. Einaudi, Ed. Harvard University press, 1965.

[33] R. Nijsse, "Le poème Électronique se répète," *Cement*, vol. 4, pp. 9–13, 2008.

[34] M. Oosterhuis, "A parametric structural design tool for plate structures," Master's thesis, TU Delft, 2010.

[35] B. Peerdeman, "Analysis of thin concrete shells revisited: opportunities due to innovations in materials and analysis methods," Master's thesis, TU Delft, 2008.

[36] L. Piegl, "On nurbs: a survey," *IEEE Computer Graphics and Applications*, vol. 11, pp. 55–71, 1991.

[37] J. Przemieniecki, *Theory of matrix structural analysis*. MC Graw Hill Book Company, 1968.

[38] M. Quack, "Dubbel gekromd gevelelement, van ontwerp naar uitvoering," Master's thesis, TU Delft, 2001.

[39] E. Ramm, "Shape finding of concrete shell roofs," *IASS journal*, vol. 45, pp. 29–39, 2004.

[40] ——, "Heinz isler shells- the priority of form," *IASS journal*, vol. 52, pp. 143–154, 2011.

[41] H. Schek, "The force density method for form finding and computation of general networks," *Computer methods in applied mechanics and engineering*, vol. 3, pp. 115–134, 1974.

[42] H. Schipper, "Double-curved precast concrete elements," Ph.D. dissertation, Tu Delft, 2015.

[43] H. Schipper, S. Grunewald, and P. Raghunath, Eds., *Rheological parameters used for deliberate deformation of a flexible mould after casting*. TU Delft, 2013.

[44] staff, "The sydney opera house," *Concrete Construction*, vol. September, p. 2, 1967.

[45] ——, "Segmentation, us air museum, duxford, cambridgeshire," *Mix, by C&CAA*, vol. December, pp. 6–7, 2001.

[46] R. Ter Maten, "Ultra high performance concrete in large span shell structures," Master's thesis, TUDelft, 2011.

[47] S. Timoshenko and S. Woinowsky Krieger, *Theory of Plates and Shells*. McGraw Hill Book Company, 1959.

[48] B. Topping and A. Khan, "Parallel computation schemes for dynamic relaxation," *Engineering computations*, vol. 11, pp. 513–548, 1994.

[49] J. Vambersky and L. Wagemans, *Special Structures, course CT5251*, J. Coenders, Ed. TU Delft, 2008.

[50] W. Van Dijk, M. Falger, and R. Sterken, "Scheepsbouwtechniek - ovt," *Cement*, vol. 2, pp. 34–41, 2013.

[51] e. a. van Nijhuis, J.W., "Typen vegetatiedaken, voor- en nadelen, http://ecoengineering.groenweb.nl/content/groene-daken-techniek," http://ecoengineering.groenweb.nl/content/groene-daken-techniek, 2009.

[52] M. van Roosbroeck, "The construction of precast concrete shells, morphology-segmentation-production method," Master's thesis, TU Delft, 2006.

[53] D. Veenendaal, "Evolutionary optimization of fabric formed structural elements," Master's thesis, TU Delft, 2008.

[54] R. Verhaegh, "Free forms in concrete," Master's thesis, TU Eindhoven, 2010.

[55] E. Vicenzino, G. Culham, V. H. Perry, D. Zakariasen, and T. S. Chow, "First use of uhpfrc in thin precast concrete roof shell for canadian lrt station," *PCI journal*, vol. September, pp. 50–67, 2005.

[56] H. Vidal, "Method and apparatus for moulding curved concrete sections," European Patent EP0 238 168 A1, 1986.

[57] K. J. Vollers and A. Rietbergen, "A method and apparatus for forming a double curved panel from a flat panel," International Patent WO 2009/002 158 A1, 2008.

[58] ——, "Werkwijze en mal voor het vervaardigen van een gebogen paneel," Netherlands Patent NL2 001 738 C2, 2010.

[59] R. Weston, *Utzon- Inspiration, vision, architecture*. Edtion Blondal, 2002.

Contact information

Personal data

Name: S.J.Witterholt

Studynumber: 1320173

Master: Building Engineering, Structural Design

Tel.: 0625004881

Email: S.J.Witterholt@student.tudelft.nl

Graduation Committee

- Prof. Ir. R. Nijsse
  Structural and Building Engineering, TU Delft / ABT
  R.Nijsse@tudelft.nl
- Dr. Ir. H.R.Schipper
  Structural and Building Engineering, TU Delft
  H.R.Schipper@tudelft.nl
- Dr. Ir. P.C.J. Hoogenboom
  Structural Mechanics, TU Delft
  P.C.J.Hoogenboom@tudelft.nl
- Dr. Ir. S. Grunewald
  Concrete Structures, TU Delft / Laboratory Magnel for Concrete Research, Ghent University
  S.Grunewald@tudelft.nl
- Ir. J.A.M. van Vliet
  Raadgevend Ingenieur, ABT
  H.V.Vliet@abt.eu

Appendix A

Top displacement hemispherical dome with potential energy

To derive the top displacement of the hemisphere use is made of an exam question of the course Theory of elasticity CT5141 (date: 25/01/2006). With the use of potential energy a formula for the deflection of the dome is derived, beginning with an assumed displacement of:

$$u_z = C2 * cos(2 * \varphi) + C1 * cos(\varphi)^2$$

$$u_\varphi = C3 * sin(2 * \varphi) + C4 * sin(4 * \varphi)$$

Furthermore, use is made of the following formulas for spherical domes, where it is assumed that the Poisson's ratio ν is zero:

$$\varepsilon_{\varphi\varphi} = \frac{1}{a} * (\frac{du_\varphi}{d\varphi} + u_z)$$

$$\varepsilon_{\theta\theta} = \frac{1}{a} * (u_\varphi cot\varphi + u_z)$$

$$n_{\varphi\varphi} = E * t * \varepsilon_{\varphi\varphi}$$

$$n_{\theta\theta} = E * t * \varepsilon_{\theta\theta}$$

The expression for the potential energy became:

$$E_{pot} = \int_{\phi=0}^{\frac{1}{2}\pi} \int_{\theta=0}^{2\pi} \left(\frac{1}{2} n_{\phi\phi}\varepsilon_{\phi\phi} + \frac{1}{2} n_{\theta\theta}\varepsilon_{\theta\theta} + u_z p \cos\phi - u_\phi p \sin\phi\right) a \sin\phi \, d\theta \, a \, d\phi$$

While using Maple most of the units are called differently in order to avoid the confusion which came with using the initially used notations in the program. The calculation input and output (short version) can be found in Figure A.1. In order to calculate the final deflection at the top of the hemisphere, u_z is calculated for an angle $\varphi = 0$. When the determined values for C1 and C2 are incorporated in the formula this yields $u_z = -1,97\frac{pa^2}{Et}$.

$$w := C2 \cdot \cos(2\,H) + C1 \cdot \cos(H)\cos(H);$$
$$v := C3 \cdot \sin(2\,H) + C4 \cdot \sin(4\,H);$$
$$e := \frac{1}{a} \cdot ((diff(v, H)) + w);$$
$$f := \frac{1}{a} \cdot (v \cdot \cot(H) + w);$$
$$n := \mathrm{E} \cdot \mathrm{t} \cdot e\ ;$$
$$m := \mathrm{E} \cdot \mathrm{t} \cdot f;$$
$$s := int\left(\left(\frac{1}{2} \cdot n \cdot e + \frac{1}{2} \cdot m \cdot f + w \cdot p \cdot \cos(H) - v \cdot p \cdot \sin(H)\right) \cdot a \cdot \sin(H), K = 0\,..2\,\mathrm{pi}\right);$$
$$u := int\left(s \cdot a, H = 0\,..\frac{1}{2}\mathrm{pi}\right);$$
$$u1 := diff(u, C1);$$
$$u2 := diff(u, C2);$$
$$u3 := diff(u, C3);$$
$$u4 := diff(u, C4);$$
$$solve(\{u1, u2, u3, u4\}, \{C1, C2, C3, C4\});$$
$$evalf(\%);$$

$$\left\{C1 = -\frac{1.359375000\,a^2\,p}{E\,t}, C2 = -\frac{0.6093750000\,a^2\,p}{E\,t}, C3 = \frac{0.6969572368\,a^2\,p}{E\,t}, C4 = -\frac{0.02158717105\,a^2\,p}{E\,t}\right\} \quad \textbf{(1)}$$

Figure A.1: Deflection of a hemisphere: Maple input and output